



The Effects of Rocket Exhaust on Stratospheric Ozone: Chemistry and Diffusion

Prepared for:

Environmental Management Division
USAF Space and Missile Systems Center
El Segundo, CA

Prepared by:

TRW Space & Electronics Group

Peter D. Lohn
Eric Y. Wong

in coordination with:

Darryl D. Spencer, Roger Meads, Luisa T. Molina and Mario J. Molina
Department of Earth, Atmospheric and Planetary Sciences
and Department of Chemistry
Massachusetts Institute of Technology
Cambridge, MA

and

Peter S. Connell, John J. Walton, Joyce E. Penner and Charles O'Connor
Lawrence Livermore National Laboratory
Livermore, California

August 1996

Report Documentation Page

Report Date 00081996	Report Type N/A	Dates Covered (from... to) -
Title and Subtitle The Effects of Rocket Exhaust on Stratospheric Ozone: Chemistry and Diffusion		Contract Number
		Grant Number
		Program Element Number
Author(s) Lohn, Peter D. , Wong, Eric Y.		Project Number
		Task Number
		Work Unit Number
Performing Organization Name(s) and Address(es) TRW Space & Electronics Group One Space Park Redondo Beach, CA 90278		Performing Organization Report Number
Sponsoring/Monitoring Agency Name(s) and Address(es) Environmental Management Division USAF Space and Missile Systems Center El Segundo, CA		Sponsor/Monitor's Acronym(s)
		Sponsor/Monitor's Report Number(s)
Distribution/Availability Statement Approved for public release, distribution unlimited		
Supplementary Notes		
Abstract		
Subject Terms		
Report Classification unclassified	Classification of this page unclassified	
Classification of Abstract unclassified	Limitation of Abstract UU	
Number of Pages 151		



The Effects of Rocket Exhaust on Stratospheric Ozone: Chemistry and Diffusion

Prepared for:

Environmental Management Division
USAF Space and Missile Systems Center
El Segundo, CA

Prepared by:

TRW Space & Electronics Group

Peter D. Lohn
Eric Y. Wong


in coordination with:

Darryl D. Spencer, Roger Meads, Luisa T. Molina and Mario J. Molina
Department of Earth, Atmospheric and Planetary Sciences
and Department of Chemistry
Massachusetts Institute of Technology
Cambridge, MA

and

Peter S. Connell, John J. Walton, Joyce E. Penner and Charles O'Connor
Lawrence Livermore National Laboratory
Livermore, California

Approved by:


John J. Lamb, Ph.D.
Program Manager

August 1996

The Effects of Rocket Exhaust on Stratospheric Ozone: Chemistry and Diffusion

CONTENTS

1. Introduction and Summary	1
2. Upgraded Kinetics and Diffusion Models: TITAN III-C Validation	3
3. Stratospheric Ozone Depletion Caused by a TITAN III Launch	10
4. Liquid Rocket Engine Effects on Stratospheric Ozone	15
5. Post-Launch Depletion of Stratospheric Ozone	17
6. Summary and Recommendations	28
7. References	31

1. Introduction and Summary

The Environmental Management of the Space and Missile Systems Center (SMC) has set out to evaluate the depletion of stratospheric ozone caused by Air Force activities in space. Recent work supported by SMC included an assessment of the impact of deorbiting debris on stratospheric ozone (Ref. 1.1) and the potential for reduction of ozone destruction by use of alternate propellants for launch vehicle rocket engines (Ref. 1.2). A key goal of the SMC effort is to upgrade requirements for the prototype high-resolution ozone imager (HIROIG) (Ref. 1.3). The present work provides inputs for further HIROIG requirement resolution. It addresses the effects of rocket exhaust on stratospheric ozone. The local, short time, effect (as measured by HIROIG) is evaluated as is the ultimate global effect. Consideration of both short time and global effects enable connection of launch predictions and measurements of ozone depletion to the ultimate, long term depletion of stratospheric ozone. The present effort extends the work reported in Reference 1.4 in which a methodology was described which allows a quantitative assessment of the impact on stratospheric ozone by rocket exhaust.

The primary results of the present study are summarized as follows:

- 1) A validated methodology has been established. Kinetics and diffusion model upgrades (inclusion of NO, chlorine, and heterogeneous mechanisms; diffusion

model validated and anchored to in situ data) have been applied to a TITAN III launch for which in situ measurements of ozone depletion are available. Good comparison with this data provides a validation of the present methodology.

2) Analysis of the SRM-induced depletion of ozone during a TITAN III launch was addressed. Local ozone depletion is presented: the HIROIG sensor can be expected to view a local ozone hole of several kilometers radius and of duration from ten minutes to nearly an hour after launch. It needs to take into account possible polarization effects caused by alumina particle formation. This can be achieved by using three identical sensors sensitive to light polarized in different planes. Details of the configuration are provided in Chapter 6. Extension to post-launch times is discussed.

3) Loss of stratospheric ozone loss caused by liquid rocket engine boosters is evaluated (the primary loss is caused by nitric oxide). The effects are insignificant when compared to SRM boosters. Two considerations lead to this conclusion:

i) The NO catalytic cycle mechanism causes less ozone destruction than that of chlorine. Furthermore, present liquid boost engines (RP-1/LOX; LH₂/LOX) are not nitrogen-based thus leaving afterburning as the only process by which NO can be produced. Afterburning in the stratosphere produces very little nitric oxide.

ii) Presently, all large-thrust U.S. launch vehicles are chlorine-based SRMs that are capable of producing large amounts of chlorine in the boost phase.

2. Upgraded Kinetics and Diffusion Models: TITAN III-C Validation

Kinetics Upgrade

Destruction of ozone in the stratosphere by rocket exhaust may be caused by several mechanisms. Homogeneous reactions which destroy ozone through the chlorine or nitric oxide catalytic cycles and heterogeneous reactions in which chlorine-bearing reservoir species such as chlorine nitrate act on the surface of Al_2O_3 particles to release chlorine are the primary candidate mechanisms. The heterogeneous mechanism associated with aluminum oxide particles from SRMs was found to be unimportant (Ref. 1.4) relative to the effects of chlorine or nitric oxide produced in the afterburning region. Past work focused on either the chlorine and aluminum oxide mechanisms or on the nitric oxide mechanisms (Refs. 1.1, 1.2, 1.4), thus assuming insignificant inter catalytic cycle interactions. The present task combined both reaction packages which accounts for ozone depletion effects of Al_2O_3 particles, chlorine, and nitric oxide. The reaction rates are given in Appendix I and are drawn from References 2.1 through 2.5.

The rate constants for the photochemical reactions were calculated both in the stratosphere and the troposphere in order to estimate possible variations caused by solar absorption. Rate constants for the troposphere were required for validation

purposes. The coefficients were estimated by integrating the product of the solar flux (I), collision cross section (α), and quantum efficiency (ϕ):

$$\int \phi \alpha I d\lambda,$$

since primary photochemical reactions are considered here, the quantum yield and absorption cross section are considered altitude invariant.

The solar intensity at 7 km and 22 km was calculated using the MODTRAN transmission code. The absorption and quantum efficiency were taken from Reference 2.1. The 22 km values calculated are virtually identical to those used in Reference 1.4. The values for 22 km and 7 km are the same (to one significant figure) except for the rate for HNO_3 dissociation for which the 7 km value is about 1/3 of the 22 km value.

TITAN III In Situ Data

Stewart and Gomberg (Ref. 2.6) took a set of data in the plume of a TITAN III launch. Ozone, NO and NO_2 were measured by aircraft passes through the plume/wake at two times, 5 minutes and 34 minutes, after the passing of the launch vehicle with its SRMs. The Stewart and Gomberg results are used to firm up our understanding of the diffusion of rocket exhaust plumes. Their results are also used to establish (by comparison with direct in situ measurements of ozone loss) the

validity of our overall diffusion/kinetics approach for calculation of ozone depletion as caused by rocket exhaust.

The altitude of the observations is not cited in their report and the authors are no longer with NASA Langley. We were, however, able estimate the altitude by two approaches:

- 1) the measured mixing ratio for ozone is 50 ppb. This is the level expected at about 7 km;
- 2) the data was taken from a Cessna 402. Conversations with an aviation expert (Ref. 2.7) indicates that the maximum altitude achievable with a (turbocharged) Cessna is about 25,000 ft (7.6 km).

Based on these considerations we proceed under the assumption that the measurements were taken at seven kilometers.

Analysis Approach for TITAN III Data

The TITAN III plume flowfield was calculated by use of the industry standard SPF-II (Standard Plume Flowfield) code. The nozzle exit conditions were taken from the Stewart and Gomberg report. The TITAN III uses Thrust Vector Control (TVC) above 10 km. We have calculated the plume flowfield for both TVC and non-TVC conditions. The calculated NO levels for TVC are somewhat greater since the TVC

dumps N_2O_4 into the nozzle. However, the major source of plume NO is from afterburning.

The hot plume code (SPF) results were taken out to several thousand nozzle diameters. The "cold wake" initial profiles were taken after the plume had nearly come to rest relative to the ambient atmosphere. The cold wake profiles were then used to perform a diffusion/reaction calculation by using the TRW-originated cold wake code (described in Ref. 1.4). The TITAN III has two solid motors. The resultant plume/wake size is assumed to be twice (by area) that calculated by the single SRM plume SPF calculation.

Specification of Diffusion Coefficient

The remaining consideration for modeling the TITAN III plume is the diffusion coefficient. Eddy diffusivity was discussed in detail in Reference 1.4. The specification of the diffusion model by examination of the plume data (of Hoshizaki, Ref. 2.8) and other data of the spatial scale analogous to a booster plume was discussed. Postulation that the apparent eddy diffusion coefficient is proportional to the plume size was addressed and an expression for eddy diffusion coefficient was put forth (scale-dependent diffusion is also discussed in Reference 2.9):

$$K = br,$$

where K is the apparent eddy diffusion coefficient, m^2/s ;

r is the plume radius in meters;

b is an empirically-derived value;

and $b=1.1$ is the average value of a range from 0.6 to 1.3.

Use of this diffusion model to determine the diffusion coefficient ($b=1.1$) produces a result that is not in agreement with Stewart and Gombert measurements: the plume diffuses more rapidly than the measurements suggest. Stepping back, we then attempt to determine if the eddy diffusivity in the troposphere could be lower than the result appropriate for the stratosphere. Particularly we examine other data to determine if the eddy diffusivity might be less than the value ($b=1.1$) the model predicts.

The data of Randerson (Ref. 2.10) is considered. Randerson looked at the horizontal spread of a nuclear cloud in the lower-mid troposphere (4 km-5 km). At early times, of duration a few minutes, the standard deviation of horizontal diffusion (σ_y) was estimated from cloud size measurements. The apparent turbulent eddy diffusion coefficient is estimated then from the result of Taylor (Ref. 2.11) by the relationship: $K_H = \frac{\sigma_y^2}{2xt}$. Use of the Randerson data (with σ_y = cloud diameter/4.3) and scaling linearly results in a eddy diffusivity in the range of 10-30 m²/s for the initial cold wake of radius 170 m (as opposed to the value of 187 m²/s if the average value of $b=1.1$ is used). We fix the value for the initial cold wake at 20 m²/s. This

approach results in a b value of approximately 0.1 (instead of 1.1) and is at the lower edge of the envelope of data for stratospheric diffusion as shown in Figure 2.1.

Results of Comparison of TITAN III Data with Model

Using the revised eddy diffusivity model ($b=0.1$) the cold wake analysis is undertaken. The results are shown Figures 2.2-2.5 for several times. The data of Stewart and Gomberg is shown on the plots. A few comments about the in situ measurements are useful:

- 1) the measurements (ozone, NO, NO₂) are taken at five minutes and thirty four minutes after the launch. The earlier time is within the time for which the cold wake diffusion results are most applicable. At later times, beyond ten minutes, the effects of wind shear can start to become dominant. We show calculated results at later times to give a more thorough comparison with the measurements.
- 2) the instruments were not expected to be accurate at 5 parts per billion. The centerline results are near five parts per billion (presumably indicating a value between zero and 5 ppb) and not included in the comparison.

The results show reasonable agreement between calculated and measured ozone, NO and NO_x concentrations. The concentration of ClO which is the key product of the primary mechanism for ozone loss is also included to illustrate the importance

of the chlorine catalytic cycle. The depletion of ozone caused by the NO mechanism and heterogeneous Al_2O_3 mechanism are small relative to that caused by chlorine. The results at later time (27 and 40 minutes) are plotted and compared with measured values at 34 minutes. The measured size of the ozone "hole" is in reasonable agreement with these two calculated results. The limitations of the diffusion model (mainly lack transport convection terms), again, should start to become important for times on the order of tens of minutes and thus the validity of the model is supported by the good agreement at five minutes after launch.

3. Stratospheric Ozone Depletion Caused by a TITAN III Launch

The ozone loss caused by a complete TITAN III-C pass through the stratosphere was evaluated by calculation at altitudes of 15, 20, 25, 30, 35, and 40 kilometers. The launch trajectory (for 2.4 MLb thrust) was verified by comparison with several sources. The trajectory is characterized in Figures 3.1 and 3.2. The state variables (velocity, altitude) are used to drive a SPF plume flowfield calculation. Inputs to the SPF "hot plume" calculation are vehicle altitude and nozzle exit plane conditions (species concentrations, velocity, temperature, pressure and relative speed). The velocity differential (the difference between the vehicle velocity and the exhaust plume velocity) drives mixing in the shear layer. Mixing with the ambient atmosphere spreads the plume and brings it to rest. Mixing and combustion of the burnable plume species (H_2 , CO) with ambient oxygen produces a radical-rich afterburning region (e.g., O, OH, H) leading to the thermal decomposition of HCl into chlorine. The chlorine mechanism is the main cause of ozone destruction by SRM exhaust. The production of chlorine by afterburning is thus a key step towards ozone destruction and requires careful evaluation of the "hot plume" dynamics and chemistry (Reference 1.4 discusses the afterburning mechanism).

Results of the initial exhaust plume calculation are shown in Figures 3.3 and 3.4. The figures show concentrations of nitric oxide and atomic chlorine as a function of

altitude: from 15 km to 40 km. In addition the plume size is shown. The plume size increases with altitude. This effect results largely from the decrease in ambient pressure with altitude. A corresponding decrease in concentration is estimated with the greater plume diameter and is physically consistent with the plume coming to rest and into (near) dynamic equilibrium with the ambient atmosphere. The levels of chlorine are largely determined by afterburning while the levels of nitric oxide are slightly enhanced by the N_2O_4 dump by the TVC (Thrust Vector Control) with the major contribution from afterburning.

Cold Wake Calculations

The upgraded and validated cold wake code (includes NO, Cl, heterogeneous mechanisms; validated, anchored diffusion model) was applied to analysis of ozone destruction caused by the SRM launch. The initial plume concentrations were those calculated by the hot wake analyses. The eddy diffusivity for the stratosphere was scaled by the relationship described in the previous section ($K = 1.1 \times \text{radius}$: as discussed in Ref. 1.4 and based on stratospheric plume dispersion data from Ref. 2.8). (Additional validation of the present diffusion model was presented in Reference 3.1.) A calculation of the cold wake diffusion and chemical reactions was made for velocities from 15 km to 40 km. The main interest is in the early time diffusion-driven behavior which occurs in tens of minutes after launch (and before ambient ozone diffuses back into the). The radial and centerline species

distributions are shown in Figures 3.5-3.7 are shown for an altitude of 20 kilometers. A ozone hole is formed initially in the "hot plume" and continues to increase in size in the cold wake by diffusion and reaction. The ozone hole increases in size for a few hundred seconds to a radius of approximately 500 to 1000 meters. Ozone backfills (as caused by diffusion processes) into the hole as time passes and at 500 seconds (Figure 3.6) the ozone concentration at the axis has recovered to 50% of the ambient value. The process is controlled by the rate at which plume species diffuse into the ambient atmosphere. The process of ozone loss is controlled by the reaction of ozone with chlorine (with ClO as a product) and the subsequent re-production of chlorine by photo reactions and reactions associated with ClO. It is this cyclic regeneration of Cl that causes the generation of an ozone hole. In an average sense, approximately five to ten ozone molecules are consumed by each original plume chlorine atom during this early time before diffusion fills up the hole. The total loss of ozone is somewhat greater than the size of the hole indicates since the hole begins to fill when the radially-inward diffusion of ozone exceeds the ozone loss.

Results for ozone loss calculations at other altitudes of the stratosphere are shown in Figures 3.8 to 3.12. The centerline values of several species are shown. The time to "fill the axis" with ambient ozone is seen to take between 1000 seconds at 20 km to about 2000 seconds at 40 km. A measure of the plume size (and age) can be made by taking the time when the centerline value is about 25% of the ambient

value and the location where the ozone concentration is approximately 90% of the ambient value. These values are shown in the following table:

Altitude, km	Time, s	Radius, m
15	1400	3000
20	1200	2000
25	1200	2500
30	1500	4000
35	1800	11000
40	2000	7000

The ozone void is seen to be larger and lasts to somewhat longer times at higher altitudes. Contributing factors to these effects are the larger size of the hot plume caused by expansion to lower ambient pressure, more rapid diffusion of the larger plume, and smaller ambient ozone concentrations at high altitude. The decrease in size at 40 km may be caused by the apparent locking up of more chlorine as HCl as shown in Figure 3.4.

The behavior of the cold wake is strongly dependent on turbulent mixing with the atmosphere and is characterized by eddy diffusivity. The effect of uncertainties in

eddy diffusivity can be estimated by calculating the plume growth and chemistry for two diffusivity models within the data range of Figure 2.1. Specifically $b=0.6$ and 1.5 were used to calculate the cold wake at an altitude of 20 km. Centerline species concentrations are shown in Figures 3.13 and 3.14. The time to fill in the ozone hole is seen to range from about 600 seconds (maximum diffusion) to 2000 seconds (minimum diffusion). These last two figures demonstrate the importance of having an accurate representation of the turbulent mixing that drives the dispersion of the cold wake.

4. Liquid Rocket Engine Effects on Stratospheric Ozone

The effects of liquid rocket engines on stratospheric ozone were addressed in Reference 1.2. Two propellant combinations were addressed: LH₂/LOX (720 klb thrust) and RP-1/LOX (810 klb thrust). The loss of ozone was found to “exhibit no deleterious effect on the environment” which translates extremely small ozone loss. The sole mechanism considered was destruction by NO and NO₂ produced by afterburning. The lack of ozone destruction is a result of the lack of NO/NOX in the plume. Afterburning temperatures must be in excess of 2000 K in order to produce appreciable NO/NOX but for liquid systems such a high temperature is not reached by afterburning in the stratosphere.¹ This effect has been discussed in Reference 4.1.

The remaining liquid engine to discuss is one in which NO is produced directly by use of N₂O₄ as an oxidizer. No U.S. launch vehicle uses NTO in the stratosphere but for completeness we are compelled to examine its potential effect.

¹ In contrast, HCl can decompose to form Cl at lower temperatures as indicated by a much lower activation energy. Hence formation of chlorine from HCl by afterburning is an important mechanism for SRMs at stratosphere altitudes.

A hypothetical 2.4 MLb class liquid thruster plume is examined by taking the Titan III cold wake start conditions and turning off the chlorine-related chemistry. The NO/NO₂ concentrations are about those from an MMH/NTO thruster (mole fraction of NO of nearly 10⁻²). The results of the cold wake analysis (at 20 km) are shown in Figures 4.1 to 4.3. An ozone hole is seen to open up but then close down by 400-500 seconds. The "depth" of the hole is not as pronounced as for the SRM wake. The ozone levels in the hole are about 25 to 50% of the ambient value whereas for the SRM the in-the-hole ozone concentrations are several orders of magnitude less than the ambient value. Thus the in-the-hole column density effect of the liquid engine wake is considerably less than that effect caused by an SRM. However in the hole the liquid engine wake does consume 50% of the ozone molecules in the ozone hole that it produces.

5. Post-Launch Depletion of Stratospheric Ozone

The previous sections have discussed depletion of ozone by rocket exhaust at times shortly after the launch. The primary interest for assessment at early time is to assess the opening of a local ozone hole in the wake of a launch thruster. The question of global impact is also an important matter. The ultimate assessment of global impact must be evaluated by application of global transport/chemistry models. Results from one such model will be discussed at the end of this section.

The local ozone hole described in sections 2, 3, and 4 persist for tens of minutes when driven by chemical reactions and turbulent diffusion. The plume-induced species diffuse and ultimately reach concentrations equivalent to the corresponding background levels or, as in the case of chlorine, react to form a stable compound that prevents that SRM-borne chlorine atom from further destruction of ozone and/or precipitates out of the stratosphere. The effects of wind shear can however complicate this process. As an example, the physical process of large scale vertical wind shear (or strain) can act to stretch the plume and to slow the radial growth. This effect could serve to hold the ozone-attacking species concentration to high levels for a longer period of time and allow, by diffusion of ambient ozone to the distorted plume/wake, cause additional loss of ozone. This process of course is

complicated by fluctuations in the wind field which could make the process complex and require statistical treatment. The work of Prather (e.g., Ref. 5.1) presents a thorough discussion of detailed modeling of the effects of wind-induced strain .

An order-of-magnitude assessment of global effects can be built up by first order considerations. First, the early-time local hole driven by the TITAN III is approximately 2000 to 4000 meters radius at altitudes 15 to 30 km (altitude range for maximum ozone concentration). Taking the 4000 m value we get an estimate (geometric) of one in 10 million ozone molecules destroyed shortly after launch for a 2.4 Mlb-class launch vehicle SRM.

The result can be carried out further in time (for a chlorine-containing propellant) by examination of the production/loss rates after diffusion to ambient densities. At this later time chlorine is replenished from ClO by time scales on the order of ten seconds to a few hundred seconds by reaction with ambient species (e.g., NO). However at times of the order of a few hundred seconds chlorine can react to form relatively stable compounds, such as chlorine nitrate. Chlorine nitrate dissociates in approximately 6 hours to form chlorine again. During this time roughly 20 or more ozone molecules per Cl radical can be lost (estimated by examination of characteristic reaction times) to recycled chlorine with 20 or more being lost every six (or so) hours. During a 5 to 10 day period Cl will react with various compounds (e.g., hydrocarbons) to form HCl which is dissociated in approximately one half

year. A 2.4 MLb SRM deposits about 750 kilogram moles of free chlorine (including Cl_2) into the stratosphere per launch resulting in a potential of $(750/2) \times 6 \times 10^{26} \times ((5 \text{ to } 10) \times 24/6) \times 20 = (1.8 \text{ to } 3.6) \times 10^{32}$ ozone molecules lost (assuming half of all the chlorine is freed from HCl during afterburning as indicated by the SPF plume results) in one year as a result of a launch. There are approximately 4×10^{37} ozone molecules in the stratosphere and hence the percent of stratospheric ozone molecules lost per launch (2.4 MLb SRM) per year may be estimated as 0.0005% to 0.001% per year per launch. The exchange time from stratosphere to troposphere is estimated to be of the order of one year. If this time is representative of the time for launch-induced chlorine species to leave the stratosphere then the global impact of one SRM launch would be of the order of 0.0005% to 0.001% destruction of stratospheric ozone.

Global Model Results: Global Effects on Stratospheric Ozone from Titan Rocket

Exhaust: Background

The following discussion is derived from the work performed by LLNL personnel using their 2-D global model. For more detailed description of the model and discussion of the results, the companion report provided by LLNL is recommended. Depletion of ozone in the stratosphere has been linked to the release of man-made chlorofluorocarbon (CFC) transported into the stratosphere and subsequently photodissociated into active chlorine that destroy ozone through the chlorine catalytic cycle. The launch of Titan rockets and similar solid rocket motors by the

Air Force, which generate large amount of chlorine-containing exhaust species such as HCl, Cl and Cl_2 directly into the stratosphere certainly add to the burden of current stratospheric chlorine. The purpose of this section is to quantify the chlorine release by Titan-type rocket motors and determine the potential global impact on the stratospheric ozone in a global steady state. In addition, the transport of the exhaust plume in the stratosphere and the impact area on the ground arriving from the direct line-of-sight of the sun and the plume were examined.

The launch scenario considered here consists of 10 Titan launches (with two SRMs firing simultaneously) per year which translates into approximately 378,000 kg of chlorine injection into the stratosphere. The launches were assumed to take place at Cape Canaveral located at 28°N latitude and 280°E longitude. The chlorine from these launches are used as a stratospheric source of Cl_y and is assumed to be in the form of HCl for global calculations using Lawrence Livermore National Laboratory (LLNL) 2-D model (Ref. 5.2). In these global calculations, analysis were performed for several modeling years until a steady state in which the Cl_y injection is balanced by that transported into the lower troposphere is obtained. Results reported here represent global steady state solutions illustrated in different months of a year. The calculation domain in all the following analyses is limited between the ground and at a altitude of 85 km in the atmosphere. The boundary conditions required for

the solution of the 2-D model transport equations are a set of specified species concentrations in ground level and zero flux at the upper atmosphere.

For the cold plume transport analyses, LLNL Grantour Model (refer to the companion report by LLNL, Ref. 5.2), a global model that treats the dispersion of pollutants and their chemical interaction in the atmosphere was used (although the chemistry part was not exercised here). The model calculates the advection of plume parcels by using stratospheric wind field data supplied by the Goddard Data Assimilation Office. These wind data have a resolution of 4x5 degrees in the horizontal, and approximately 3 km in the vertical and 6 hours in time. In the following calculations, *ozone in the stabilized plume is assumed to be completely depleted*. Cold plume initial conditions consist of species concentrations and plume size of the Titan exhaust as a function of vehicle altitude (presented in previous sections). The method of obtaining these conditions had been described previously by Denison et al. (Ref. 1.4). The amount of chlorine injected is determined by the time for the Titan to travel through the stratosphere, which in turn depends on the pitch profile adopted in the analysis. In the trajectory calculation the flight path angle is set to zero initially and increases by 1 degree per second at 62 seconds after launch (roughly at altitude 10 km) until it reaches 45 degrees to stay. Based on this trajectory profile it takes approximately 40 seconds to travel through the stratosphere.

Results: Global Effects

The calculated steady state Cl_y enhancement (in ppt) defined as the perturbed chlorine relative to the reference atmosphere of total inorganic chlorine, is presented in Figures 5.1-5.2 for January and July respectively, using the LLNL 2-D model. The reference atmosphere was assumed to contain natural and anthropogenic Cl_y at a background level of 3500 ppt. In general, the enhancement is the largest in the vicinity and north of the launch site, in the upper stratosphere, consistent with the prevailing northward zonally averaged meridional circulation. In January, an enhancement of 5 ppt is seen to spread over a range of 40 degrees in latitude corresponding to approximately 4000 km. In July, however, Cl_y is enhanced more than in January in the area of launch site by 2 ppt due to weaker summer circulation which tends to confine the exhaust emissions to a smaller region. In the lower stratosphere, the Cl_y enhancement is less, about 1 ppt at 20 km. In steady state, which takes about 2.6 model years, Cl_y enhancement is seen to have spread to the southern hemisphere. The level of enhancement is typical smaller than in the northern hemisphere, by about 3 ppt at launch site.

Figures 5.3-5.4 show the results of local % ozone change due to continuous Titan launches at 10 per year (after ozone change due to CFCs is subtracted out). During the winter, the calculations show northward transport and mixing between 30°N and the North Pole leading to larger ozone depletion in this region than in other region of the northern hemisphere. In the same time, the model shows southward

mixing and transport between 30°S and the South pole leading to larger ozone depletion although the level of destruction is typically smaller than its northern counterpart by a factor of 2. During the summer, the transport and mixing both in the northern and southern hemisphere are somewhat similar. As illustrated in Figure 5.4 the largest ozone depletion region is between 30°N and the North Pole, and 30°S and the South Pole. In both winter and summer, the largest ozone destruction occurs in the upper stratosphere between 30 to 60 km, corresponding to large Cl_y enhancement in the same region.

Ozone destruction caused by Titan rocket launches peaks about 0.06% at 60°N, and 0.03% at 60°S. In mid-latitudes, the destruction is smaller typically at .01% or less. It is interesting to note that in view of small perturbations in chlorine injection, these results calculated by using detailed global model can be linearly scaled according to the amount of injection. The work reported by Prather et al. (Ref. 5.3) in assessing the Space Shuttle impact on stratospheric ozone has concluded that at an injection rate of 725,000 kg of chlorine per year, the largest ozone depletion was found to be 0.10% in steady state. Their analysis was performed using a variety of 2-D and 3-D global models. In the current analysis, however, Titan exhaust was assumed to deposit 400,000 kg of chlorine in the stratosphere, which by using linear scaling, the global ozone should be on the order of .055%. Of course, this value is essentially the same as that predicted by using the LLNL 2-D model, thus

confirming the linear scaling law under small chlorine perturbation proposed in a TRW internal report (Ref. 5.4).

Results: Cold Plume Transport

Plume transport is largely determined by the seasonal changes in the stratospheric winds in magnitudes and directions, and the launch trajectory azimuth. The plume will be transported differently even at the same time of the year due to the significant variances in the stratospheric winds. As noted in Ref. 5.5 from the wind profile data derived from the NASA/AF Range Reference Atmosphere, as well as wind profiles from Handbook Geophysics 1985 (Ref. 5.6), the mean zonal wind is typically a factor of 2 of the zonal variance and the meridional wind is the same order as its variance. As seen in Figures 5.5-5.6 (taken from Handbook Geophysics 1985 for Wallops Island 38°N--Ref. 5.5) the mean direction and magnitude of the stratospheric wind is from the west in the northern winter and is from the east in the summer. In general, the wind speed increases with altitudes. Furthermore, the zonal wind speed exceeds that of meridional wind by a factor of 4. While eddy diffusive mixing would erode and expand the plume, the horizontal shearing over the first several hours is dominant, leading to significant attenuation in the vertical plane normal to the plume segments. However, plume diffusive processes were not included in these calculations.

In all the following plume transport calculations the plume is divided into 8 vertical segments arranged in different altitudes in the stratosphere. The location of the plume is illustrated in terms of projected location on ground through the line of sight of the sun and the plume. The computed plume location 2 hours after launch in Cape Canaveral at 6 A.M. in the winter is shown on Figure 5.7. Due to the prevailing wind from the west and from the south, the plume segments are seen to have moved from the launch site (designated as a square box in the figure) diagonally to the north east direction. The plume segments in the upper stratosphere are stretched to larger extent than those in the lower stratosphere due to the increase in wind speed in upper atmosphere. In 2 hours, the plume had moved approximately 100 km latitudinal and 200 km longitudinal directions. Similar plume behaviors are seen in Figures 5.8-5.9 which show the migration of the plume at 4 and 9 hours after launch. Interestingly, due to low wind speed in the lower stratosphere, the remnant of the plume in this region stayed on even 9 hours after launch. This means that locations within the projected area of the plume above will be exposed to atmospheres somewhat depleted in ozone for a long period of time. The extent of this affected area and the level of ozone depletion at times of 2, 4 and 9 hours after launch are shown in Figures 5.10-5.12. To be conservative, all ozone molecules in the regions occupied by the plume are assumed to be completely consumed: infinite rate chemistry is implied. As expected the affected area increases with time and the percentage of ozone loss decreases with time. In the worst case, an area of 20 km^2 , probably directly below the plume in the

vicinity of the launch site the level of ozone destruction is 0.15% in the 2 hours after launch. After 9 hours, the level of depletion is roughly reduced by a half to 0.075% over an area of 60 km².

The computed plume transport for July are shown in Figures 5.13-5.15 at 2, 4 and 9 hours after launch. Clearly in 2 hours after launch, the plume had moved from the source point to the west consistent with the prevailing direction of the zonal wind which is from the east. The magnitude of the meridional wind is small compared with the zonal wind by an average factor of 20, as demonstrated by relatively small movement in the meridional direction. This behavior carries over to large time plume transport at 9 hours after launch. Again the plume segments in upper stratosphere were stretched more than those in the lower atmosphere because of much larger wind speed in the upper atmosphere. In 2 hours, the plume is seen to have moved by 200 km longitudinally, and essentially 0 km latitudinally. A comparison between the winter and summer figures appears to show that in winter launches, the plume tend to linger in the vicinity of the launch site for a long time while in the summer launches, the closest plume segment to the launch site had migrated 200 km to the west. If this model prediction is true, it certainly implies that in the vicinity of the launch site, summer launches may be more benign than the winter launches in terms of ozone depletion.

Figures 5.16-5.18 show the level of ozone depletion in the direct line-of-sight from the sun. Due to overlapping of different plume segments in the direction of the sun light, the extent of diminishing ozone along the line-of-sight is seen to be generally higher than in the winter launches. At 2 hours after launch the ozone loss is about 0.25% with affected area of about 10 km². After 9 hours, the affected area had increased to 1000 km² at an ozone depletion level about half that in earlier times.

Concluding Remarks

Based on the scenario of 10 Titan launches per year the analysis results showed that global stratospheric ozone was perturbed only slightly, probably within the range of seasonal variations. In earlier times after the launch, the level of ozone column density loss is about 0.25% over an area of 20 km² after 2 hours, and after 9 hours, the plume size had increased and the influenced area is increased to about 70 km² at approximately 0.1%. From a global steady state standpoint, the effect is larger in the Pole regions and relatively small in other areas. In the north pole region, the loss peaks at about 0.06% while the rest of the globe has a loss of about 0.01%. Because of the assumption of complete ozone loss within the stabilized plume, the "line of sight" ozone depletion calculated here represents a conservative or worst case assessment. Consideration of plume diffusion would increase the area of the surface plume footprint, but would probably not increase the ozone loss in the direct beam.

6. Summary and Recommendations

Based on the calculations in the previous chapters, we are in a position to recommend specific parameters for the HiRoig Sensor. The initial design configuration of a sensor that will measure backscattered solar ultraviolet radiation in the launch corridor is affirmed. The instrument will be required to measure ozone (a strong UV absorber) as well as other UV absorbing species such as Cl_2 and ClO . This report has shown that these species are the primary species of interest. A spectral resolution of 2 nanometers is required to obtain an altitude profile of ozone depletion with a spatial resolution of 3 to 5 kilometers. The sensor should operate in the "push broom" mode in order to track a plume that may begin to disperse quickly (minutes to several hours), due to stratospheric wind shears.

Based on the results of this study, TRW concurs with USAF initial specifications for the focal plane detector (CCD) which measures a 100 point spectrum in each of 100 pixels. The instantaneous field of view of 1 kilometer (in-track) by 100 km (cross-track) when the sensor is pointed toward nadir should provide the field of view required, based on the TRW modeling study.

Methodology for calculation of ozone depletion caused by rocket launches has been upgraded and applied to several systems. The chemical kinetics were upgraded and the dispersion model was validated by comparison with data.

The upgraded methodology was applied to several launch scenarios. Estimates were made on both the local ozone hole and the longer time estimates of global effects. Correct specification of the diffusion coefficient was shown to be a key to proper characterization of the local ozone hole.

The primary global impact is caused by SRM's for the following reasons:

- 1) SRM's are the current boosters of choice for all U.S. systems;
- 2) the liquid first stages that operate in the stratosphere are neither nitrogen nor chlorine-based systems;
- 3) production of NO_x, an ozone depletion agent, in the afterburning region from LOX/H₂ and LOX/RP-1 systems is relatively small in the stratosphere.

The local hole produced by a single SRM launch is approximately 2 km-4 km radius and persists for a few thousand seconds after which it fills in by diffusion. The long term global impact of a single 2.4 million pound SRM in steady state is estimated to be approximately 0.001% to .006% per year reduction of stratospheric ozone. Plume transport takes place in the upper stratosphere on a level much larger than in the lower stratosphere as a result of strong stratospheric winds. The plume tends to

remain in the neighborhood of the launch site for as long as 9-10 hours with about 70% recovery from the initial ozone depletion.

Future Work

Three additional tasks are recommended to finalize our assessment of the impact of launch vehicle exhaust on ozone:

- 1) An assessment of the effects of stratospheric wind currents on the kinematics/diffusion/reaction of the exhaust wake. A direct approach is to add the convection terms to the TRW diffusion model so that wind shear effects can be included. The methodology of Prather (Ref. 5.1) would be used to extend results from the extended TRW model to longer times;
- 2) An assessment of the effects of multiple engines (e.g., the two strap-on configuration of TITAN III and IV). The interaction of the exhaust plumes will cause regions of sharply increased temperature and density and lead to larger concentrations of atomic chlorine and nitric oxide and thus cause greater impact on stratospheric ozone;
- 3) A compilation of projections for all classes of U.S. boosters in order to support estimates of the effect of various launch scenarios on stratospheric ozone.

7. References

- 1.1 "The impact of Deorbiting Space Debris on Stratospheric Ozone," P. D. Lohn, E. Y. Wong, M. J. Molina, M. R. Denison, J. J. Lamb, Prepared by TRW for Space and Missile Systems Center, May 31, 1994.
- 1.2 "Utilization of Alternate Propellants to Reduce Stratospheric Ozone Depletion," Prepared by TRW for Space Defense and Missile Systems Center, May 31, 1994.
- 1.3 "System Requirements Review for the High-Resolution Ozone Imager (HIROIG)," D.L.McKenzie et.al., Aerospace Report No. TR-93(3231)-2, Sep. 15, 1993.
- 1.4 "Solid Rocket Exhaust in the Stratosphere: Plume Diffusion and Chemical Reactions," M. R. Denison, J. L. Lamb, W. D. Bjorndahl, E. Y. Wong, P. D. Lohn; Journal of Spacecraft & Rockets, v31,n3, pages 435-442, May-June 1994.
- 2.1 "Chemical Kinetics and Photochemical Data for Use in Stratospheric Modeling," W.B. DeMore et al, JPL Publication 90-1, January 1, 1990.
- 2.2 "Evaluated Kinetic and Photochemical data for Atmospheric Chemistry: Supplement III," Journal of Physical Chemical Reference Data, v18,n2, 1989, p. 881.

- 2.3 Aeronomy of the Middle Atmosphere, 2nd ed., D. Reidel Pub., 1986.
- 2.4 Anon., "Scientific Assessment of Stratospheric Ozone: 1989," World Meteorological Organization, global Ozone research and Monitoring Project, Rept. 20, Geneva, Switzerland.
- 2.5 "Stratospheric Chemistry of Aluminum Oxide Particles," M. J. Molina et al, Report to TRW, June 1994.
- 2.6 "The Production of Nitric Oxide in the Troposphere as a Result of Solid-Rocket-Motor Afterburning," R. B. Stewart and R. I. Gomberg, NASA TN D-8137, 1976.
- 2.7 Private communication with Donald G. Crawford, Crawford Aviation, Torrance CA., 1995.
- 2.8 "Aircraft Wake Microscale Phenomena," The Stratosphere Perturbed by Propulsion Effects, Climatic Impact Assessment Program, U.S Dept. of Transportation, CIAP Monogram, 3, Washington, DC, Sept. 1975, Chap.2, pp 60-73.
- 2.9 "Scale-Dependent Diffusion," J.J. Watson, Applied Meteorology, v12, n3, April 1973, pp. 547-549.
- 2.10 "Temporal Changes in the Horizontal Diffusion Parameter of a Single Nuclear Debris Cloud," D. Randerson, J. Appl. Meteor. v11, 1972.
- 2.11 "Diffusion by Continuous Movements," G.I. Taylor, Proc. London Math. Soc. A20, pages 196-212, 1921.

- 3.1 "Characteristics of Alumina Particles from Solid Rocket Motor Exhaust in the Stratosphere," E.J. Beiting, Aerospace Corp. Report No. TR-95(5231)-8, Sep. 1996.
- 4.1 "Computer Model Calculations of NO_x Production in Rocket Motors and Plumes," P.F. Zittel, Aerospace Corp. Report No. TOR-96(1306)-1, Nov. 1995.
- 5.1 "Global Impact of the Antarctic Ozone Hole: Chemical Propagation," M. Prather and A.H. Jaffe, *J. Geophysical Res.*, **v95,nD4**, pages 3473-3492, March, 1990.
- 5.2 LLNL Report, 1996.
- 5.3 "The Space Shuttle's Impact on the Stratosphere," *J. Geophysical Res.*, **v95,nD11**, pages 11583-18590, October 1990.
- 5.4 "Global Estimate of the Impact on Stratospheric Ozone due to Deorbiting Space Debris," E.Y. Wong, TRW Interoffice Correspondence, April 26, 1995.
- 5.5 "Local Effects of Solid Rocket Motor Exhaust on Stratospheric Ozone," M. Ross, *J. Spacecraft and Rockets*, **v.3,n1**, pages 144-153, Jan.-Feb. 1996.
- 5.6 Handbook of Geophysics and the Space Environment, ed. A.S. Jursa, Chapter 17, 1985.

Appendix I

Cold Wake Reactions and Rates: Arrhenius form; cm³/molecule-s.

Reaction	A	E/R(K)	n
S+HCl→HCl.S	a		
HCl.S+ClONO ₂ →Cl ₂ +HNO ₃ .S	a		
Cl ₂ +hν→Cl+Cl	3.0E-3		
Cl+O ₃ →ClO+O ₂	2.9E-11		
ClO+O→Cl+O ₂	3.0E-11		
ClO+HO ₂ →HOCl+O ₂	4.8E-13	-700	
OH+O ₃ →HO ₂ +O ₂	1.6E-12	940	
HOCl+hν→OH+Cl	5.0E-4		
NO+O ₃ →NO ₃ +O ₂	2.0E-12	1400	
ClONO ₂ +hν→NO ₃ +Cl	5.0E-5		
NO ₃ +hν→NO+O ₂	2.0E-2		
Cl ₂ O ₂ +M→ClO+ClO+M	1.0E-3		
Cl ₂ O ₂ +hν→2Cl+O ₂	1.E-3		
OH+CO→CO ₂ +H	7.3E-18	-373	1.5
ClO+NO→Cl+NO ₂	6.4E-12	-290	
ClO+NO ₂ +M→ClONO ₂ +M	4.65E-23	-3.4	
ClO+ClO+M→Cl ₂ O ₂ +M	1.45E-23	-3.6	
H+O ₂ +M→HO ₂ +M	5.7E-321.6		
OH+O→H+O ₂	2.2E-11	-120	
OH+H ₂ →H ₂ O+H	5.5E-12	2000	
OH+OH→H ₂ O+O	4.2E-12	240	
OH+OH+M→H ₂ O ₂ +M	6.9E-31	0.8	
OH+HO ₂ →H ₂ O+O ₂	4.8E-11	-250	
OH+H ₂ O ₂ →H ₂ O+HO ₂	2.9E-12	160	
HO ₂ +O→OH+O ₂	3.0E-11	-200	
HO ₂ +H→OH+OH	8.1E-11		
HO ₂ +H→H ₂ +O ₂	8.8E-12		
HO ₂ +HO ₂ →H ₂ O ₂ +O ₂	2.3E-13	-600	
H ₂ O ₂ +O→OH+HO ₂	1.4E-12	2000	
N+O ₂ →NO+O	1.5E-11	3600	
N+NO→N ₂ +O	3.4E-11		
NO+O+M→NO ₂ +M	9.0E-32	1.5	

Reaction	A	E/R(K)	n
NO+HO ₂ →NO ₂ +OH	3.7E-12	-240	
NO+NO ₃ →NO ₂ +NO ₂	1.7E-11	-150	
NO ₂ +O→NO+O ₂	6.5E-12	-120	
NO ₂ +O+M→NO ₃ +M	9.0E-32	2	
NO ₂ +OH+M→HNO ₃ +M	2.6E-30	3.2	
NO ₂ +NO ₃ +M→N ₂ O ₅ +M	2.2E-30	4.3	
NO ₃ +O→NO ₂ +O ₂	1.0E-11		
O+O ₂ +M→O ₃ +M	6.0E-34	2.3	
O+O ₃ →O ₂ +O ₂	8.0E-12	2060	
H+O ₃ →OH+O ₂	1.4E-10	470	
NO ₂ +O ₃ →NO ₃ +O ₂	1.2E-13	2450	
OH+HNO ₃ →H ₂ O+NO ₃	7.2E-15	-785	
SO+O ₂ →SO ₂ +O	2.6E-13	2400	
SO+O ₃ →SO ₂ +O ₂	3.6E-12	1100	
SO ₂ +OH+M→HSO ₃ +M	3.0E-31	3.3	
HSO ₃ +O ₂ →HO ₂ +SO ₃	4.0E-13		
SO+NO ₂ →SO ₂ +NO	1.4E-11		
SO+OH→SO ₂ +H	8.6E-11		
SO ₂ +O+M→SO ₃ +M	4.0E-32	-2000	
H ₂ O ₂ +hν→OH+OH	1.6E-05		
N ₂ O ₅ +hν→NO ₃ +NO ₂	5.0E-04		
NO ₂ +hν→NO+O	8.0E-03		
HNO ₃ +hν→OH+NO ₂	1.6E-05		

a: Reaction rate expression derived from collision theory. Probability calculated from Reference 2.5. S is some surface area available for heterogeneous reaction.

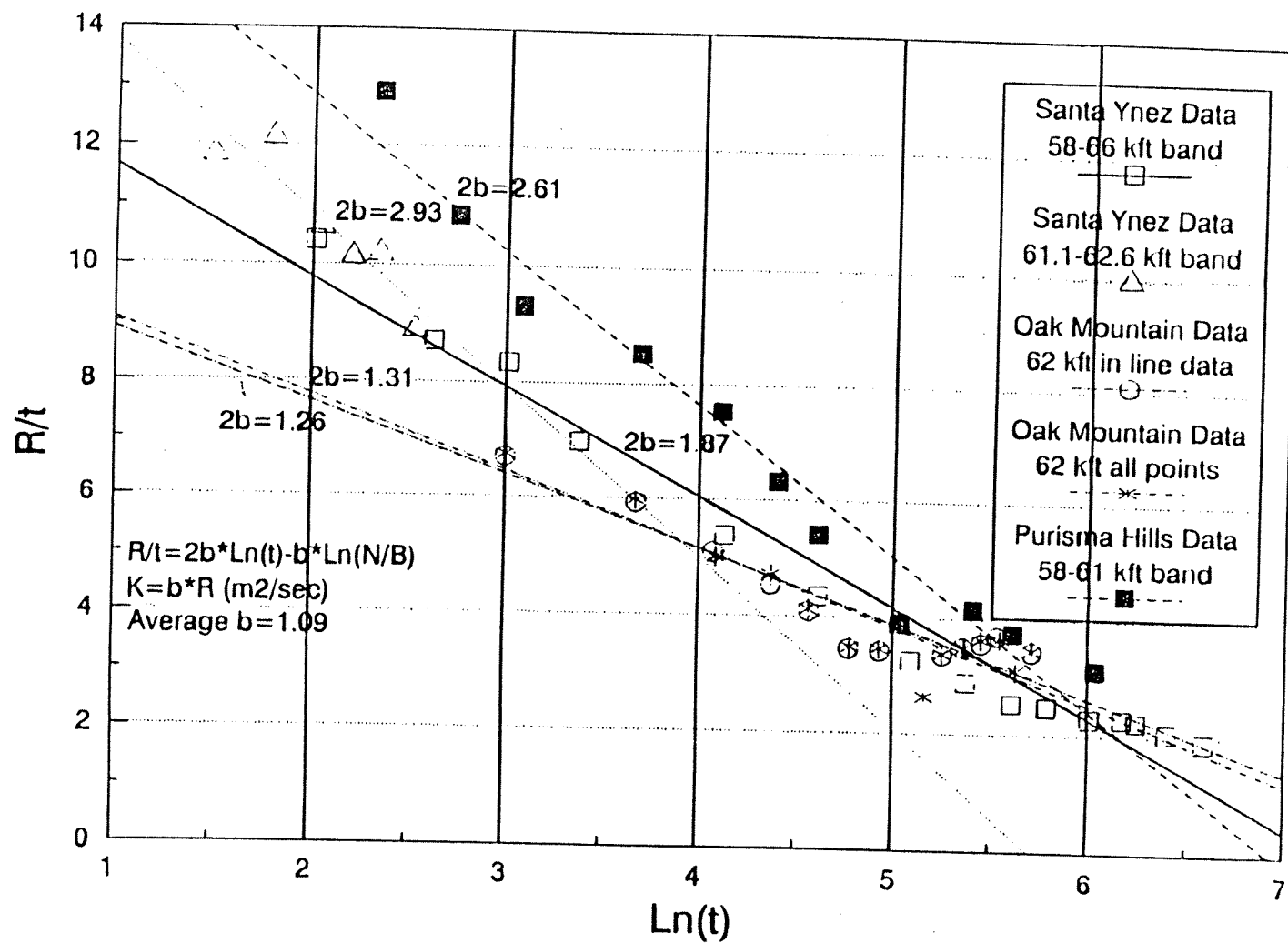
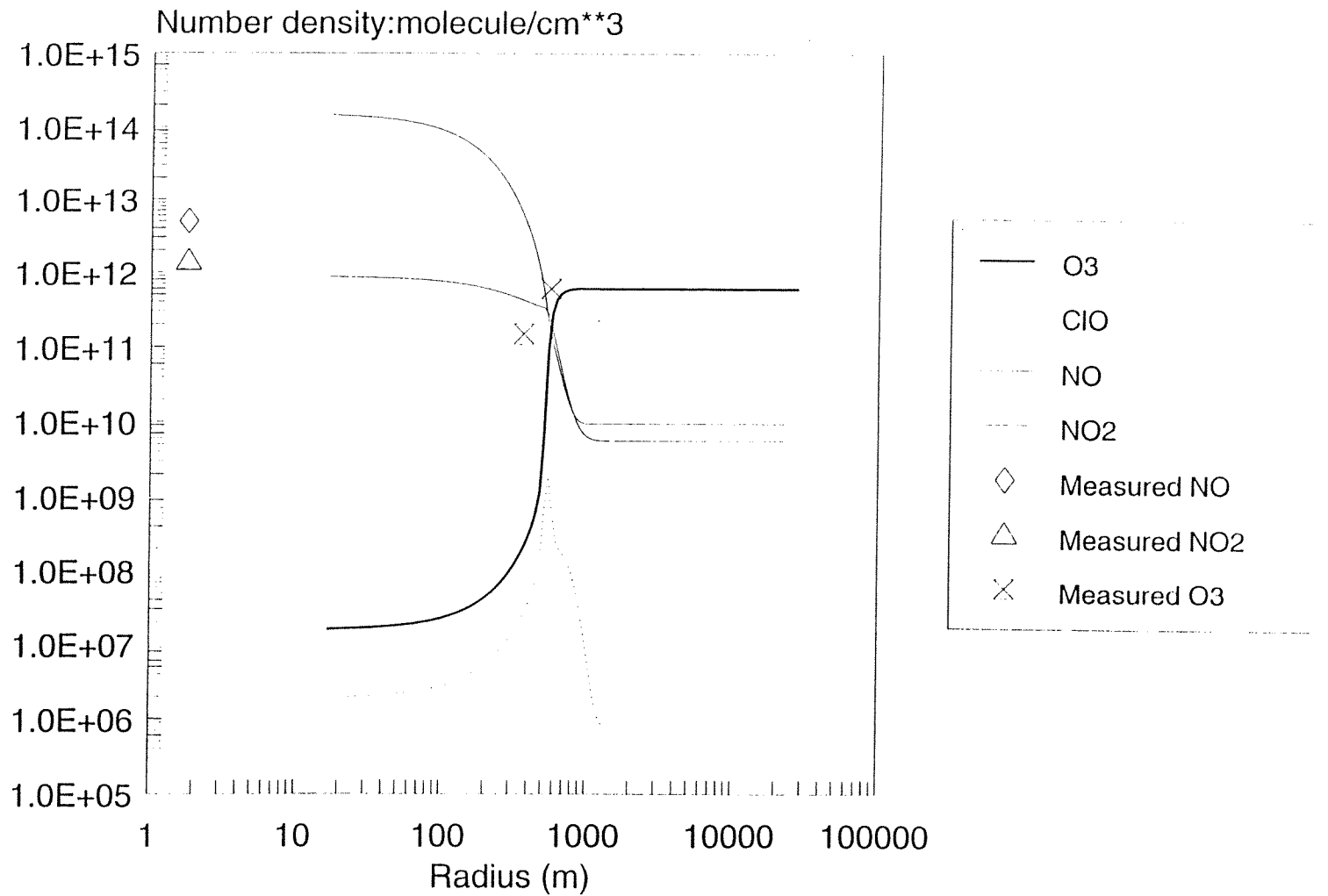


Figure 2.1. Eddy diffusion fit to rocket plume growth data assuming variable diffusivity $[N = B \exp(-r/bt)/t^2]$.

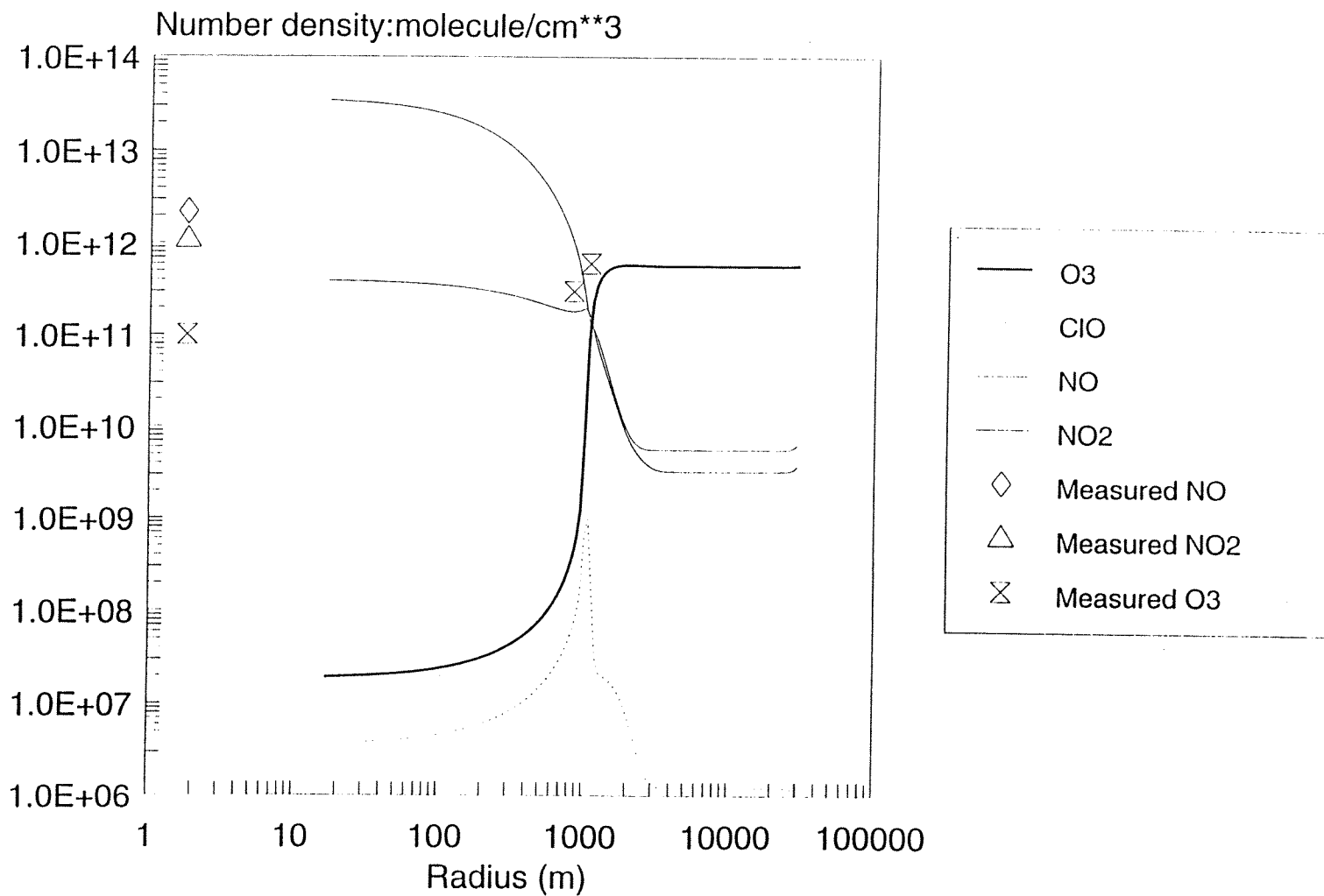
Radial Species Profile at 300s (Titan IIIC-SRM, 7km)



akt20;tcv spf

Figure 2.2.

Radial Species Profile at 1643s (Titan IIIC-SRM, 7km)



akt20;tcv spf

Figure 2.3.

Radial Species Profile at 2424s (Titan IIIC-SRM, 7km)

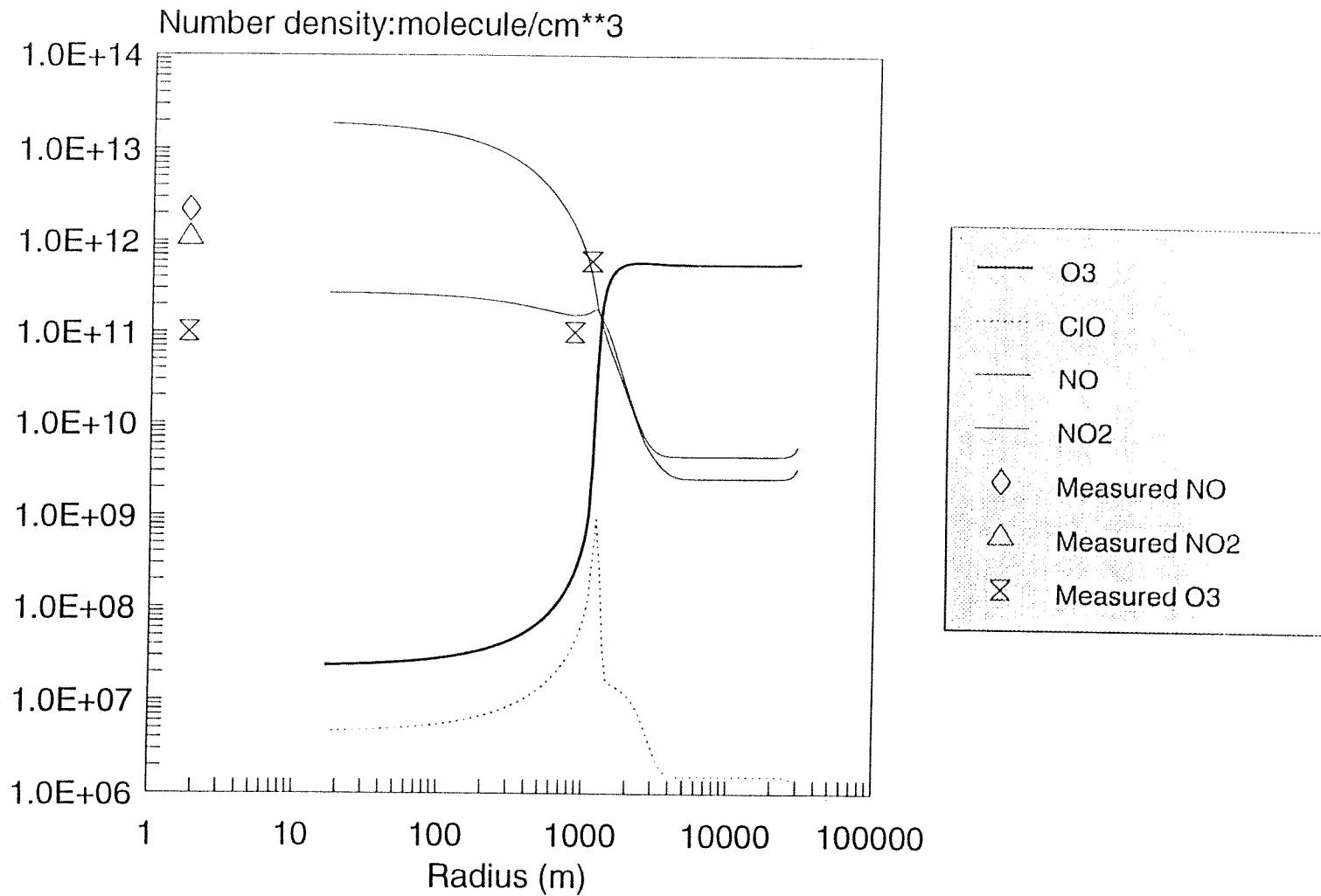
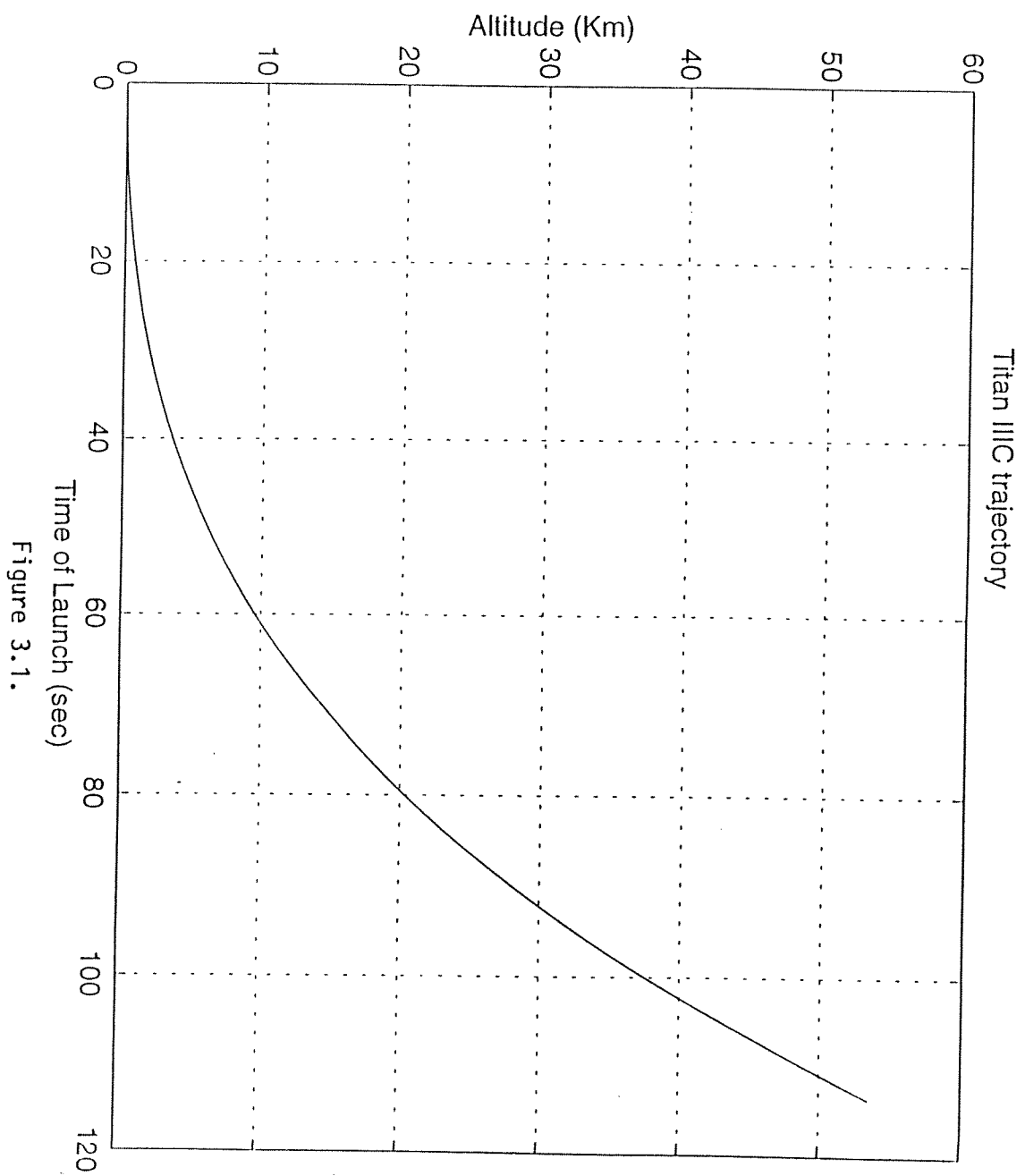


Figure 2.4.



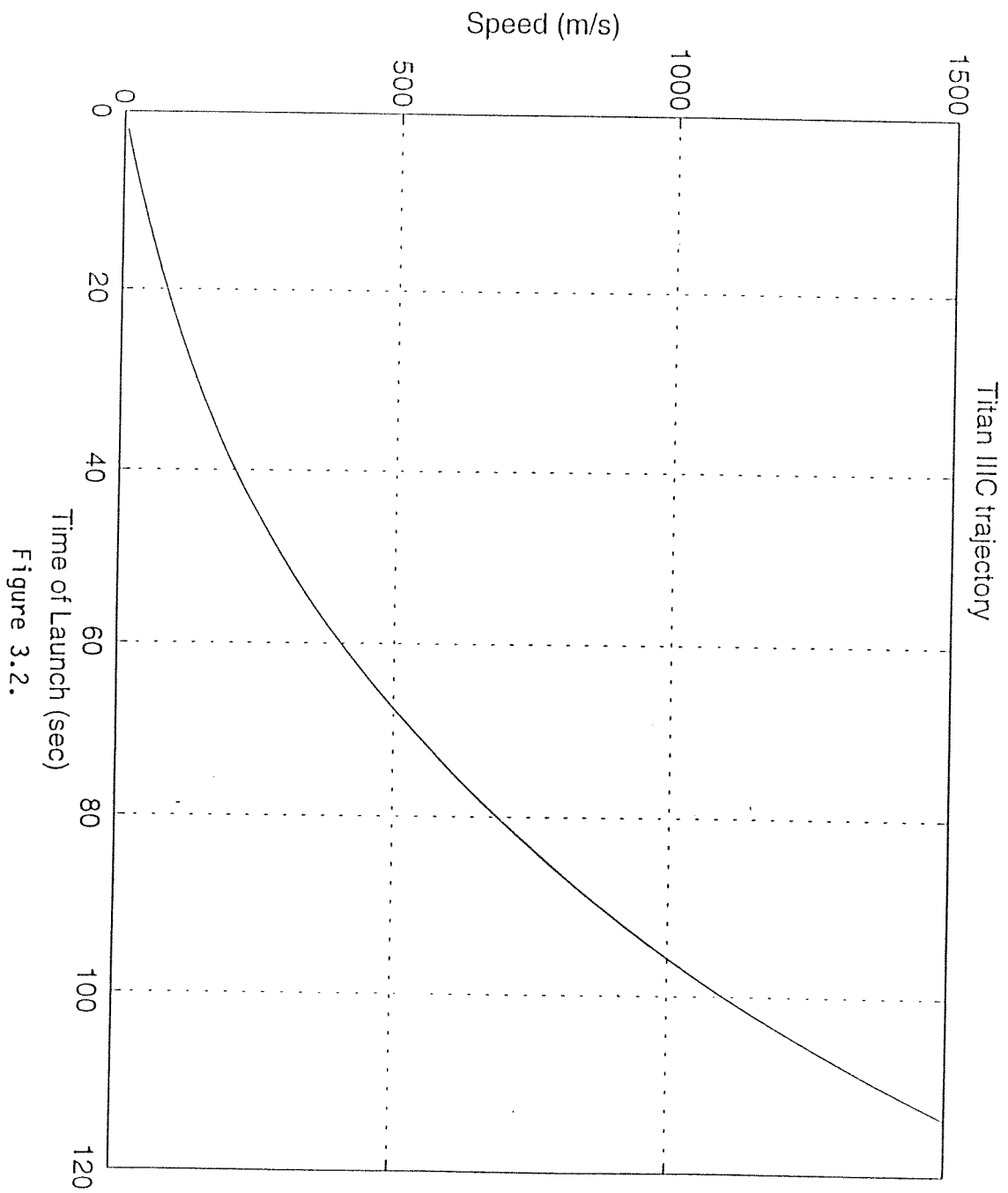


Figure 3.2.

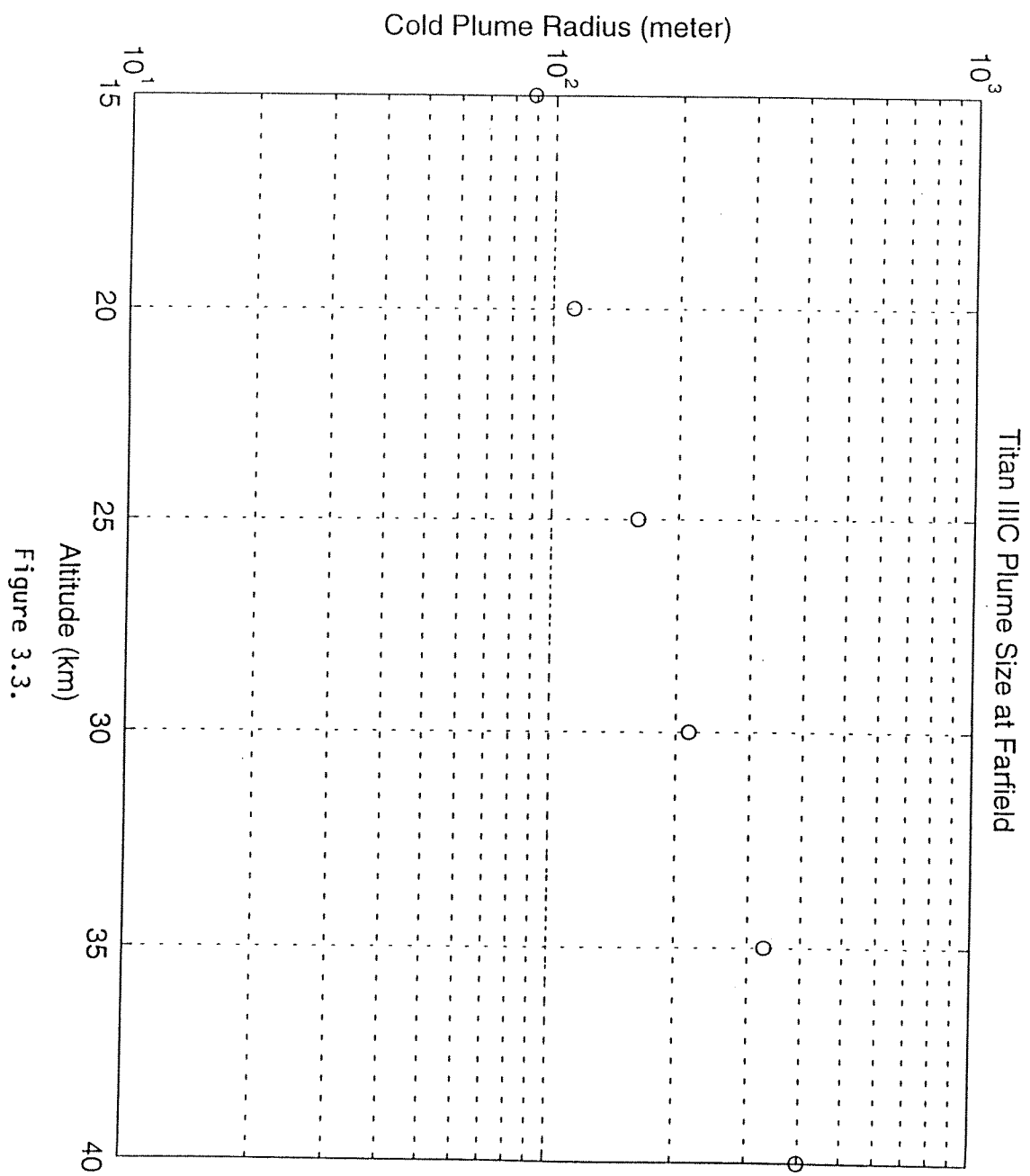


Figure 3.3.

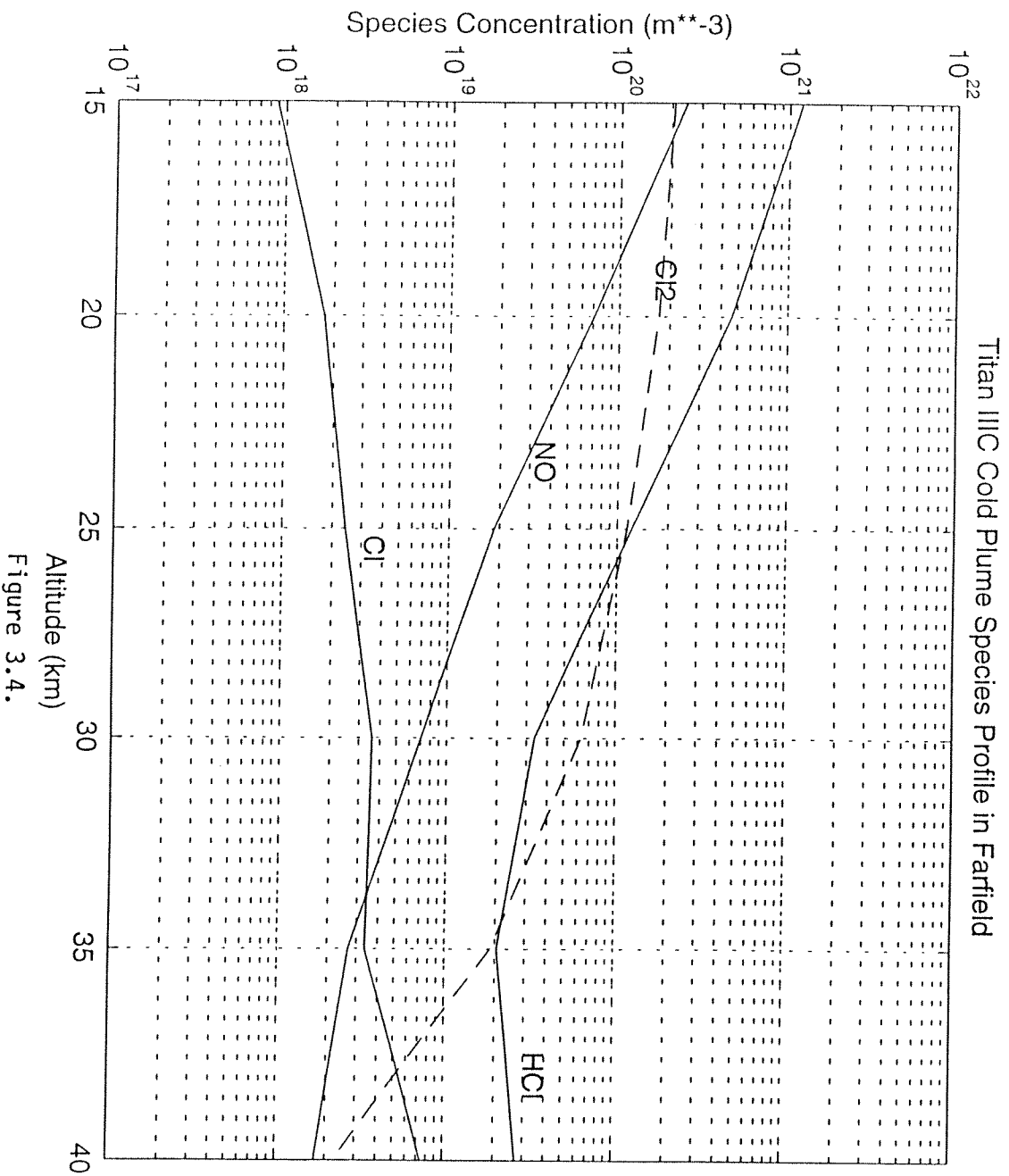


Figure 3.4.

Axial Species Profile (Titan IIIC-SRM 15km)

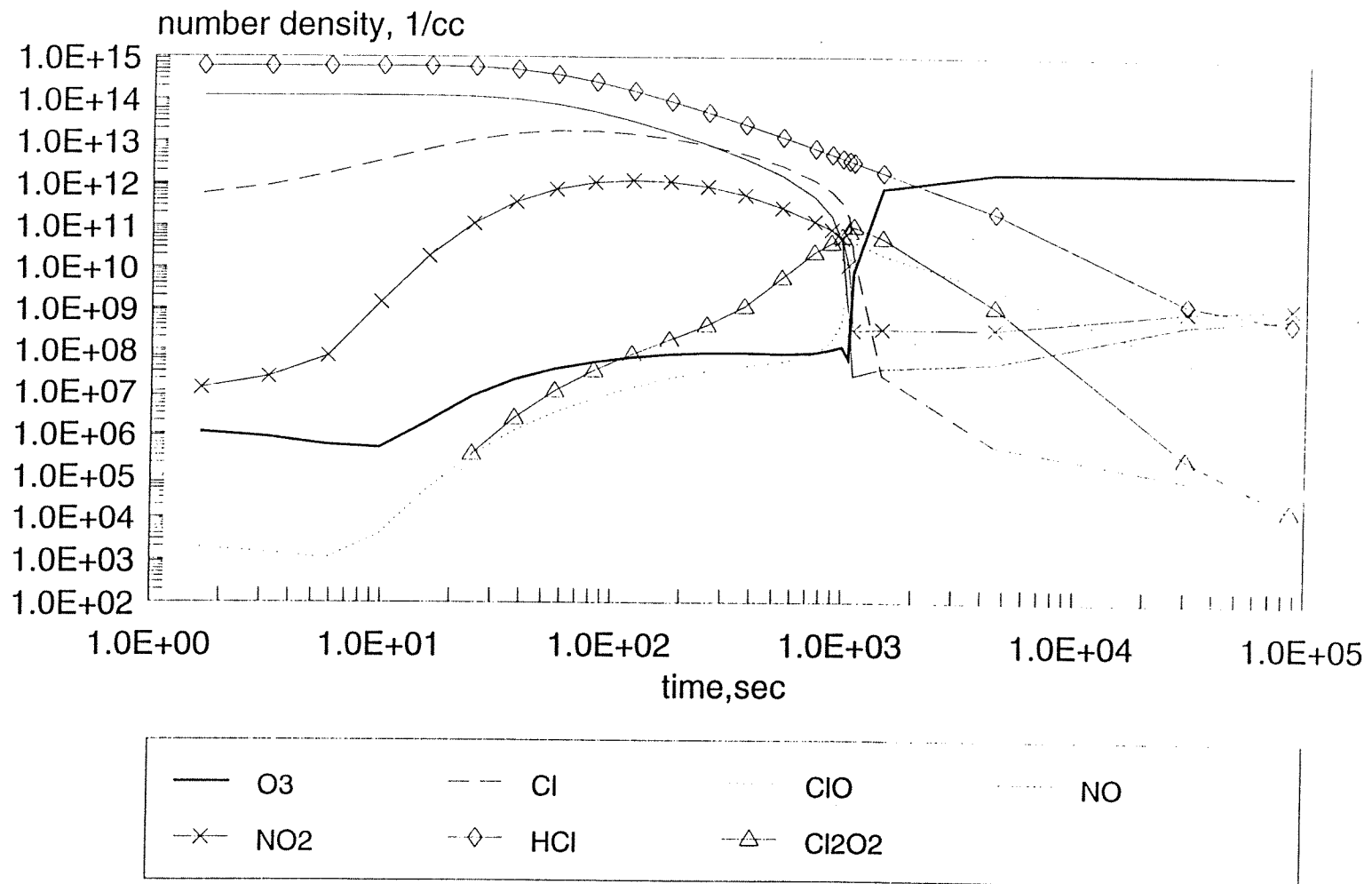


Figure 3.5.

Axial Species Profile (Titan IIIC-SRM 20km)

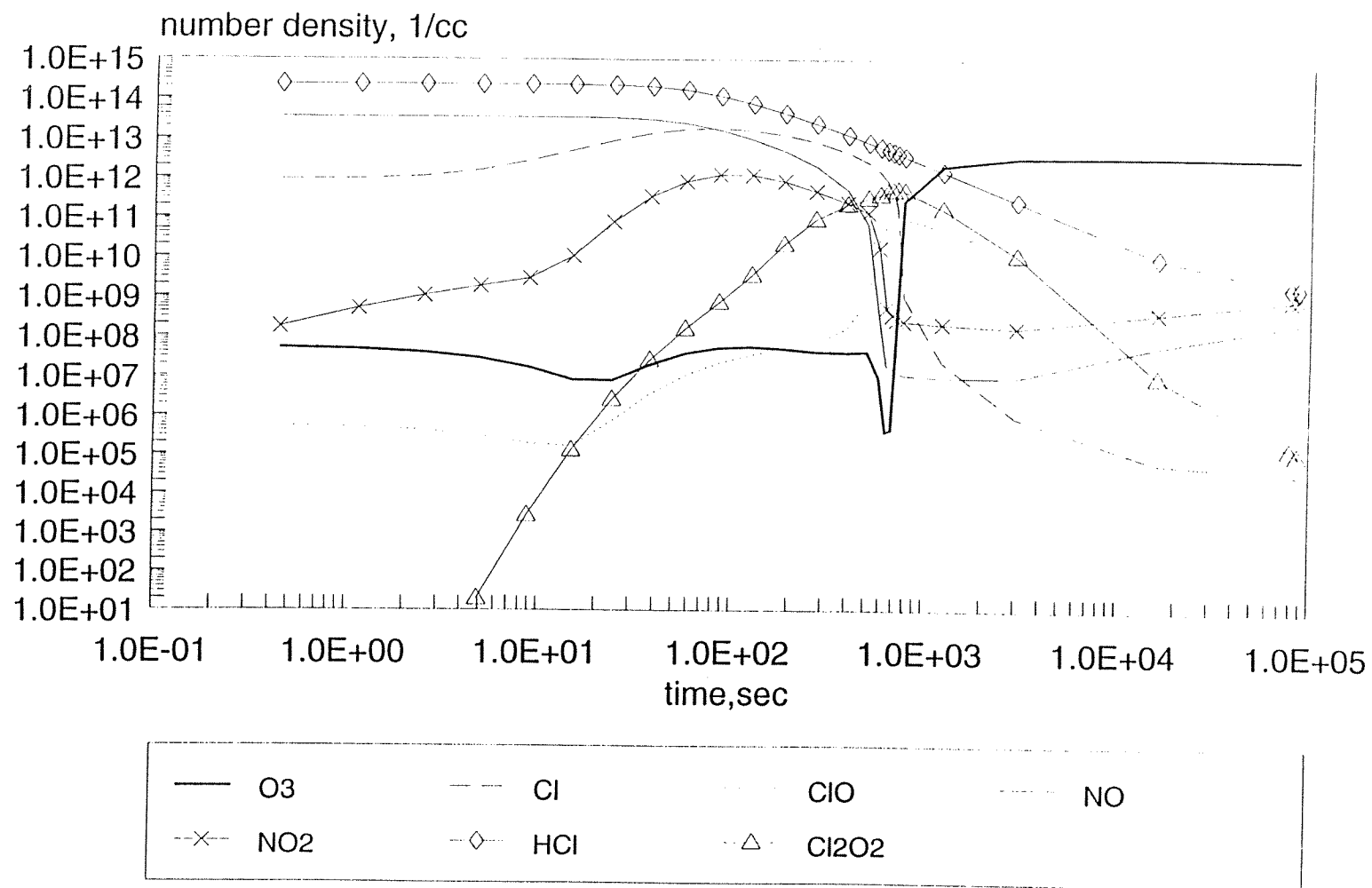


Figure 3.6.

Radial Species Profile at 125s (Titan IIIC-SRM, 20km)

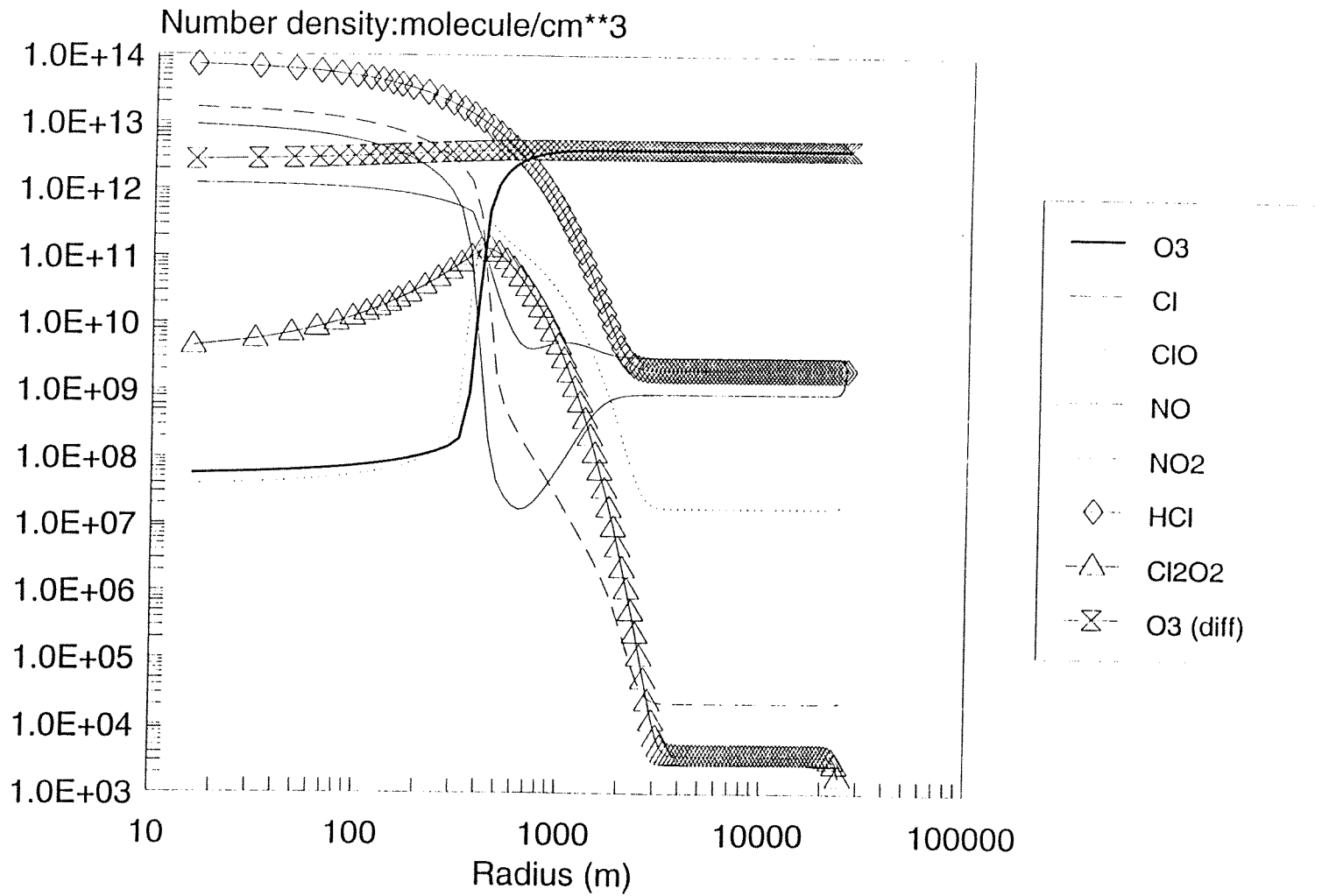


Figure 3.7.

Radial Species Profile at 500s (Titan IIC-SRM, 20km)

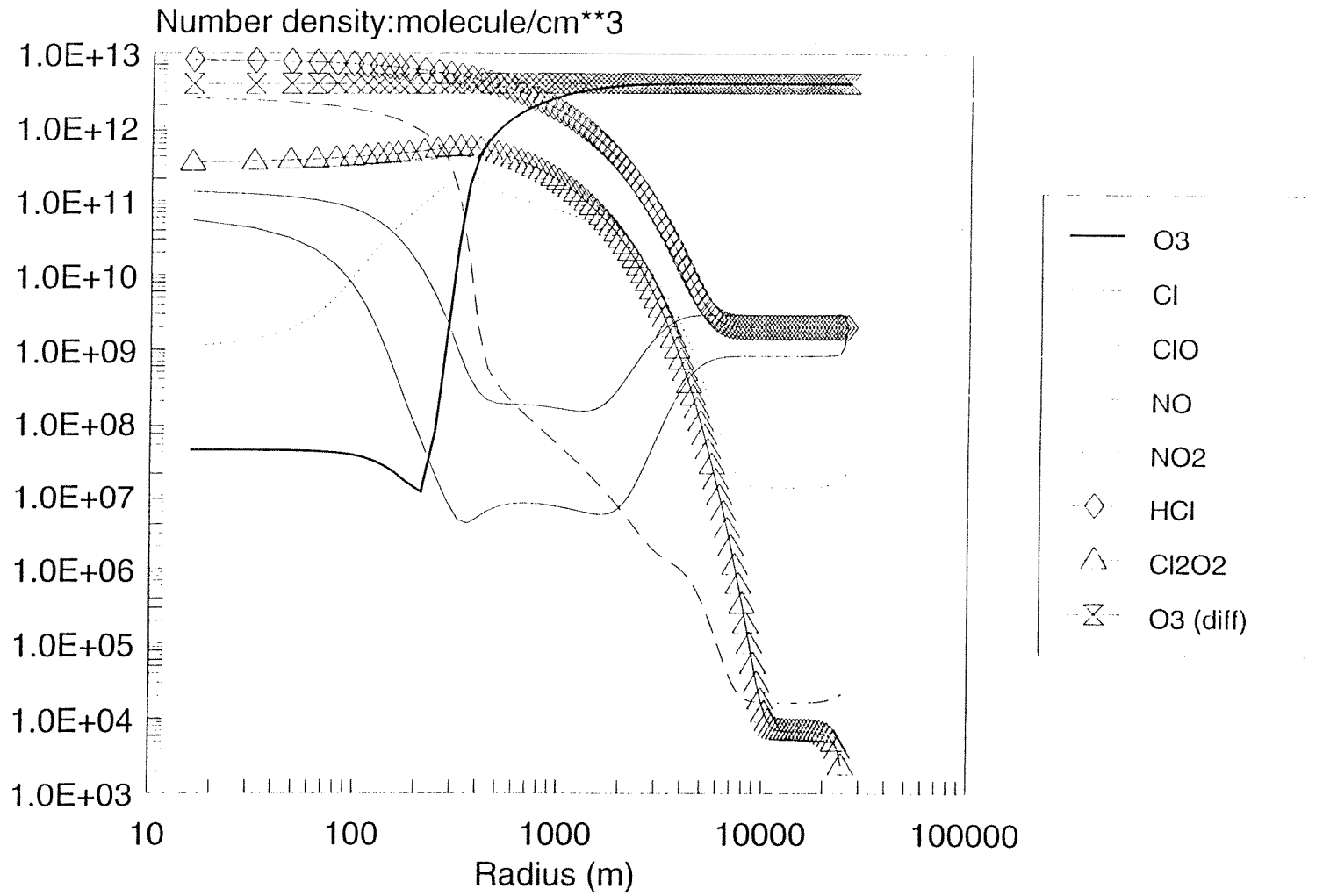


Figure 3.8.

Axial Species Profile (Titan IIIC-SRM 25km)

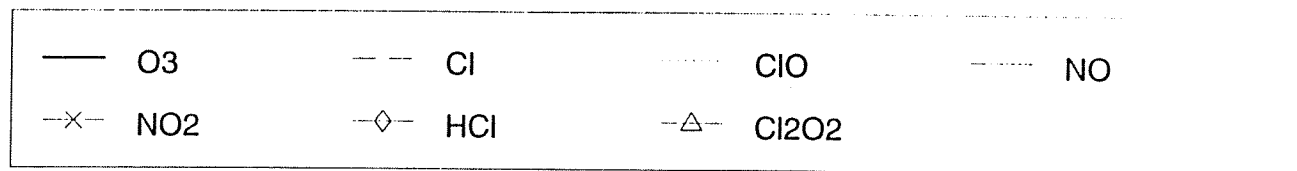
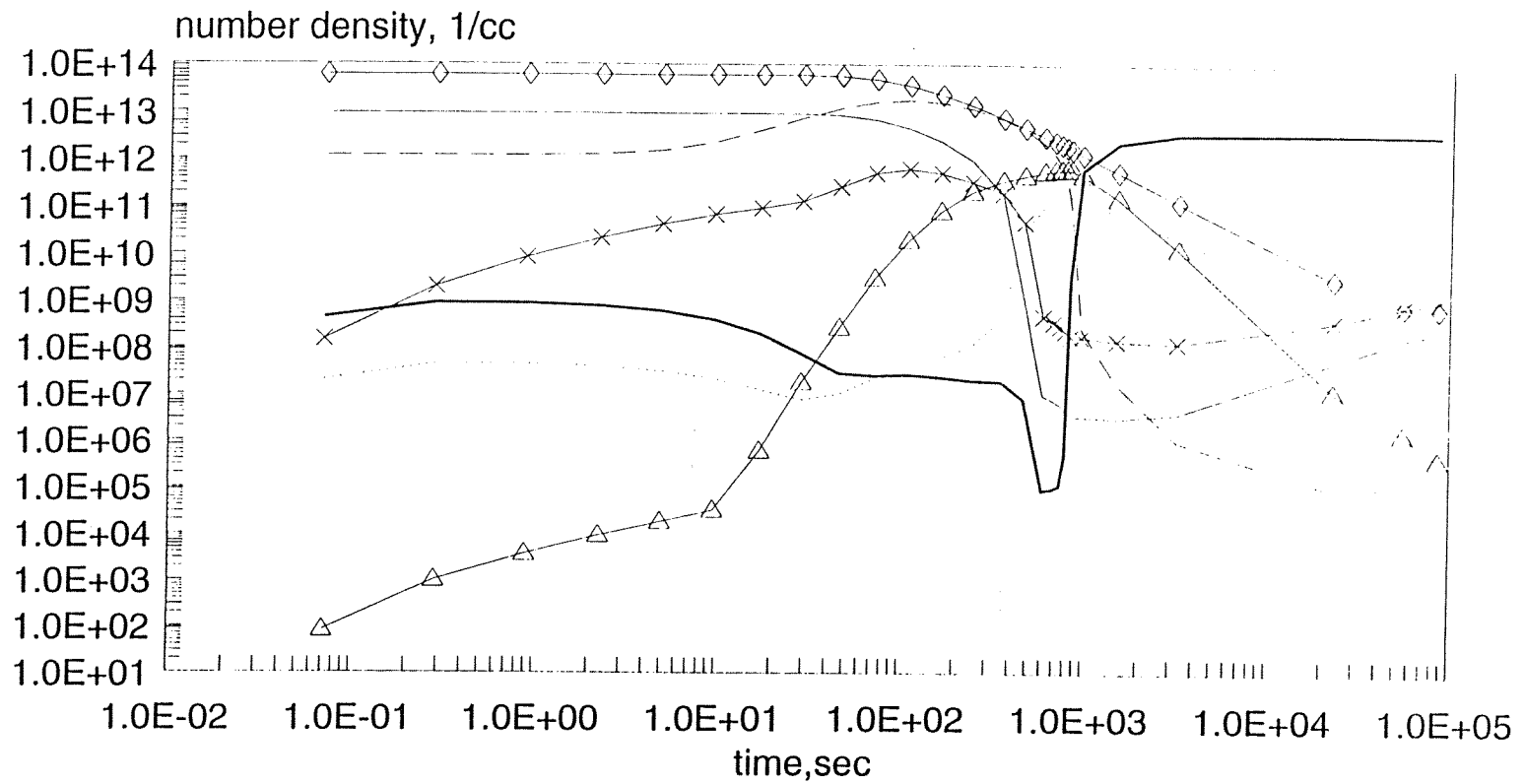


Figure 3.9.

Axial Species Profile (Titan IIIC-SRM 30km)

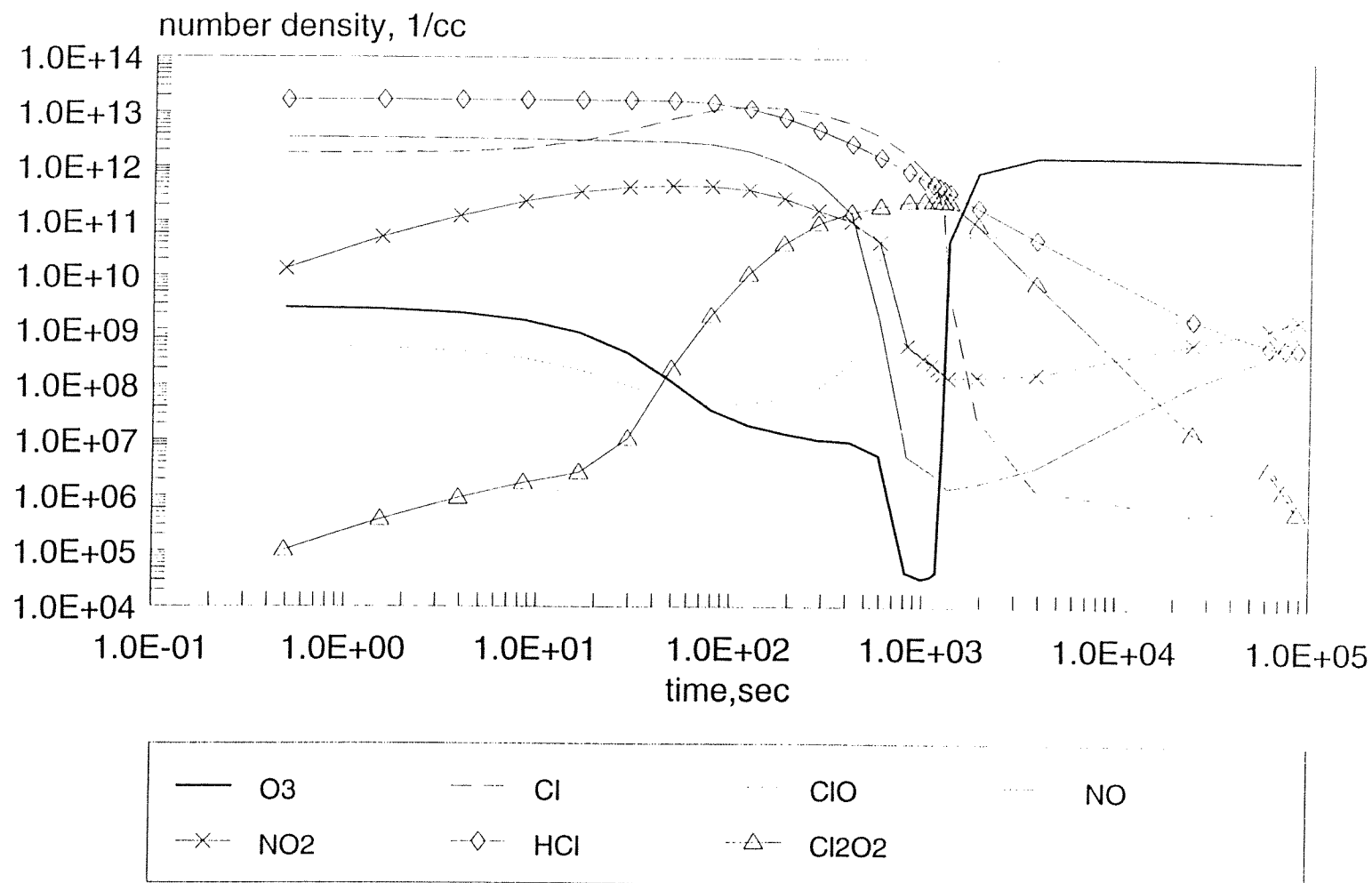


Figure 3.10.

Axial Species Profile (Titan IIIC-SRM 35km)

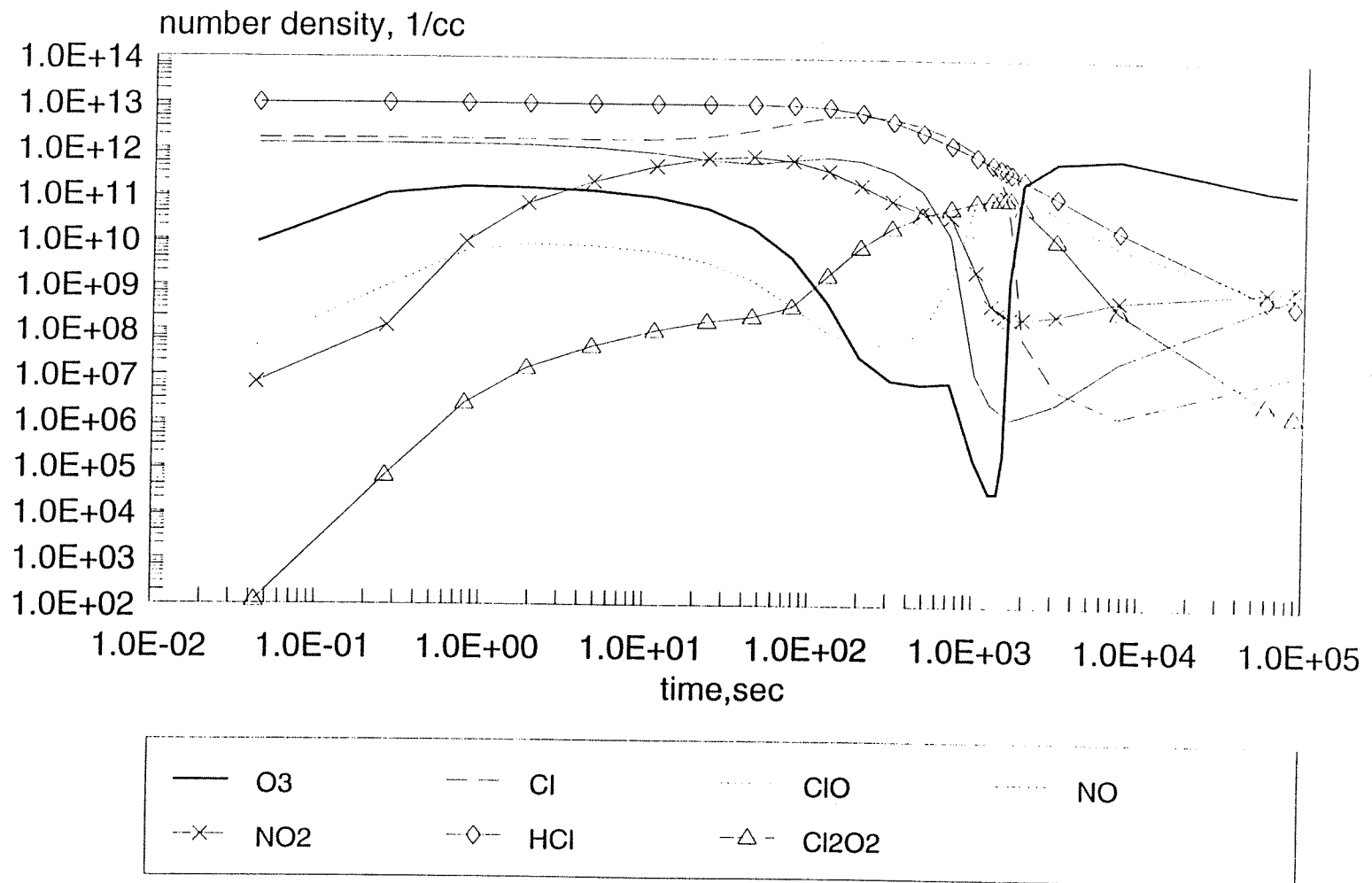


Figure 3.11.

Axial Species Profile (Titan IIIC-SRM 40km)

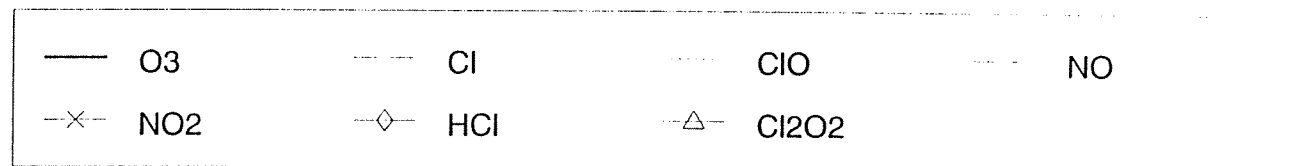
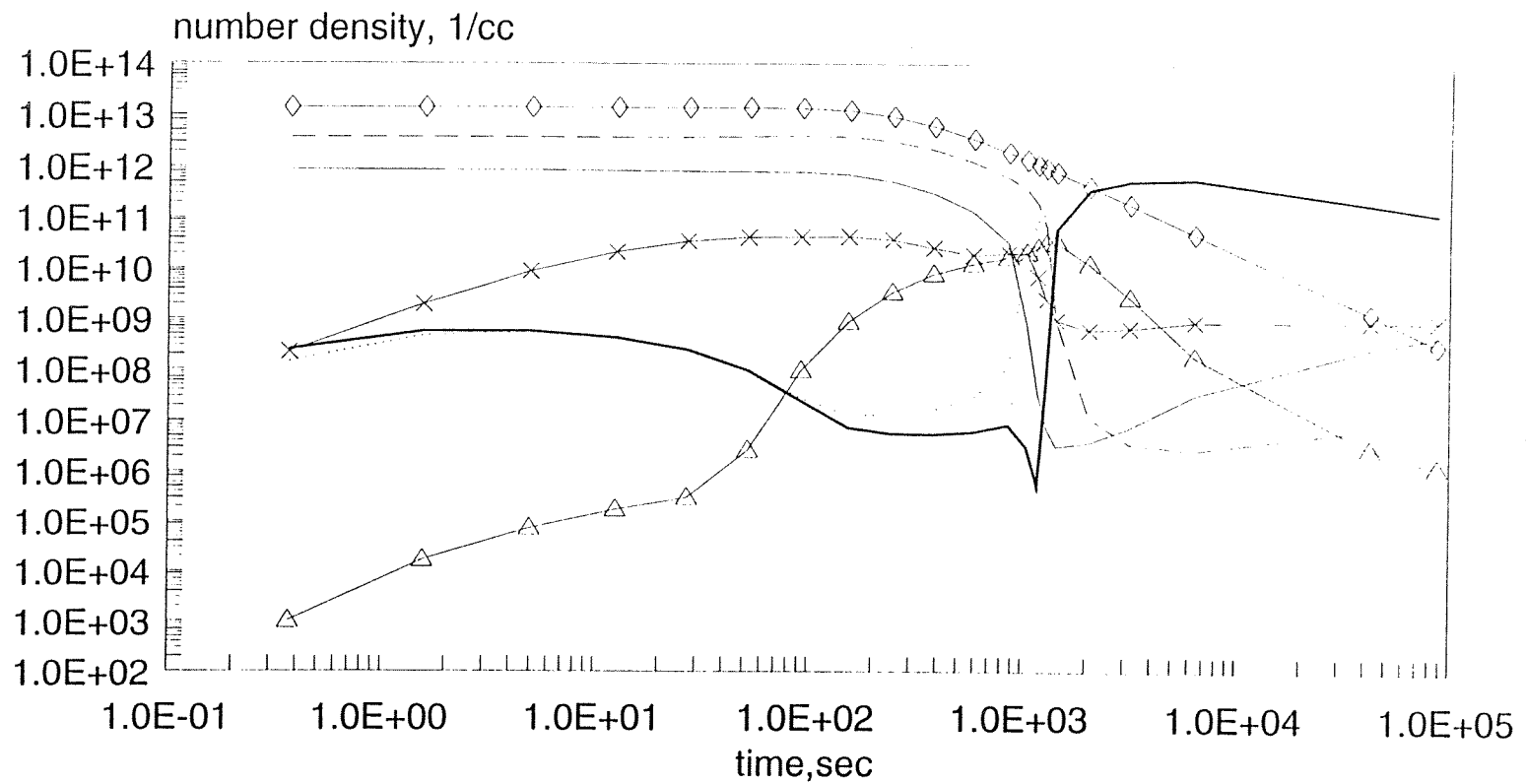


Figure 3.12.

Axial Species Profile
(Titan IIIC-SRM 20km)
eddy-diffusivity: lower estimate

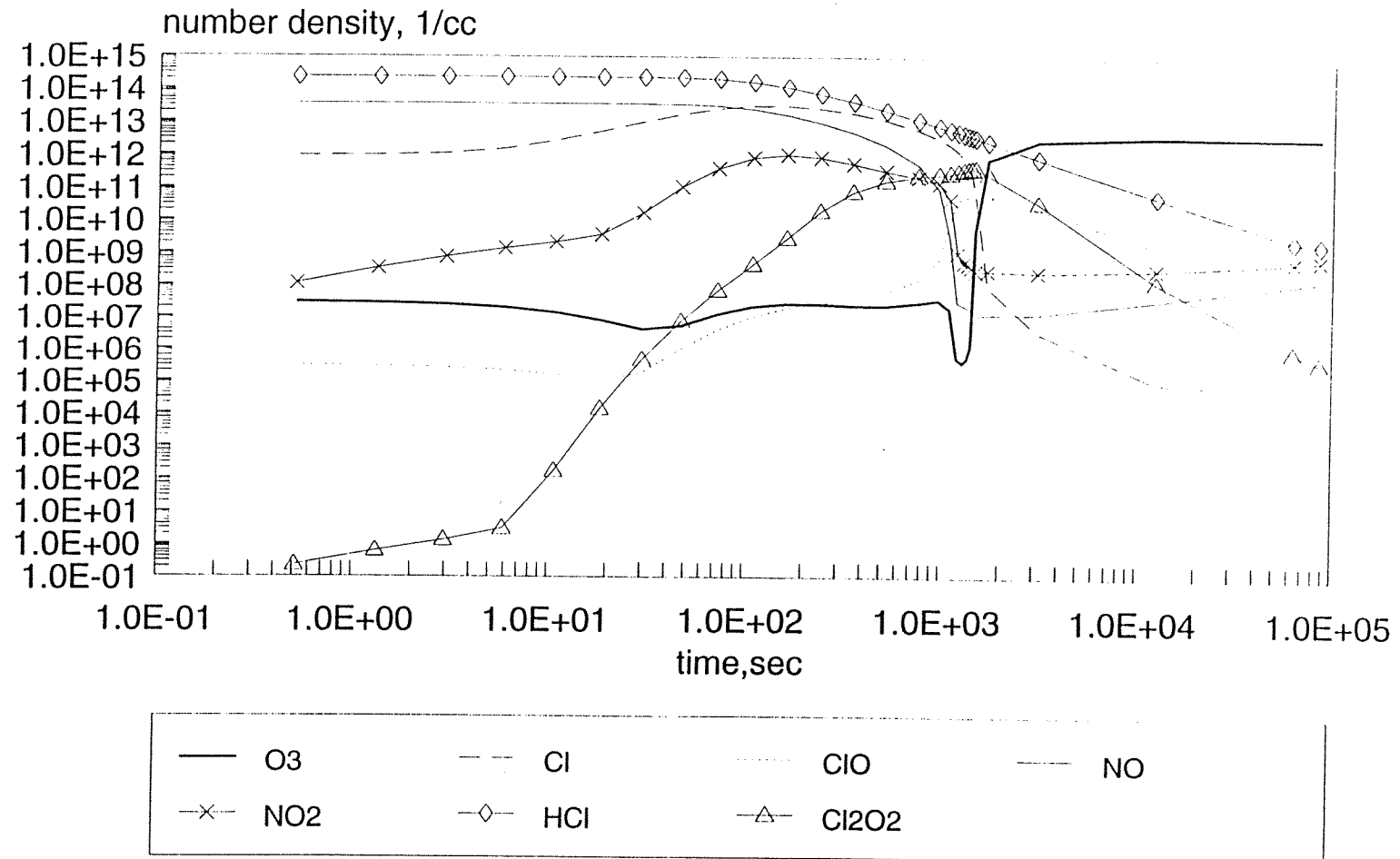


Figure 3.13.

Axial Species Profile
(Titan IIIC-SRM 20km)
eddy-diffusivity: upper estimate

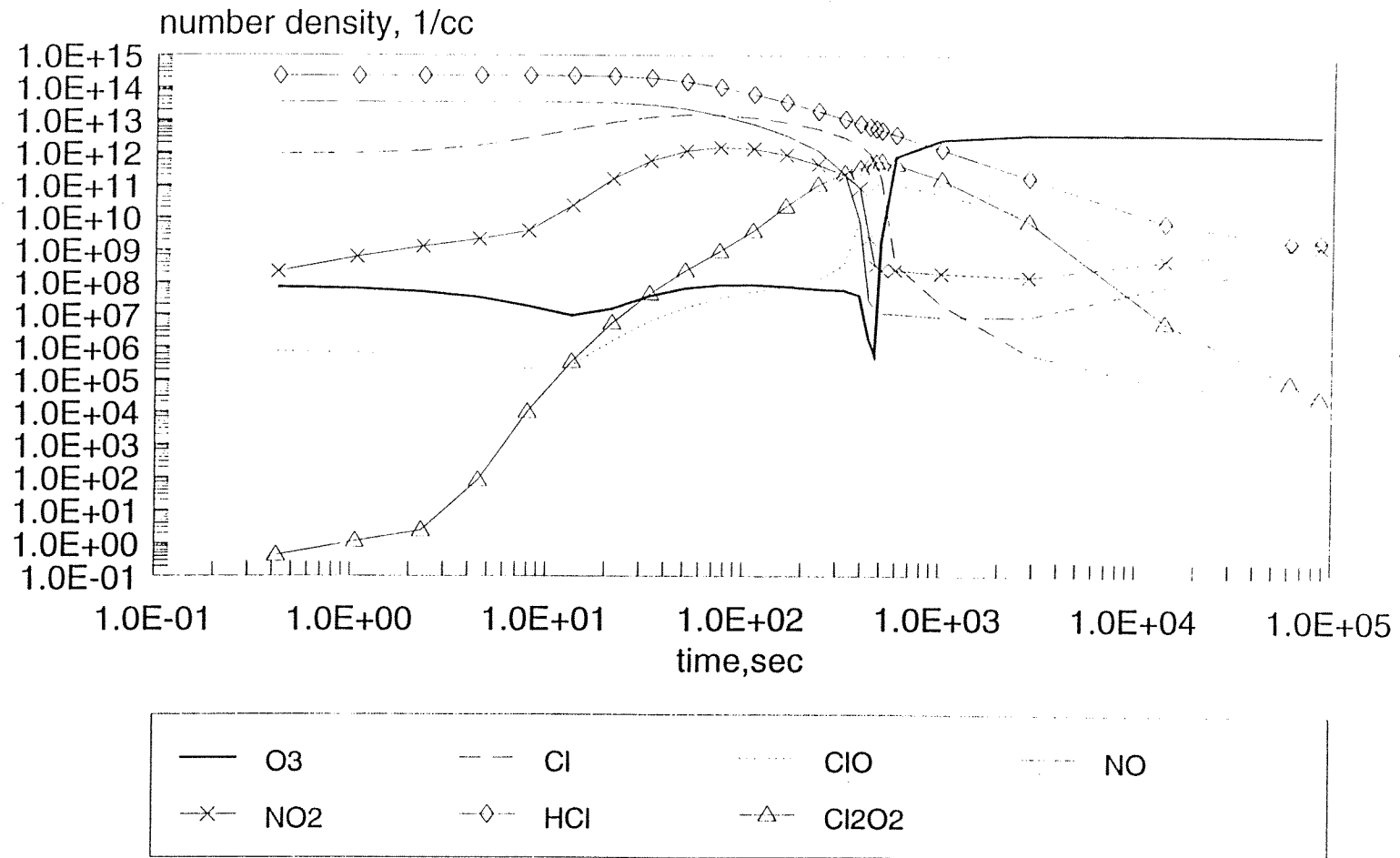


Figure 3.14.

Radial Species Profile at 110s
(one Mlb class conventional biprop)
liquid engine:NO mechanism; 20km

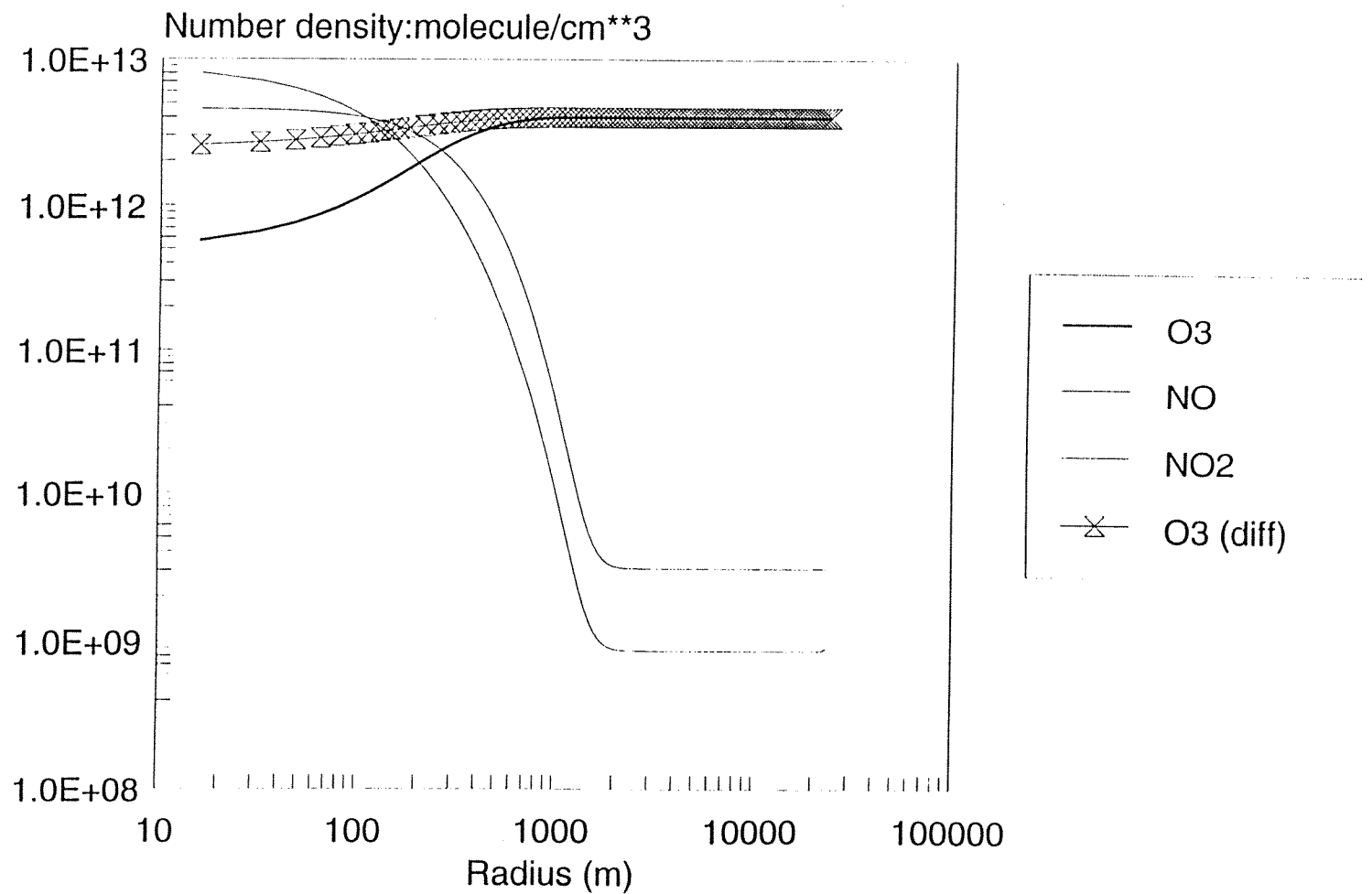


Figure 4.1.

Radial Species Profile at 515s
(one Mlb class conventional biprop)
liquid engine:NO mechanism; 20km

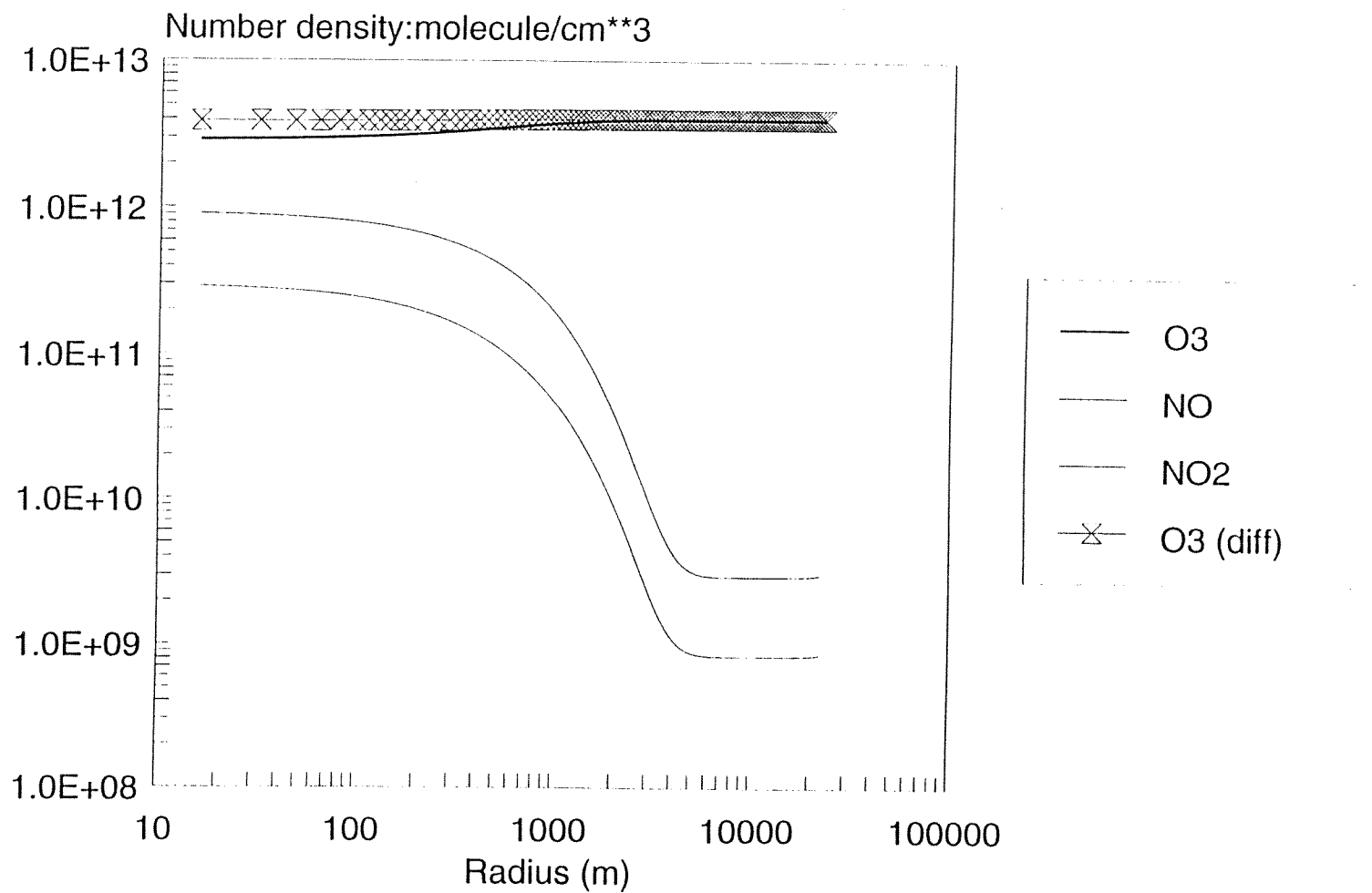


Figure 4.2.

Axial Species Profile
(one Mlb class conventional biprop)
liquid engine: NO mechanism; 20km

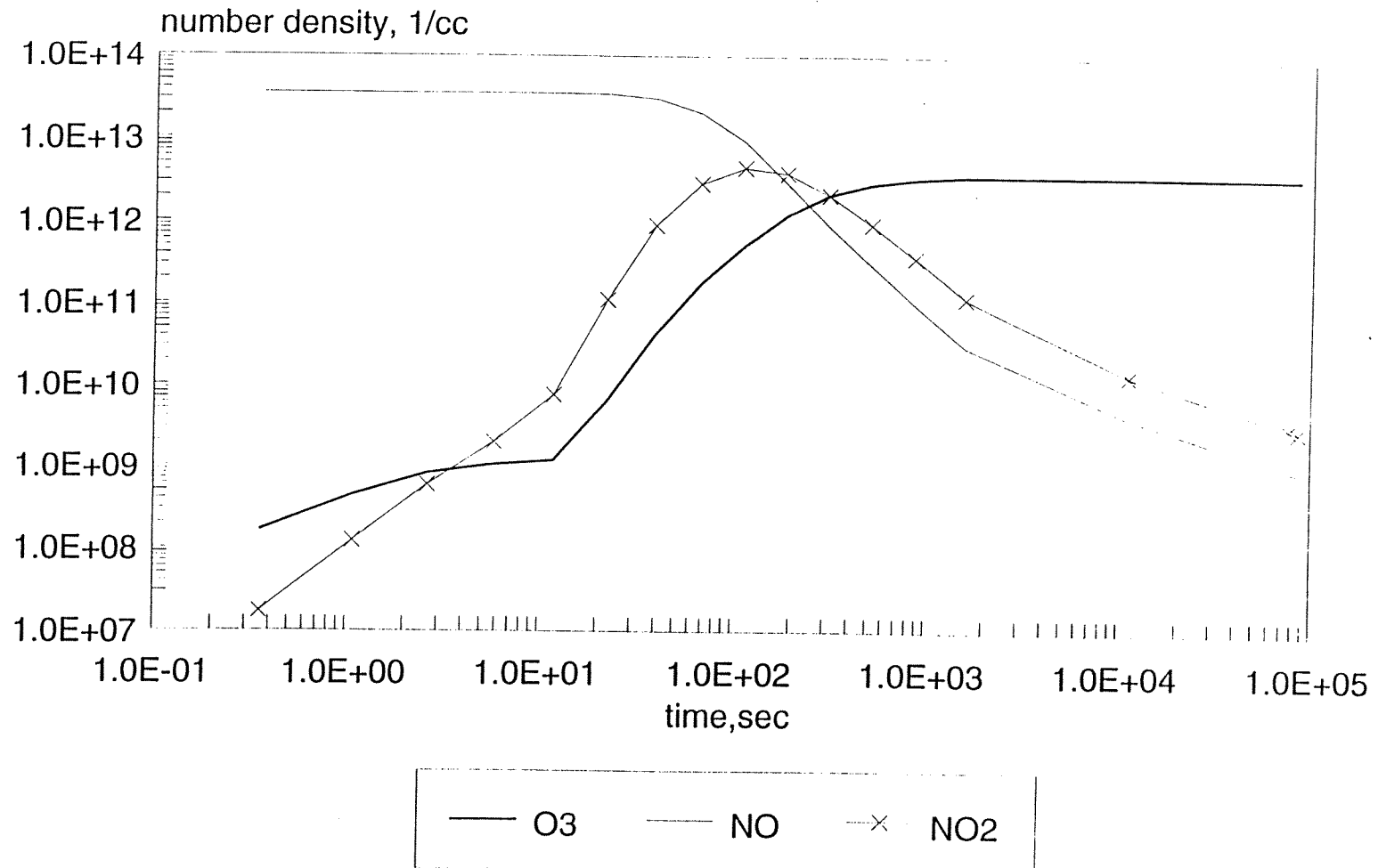


Figure 4.3.

FIGURE 5.1.

Cl₂ ENHANCEMENT IN JANUARY – TEN LAUNCH TITAN SCENARIO

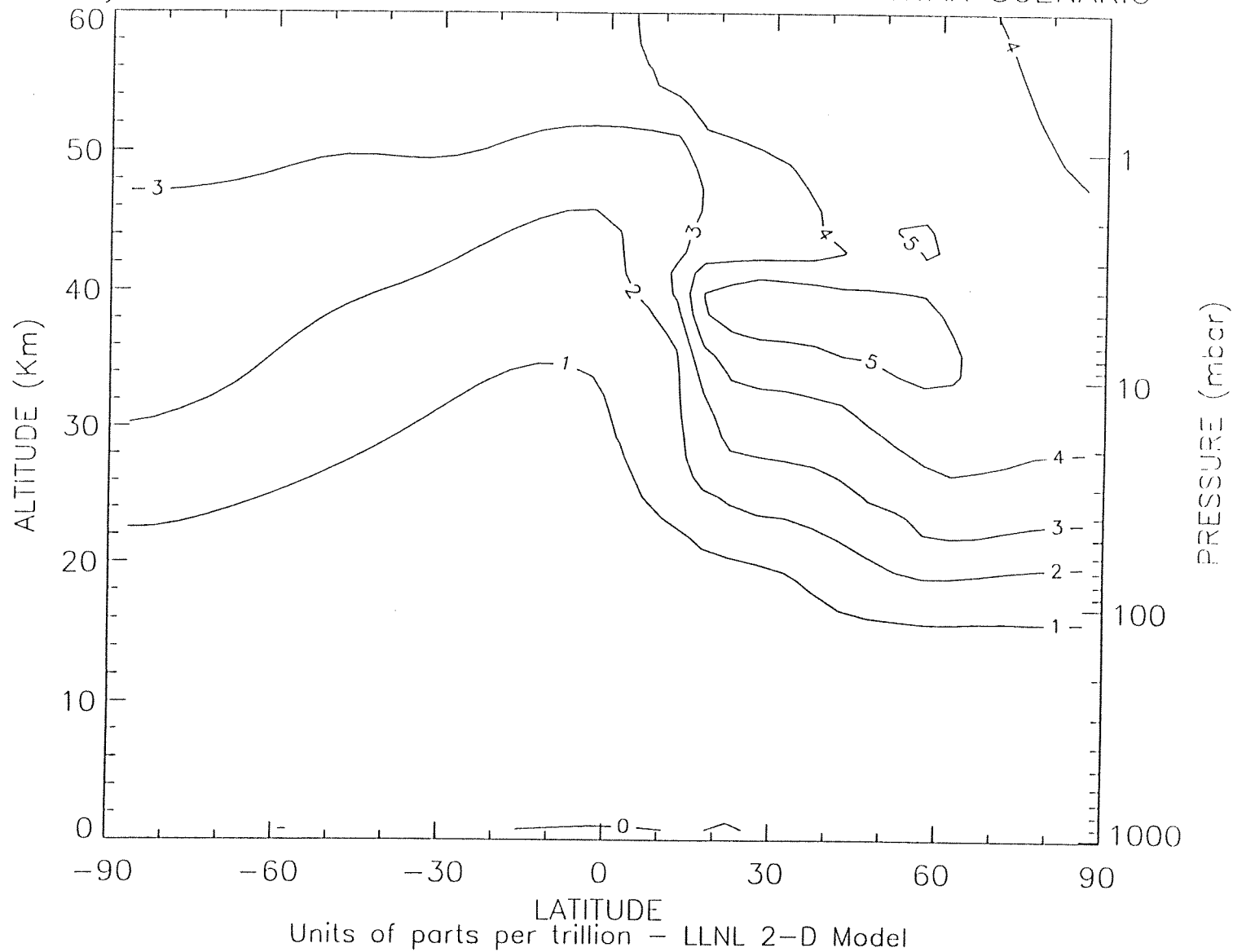


FIGURE 5.2.
Cl₂ ENHANCEMENT IN JULY - TEN LAUNCH TITAN SCENARIO

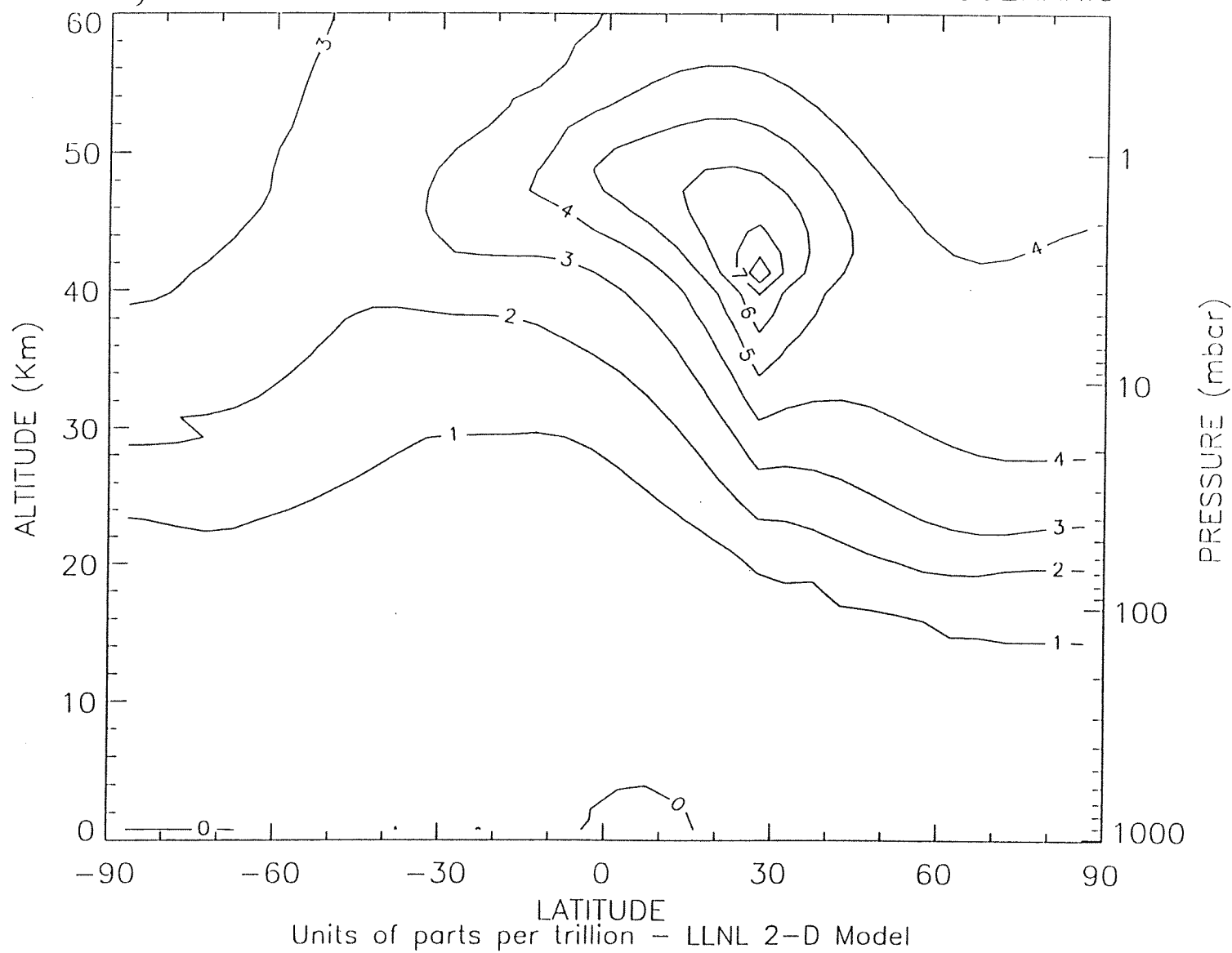


FIGURE 5.3.

LOCAL OZONE CHANGE % JANUARY – TEN LAUNCH TITAN SCENARIO

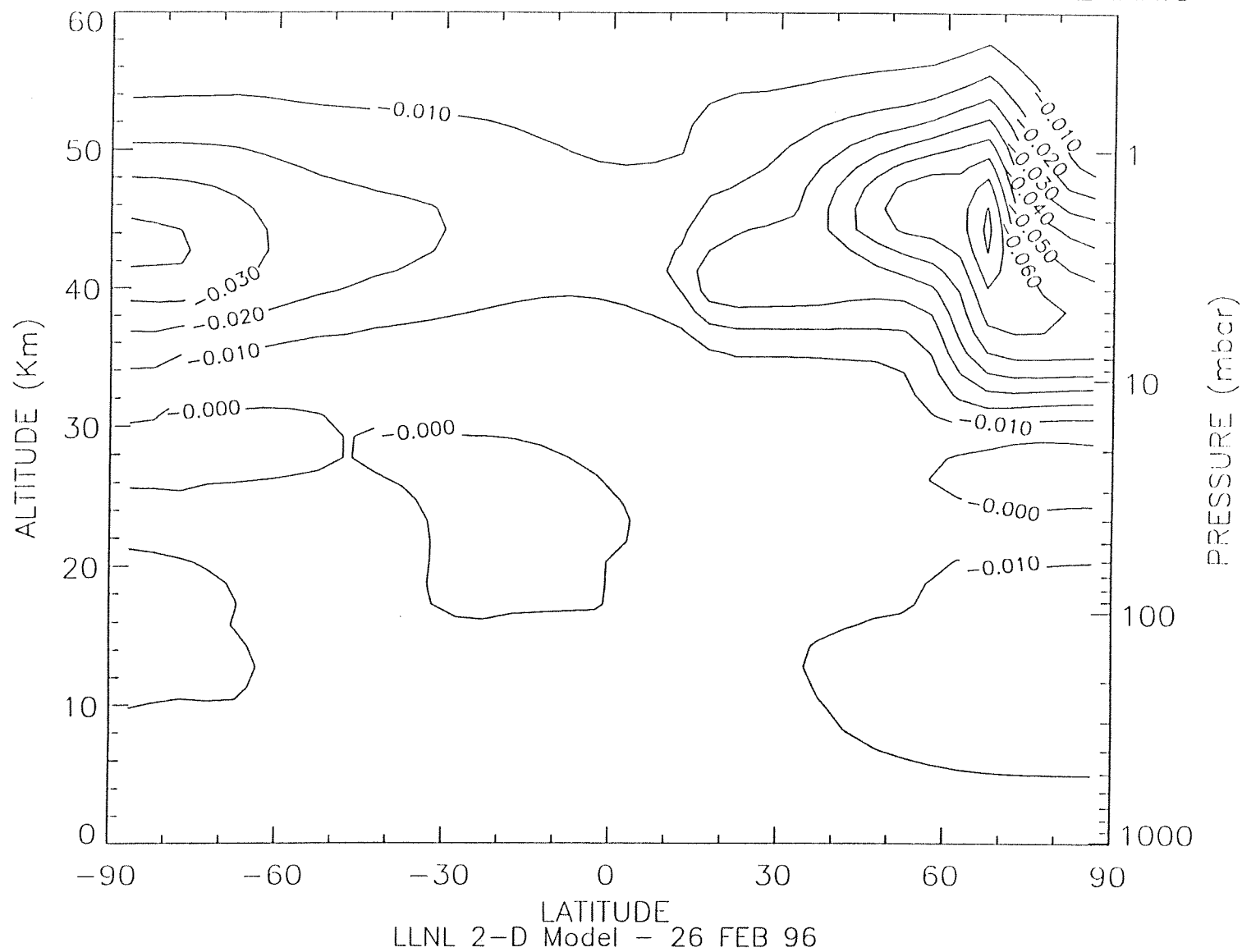


FIGURE 5.4.

LOCAL OZONE CHANGE % JULY - TEN LAUNCH TITAN SCENARIO

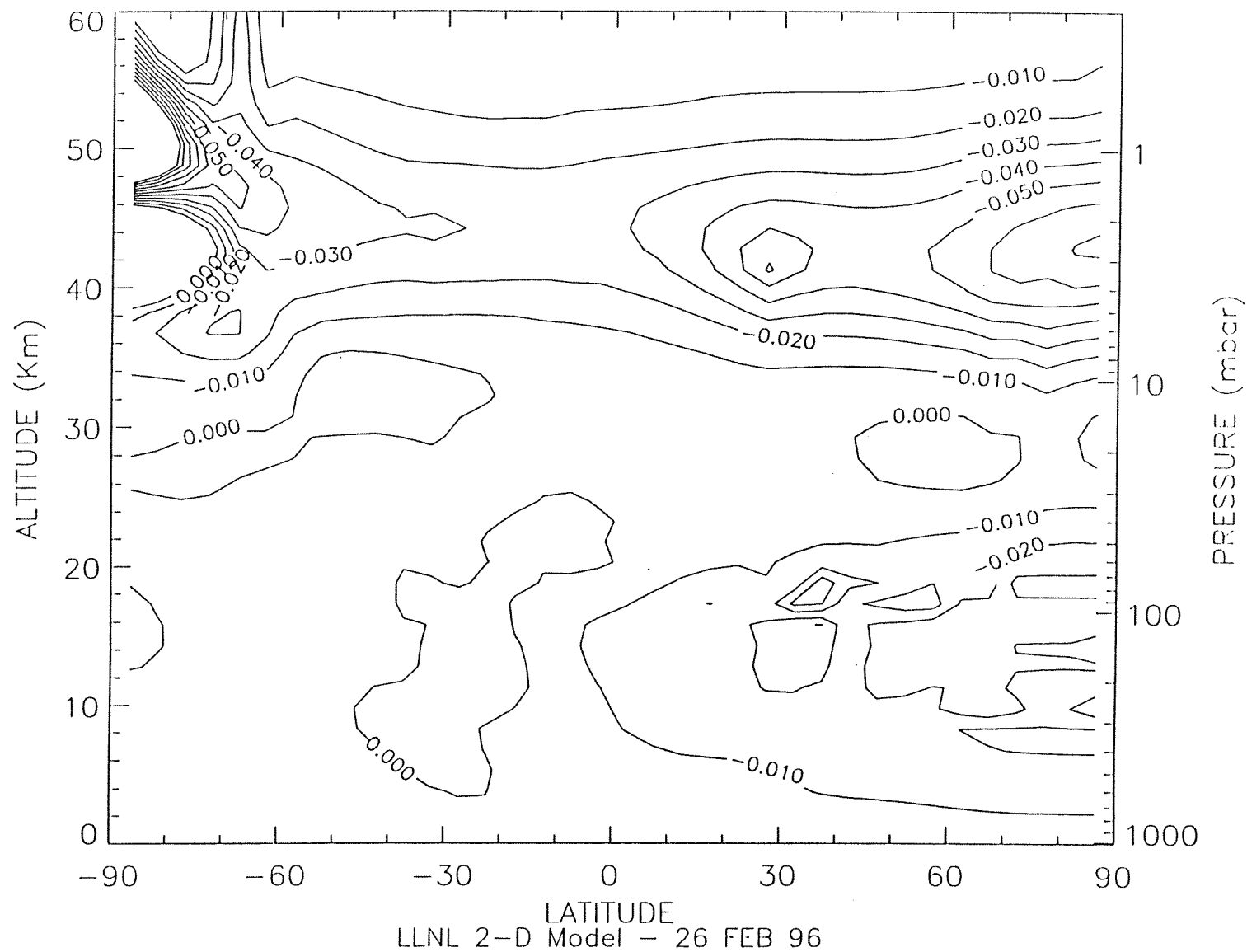


FIGURE 5.5. SEASONAL EFFECTS ON THE ZONAL WIND PROFILES AT WALLOPS ISLAND.

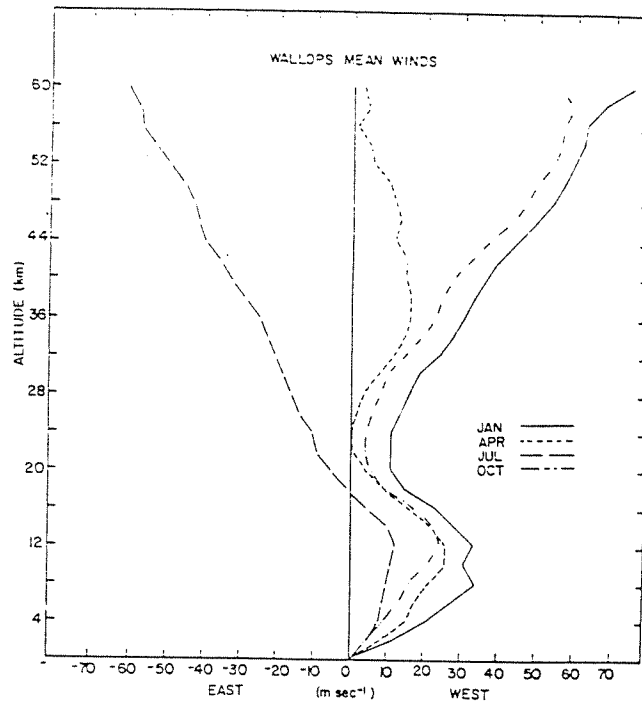


FIGURE 5.6. SEASONAL EFFECTS ON THE MERIDIONAL WIND PROFILES AT ASCENSION ISLAND.

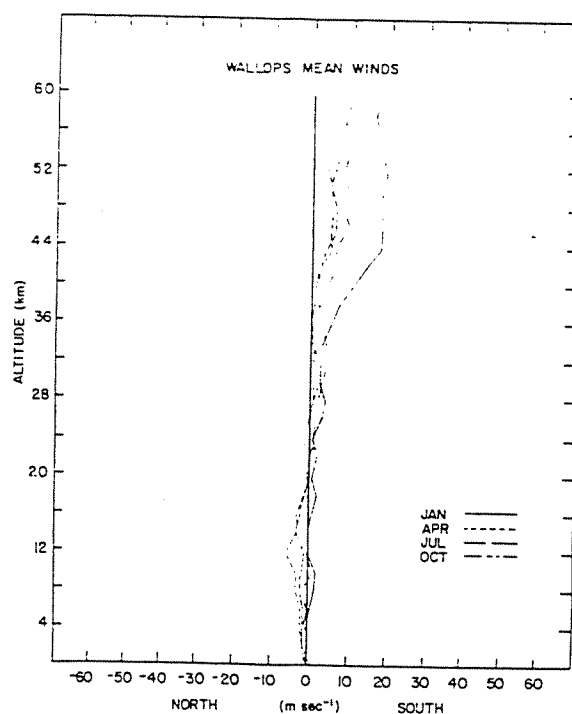


FIGURE 5.7. TITAN EXHAUST PLUME TRANSPORT IN STRATOSPHERE AFTER 2 HOURS IN JANUARY.

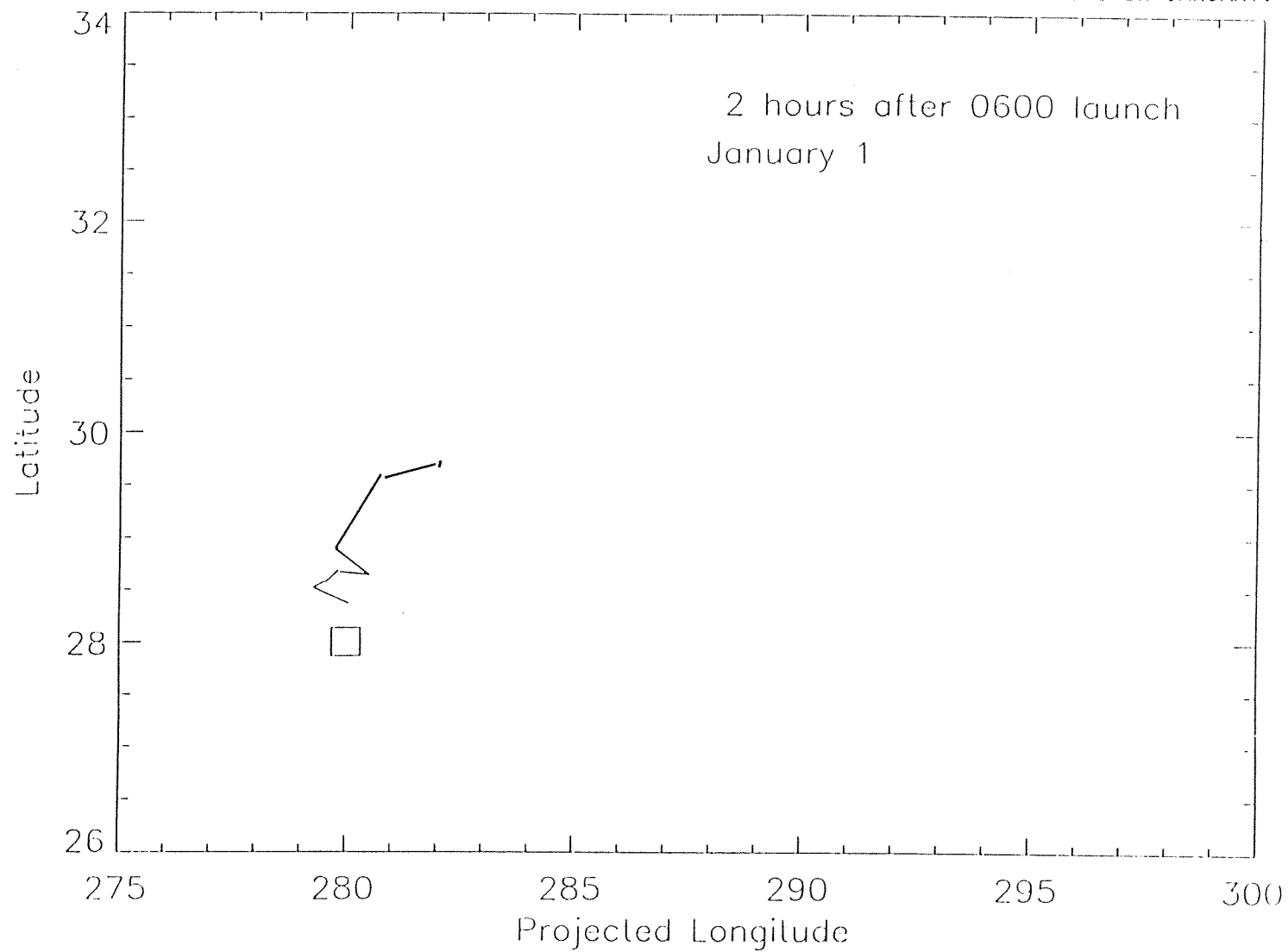


FIGURE 5.8. TITAN EXHAUST PLUME TRANSPORT IN STRATOSPHERE AFTER 4 HOURS IN JANUARY.

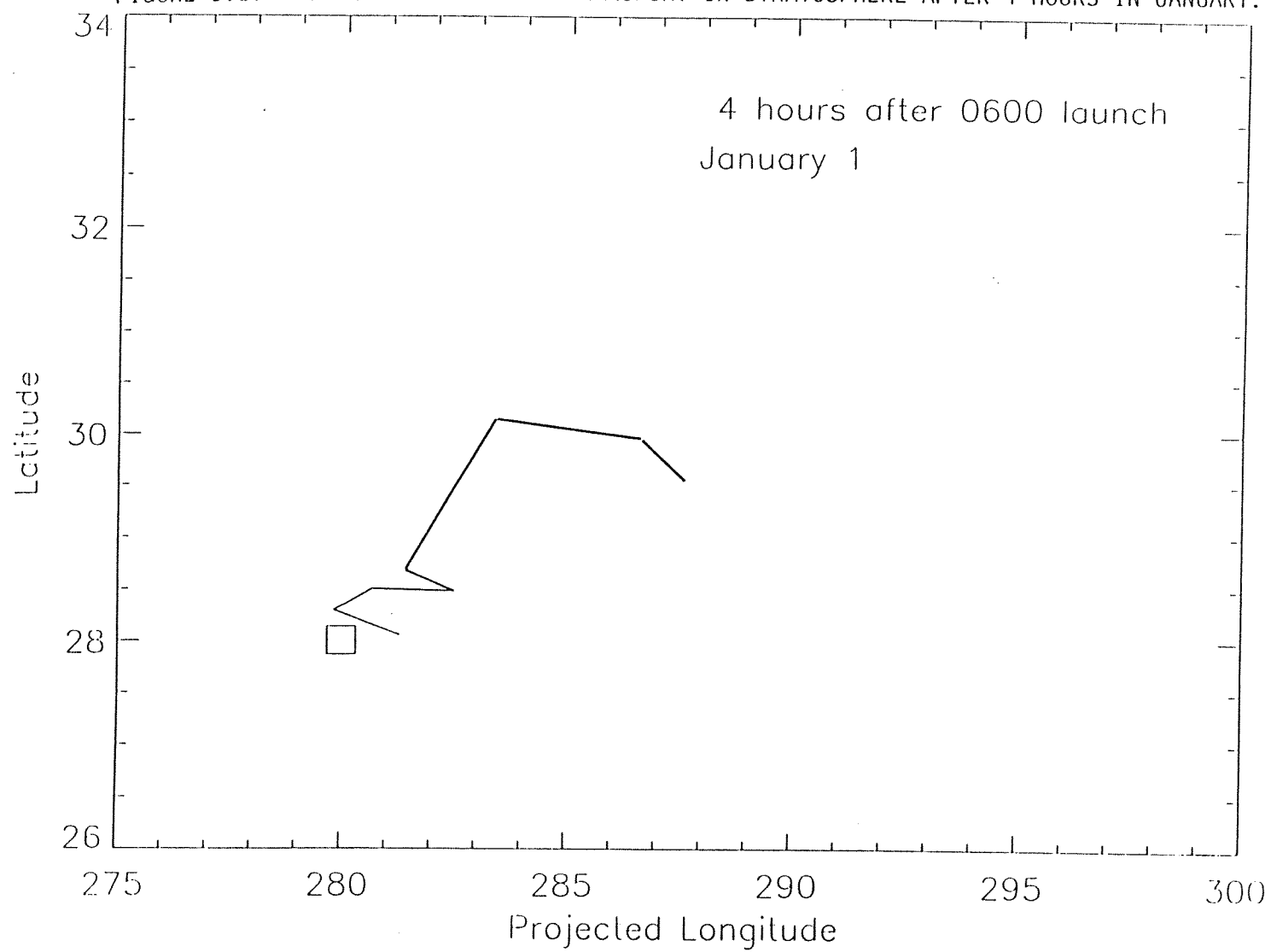


FIGURE 5.9. TITAN EXHAUST PLUME TRANSPORT IN STRATOSPHERE AFTER 9 HOURS IN JANUARY.

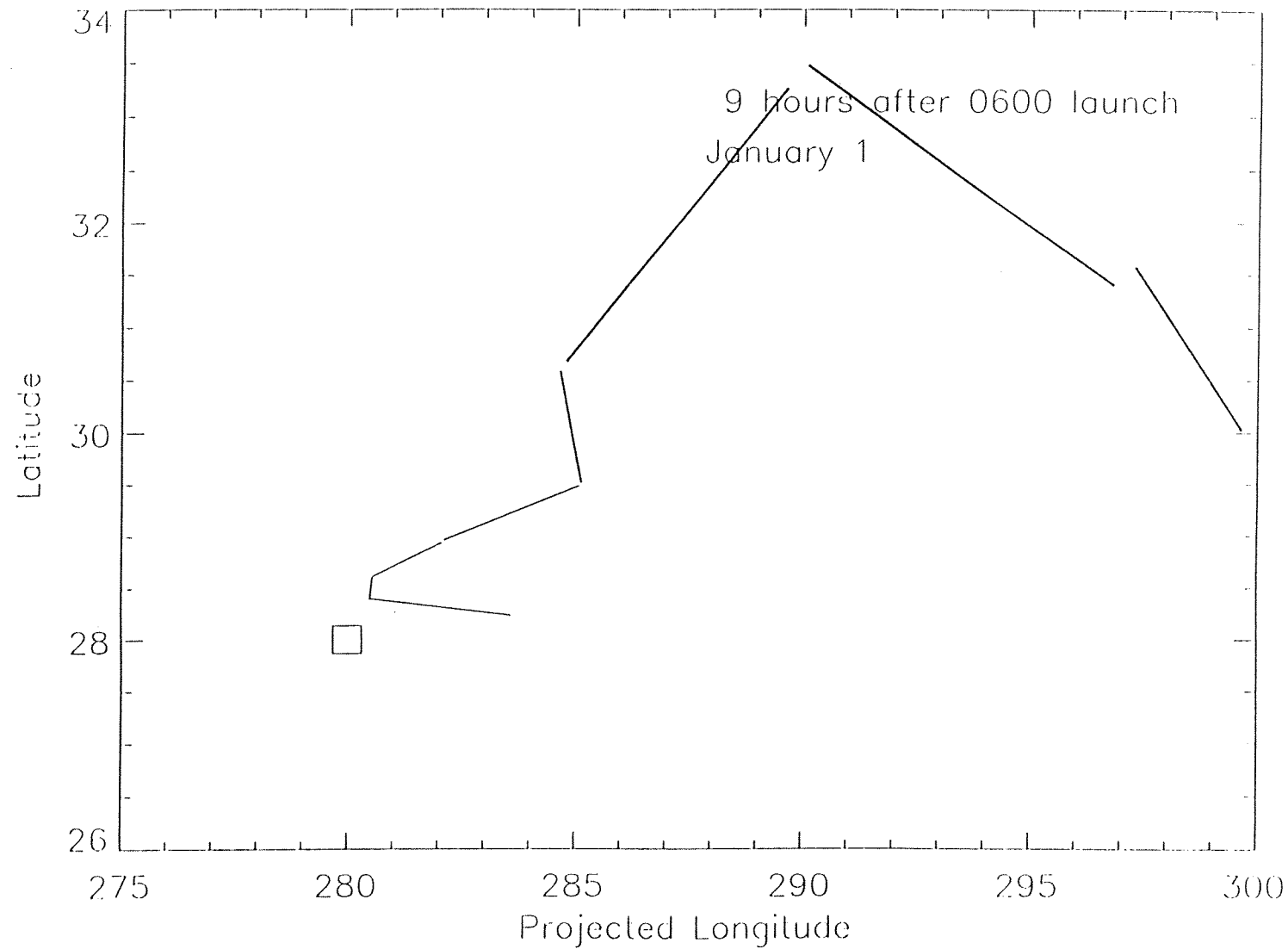


FIGURE 5.10. OZONE DEPLETION ALONG SOLAR LINE-OF-SIGHT 2 HOURS AFTER LAUNCH IN JANUARY.

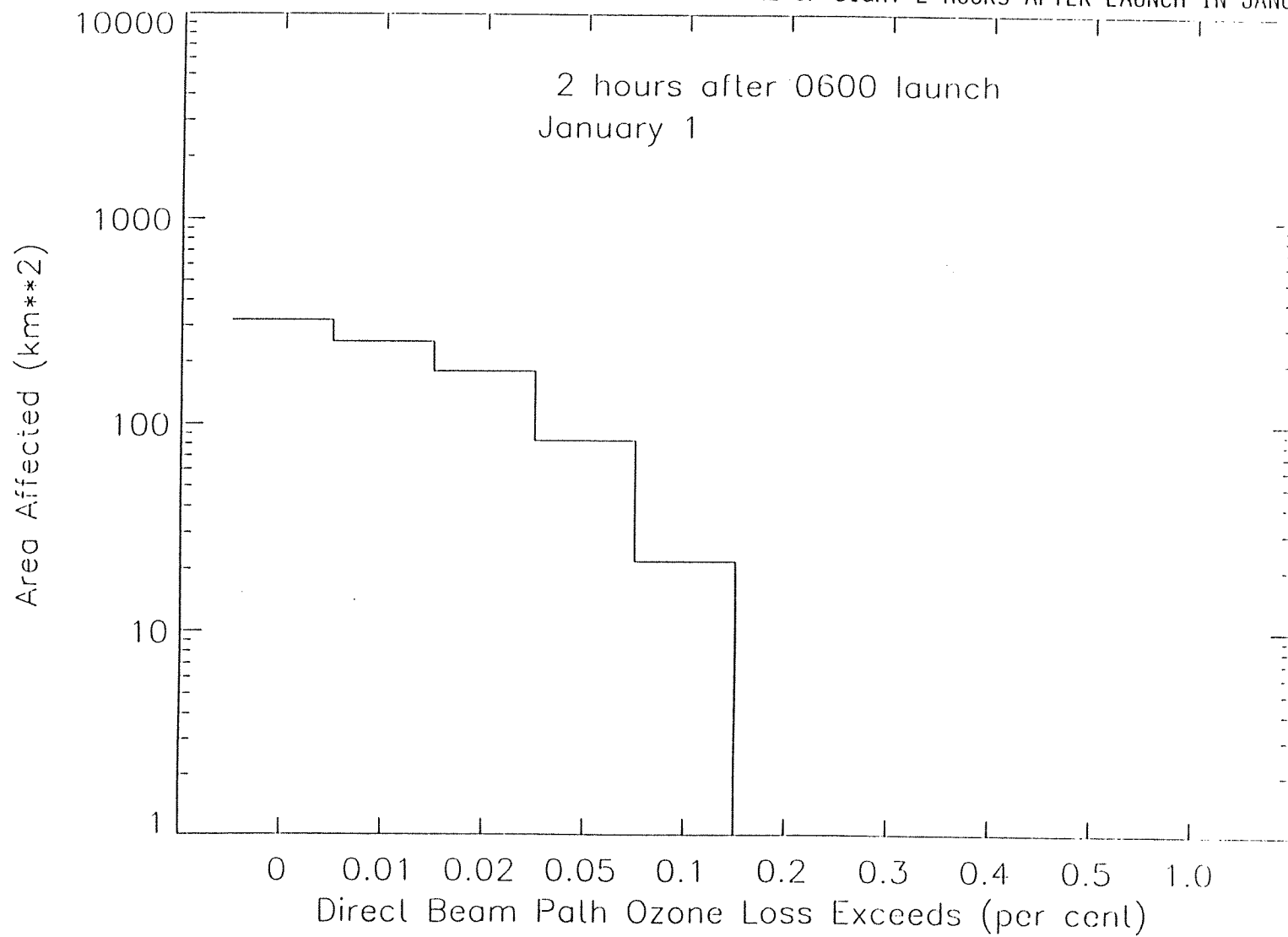


FIGURE 5.11. OZONE DEPLETION ALONG SOLAR LINE-OF-SIGHT 4 HOURS AFTER LAUNCH IN JANUARY.

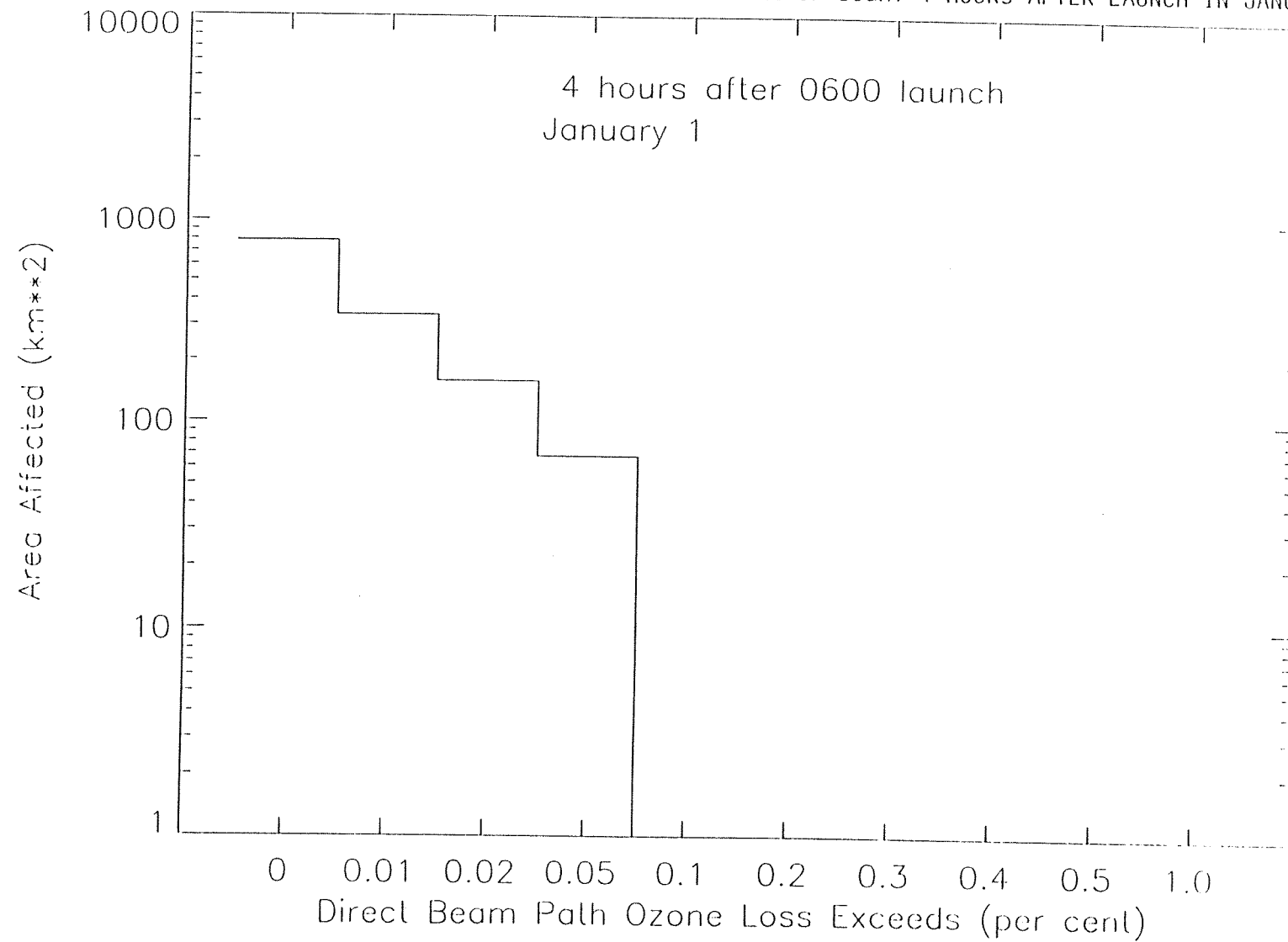


FIGURE 5.12. OZONE DEPLETION ALONG SOLAR LINE-OF-SIGHT 9 HOURS AFTER LAUNCH IN JANUARY.

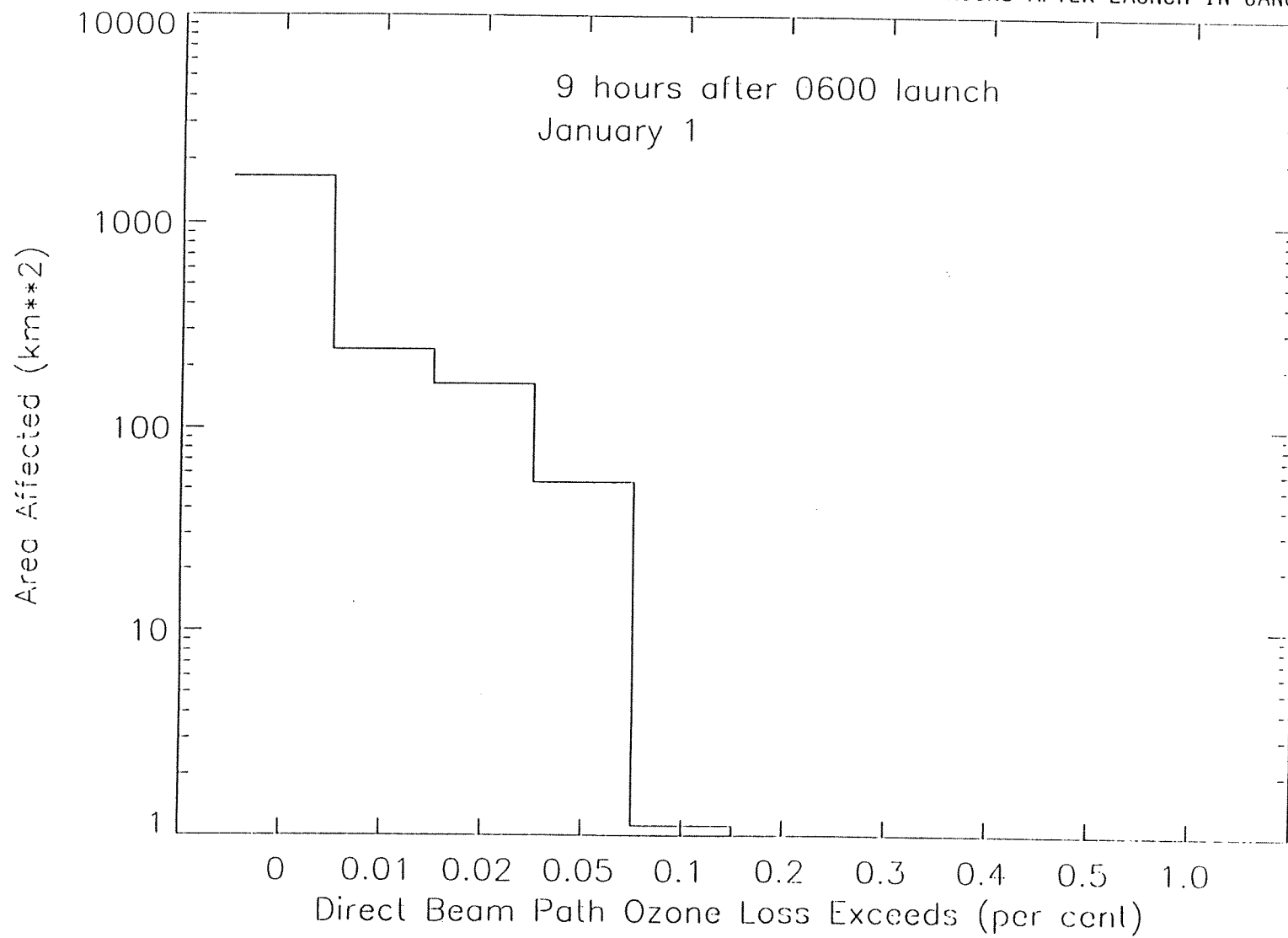


FIGURE 5.13. OZONE DEPLETION ALONG SOLAR LINE-OF-SIGHT 2 HOURS AFTER LAUNCH IN JULY.

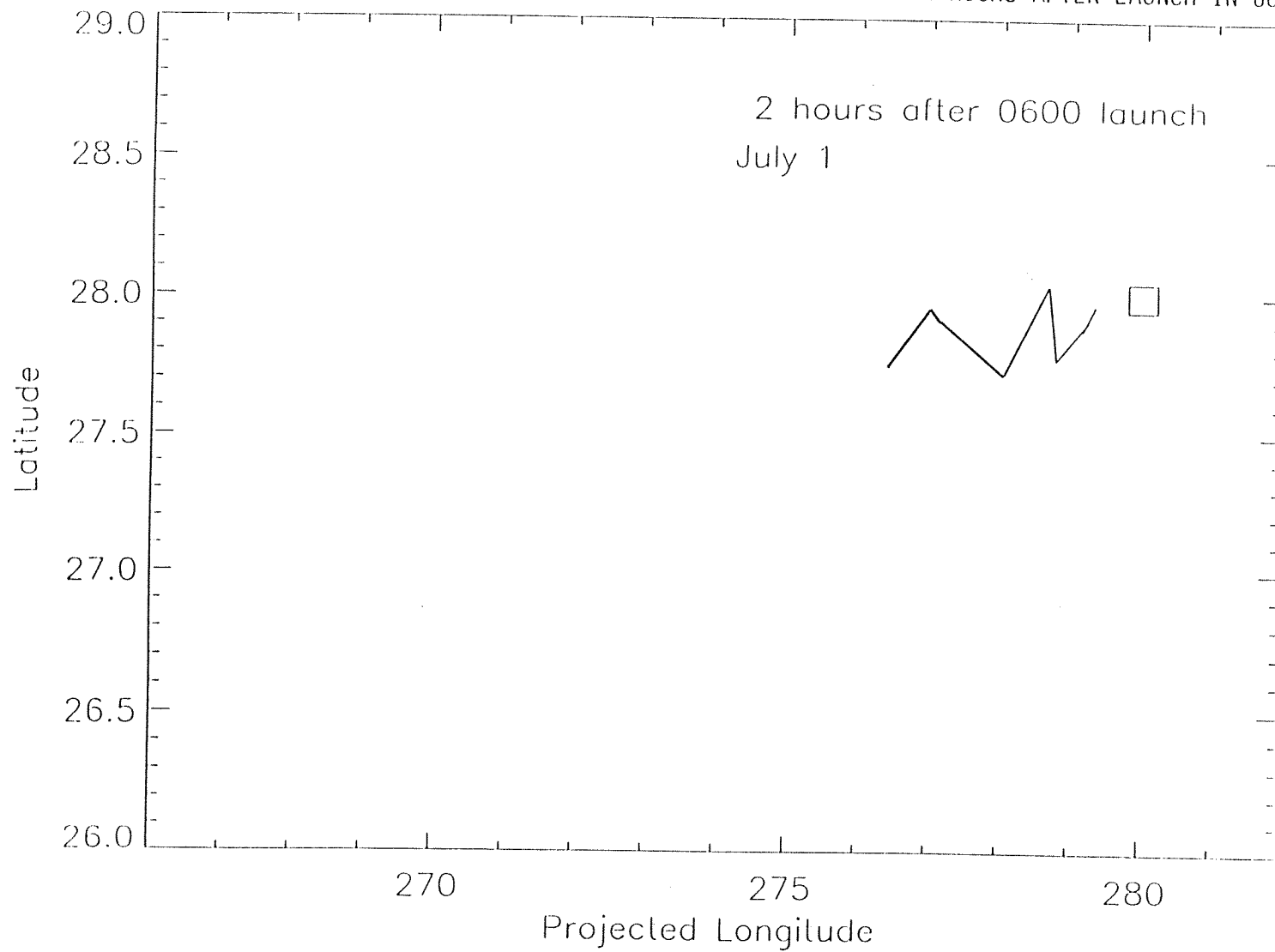


FIGURE 5.14. OZONE DEPLETION ALONG SOLAR LINE-OF-SIGHT 4 HOURS AFTER LAUNCH IN JULY.

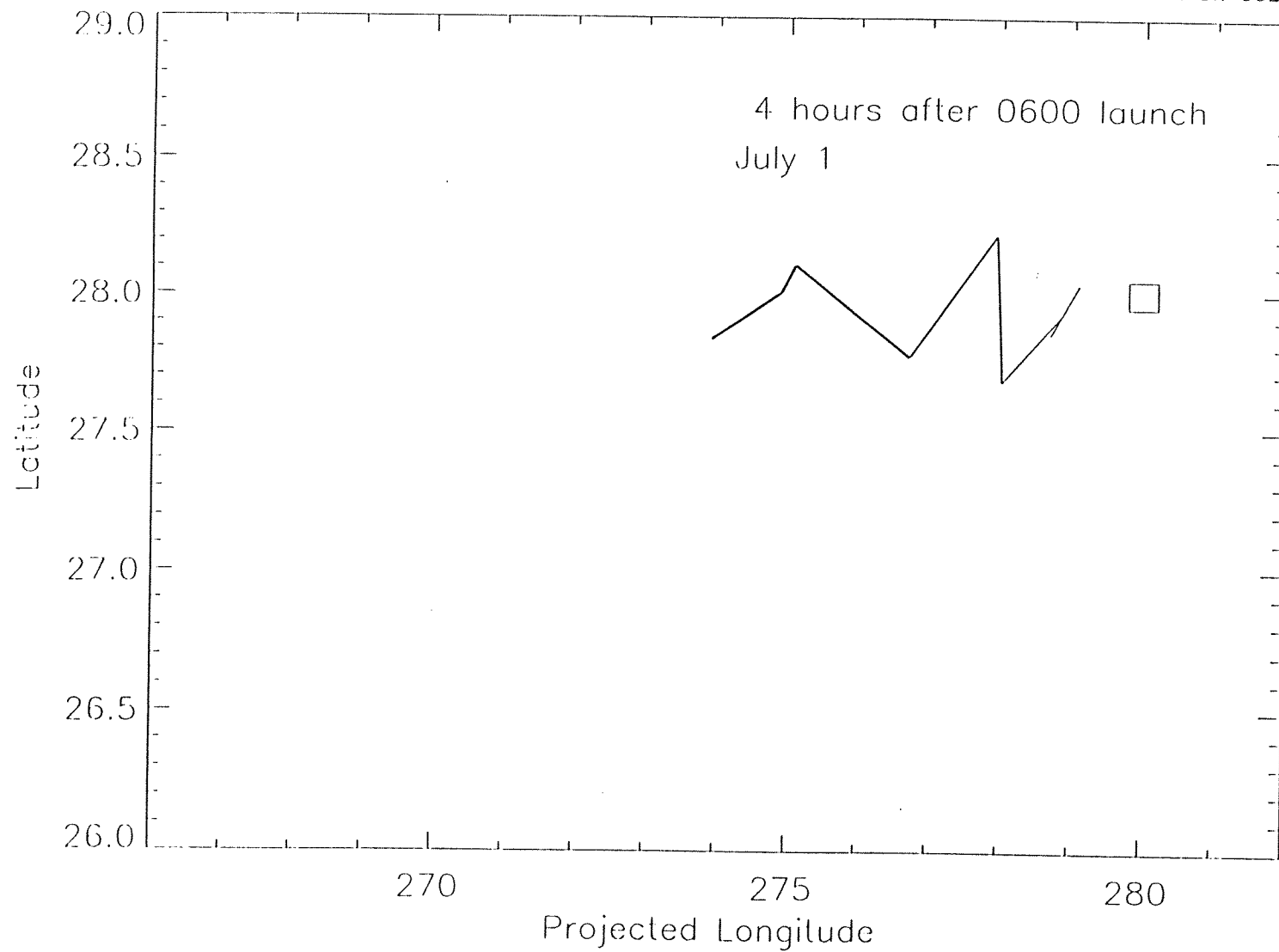


FIGURE 5.15. OZONE DEPLETION ALONG SOLAR LINE-OF-SIGHT 9 HOURS AFTER LAUNCH IN JULY.

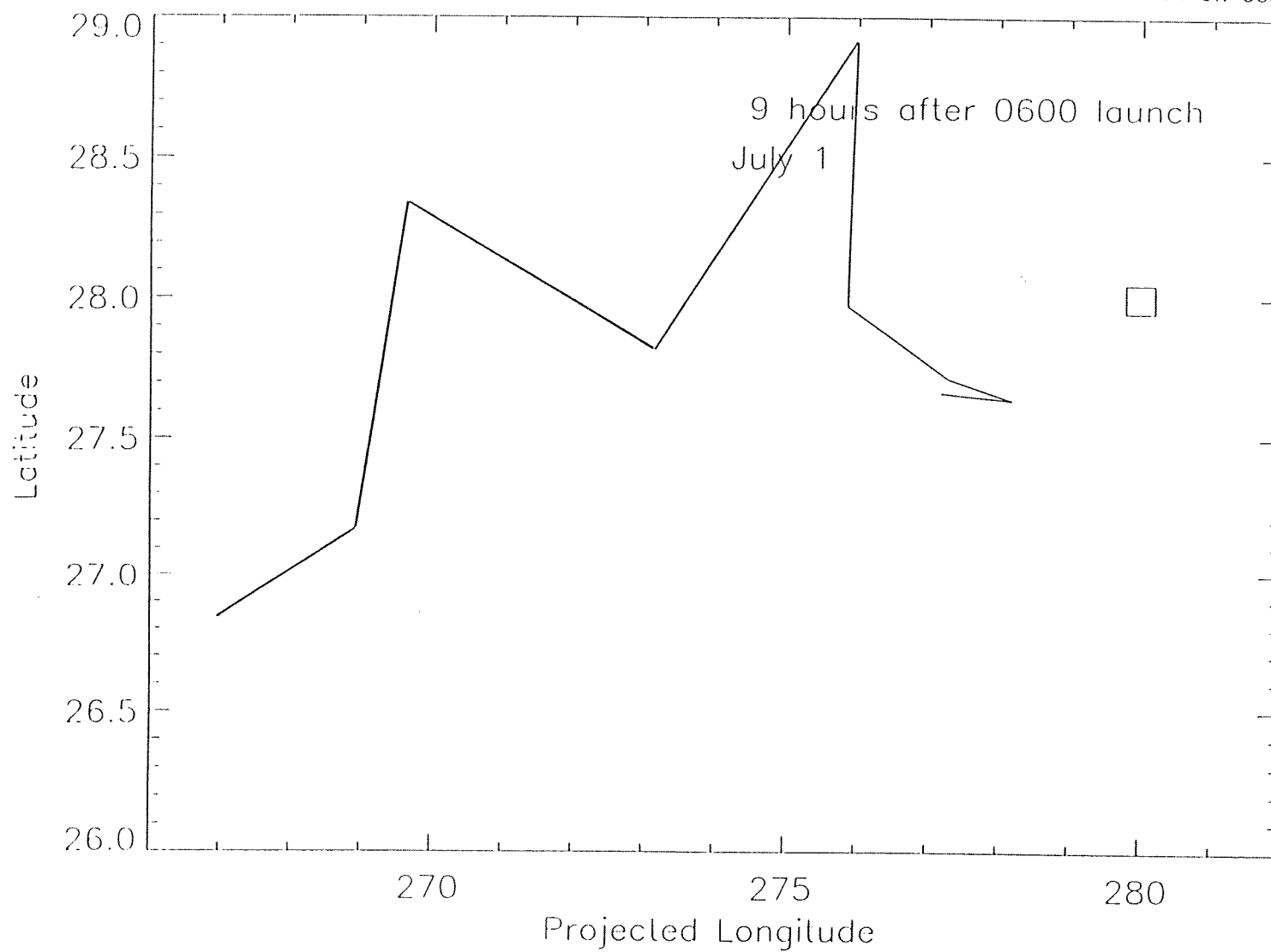


FIGURE 5.16. OZONE DEPLETION ALONG SOLAR LINE-OF-SIGHT 2 HOURS AFTER LAUNCH IN JULY.

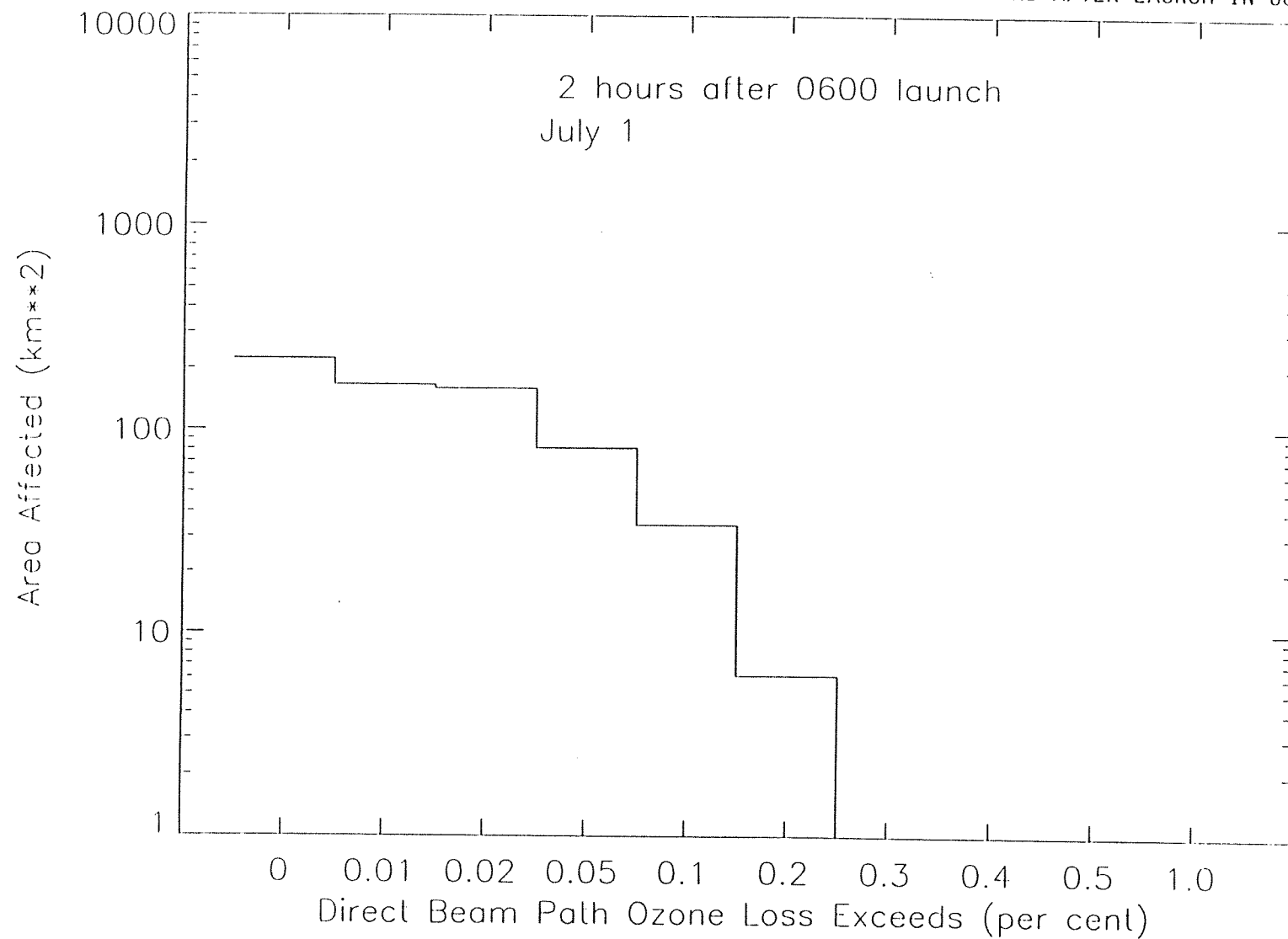


FIGURE 5.17. OZONE DEPLETION ALONG SOLAR LINE-OF-SIGHT 4 HOURS AFTER LAUNCH IN JULY.

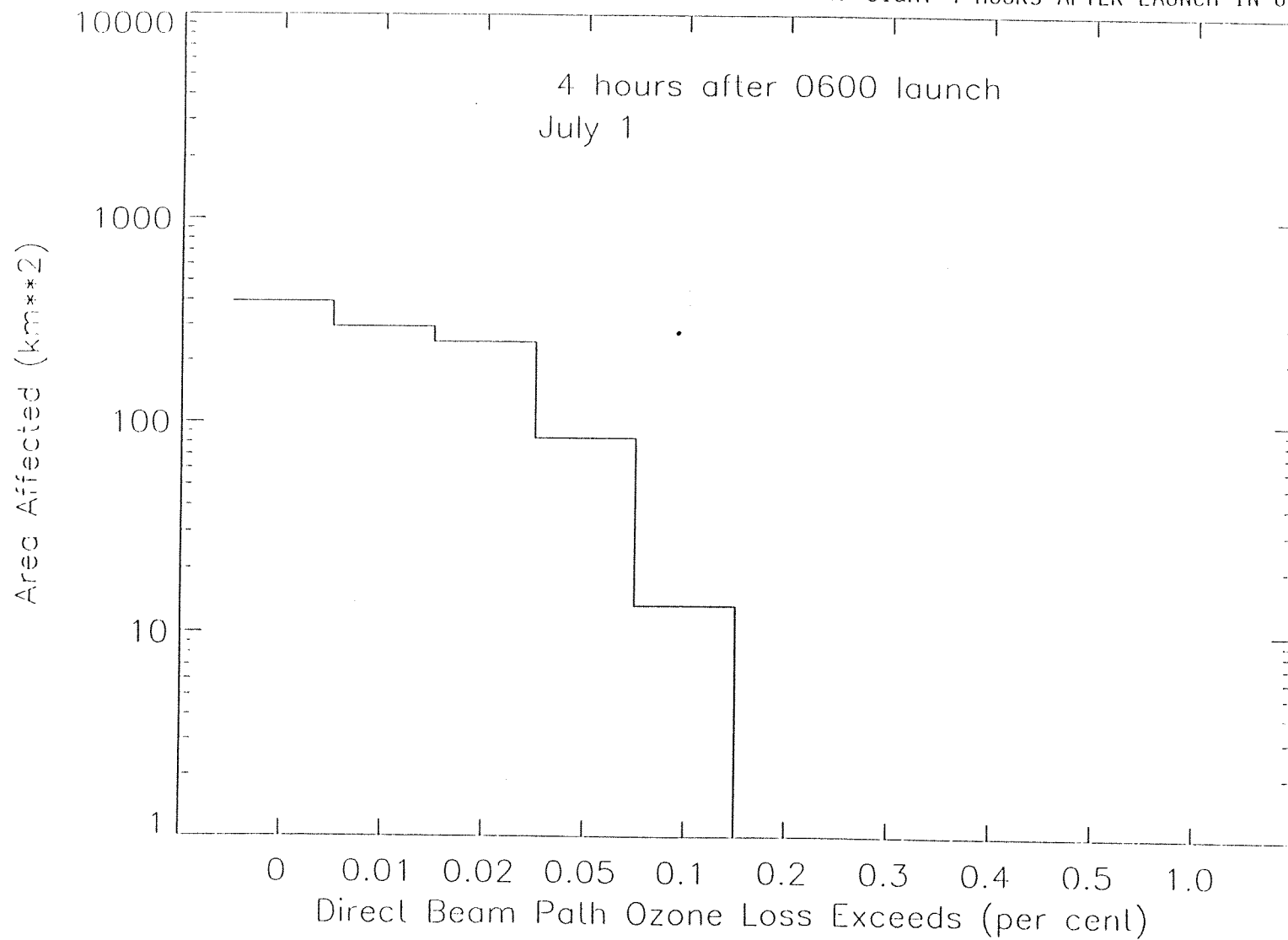
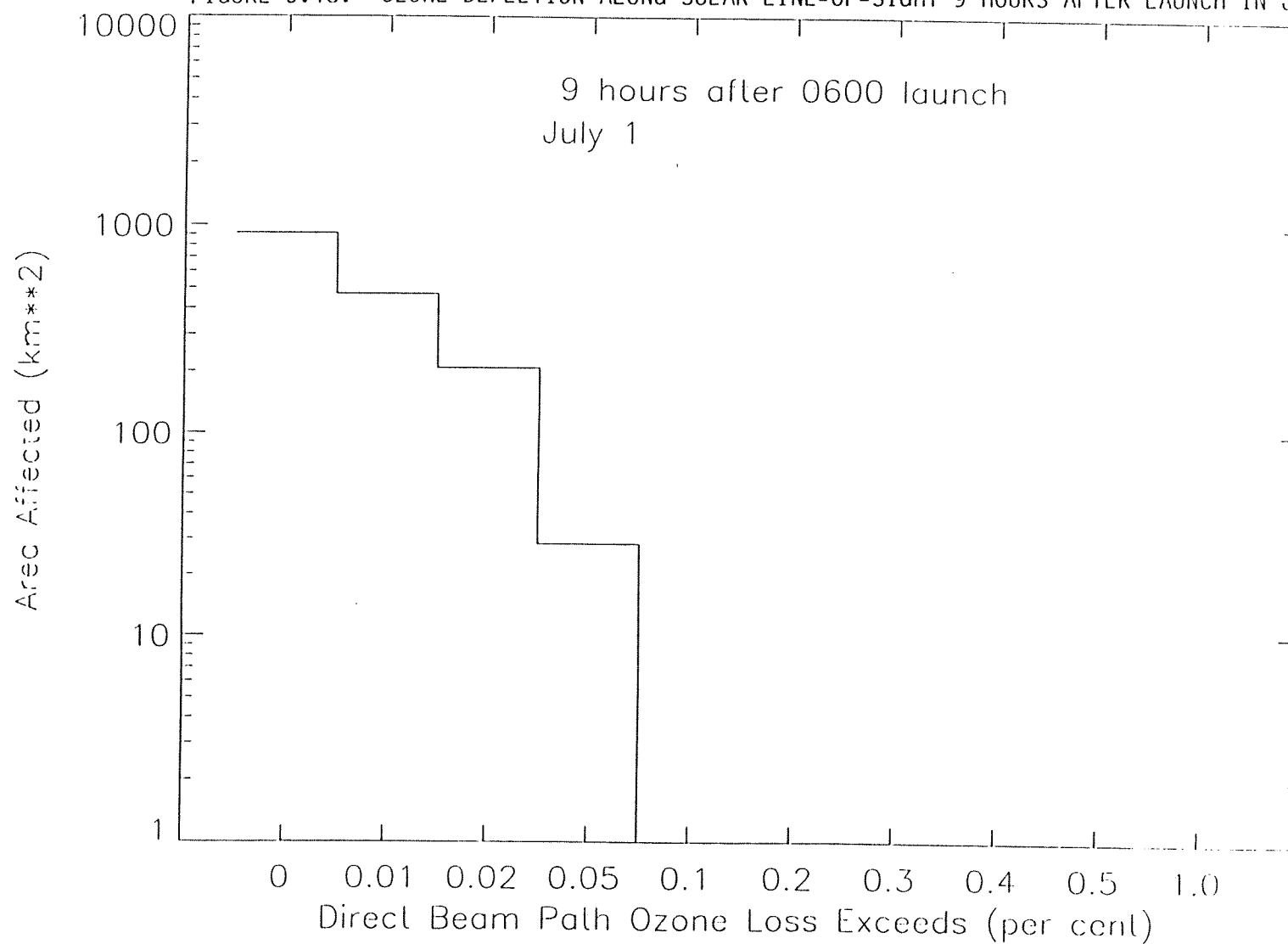


FIGURE 5.18. OZONE DEPLETION ALONG SOLAR LINE-OF-SIGHT 9 HOURS AFTER LAUNCH IN JULY.



LOCAL AND GLOBAL EFFECTS ON OZONE FROM TITAN ROCKET EXHAUST AND DEORBITING SPACECRAFT DEBRIS

A Draft Report Prepared for TRW

Peter S. Connell, John J. Walton, Joyce E. Penner, and Charles O'Connor
Lawrence Livermore National Laboratory
Livermore, CA 94550

Both the launching and deorbiting of spacecraft introduce foreign material directly into the stratosphere, a region of the atmosphere extending from around 12 to 50 km above the earth's surface. Human activities in general have little direct contact with the stratosphere (some aircraft operate in the lower stratosphere); most anthropogenic pollution of the stratosphere occurs through upward transport of long-lived gases. The question of similarities and differences between these two paths of pollutant introduction to the stratosphere arises naturally, and a careful evaluation of environmental risks associated with rocket launches is, of course, prudent.

Solid rocket motor combustion produces gases and particles that are injected into the stratosphere during the few minutes that the rocket traverses the region. Potential effects of solid rocket motor exhaust have been assessed before, with chief concern focused on the emitted chlorine-containing gases (Jackman et al., 1996, Prather et al., 1990 and Denison et al., 1994 and references therein). These earlier studies have considered topics including the global and zonally averaged effects of accumulated chlorine (Cl) emissions from indefinitely continued launch operations, the transient response to a single launch plume dispersed over a 1000 km spatial scale in a three-dimensional global model, and the early-time evolution of the plume composition in the seconds and minutes after exhaust. An important additional concern that we attempt to address in this report is the time period between establishment of the stabilized cold plume and its dispersal and the spatial range between the initial scale of hundreds of meters and the 1000 km scale of gridded global 3-D models. Can a vertically coherent region persist in which photochemical processes reduce ozone significantly?

The importance of chlorine in the stratosphere as a potentially efficient catalyzer of ozone destruction has been established over twenty years of research (WMO, 1995). The current level of abundance of inorganic chlorine-containing trace species, predominantly hydrochloric acid (HCl), in the stratosphere is about 3500 parts per trillion by volume (ppt v/v). Recent observations of these species, hydrofluoric acid (HF), and chlorofluorocarbons (CFCs) show that the surface-emitted CFCs account for the observed excess of chlorine over the naturally occurring level of around 600 ppt.

Launching of Titan and similar solid rocket motors adds to the stratospheric inorganic chlorine burden through emissions of HCl, atomic (Cl) and molecular (Cl₂) directly into the stratosphere. Before the exhaust plume disperses, plume concentrations of

these species are orders of magnitude above the background values (Denison et al, 1994). Dispersed through the stratosphere over the globe however, the additional Cl burden is small compared to the background for currently envisioned launch frequencies. Inorganic chlorine is cleared from the atmosphere by wet deposition of HCl in rain after transport processes return air from the stratosphere to the troposphere, with an overall lifetime of a few years. After several years, a continuing fixed injection rate will produce a chlorine enhancement that reaches a steady state, balanced with loss via rainout.

We report here on calculations in models in both two- and three-dimensions that address three questions in rocket/spacecraft/stratosphere interactions. We have attempted to represent the early evolution (1-50 hours) of a vertical plume in the stratosphere with a Lagrangian three-dimensional transport model driven by horizontal winds from a data-assimilating general circulation model. These horizontally sheared plume structures, illuminated by the sun, produce footprints on the surface. Depending on plume and solar orientation and plume dimensions, the possibility exists for ozone destruction in the path of the direct beam from the sun. We conducted simulations for launches in four different seasons (January, April, July, and October), surrounding a launch point (28 N, 280 E) representing Cape Canaveral.

We have also conducted global calculations of the potential steady state effects of Cl injection from a specified rate of continuous launches in a current two-dimensional model of the stratosphere including all known important ozone production and loss processes. In these calculations, we have used new estimates of the distribution of material injection as a function of altitude relevant to Titan and similar motors. The exhaust products are injected continuously and the integration is continued until the Cl enhancement levels to steady state. The distribution of the enhancement and the ozone response depend on season, latitude and launch latitude. The results support those obtained in earlier studies of Space Shuttle motor exhaust.

Finally, we have calculated the effect of increasing the steady state particulate surface area density in the stratosphere resulting from particle formation from satellite destruction on reentry. Recent stratospheric observations have demonstrated the importance of heterogeneous processes in affecting the trace constituent composition of the stratosphere and influencing the balance of ozone destroying processes. Of particular importance are processes that transform photochemically active nitrogen oxides into nitric acid, which is more stable, and processes that release active forms of chlorine from the relatively stable chlorine nitrate molecule. Laboratory studies indicate that chlorine nitrate decomposes by hydrolysis on alumina surfaces. This process, the collision of a gas phase chlorine nitrate molecule with an alumina particle, is included in the global two-dimensional model as a first order conversion of chlorine nitrate to hydrochlorous acid, HOCl, at a rate consistent with the alumina surface area density calculated to result from the reentry of orbiting spacecraft.

Data and Methodologies

Cold Plume Advection Model

The starting point for the exhaust plume advection calculations is the stabilized cold plume. The plume stabilizes when it reaches ambient temperature, after which its apparent radius is affected only by natural turbulent eddy diffusion. The plume is assumed to be axially symmetric, with the radius and exhaust composition provided by Wong and coworkers at TRW (Wong, TRW report, 1996; Denison et al, 1994) as functions of altitude in the stratosphere. While the TRW injection profile results from an analysis in which the vehicle flight profile pitches from the vertical while passing through the stratosphere, the assumption is made here that the plume is initially vertical. The profiles of radius and chlorine species concentrations are shown in Table 1.

Table 1. Cold Plume Parameter Profiles

Altitude (km)	Radius (m)	Cl	Cl ₂	HCl
7	118.8	1.22(10) ⁺	8.60(13)	1.09(15)
15	88.9	8.86(11)	2.08(14)	1.20(15)
20	111.7	1.75(12)	1.73(14)	4.65(14)
25	160.3	2.40(12)	1.14(14)	1.22(14)
30	214.5	3.60(12)	6.29(13)	3.34(13)
35	327.9	3.35(12)	1.88(13)	2.05(13)
40	398.6	7.39(12)	2.23(12)	2.71(13)

(E. Wong, TRW, private communication, 1996)

⁺ 1.22(10) = 1.22 x 10¹⁰

The plume is represented in the advection model by a vertical stack of parcels which are advected horizontally (in longitude and latitude) by winds provided by the NASA Goddard Space Flight Center Data Assimilation Office (DAO). The DAO STRATAN simulation of 1992 was used (Schubert et al., 1995), which is based on NMC and other data, and has a resolution of 4° in latitude by 5° in longitude, 25 vertical layers of which 15 are in the stratosphere, and 6 hours in time. The global three-dimensional model used here is the advection component of the GRANTOUR chemical transport model (Atherton et al., 1995). GRANTOUR is a Lagrangian parcel model in which the gridded horizontal velocities are interpolated in three dimensions to the parcel locations at every time step. In this case, advection was carried out with a one hour timestep, with gridded velocities updated every six hours. Vertical velocities were set to zero in this study, to avoid any potential numerical problems in inferring the vertical velocity from the horizontal wind

fields. Horizontal velocities are typically much faster than vertical velocities in the stratosphere.

Figures 1a-d and 2 a-d show three day average (solid lines) and instantaneous launch time (dashed line) vertical profiles of the horizontal wind components (meridional and zonal) for the four periods. Zonal winds are generally larger in magnitude than the meridional winds. At the launch latitude, the zonal wind direction is almost always from the west to the east (westerlies) except in summer when the direction reverses. Zonal wind velocities tend to increase with altitude in the winter and summer stratospheres. Meridional velocities at the launch latitude are southerlies (south to north or poleward) in the fall and winter and northerlies in the spring and summer and tend to be greater in the winter and spring. Given the horizontal resolution of the data assimilated wind products, the single profiles are similar to the time averages but can have variability with altitude similar to the average velocity magnitudes, for example the meridional velocities in April and October.

The advected parcels in GRANTOUR represent the centers of mass of the individual plume segments. As the simulation progresses, the 9 stratospheric plume parcels separate in horizontal location. Passage of the solar beam through the parcels projects their locations to the surface, according to parcel altitude and the declination and hour angle of the sun. The parcel locations are considered to be connected with 8 linear segments, representing the plume footprint at a particular time. The plume segments are assumed to maintain a circular horizontal section as they are sheared, so that a sheared plume segment can be visualized as a tilted stack of coins. Each segment represents a fraction of the total overhead column of ozone (shown in Figure 3), so that if the direct solar beam passes axially down the segment, that fraction of the total column can potentially be destroyed. If the solar beam intersects the plume segment at a sufficient angle, only a portion of that ozone column fraction would be affected by plume-related chemistry. From the hourly parcel locations, the sum of the segment footprints can be made in area and in fraction of the total ozone column that is affected by the plume.

Global Photochemistry Transport Model

In a global model, the dispersed chlorine contribution of a single launch and the transient response of ozone are quite small, and can be overwhelmed by drift in the integration of the background atmosphere and numerical significance. In this study we have considered a continuing series of launches, which produces a steady state enhancement of inorganic chlorine in the stratosphere and a steady state global ozone depletion. We used the LLNL two-dimensional model of photochemistry, dynamics, and radiation transport (Kinnison et al., 1994) to model this response for a launch frequency of 10 motors per year, continuing indefinitely. The model has a latitude resolution of 5° extending from pole to pole, and a vertical resolution of approximately 1.5 km, extending from the surface to 85 km. The third spatial dimension, longitude or the zonal direction, is averaged over the globe. The model predicts ozone abundance as a function of altitude, latitude, and season of the year, based on climatological temperature and self-consistently calculated fields of radiation and photochemical production and loss. Surface concentrations of trace gases

including N₂O, CFCs, and CH₄ are prescribed as boundary conditions, giving rise to the radical family photochemistry in the troposphere and stratosphere. The chemical mechanism incorporates about 50 species and 150 reactions.

A steady state reference atmosphere was calculated in which the source gas surface concentrations were prescribed at their observed 1990 values, producing a stratospheric burden of inorganic chlorine of about 3,500 parts per trillion. The plume exhaust was input over the single latitude zone between 25 and 30 N and vertically distributed according to the profile in Table 2.

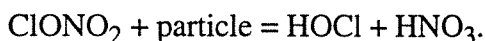
Table 2. Cl_y Injection Profile in Two-Dimensional Global Model Between 20 and 30 N Latitude.

Pressure (hPa)	Approximate Altitude (km)	Cl _y Injection Rate ⁺ (molecules/cm ³ /S)	Annual Cl _y Injection ⁺ (kt as Cl)
114	15.75	0.6189	30.9
92.3	17.25	0.5734	28.6
74.9	18.75	0.5353	26.7
60.9	20.25	0.5077	25.3
49.4	21.75	0.4905	24.5
40.1	23.25	0.4775	23.8
32.6	24.75	0.4610	23.0
26.4	26.25	0.4351	21.7
21.5	27.75	0.4071	20.3
17.4	29.25	0.3851	19.2
14.2	30.75	0.3743	18.7
11.5	32.25	0.3687	18.4
9.33	33.75	0.3552	17.7
7.58	35.25	0.3274	16.3
6.15	36.75	0.2950	14.7
4.99	38.25	0.2818	14.1
4.06	39.75	0.3040	15.2
3.29	41.25	0.3748	18.7

⁺10 motors/year

Because the input material must be dispersed meridionally over 500 km and zonally averaged around the globe, this calculation represents the response smoothed over several weeks. In this case, the input can be considered to exist entirely in the form of HCl, which is formed rapidly from Cl (and Cl₂) by reaction with the large background abundance of methane. For this run, the HCl injection was performed continuously through the integration, at a flux that summed over the year to 10 Titan motor launches, or 378,000 kg of Cl deposited into the stratosphere each year. To provide the most accurate comparison, the self-consistently derived atmospheric circulation from the reference atmosphere was prescribed for the launch-perturbed model run. The perturbations to Cl_y and ozone were calculated by difference in the fifth year of runs with and without the additional HCl input.

The LLNL two-dimensional model was also used to investigate the potential effects of ClONO₂ activation on aluminum oxide particles formed from disintegrated reentrant satellites. The reference atmosphere described above was again used. In this study the perturbation took the form of an additional term in the calculated rate constant for the reaction



The background rate constant depends on sulfuric acid aerosol surface area density and local temperature. Two values for the perturbation term were used, 5.0E-9 and 5.0E-8 seconds⁻¹. These terms were applied throughout the stratosphere and produce an augmented rate of HOCl production in the range of the TRW calculations (Wong, personal communication). The results were again determined by difference from the reference atmosphere after a suitable period of integration demonstrated that steady state had been reached.

Results

Cold Plume Advection Model

The cold plume advection calculations follow the plume evolution under representative episodic conditions for four seasons. Figures 1 and 2 above showed the horizontal winds for the selected time periods. Figure 4 shows the locations of the advected parcels from the launch time at 6 am local solar time to 12 hours after launch. The parcel traces are numbered in ascending order with altitude. The launch point is indicated by a square, and the longitudinal coordinate has been adjusted in the figures to be commensurate in distance with the latitude. One degree in both directions is roughly 100 km. The prevailing zonal winds move the plume generally to the east in all seasons except summer (July), most rapidly away from the launch longitude in winter (January) and summer. The upper parcels generally move more rapidly than the lower segments and can cover more than 1000 km in the first 12 hours. More importantly for the consideration of spatially coherent "holes" in the vertical, the plume spread top to bottom over the first 12 hours varies from a few hundred kilometers in October to 1500 km in January.

Figure 5 shows the tracks of the "shadows" the parcels make on the surface as they move and are illuminated by the sun over the daylight period following launch. These

calculations use the plane parallel approximation which is less reasonable at solar zenith angles exceeding 85 degrees, so no projections were made under these grazing incidence conditions. The atmospheric pathlength under these conditions is long and little ultraviolet reaches the surface in any case, so that this is not a problematic assumption. Comparing Figures 4 and 5, the effect of the changing solar zenith angle is seen in October, when the plume lingers around the launch point. The parcel footprints travel from west to east as the apparent solar location travels from east to west.

The footprint of the entire plume at the surface is formed by linearly connecting the "shadows" of the vertically adjacent parcels, producing a series of linked rectangles at the surface, with length determined by the parcel "shadow" locations and width determined, in the absence of diffusion, by the plume radius as a function of altitude. Figures 6 a-e through 9 a-e depict the time-evolving plume footprints. The specified cold plume radius increases with altitude and this is indicated by greater line thickness for the higher altitude plume segments (although not to scale). Latitude and longitude are not necessarily plotted to the same distance scale in these plots.

Each plume segment represents a fraction of the vertical overhead column of ozone (i.e. 10%), and, if sufficiently aligned in azimuth and zenith angle with the sun, the projected shadowed area for that segment could potentially be depleted in ozone to that corresponding extent (10%). For each segment, the area affected and the ozone loss potentially realized will also be inversely related. If sunlight passes through a segment at an oblique angle, the potential fractional ozone loss is related to the ratio of the plume thickness along the path of the direct beam to the vertical layer thickness that the segment represents. Additionally, the projections of different plume segments can intersect on the surface, producing an area subject to ozone depletion from more than one vertical segment.

From the combination of azimuths and zenith angles for the plume and the sun, we calculated the areas subject to potential ozone loss for a series of hourly intervals for the four seasons. The assumption was made, discussed further below, that the plume is devoid of ozone and that ozone outside the plume was unaffected. These results are shown in Figures 10 a-e through 13 a-e. As expected, the area affected grows as the plume segments are stretched, but the magnitude of the corresponding potential ozone loss diminishes with time. As also expected, the peak potential ozone losses occur for the April and October launches, when lower wind speeds allow the plume to remain more compact. The peak potential depletions are on the order of 1% occurring in the first few hours after launch, and affecting areas of a few square kilometers. In general, by several hours after launch, the peak potential depletion is about 0.1% over an area less than 10 square kilometers. At a potential depletion level of 0.01%, the area affected is between 100 and 1000 square kilometers. The effect of alignment of a plume segment with the solar position can be seen in the October calculation, where at 7 hours after launch (Figure 13d), the peak magnitude increases to between 0.3 and 0.4% because of the position of the sixth plume segment (Figure 9d).

Although these calculations are merely representative of four episodic atmospheric states and can not rule out the possibility of an alignment of multiple plume segments with the sun that would produce a significant ozone hole, they do indicate that such an event is apparently unlikely and increasingly so beyond a few hours after launch. A potential depletion of 1% is significantly smaller than the naturally occurring variability in overhead ozone column at both seasonal and shorter time scales, and the transient nature of the plume effect further reduces any related effects to below a reasonable level of concern.

There are several relevant considerations in the interpretation of these results. The data assimilation model that generates the winds used here is coarsely gridded in the horizontal (400 by 500 km) relative to the plume dimensions in the early hours after launch. It is also coarsely gridded in the vertical relative to sharp features (100 meter thickness) in the stratosphere often observed by in situ instruments that are presumably related to vertical shears in the horizontal winds. A more finely resolved picture of the stratospheric winds might increase the area affected by increasing the length of the more tortuous plume footprint, but might not increase the peak potential depletion as the likelihood of solar/plume alignment extending over a significant depth would be reduced in the more structured plume.

Growth of the plume radius by diffusion and the accompanying entrainment of ambient air into the spreading plume has not been considered here. Observations of plumes in the stratosphere appear to show a degree of integrity over the few hour time scale while they are sheared by the winds (Prather, private communication), so this assumption may be justified. Estimation of diffusion coefficients related to stratospheric small scale eddy turbulence is difficult and the time scales obtained tend to be short (order of minutes, Denison et al, 1994), in contrast to the apparent integrity of plumes in the stratosphere. When the plume has dispersed over the 1000 km scale after a day or two, Prather and coworkers have shown that the contribution of the chlorine from the exhaust has dropped to the 1% level over background and will be mostly tied up as inactive HCl. At early times, the very high initial levels of atomic chlorine can rapidly deplete ozone in the plume, so that these calculations, assuming total ozone loss, may represent a "worst case". Whether the competing time scales of shearing and diffusing could produce a plume a few hours old that is enlarged in radius, devoid of ozone through fast catalytic destruction, and compact with respect to shear can not be answered with the model used here. But the results of Denison and coworkers (1994) seem to show that photochemical ozone-destroying processes are too slow to keep ambient ozone from entraining and refilling the plume even after just a few minutes. Additionally, the lifetime of atomic chlorine with respect to reaction with methane and conversion to HCl is on the order of minutes. These considerations would indicate that a non-diffusing plume scenario might indeed be conservative in assessing the risks of ozone depletion.

Global Steady State Cl Perturbation and Response

The effect on stratospheric ozone of an indefinitely continuing constant rate of launches will reach a steady state when the transport-driven removal of the injected chlorine

(by the irreversible transfer of HCl from stratosphere to troposphere) balances the rate of input. In this steady state condition, a seasonally varying but annually periodic enhancement exists in the abundance of stratospheric inorganic chlorine species. As noted above, the current level of Cl_y in the mid and upper stratosphere is about 3,500 ppt and results mostly from CFC photolysis. The distribution calculated by the model in a steady state representation of current CFC surface abundances is shown in Figure 14 a and b for northern hemisphere winter and summer. The shape results from higher average illumination at the equator, yielding greater Cl release there, and the mean downward and poleward circulation in each hemisphere. To this background a continuous constant injection of HCl in the latitude bin 25 - 30 N distributed in altitude between 15 and 42 km was added. After 5 years of integration a steady state was effectively reached. The stratospheric lifetime of the added HCl, determined by dividing the stratospheric burden of excess Cl_y by the injection rate, gives a value of 2.3 years. The amount of the enhancement at steady state thus corresponds to the input from about 23 motors in this scenario (note that a single launch may involve more than one motor).

Figures 15 a and b show the resulting distribution of Cl_y enhancement in ppt for the calculated scenario of ten Titan motor launches per year. Seven ppt corresponds to 0.2% increase above the reference stratospheric Cl_y . The effects of seasonal changes in circulation can be seen by comparing the summer and winter enhancements. The peak January enhancement is between 5 and 6 ppt over a 30 degree range north of the launch latitude. Meridional circulation is stronger in the winter and moves the injected Cl_y downward and poleward. The weaker circulation in the northern hemisphere summer allows the additional Cl_y to remain longer at the launch latitude, increasing the local peak value to more than 7 ppt and leading to noticeable interhemispheric transport in the upper stratosphere. The southern hemisphere enhancement at steady state is about half of the northern hemisphere values.

The distribution of the change in ozone depends not only on the Cl_y perturbation, but also on transport and photochemical time constants and on interaction of the radical families. The maximum January destruction of -0.07% occurs at the northern and upper edge of the Cl_y peak (Figure 16a). Photochemical destruction of ozone is continuing as the air moves north through the region of high Cl_y , but is eventually slowed by the loss of solar illumination. In the southern hemisphere summer, the maximum loss is at the sunlit pole and is about half of the northern value, consistent with the Cl_y enhancement. In July (Figure 16b) the ozone loss is spread over a greater portion of the northern hemisphere and the maximum of about -0.06% occurs at the pole. Little depletion occurs in either season in the mid and lower stratosphere, where the Cl_y increase is smaller and other ozone loss processes dominate. These local responses are quite similar to the results of Prather and coworkers (1990), after scaling for their somewhat larger injection rate.

Figure 17 shows the change in total column ozone at all latitudes and seasons. The global and annual average depletion is -0.006%. The peak column losses are in the polar latitudes in the respective spring, about -0.025% in the northern hemisphere and somewhat

smaller in the southern. Depletion between 60 N and 60 S is between -0.005 and -0.010%, with little seasonal or latitudinal variation.

Global Steady State ClONO₂/Aluminum Oxide Reaction and Response

Deorbiting debris is found mostly in the form of Al₂O₃ particles, at a density of perhaps 0.1 - 1 particle per cubic meter (Wong, private communication) evenly dispersed throughout the stratosphere. Laboratory studies (Molina, 1996) have indicated that these particles may serve as sites for activation of ClONO₂, that is production of active Cl species by reaction of ClONO₂ on collision with the particle surface. This process occurs in the reference model atmosphere on the surface of sulfuric acid aerosol particles in the reaction $\text{ClONO}_2 + \text{H}_2\text{O}(\text{particle}) = \text{HOCl} + \text{HNO}_3$.

The HOCl is rapidly photolyzed, releasing the Cl to participate in ozone-destroying catalytic cycles. The presence of additional particles will augment this process, particularly at mid and low latitudes, where the sulfate aerosol particles are less efficient partners (because of lower water activity at higher temperatures). Wong has estimated that each of these particles can activate between 2E4 and 2E6 Cl per second, for a production rate of between 2E3 and 2E6 Cl per cubic meter per second. At the typical ClONO₂ stratospheric density of around 4E14 ClONO₂ per cubic meter, a first order rate constant of about 5E-9 s⁻¹ gives a processing rate of 2E6 m⁻³ s⁻¹. This first order rate constant value was specified throughout the stratosphere (designated as Case A). The actual distribution in March of ClONO₂ activation through this process is shown in Figure 18 and can be compared to sulfate activation of ClONO₂ in the reference atmosphere shown in Figure 19. Debris particle activation is between 1 and 4E6 Cl m⁻³ s⁻¹ through much of the stratosphere. It is higher in the northern hemisphere polar spring, where polar stratospheric cloud activation of HCl has produced high ClONO₂ densities. It is lower in the upper stratosphere, where ClONO₂ densities are diminished. A second case (B), was run in which the activation rate constant was increased an order of magnitude to 5E-8 s⁻¹ to ensure a numerically significant perturbation result.

Figure 20 shows the change in overhead column ozone at steady state for Case A. The global annual average ozone loss is -0.01%. As expected for small perturbations, the effect is linearly proportional to the forcing. Case B shows an average loss of -0.1%, with an essentially identical distribution in latitude and season to Case A*10. The largest losses occur in the polar springtimes, when ClONO₂ levels are enhanced by wintertime processing of HCl in the polar vortices. For short days and high levels of ClONO₂, activation by the debris particles is more competitive with ClONO₂ photolysis and produces a larger relative enhancement of active Cl species. Overhead column ozone is reduced by up to -0.07% at high southern latitudes in October. Northern hemisphere values in March are reduced by up to -0.02%. The effect is smaller in the northern hemisphere because the NH winter pole is warmer and polar activation of HCl is less efficient.

Conclusions

None of the effects of rocket motor and spacecraft operation considered here produces a significant impact on stratospheric ozone. From the global standpoint, material injected into the stratosphere during launch or deorbit has stratospheric residence lifetimes of a few years or less, which serves to limit the steady state burden. A single motor launch per year is calculated to reduce globally and annually averaged ozone by -0.0006%, with a maximum column loss at the surface of about -0.002%. These values can probably be scaled to 1000 launches per year, at which the effect (-0.6% globally and -2% maximum) is on the order of current assessments for High Speed Civil Transport fleets. Deorbiting debris particles produce an effect through activation of existing stratospheric Cl on the same order of magnitude as the additional Cl injection of 10 motors launched per year. The debris contribution to Cl activation will be substantially overshadowed by volcanic activity. Additionally, as stratospheric Cl_y diminishes in the next century because of CFC controls, the availability of ClONO_2 to activate will drop and the debris effect will diminish. The expected downward trend in ambient Cl_y levels may enhance the importance of exhaust Cl_y , however. As the balance of ozone-controlling processes changes with reduced Cl_y , the exhaust contribution will become proportionally larger. This effect deserves continued analysis.

In consideration of local ozone loss under the exhaust plume, our calculations indicate that the plume is sheared and stretched rapidly in the horizontal over just a few hours, reducing the possibility of an ozone hole with a significant depth. Local effects at the surface of up to -1% over regions of less than 10 km^2 were calculated for the less dynamically active spring and fall periods. In summer and winter, the maximum line of sight loss was around -0.5%. Regions up to 1000 km^2 are affected at levels of -0.01% in all four seasons. A more highly resolved treatment of horizontal wind velocities is not likely to increase the extent of the line of sight ozone depletions. Consideration of turbulent eddy diffusion as the plume is sheared may increase the area affected and could increase the integrated total ozone loss through processing of entrained ambient air, but indications are that photochemical processes in an entraining plume are not fast enough to keep ozone completely depressed, while processes that deactivate chlorine are quite fast. This problem could also be analyzed further with a more sophisticated chemistry/diffusion/trajectory model. In any case, daily and seasonal natural variability in overhead ozone substantially exceed these calculated effects.

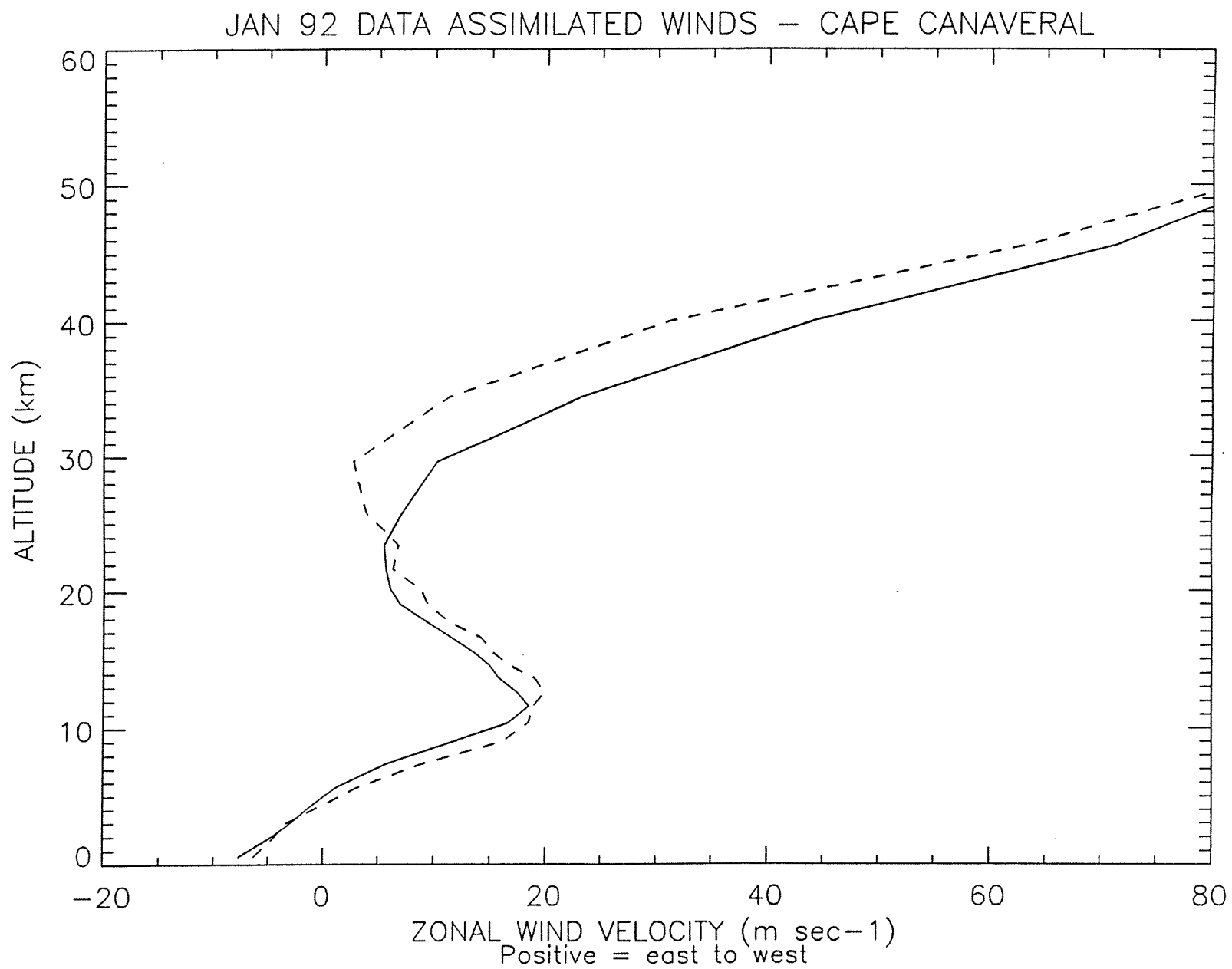


Figure 1a

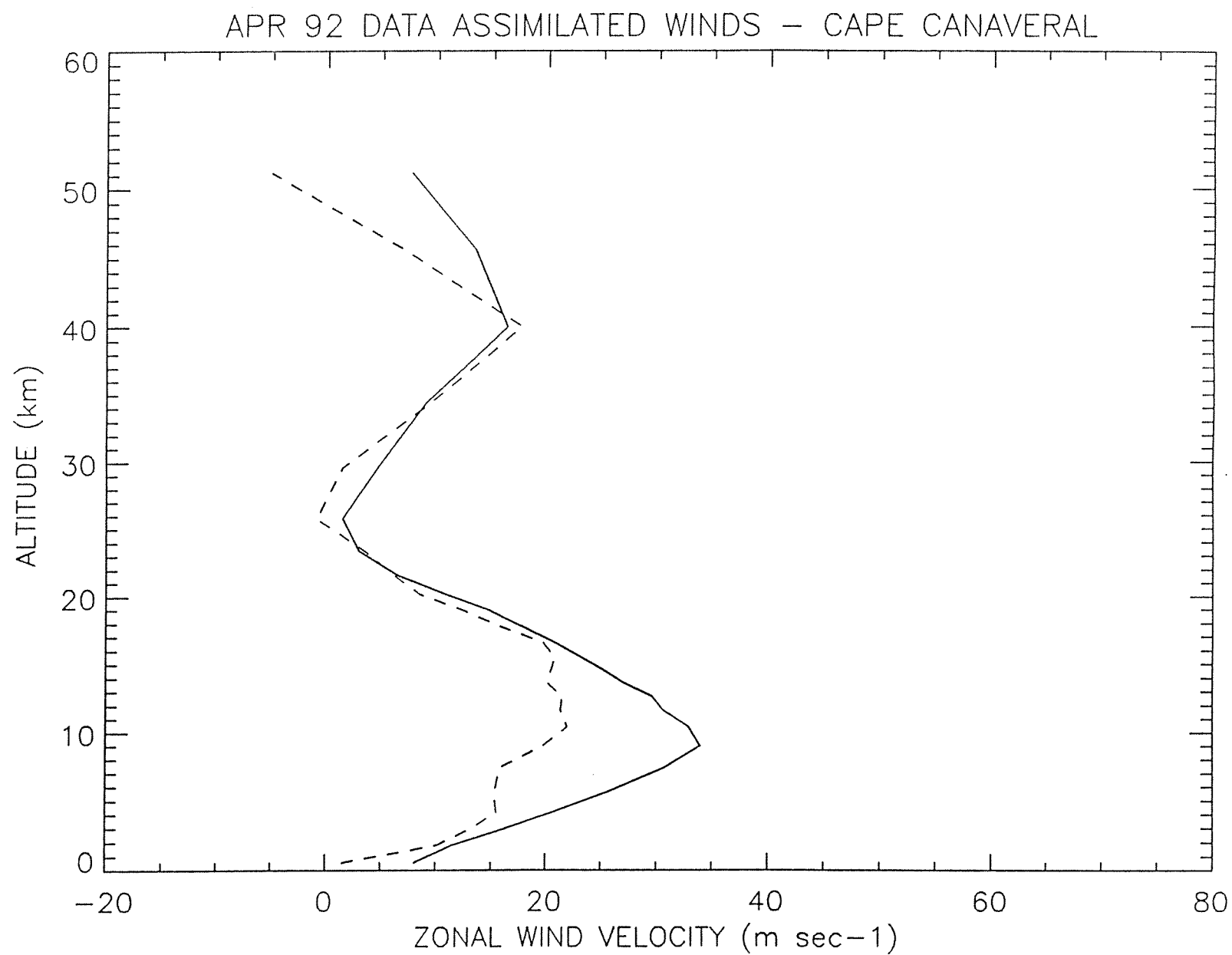


Figure 1b

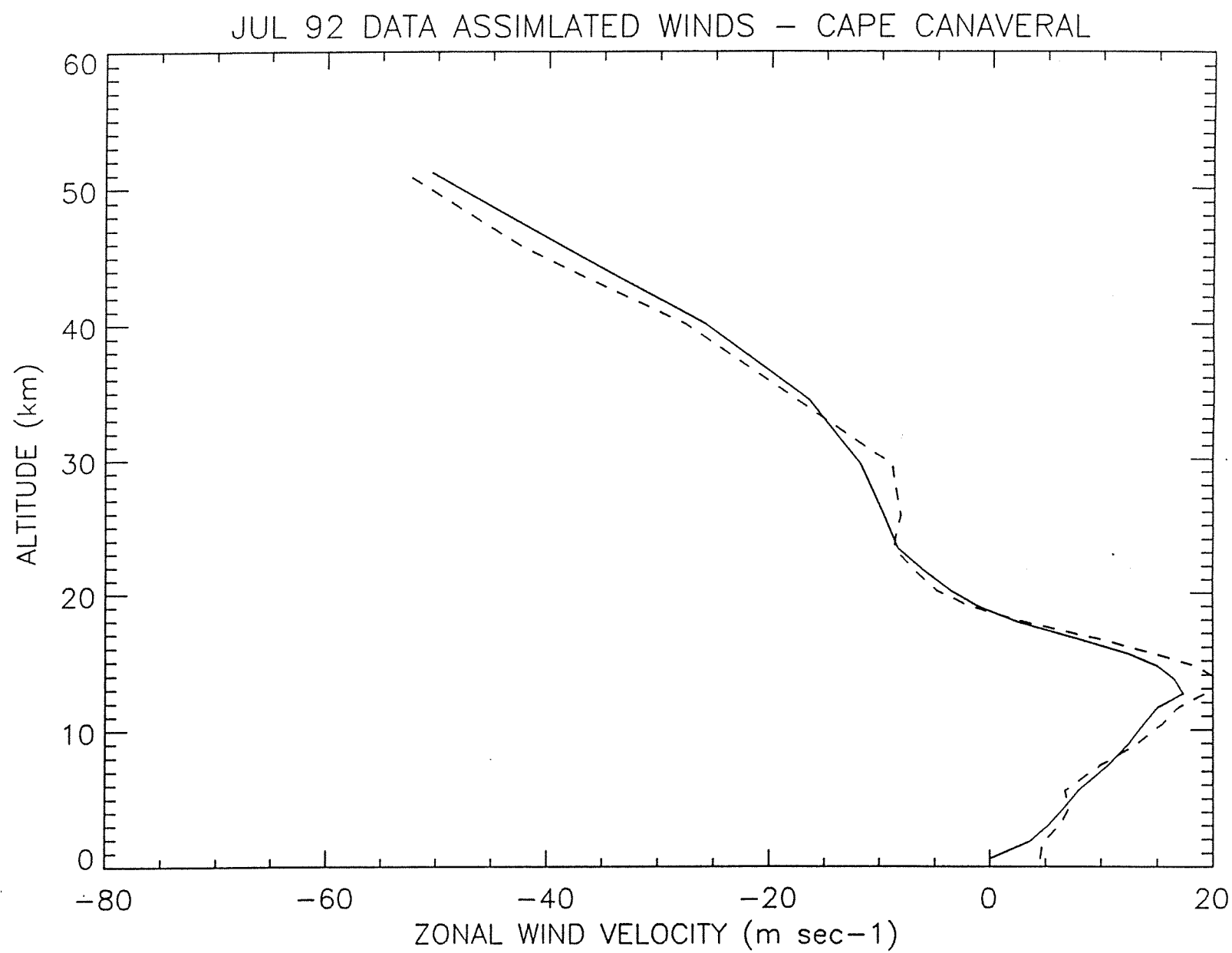


Figure 1c

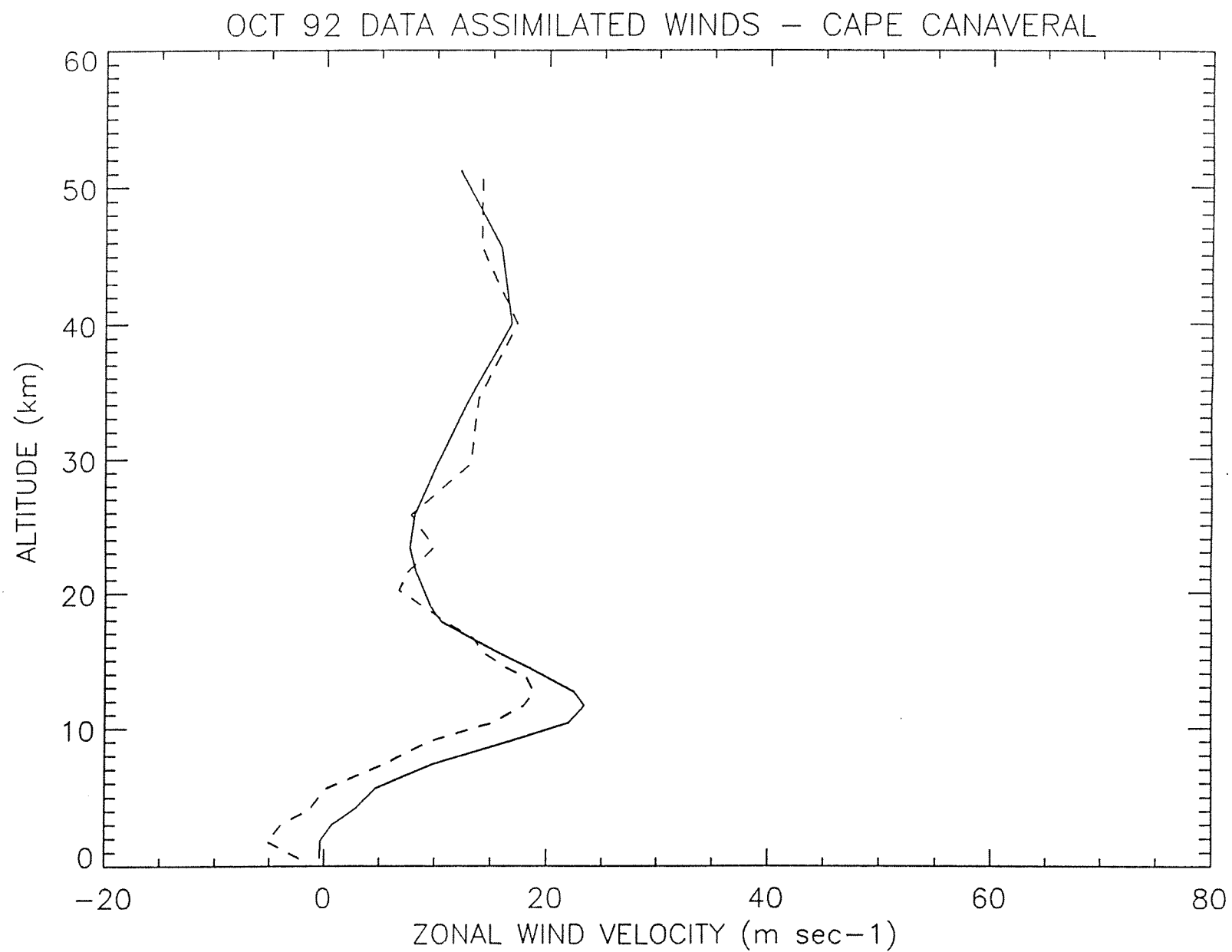


Figure 1d

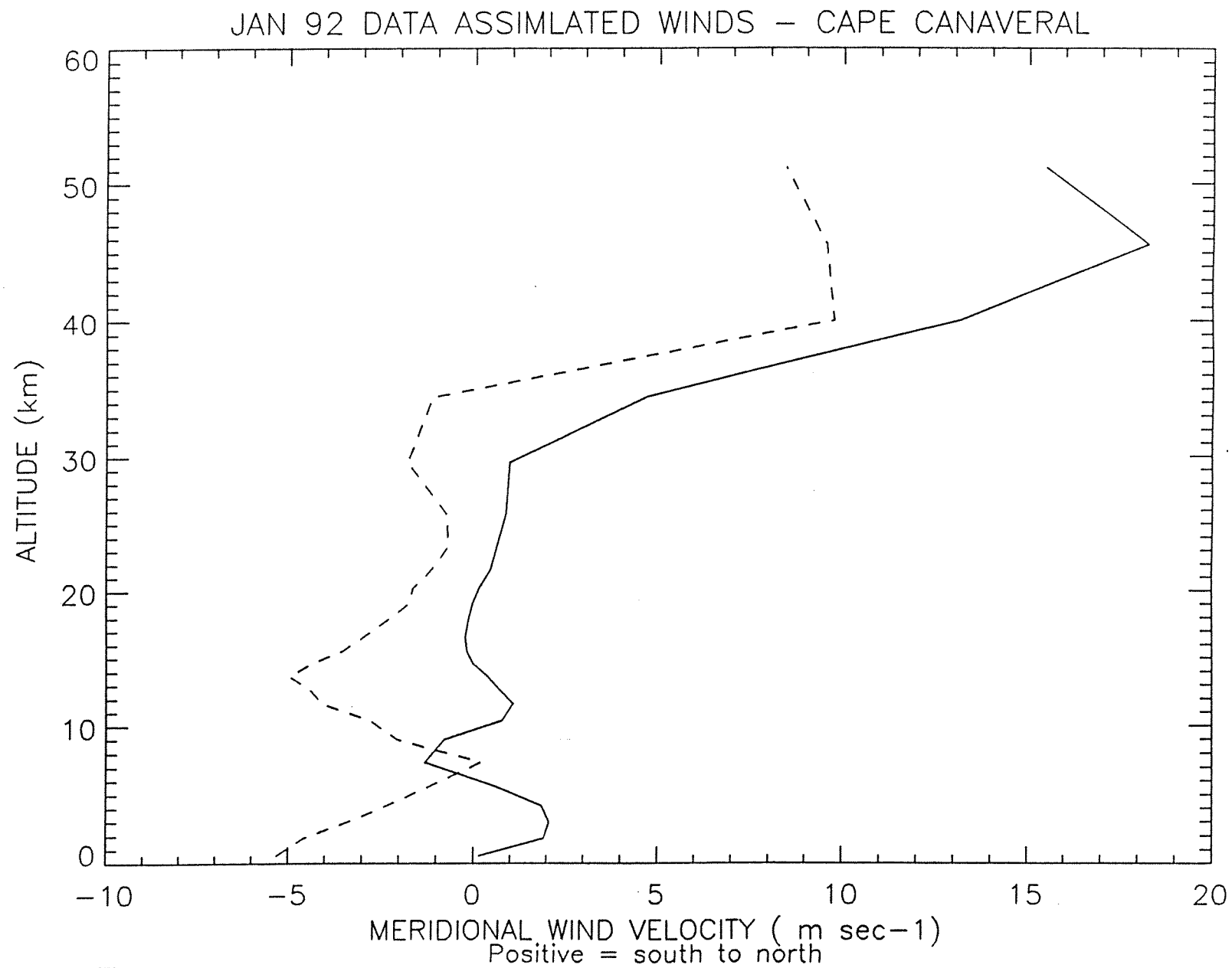


Figure 2a

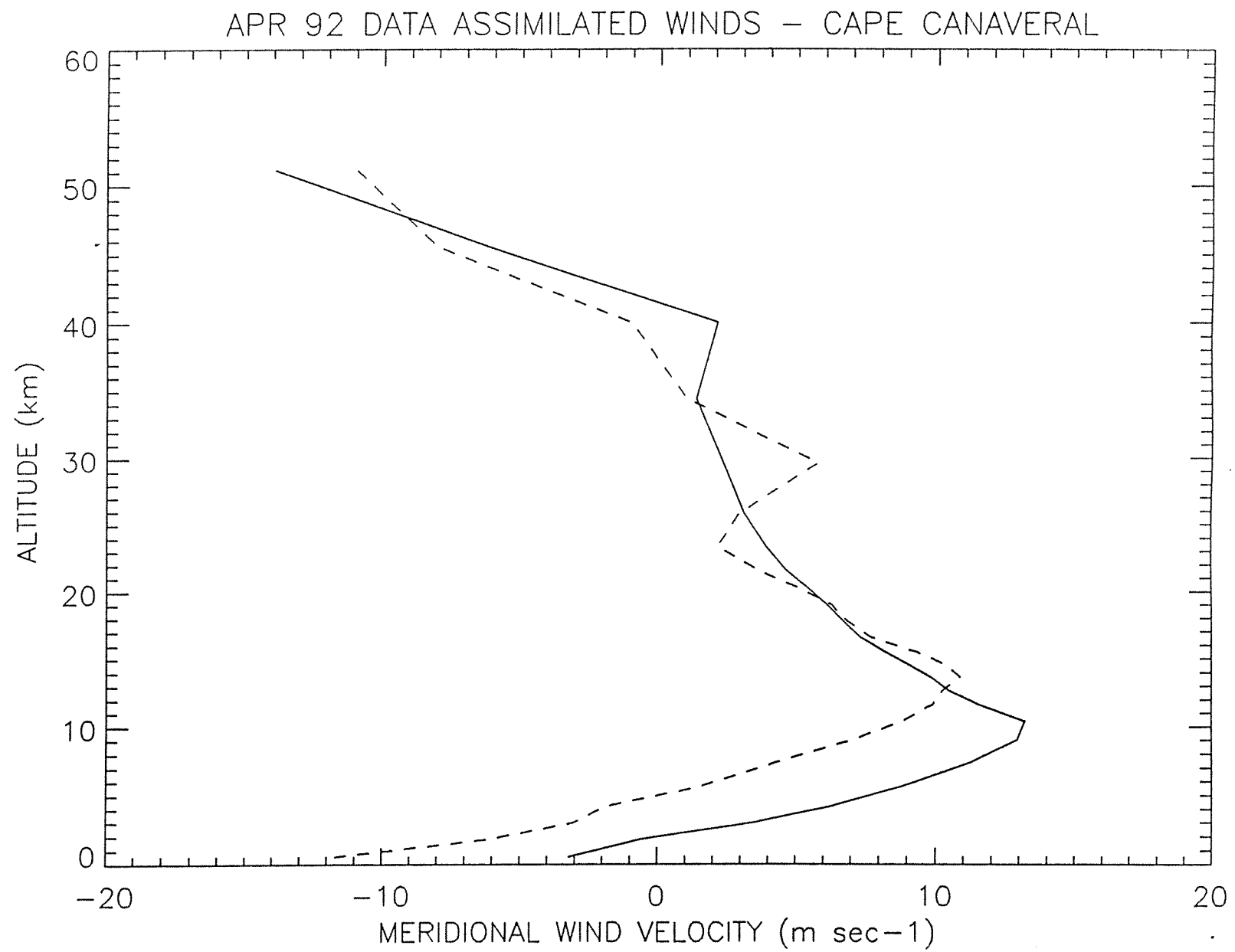


Figure 2b

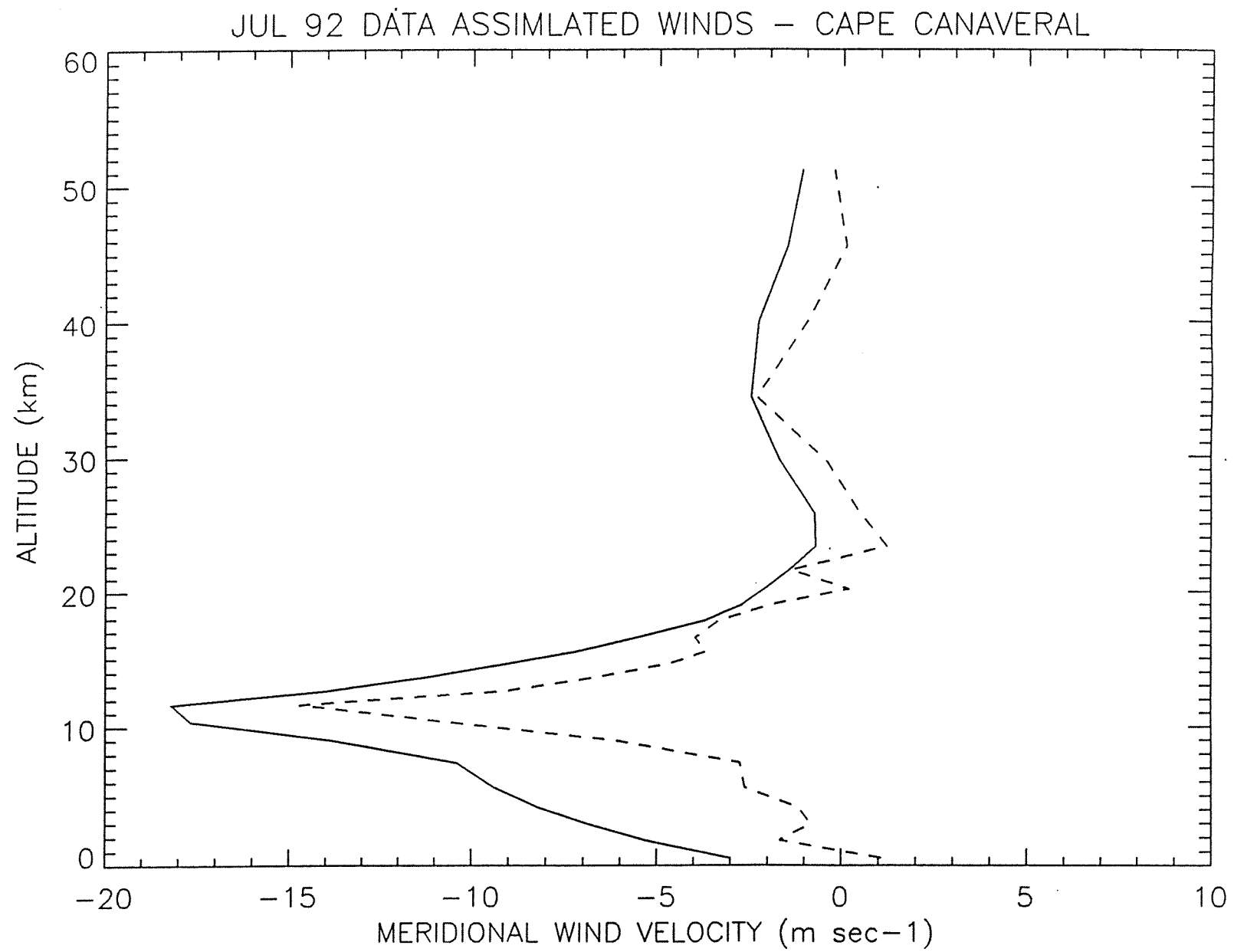


Figure 2c

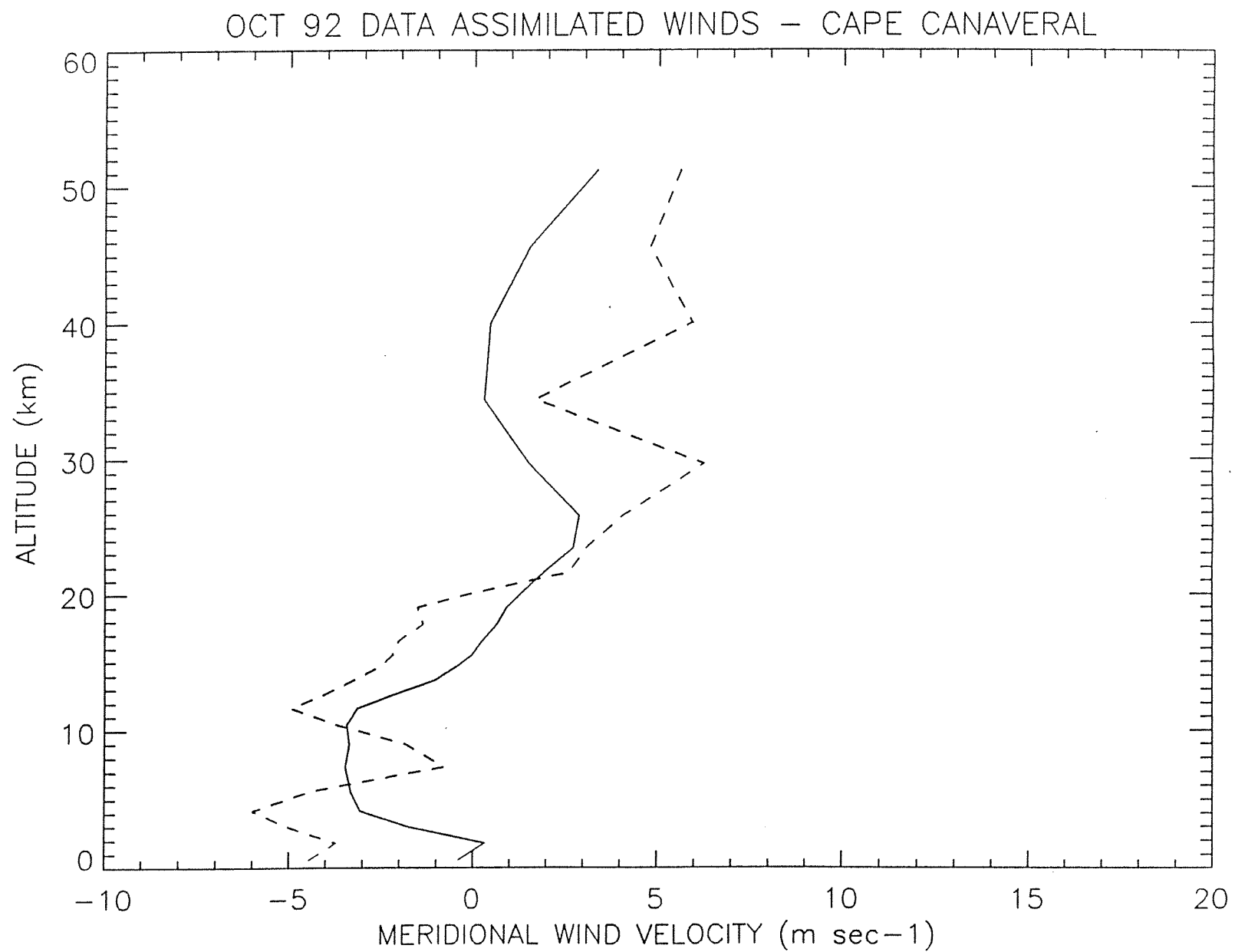


Figure 2d

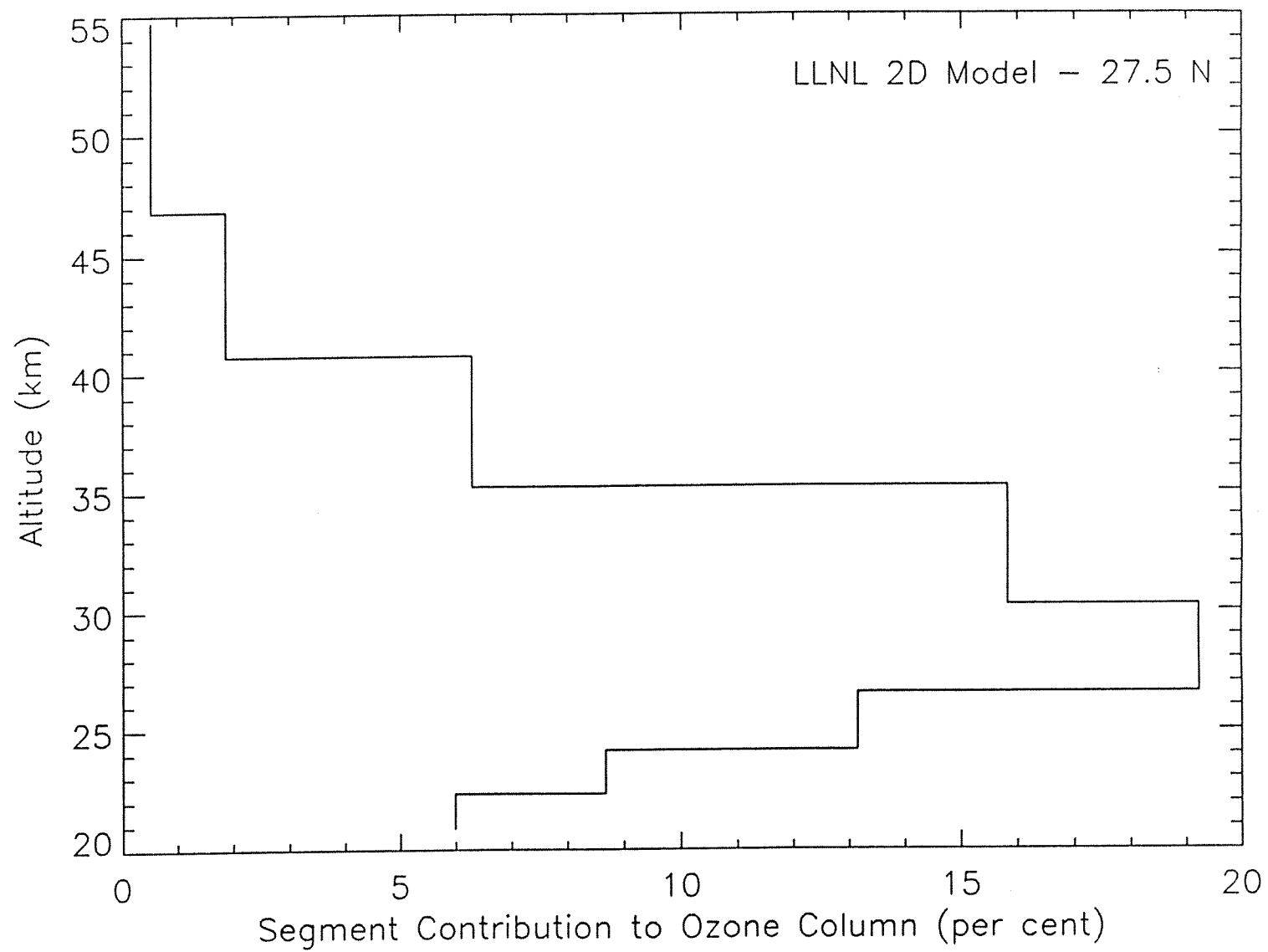


Figure 3

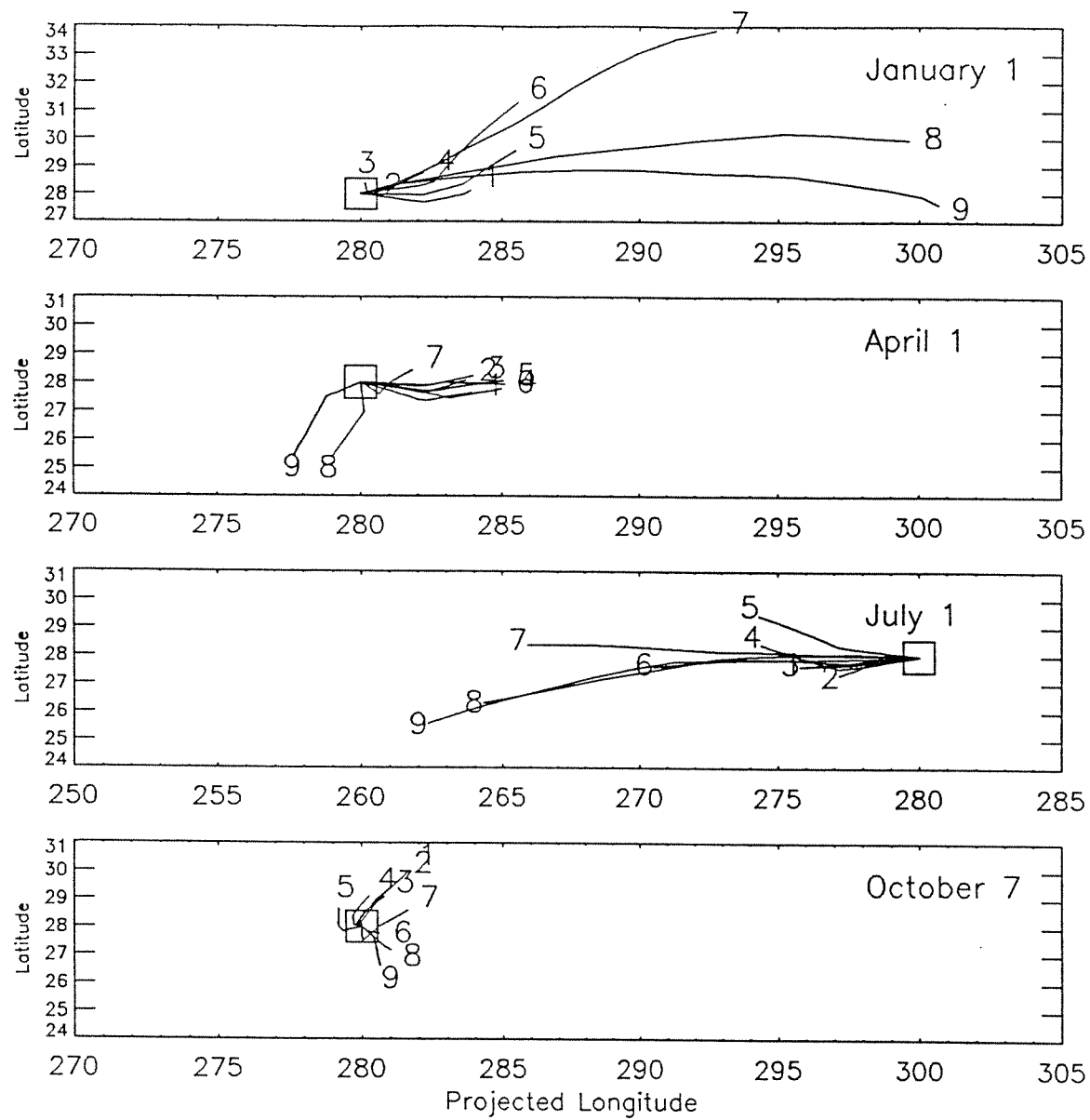


Figure 4

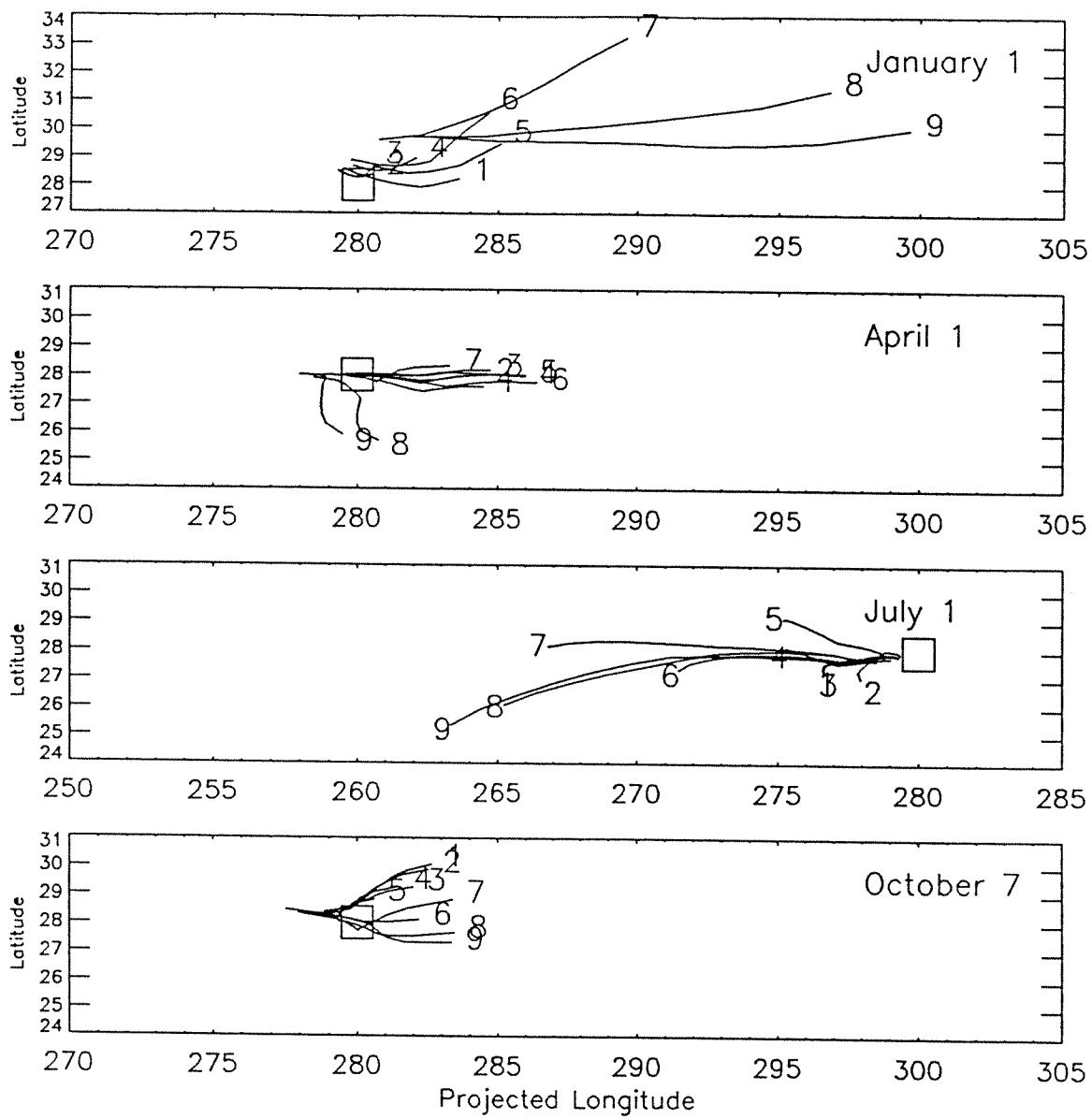


Figure 5

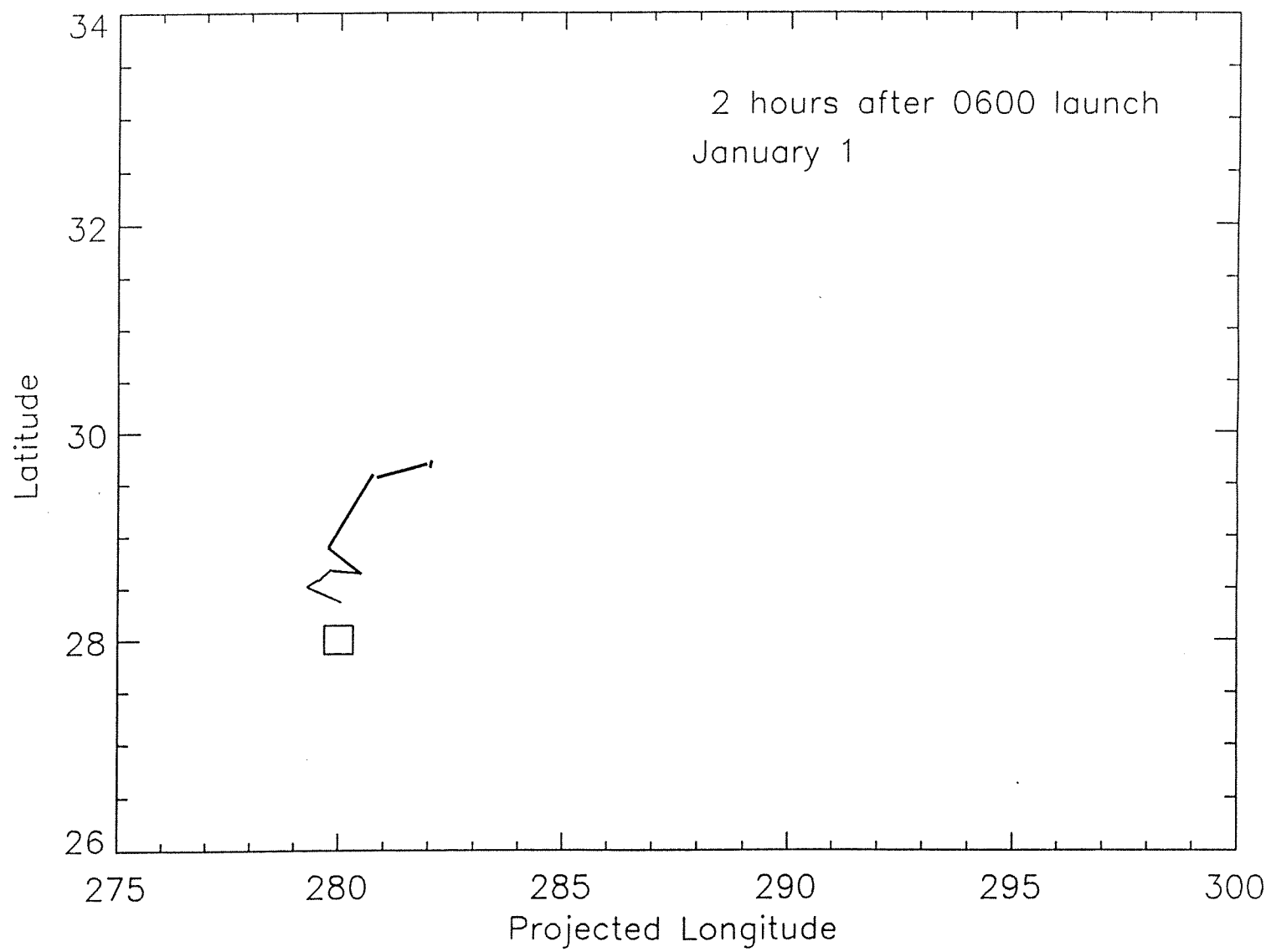


Figure 6a

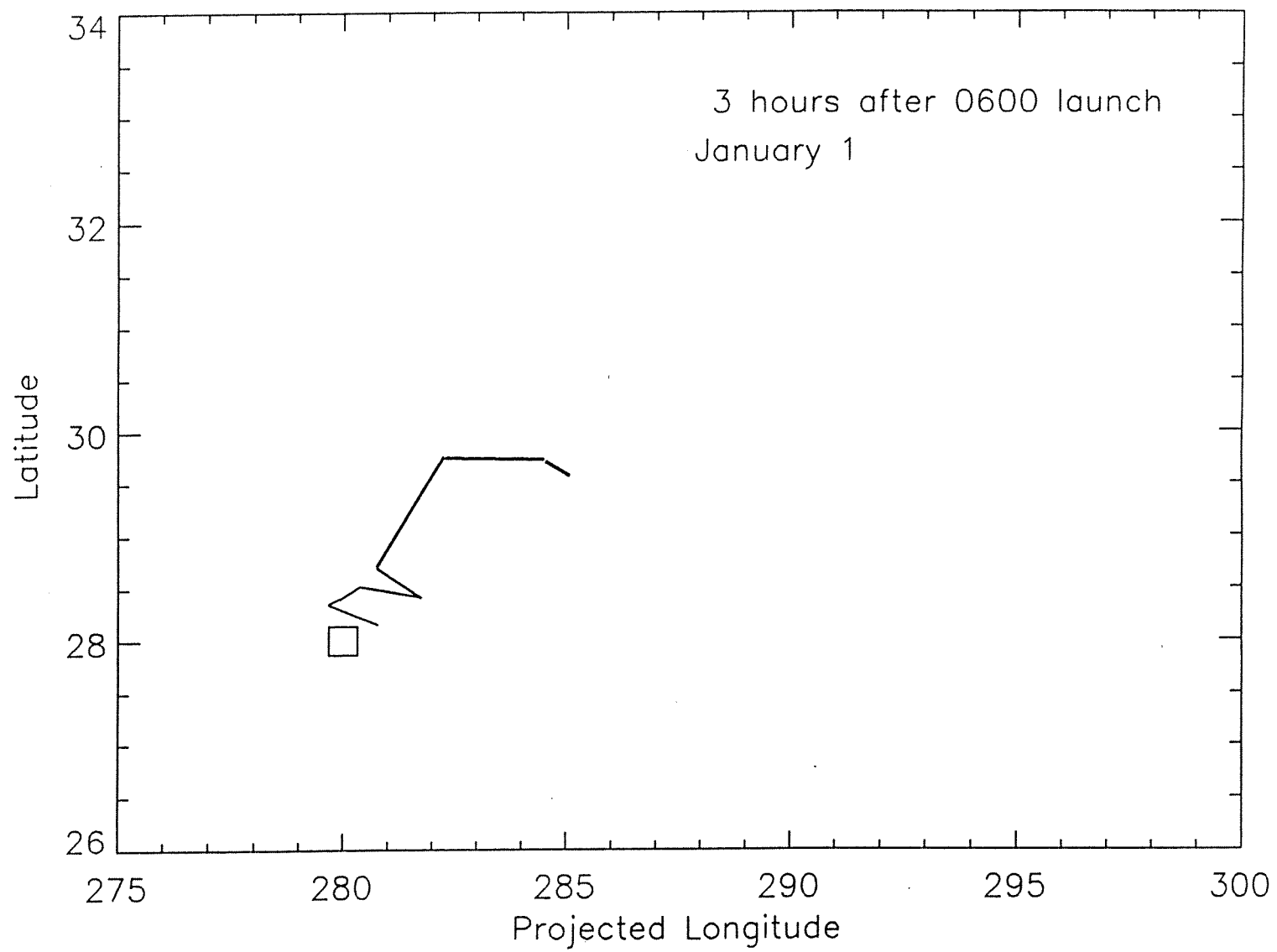


Figure 6b

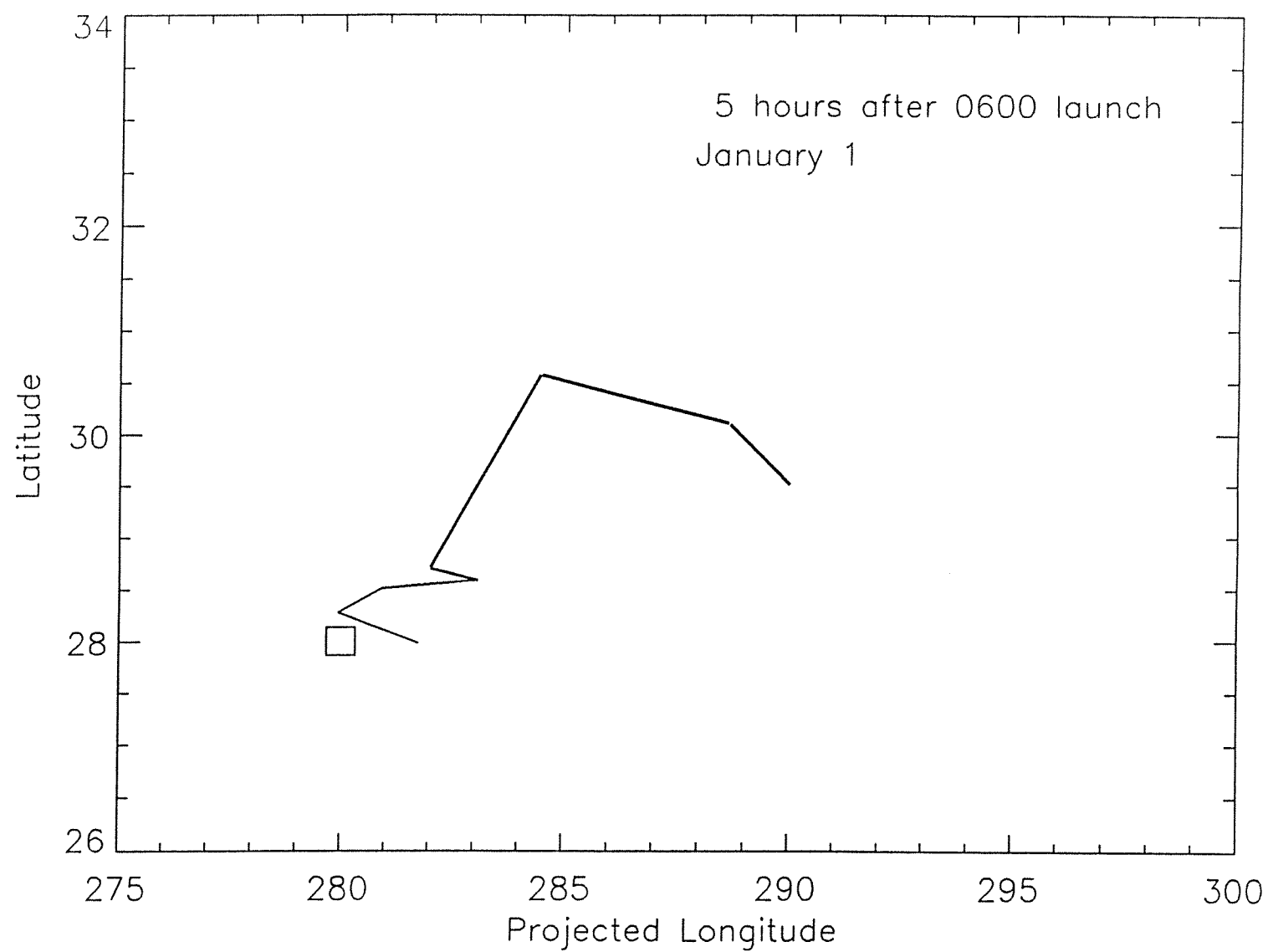


Figure 6c

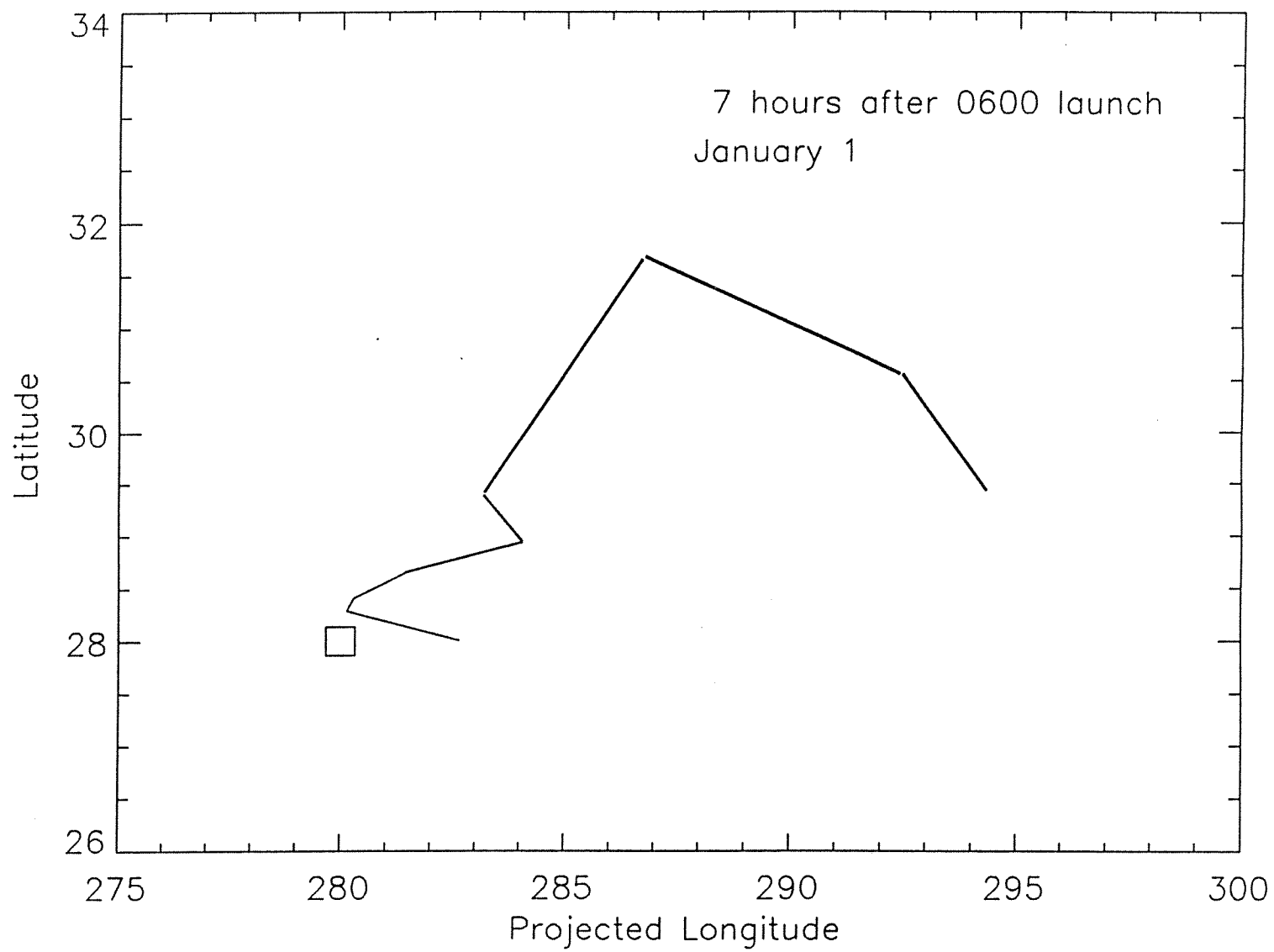


Figure 6d

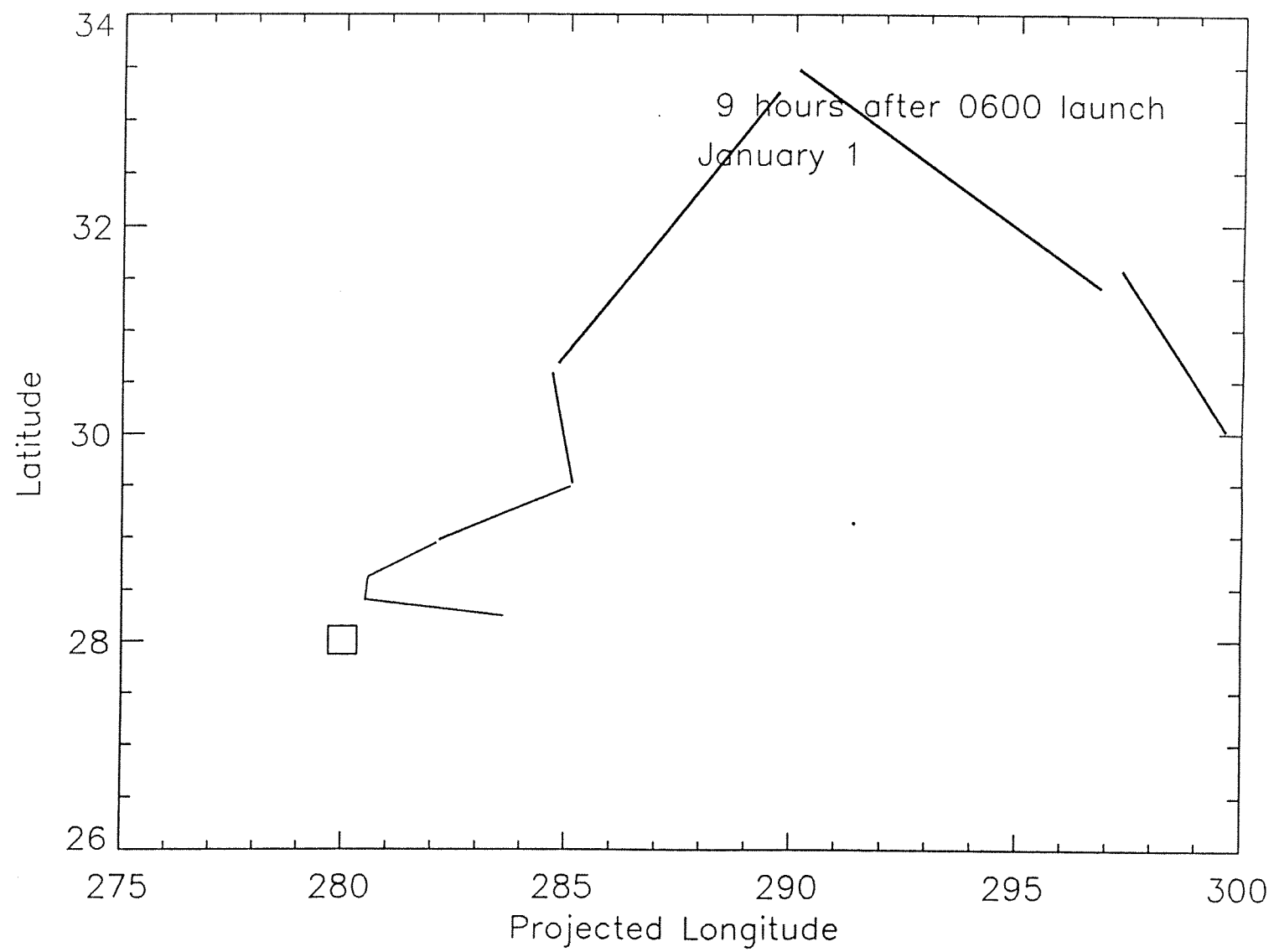


Figure 6e

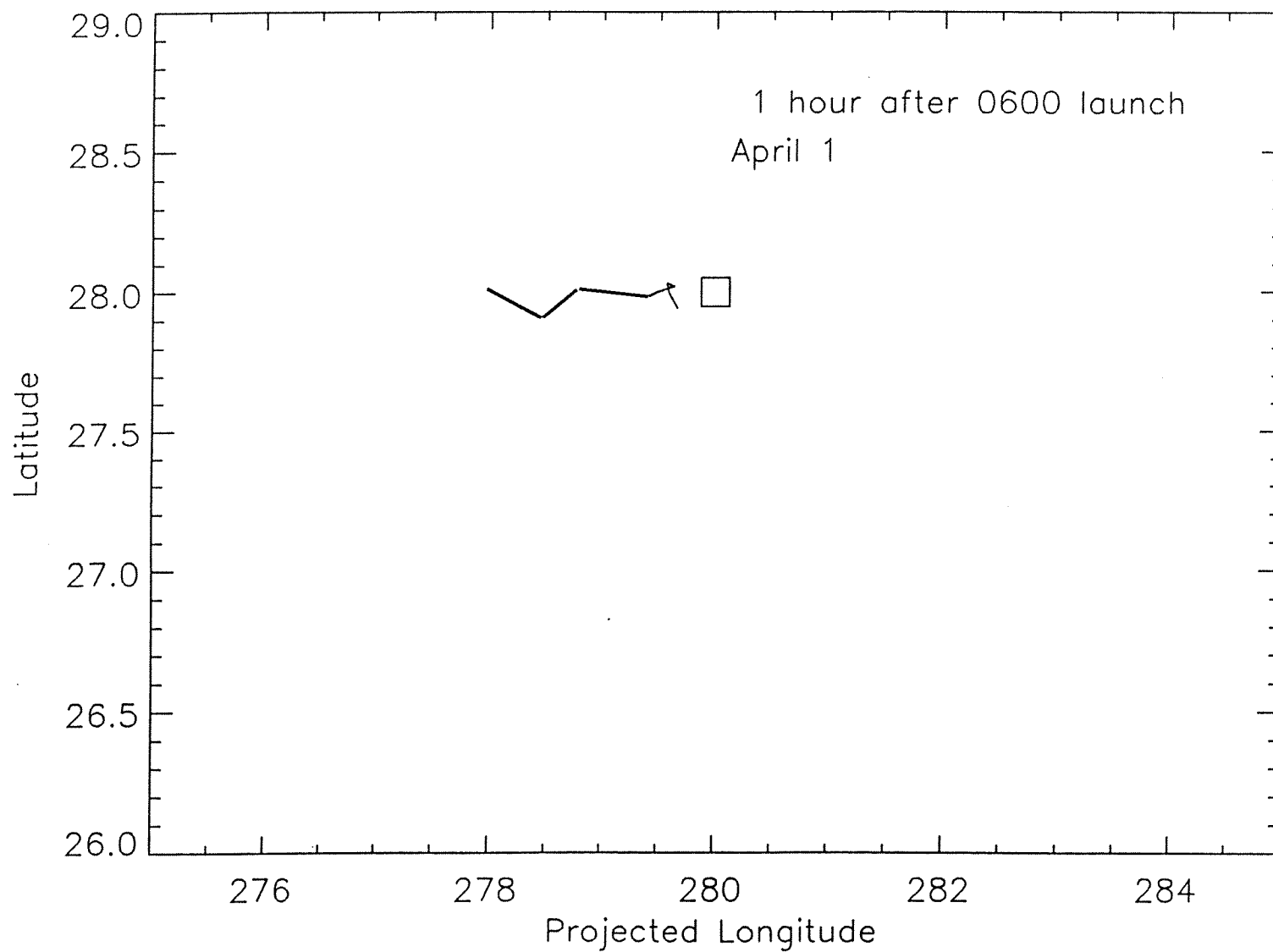


Figure 7a

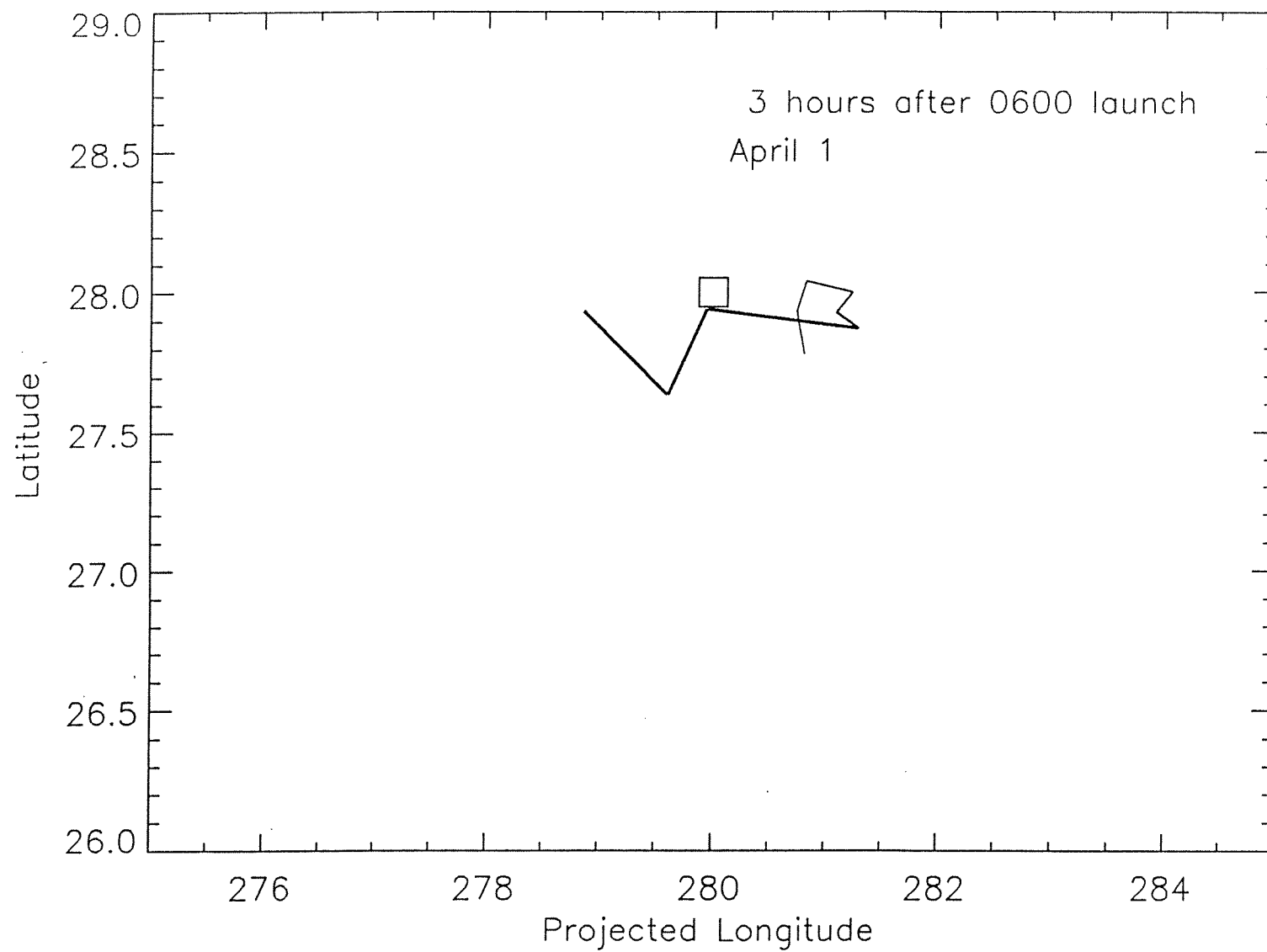


Figure 7b

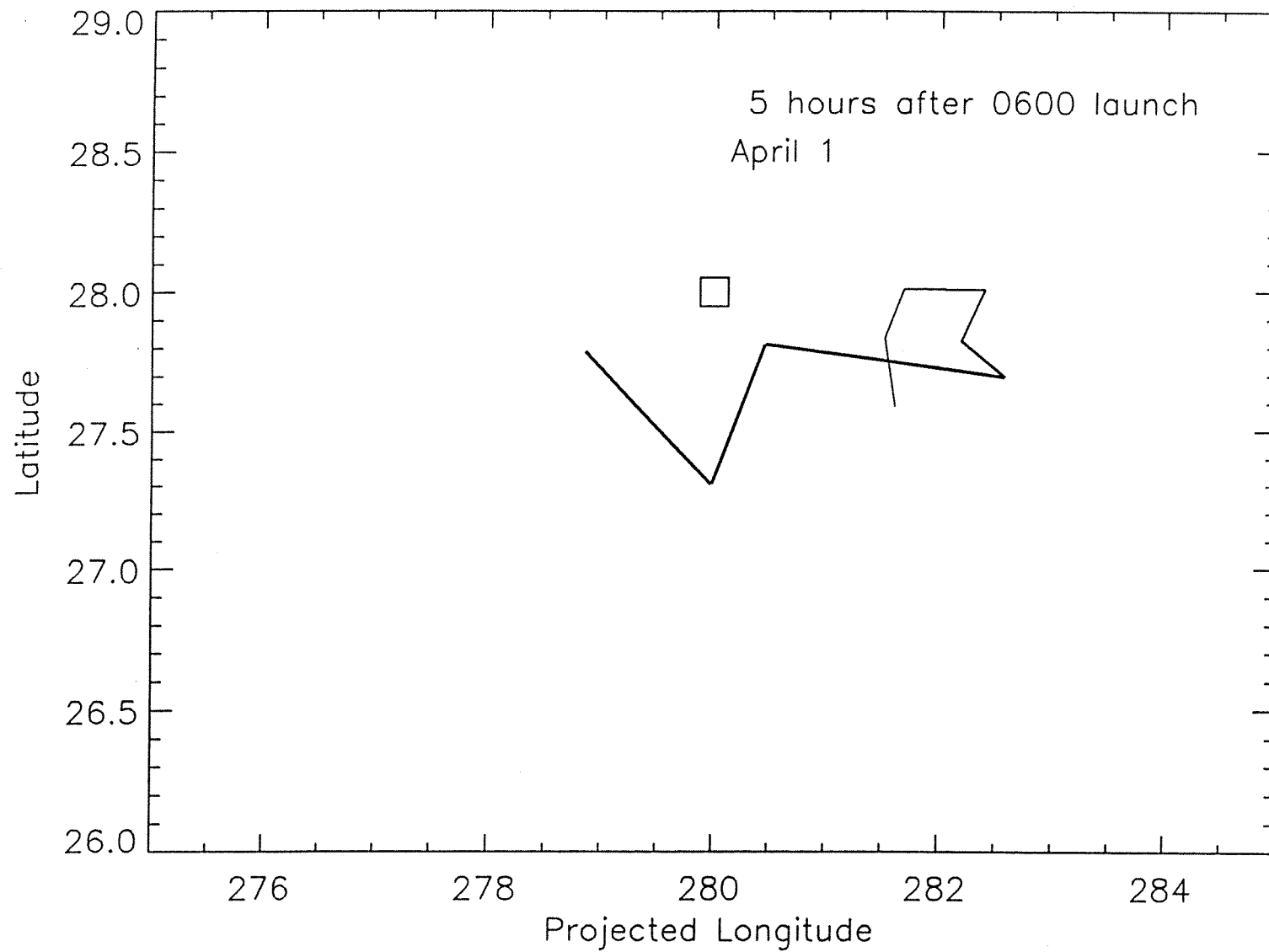


Figure 7c

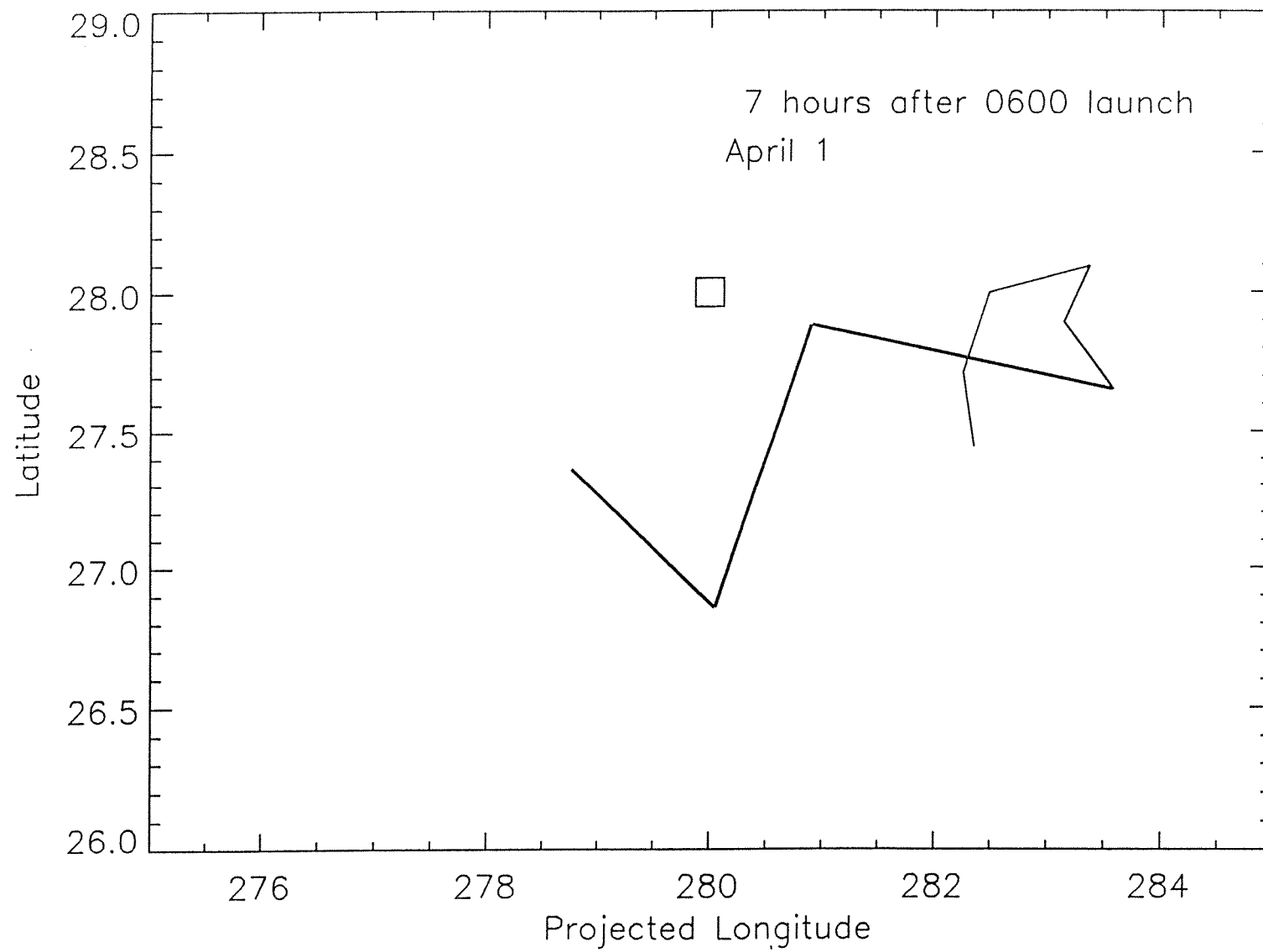


Figure 7d

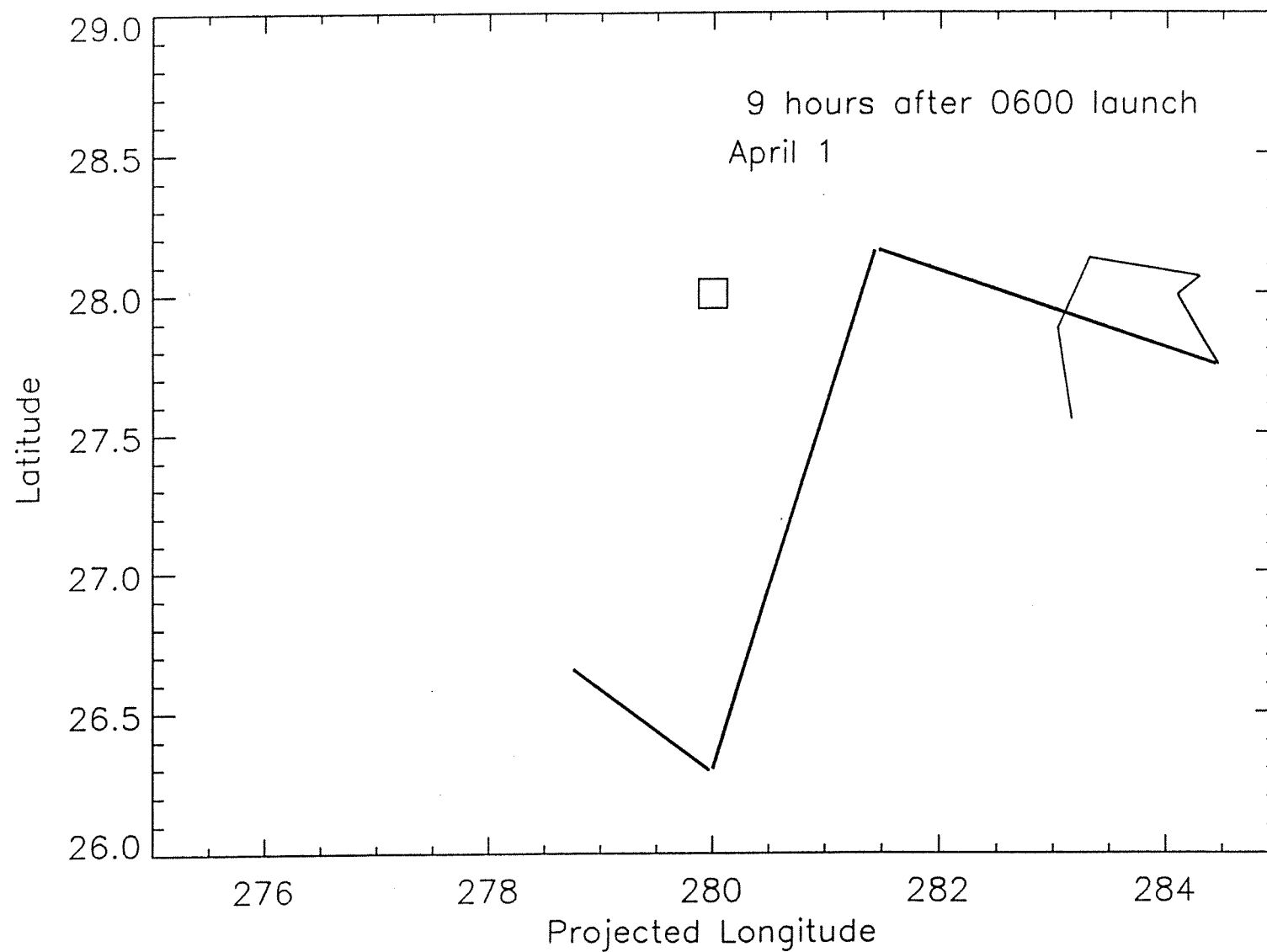


Figure 7e

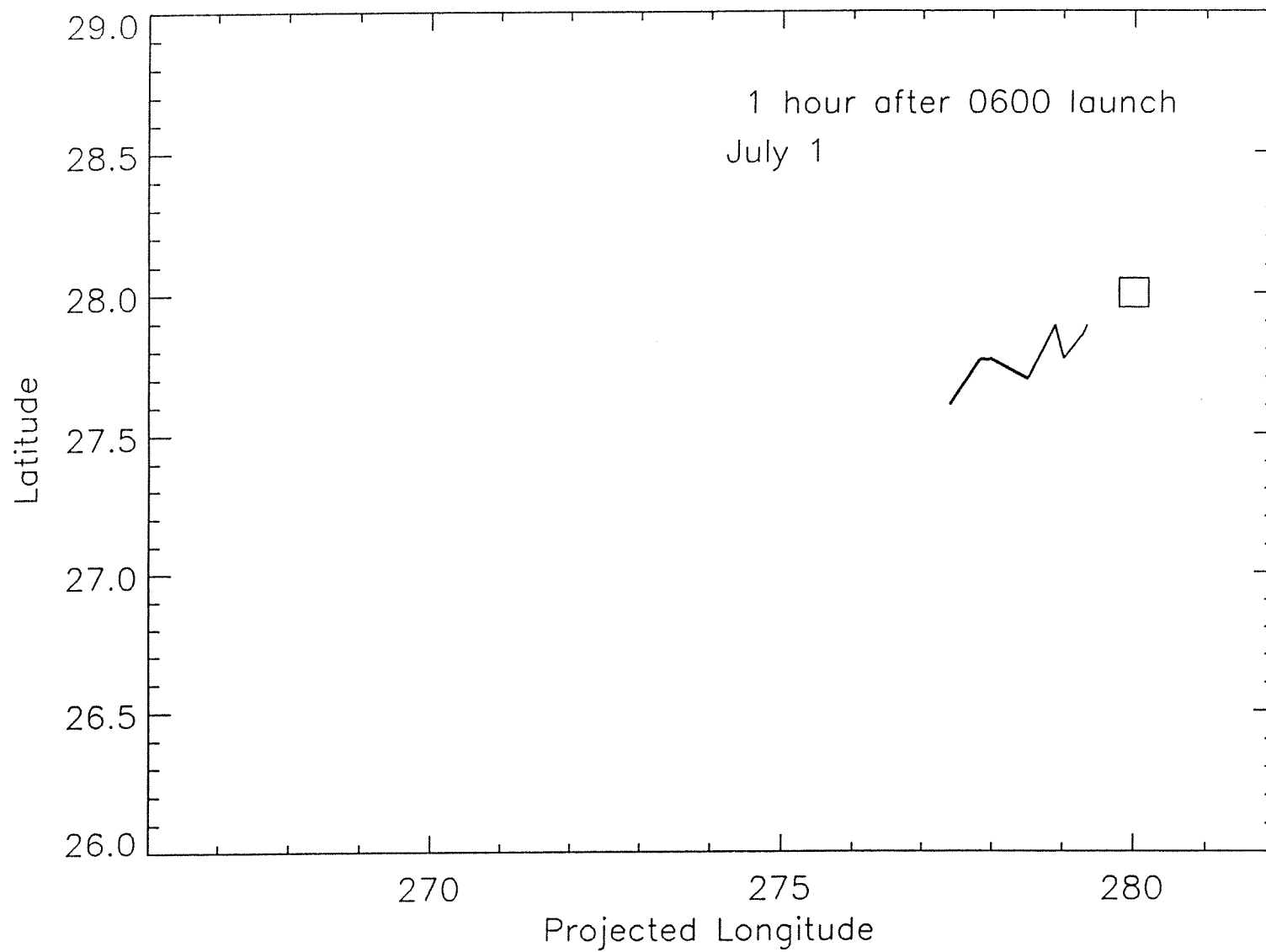


Figure 8a

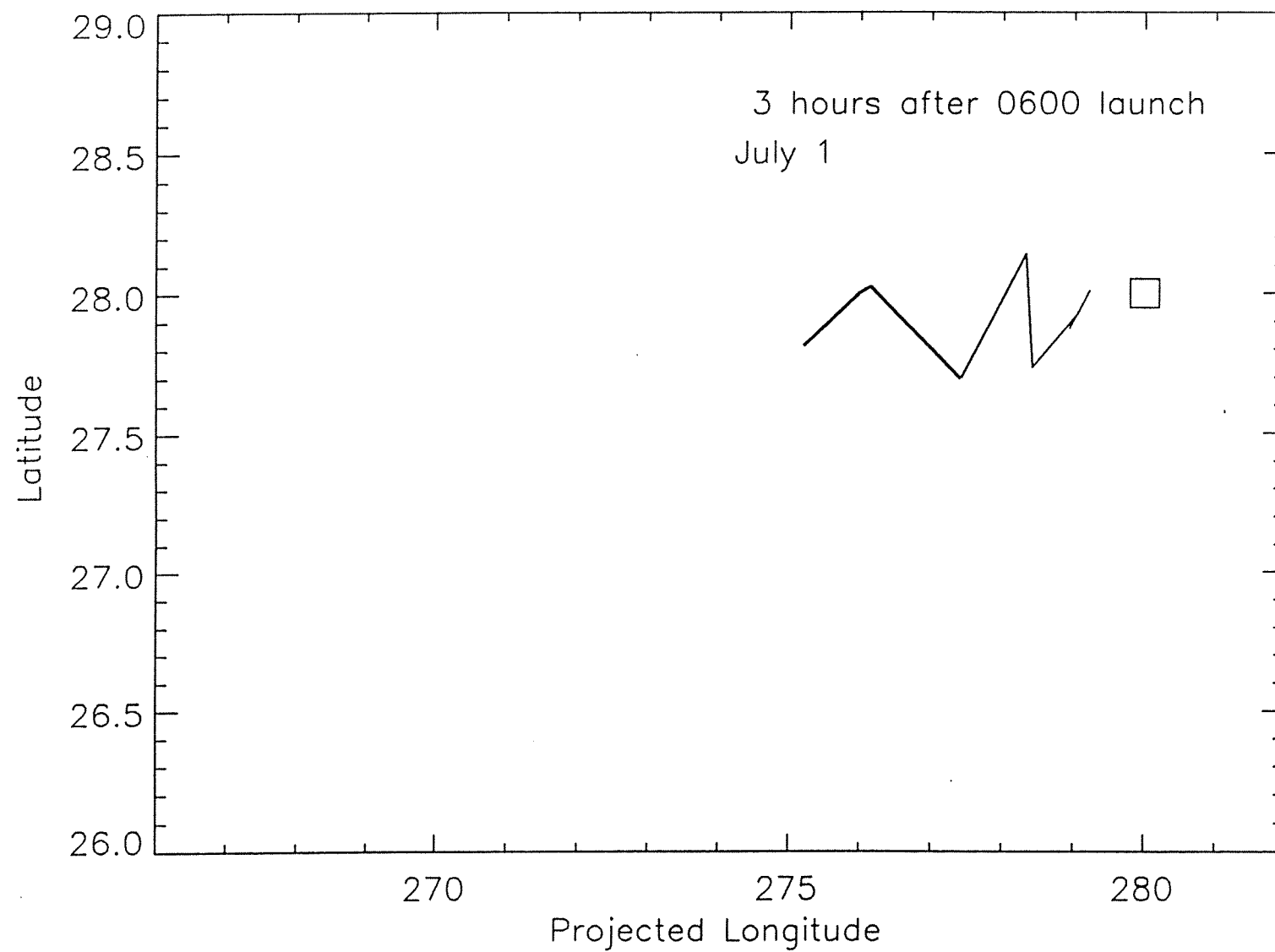


Figure 8b

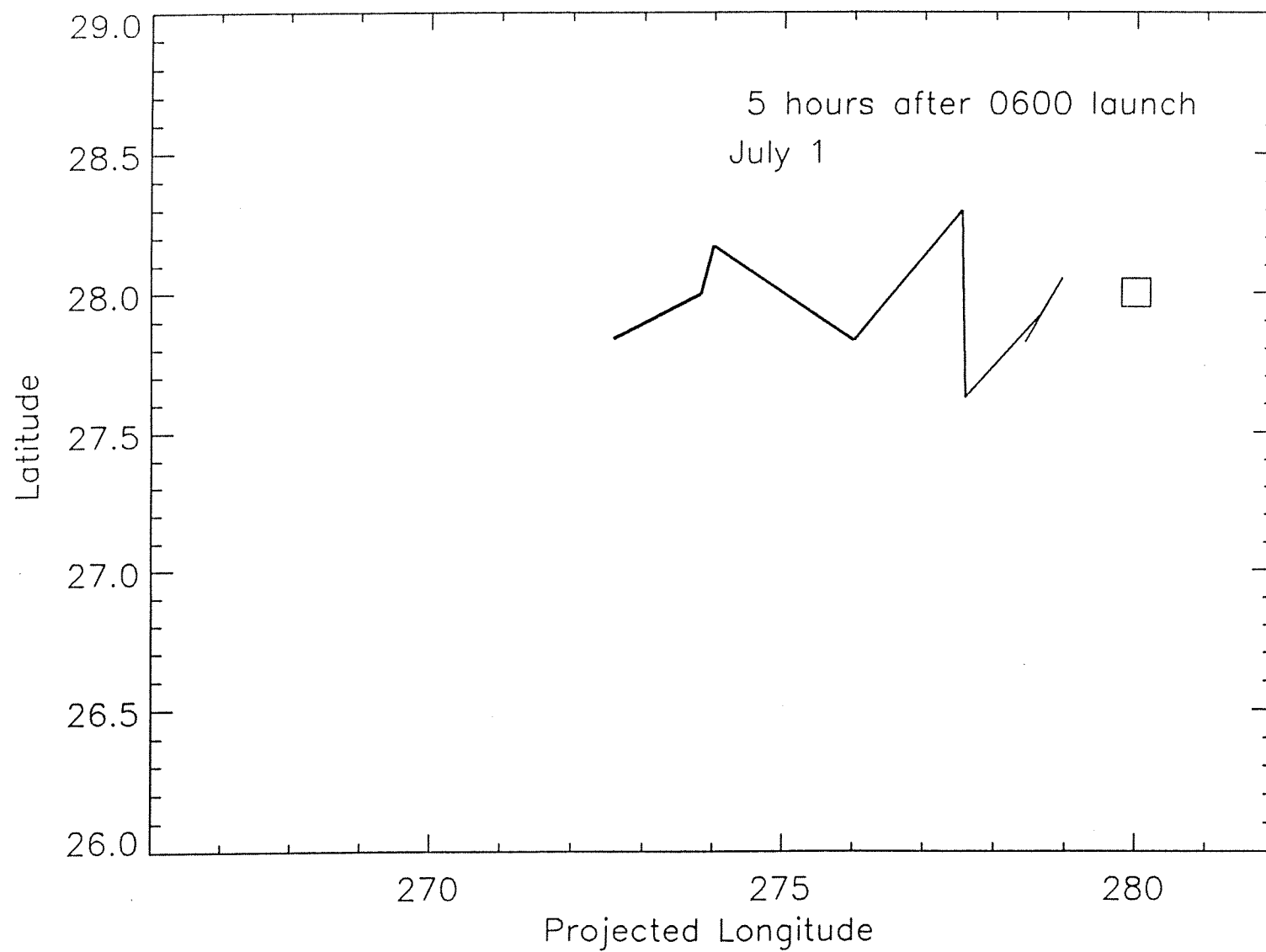


Figure 8c

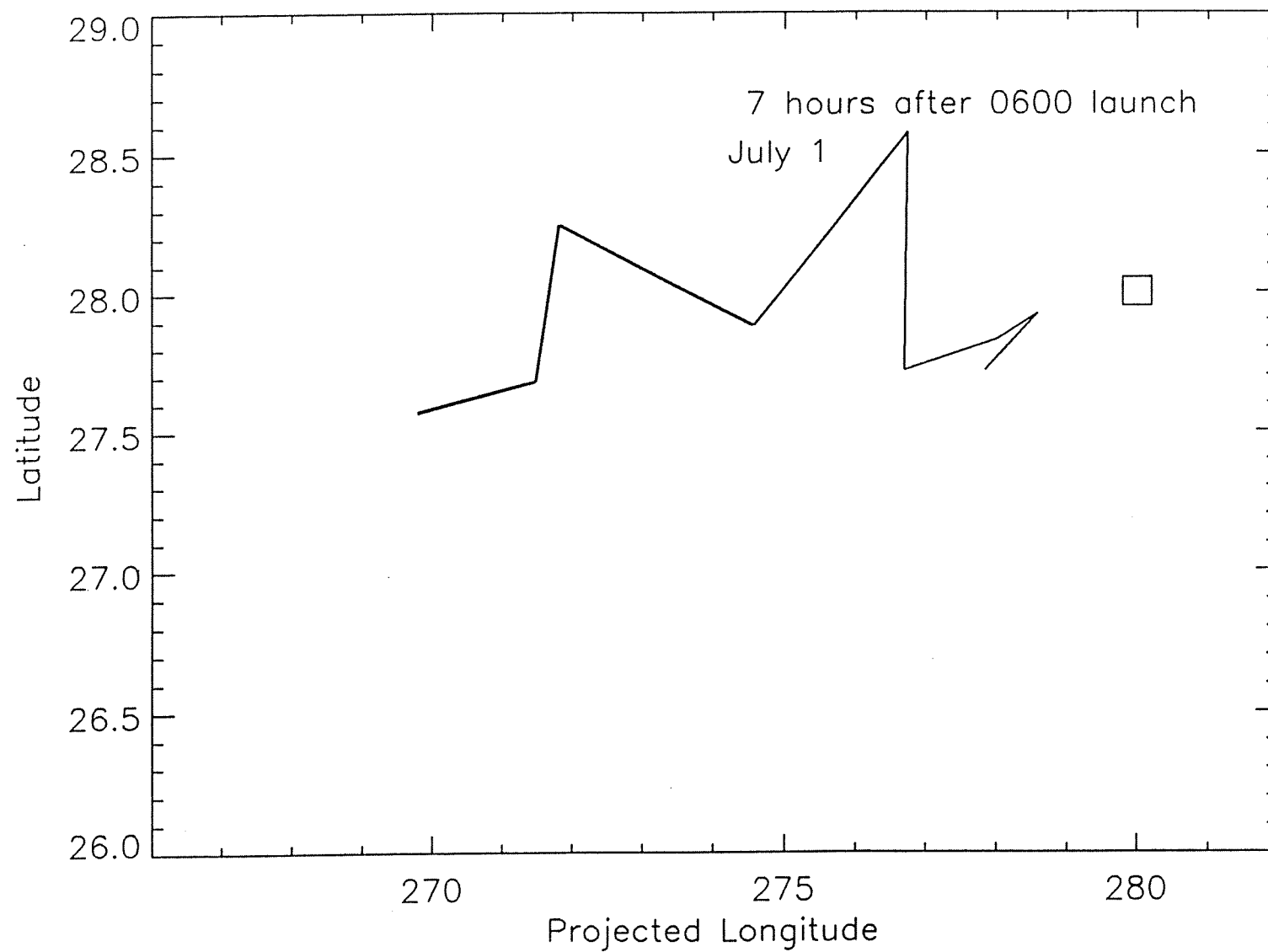


Figure 8d

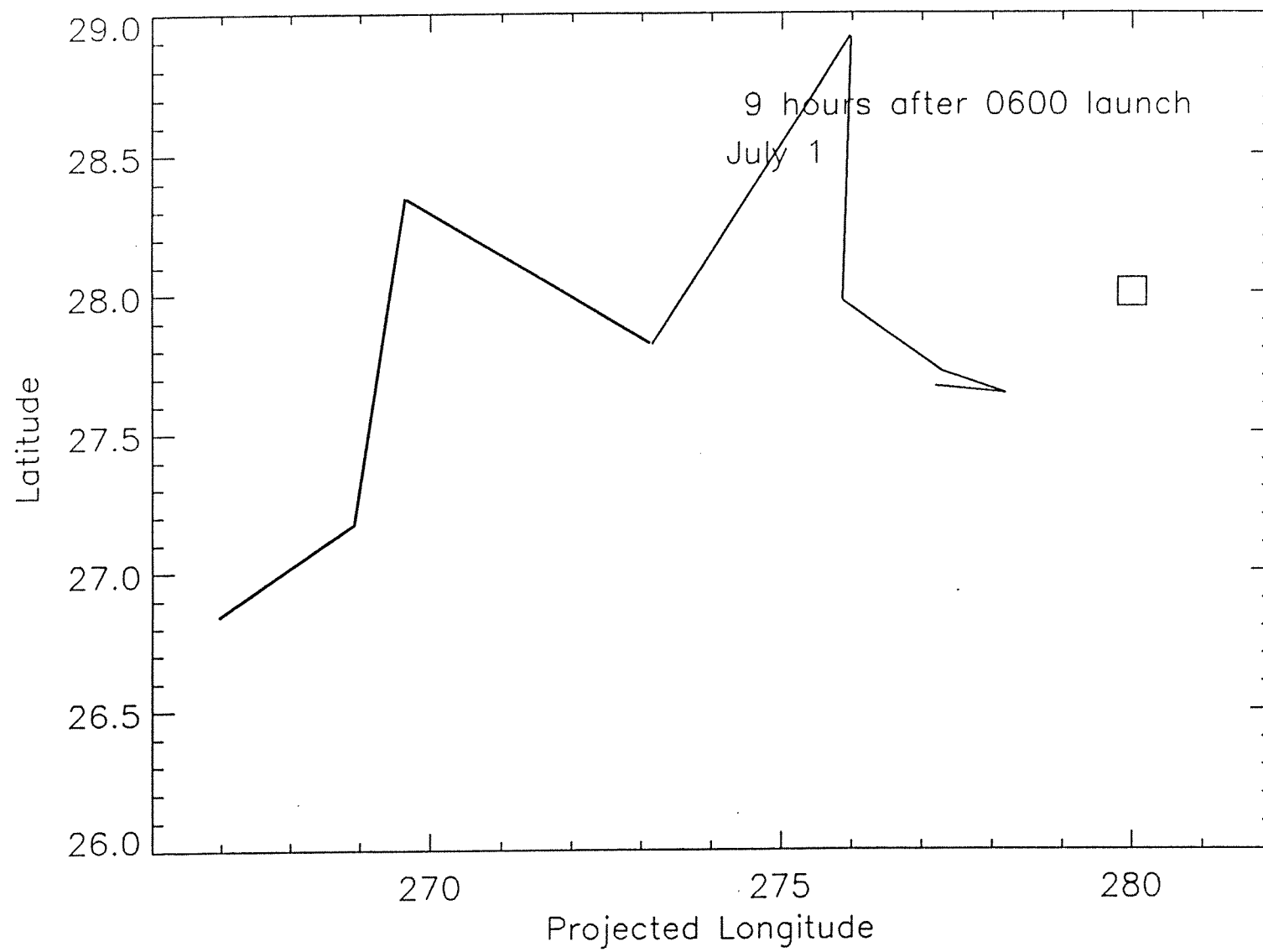


Figure 8e

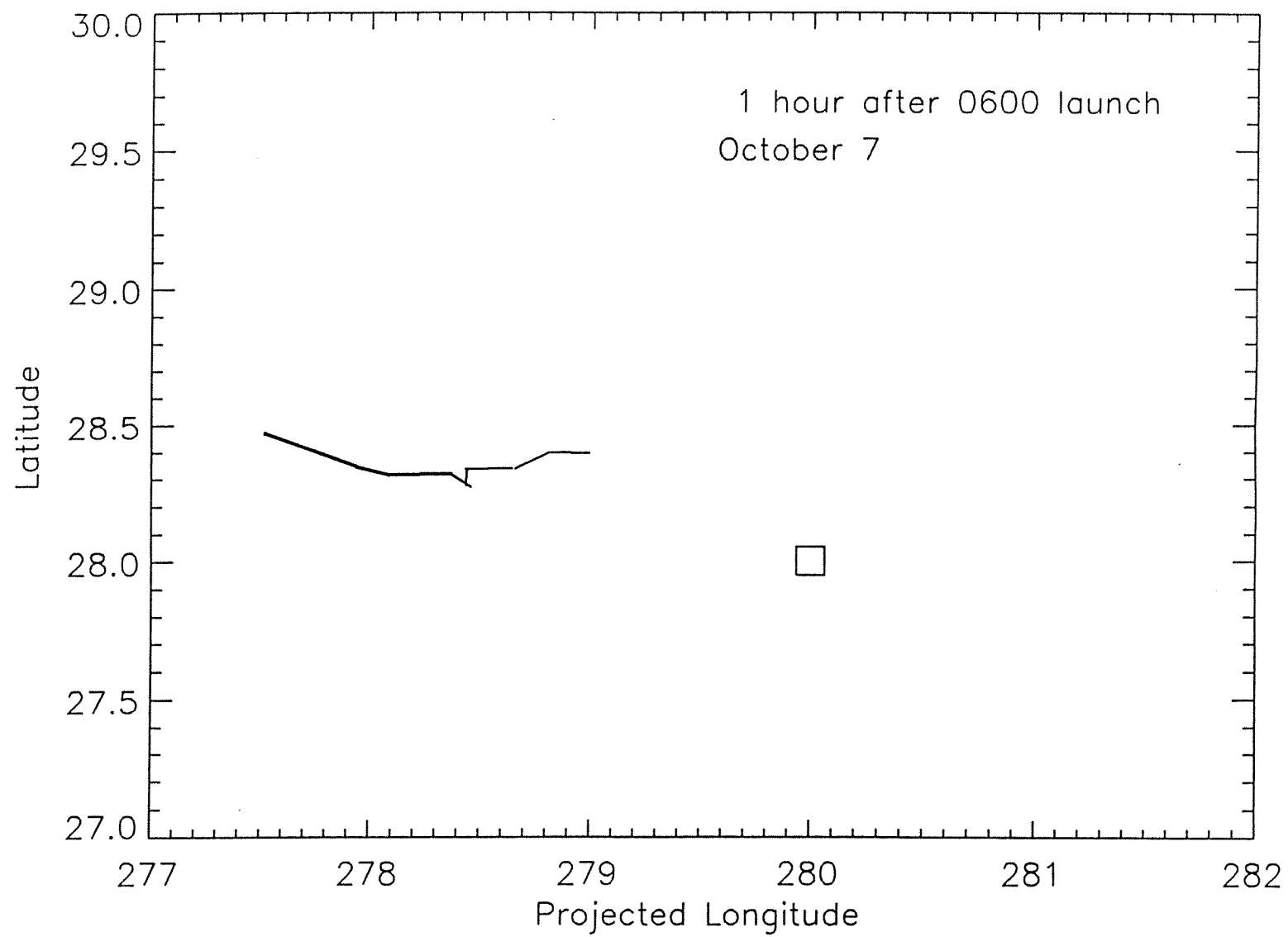


Figure 9a

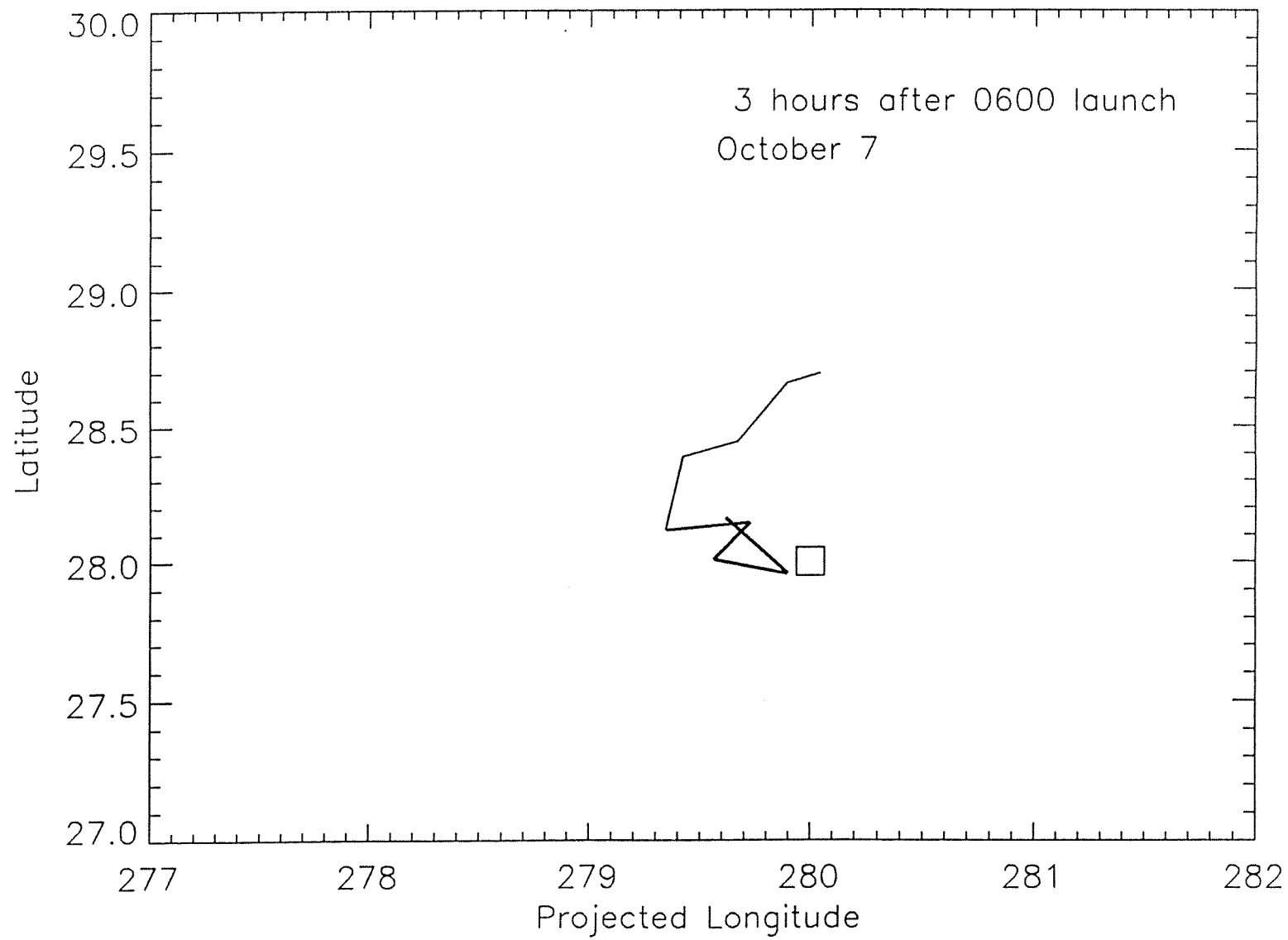


Figure 9b

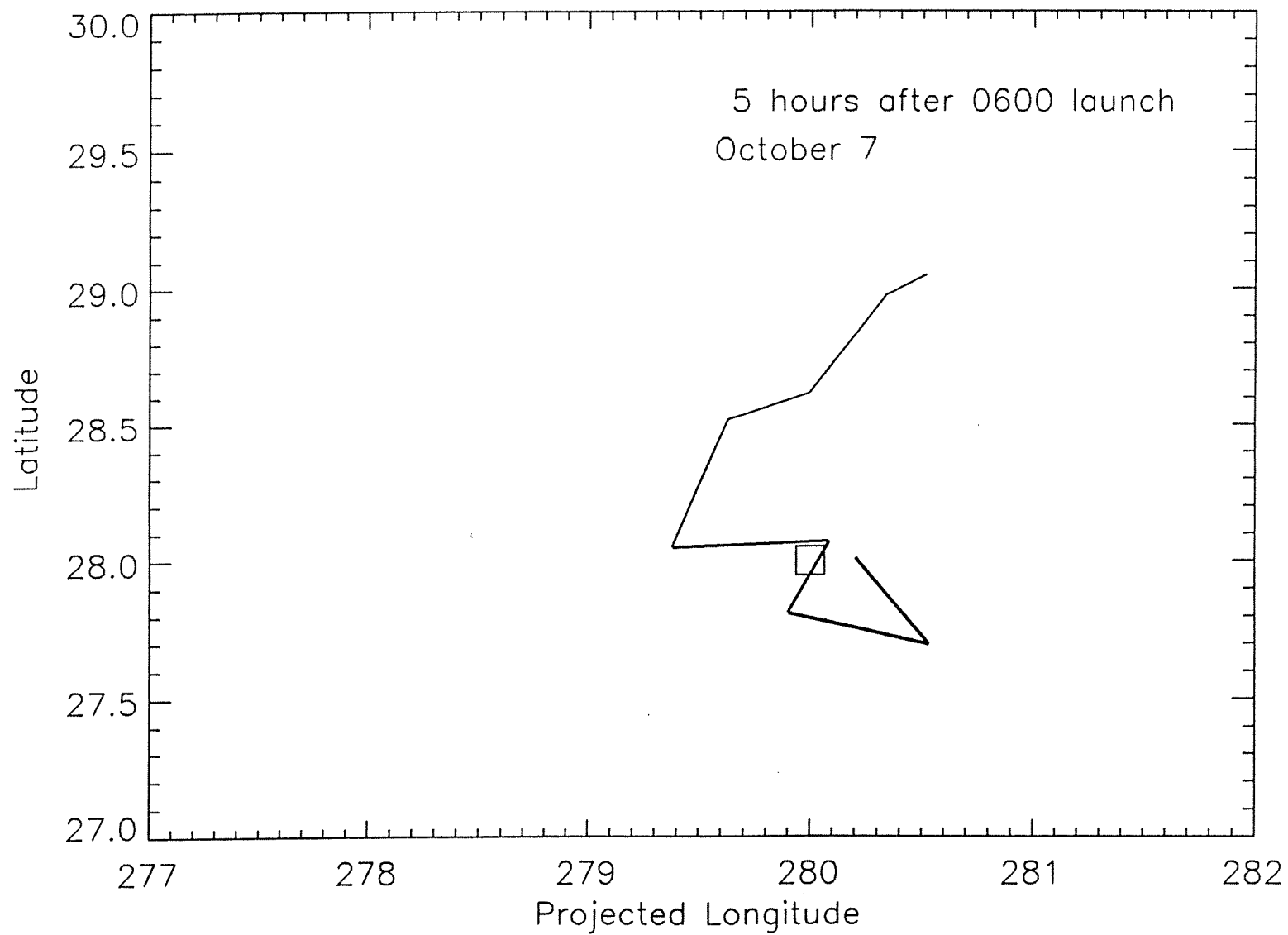


Figure 9c

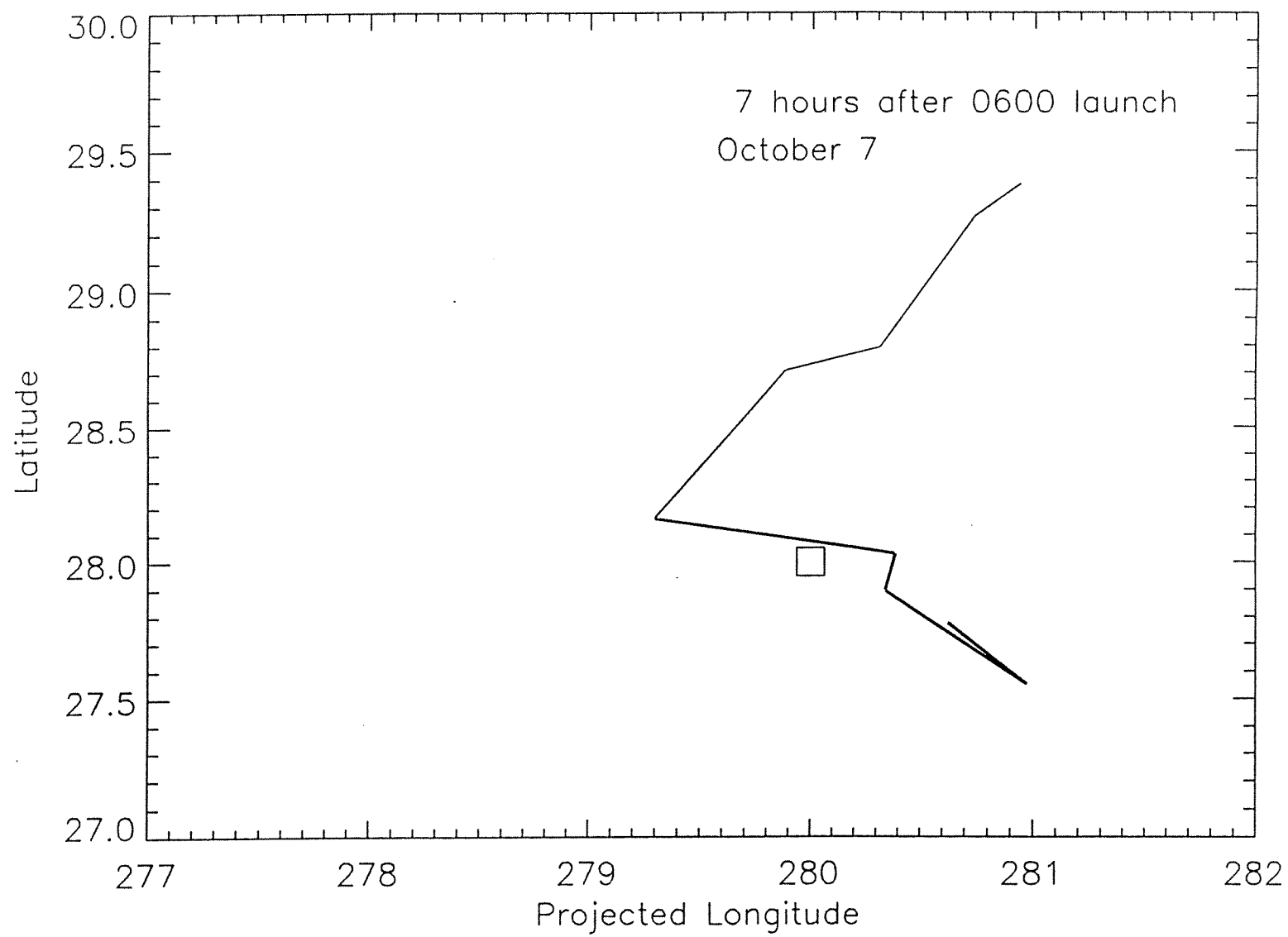


Figure 9d

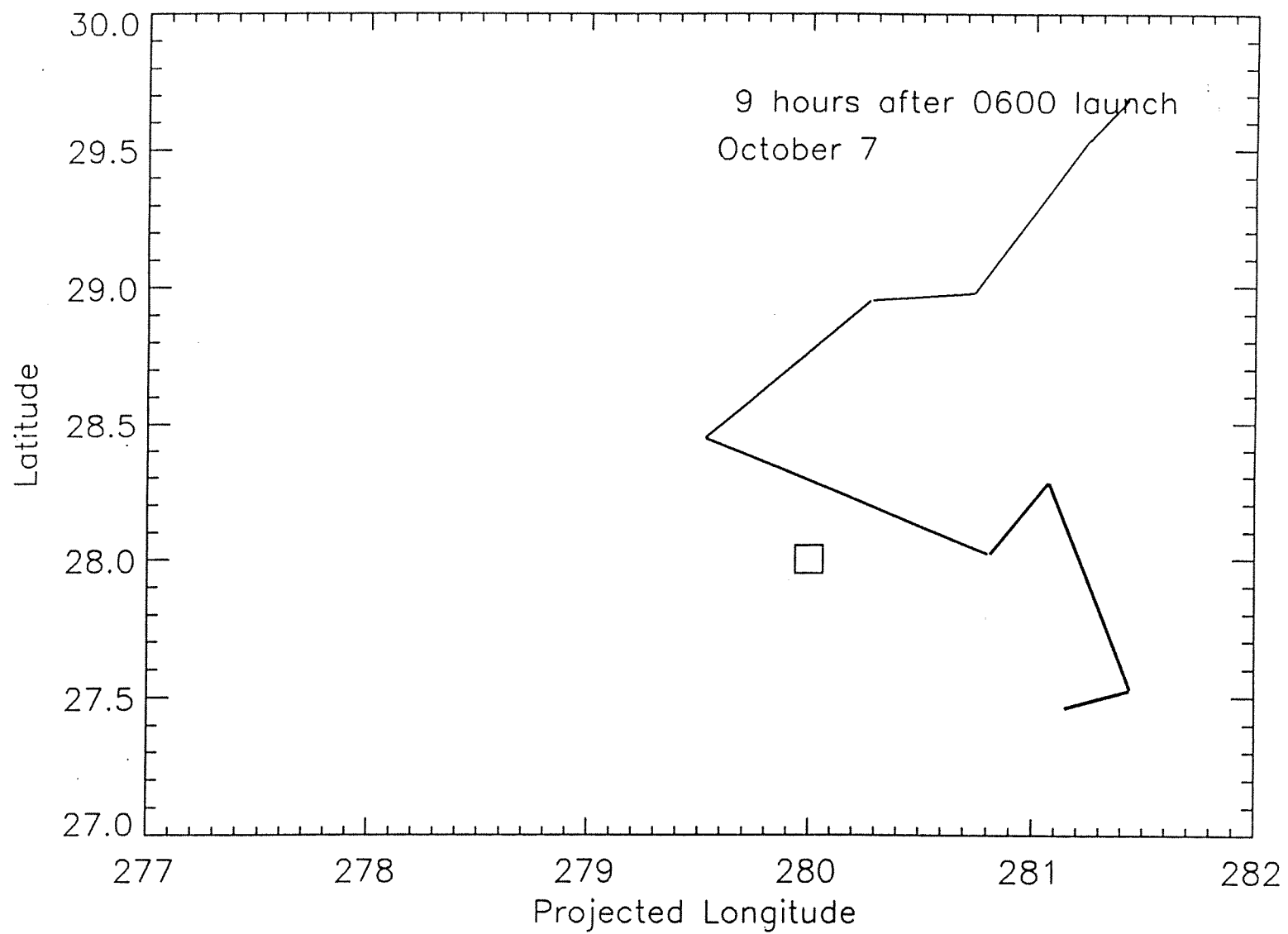


Figure 9e

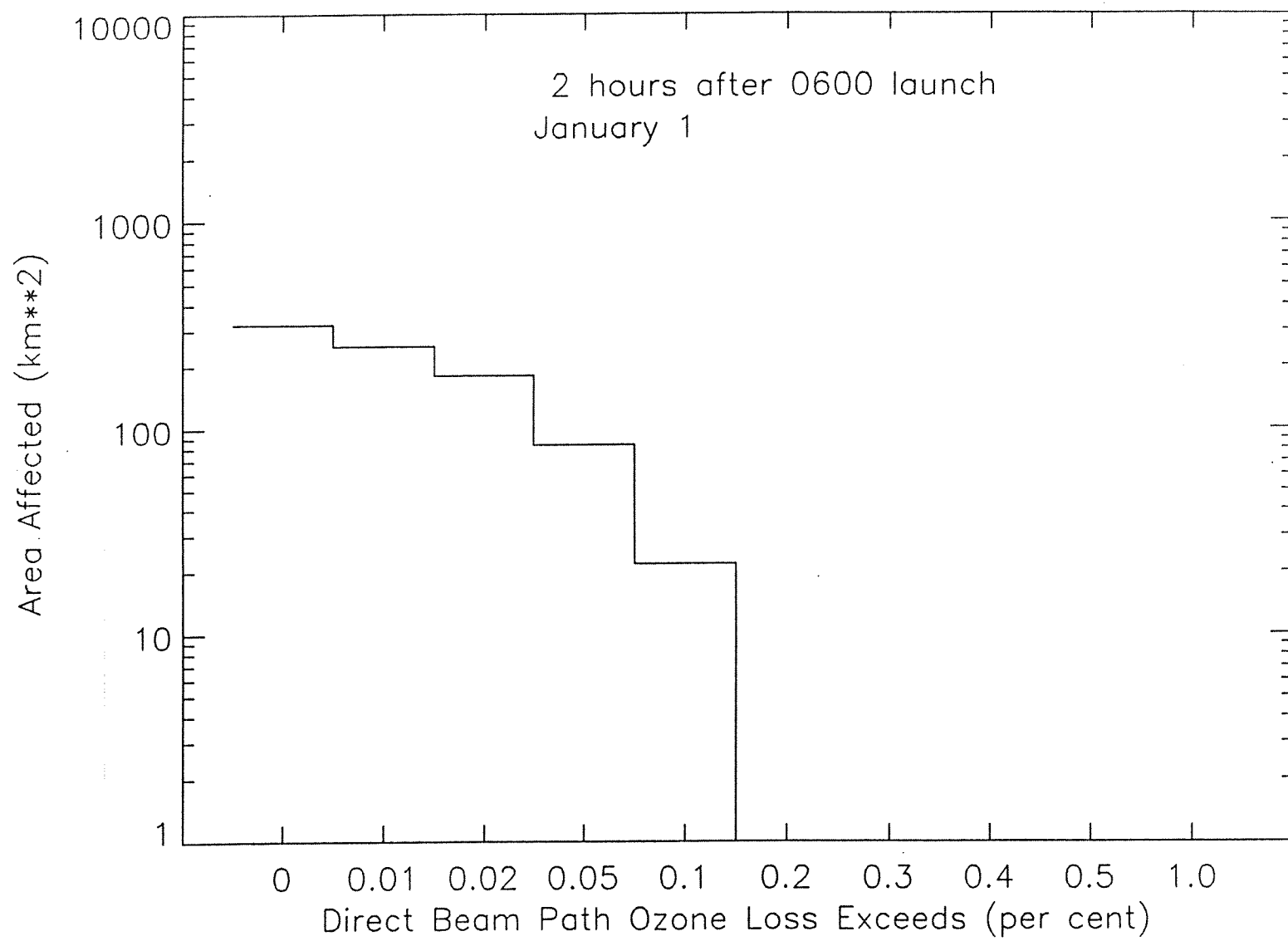


Figure 10a

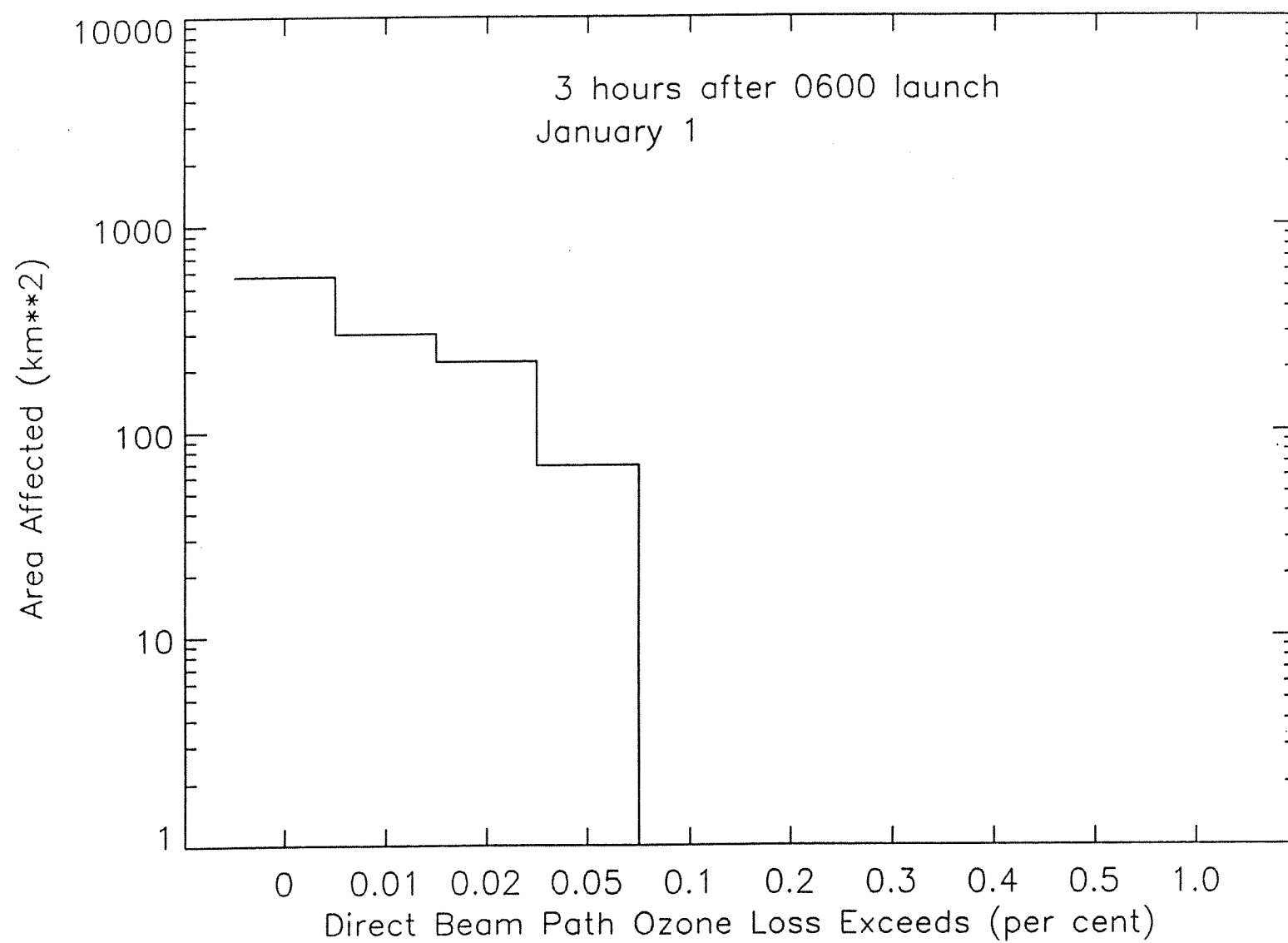


Figure 10b

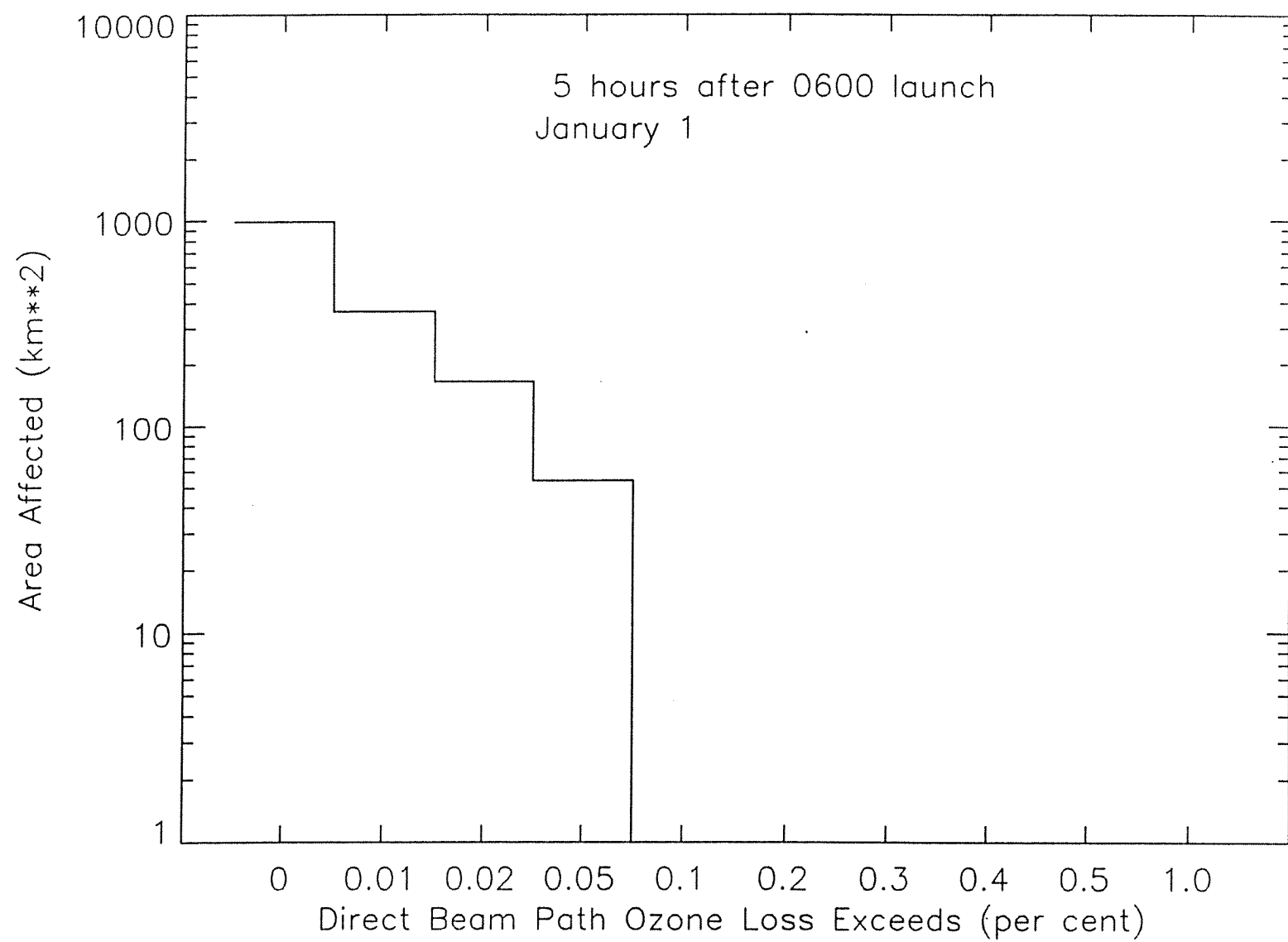


Figure 10c

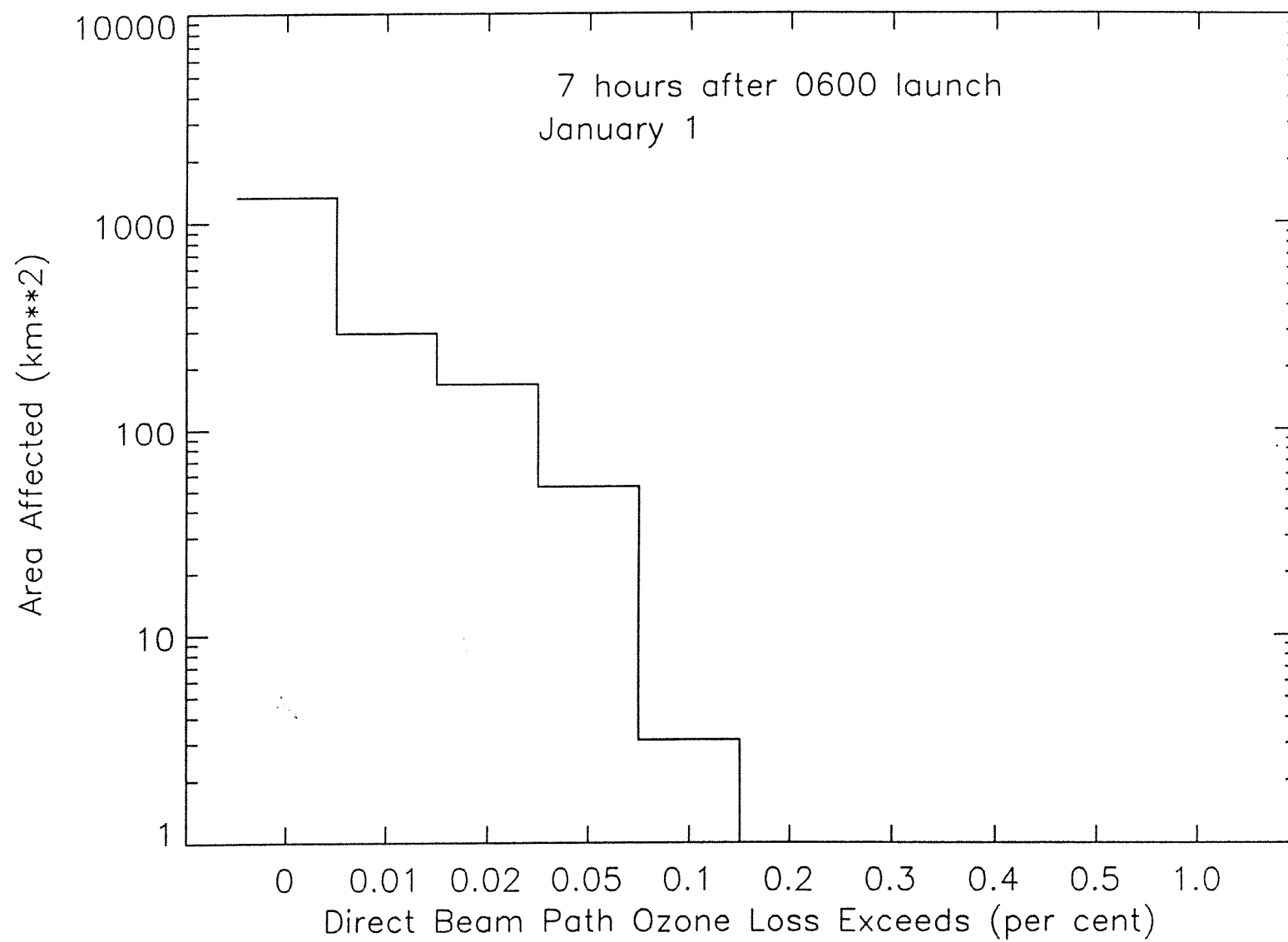


Figure 10d

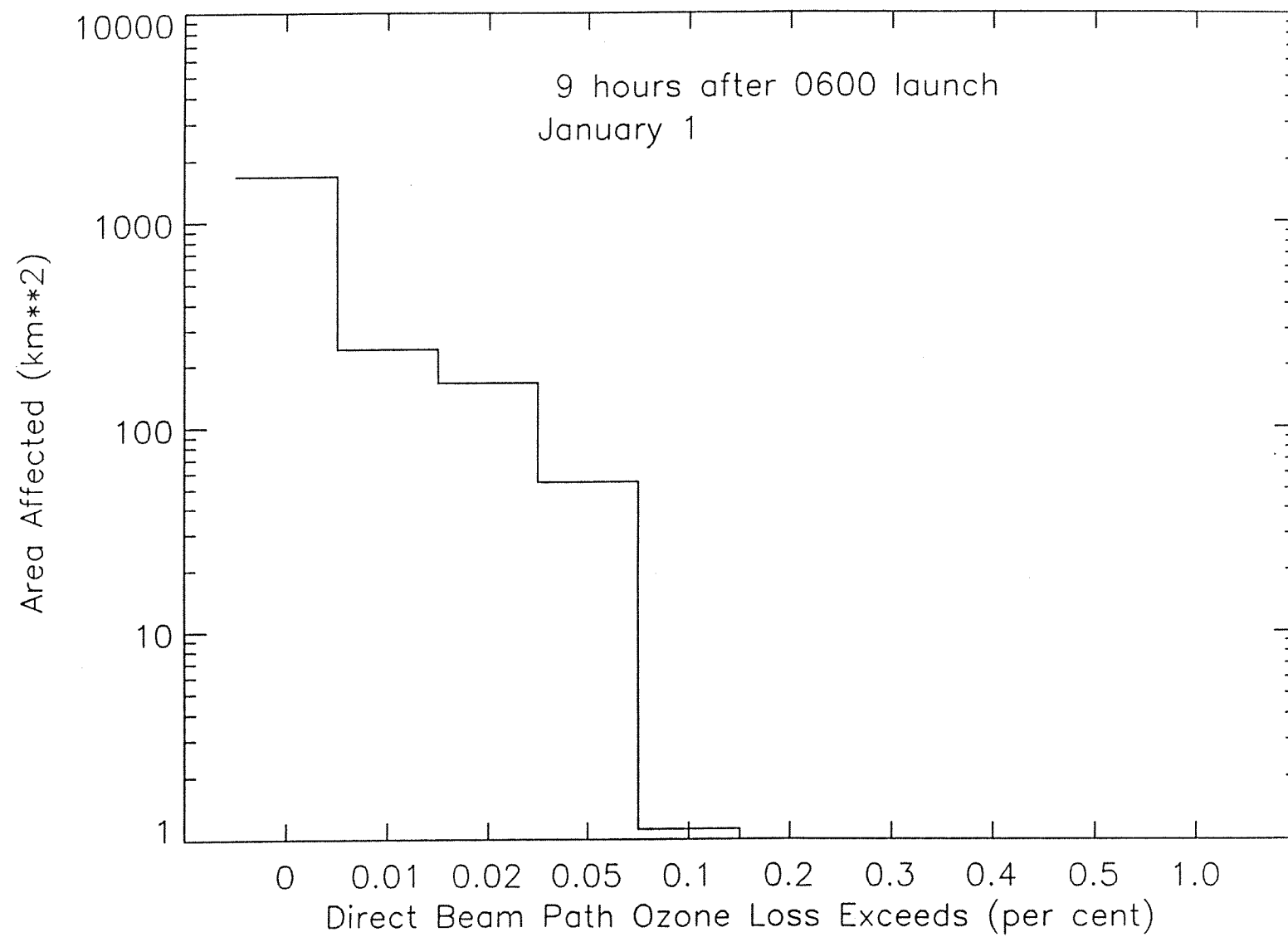


Figure 10e

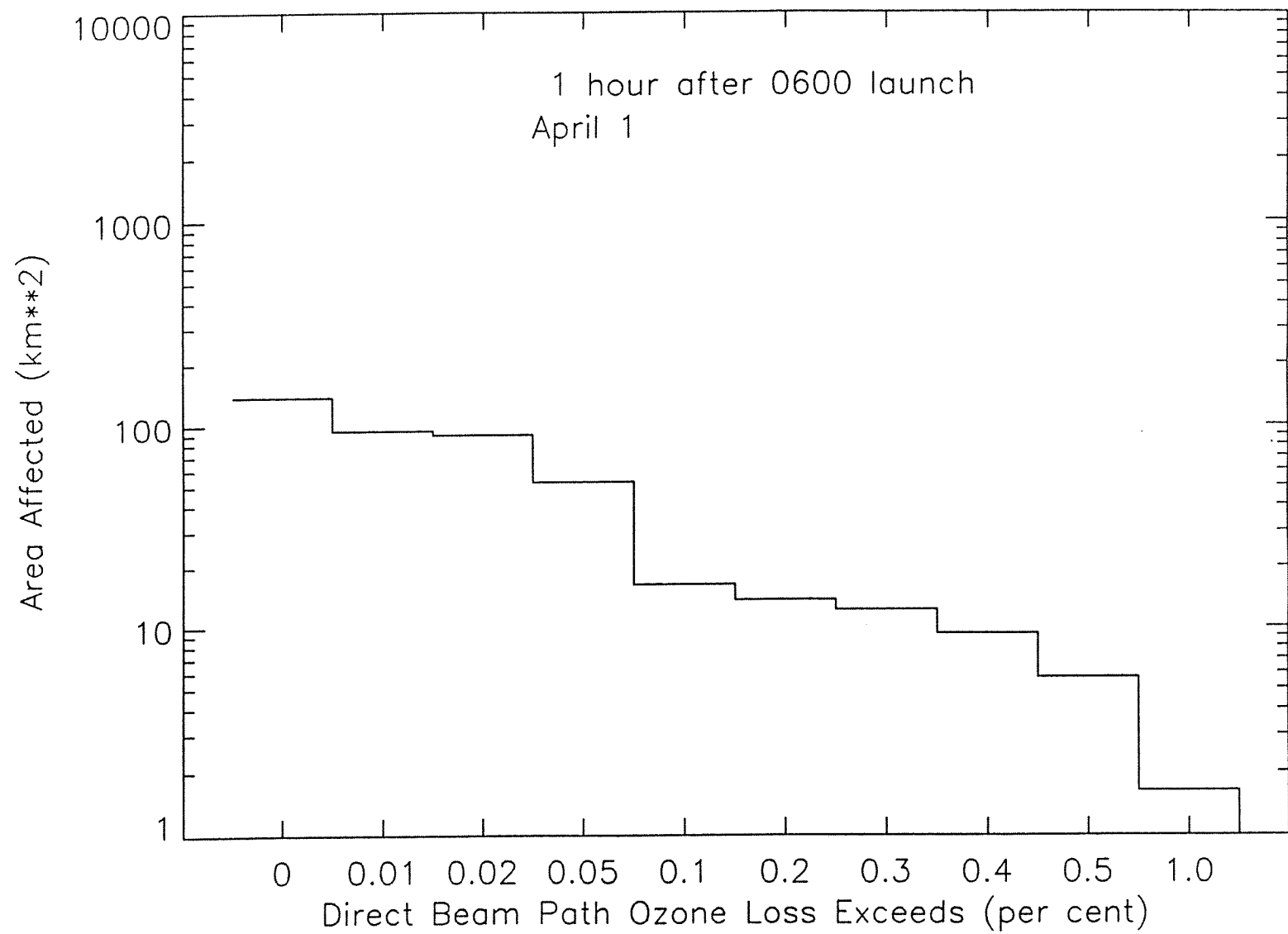


Figure 11a

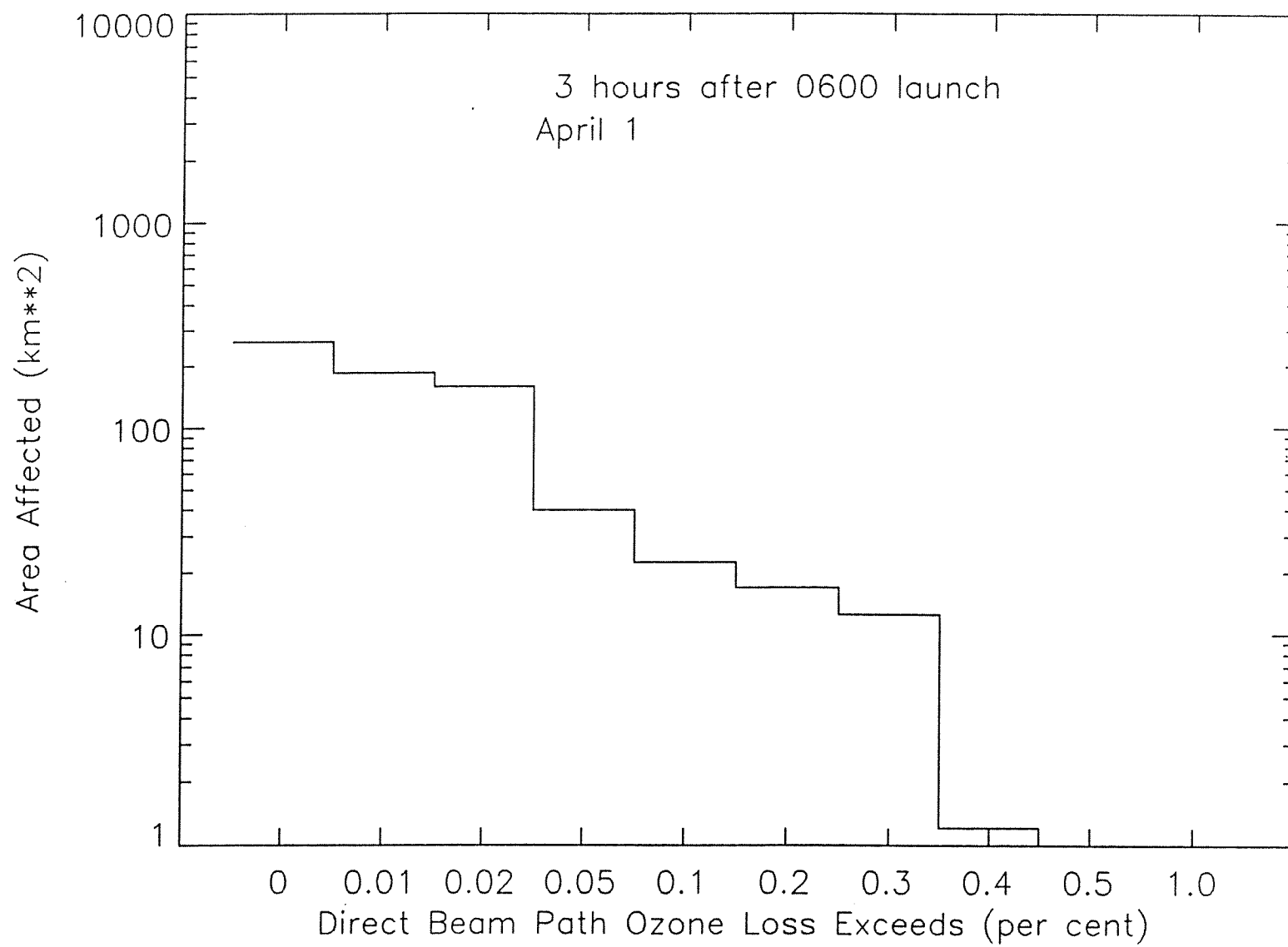


Figure 11b

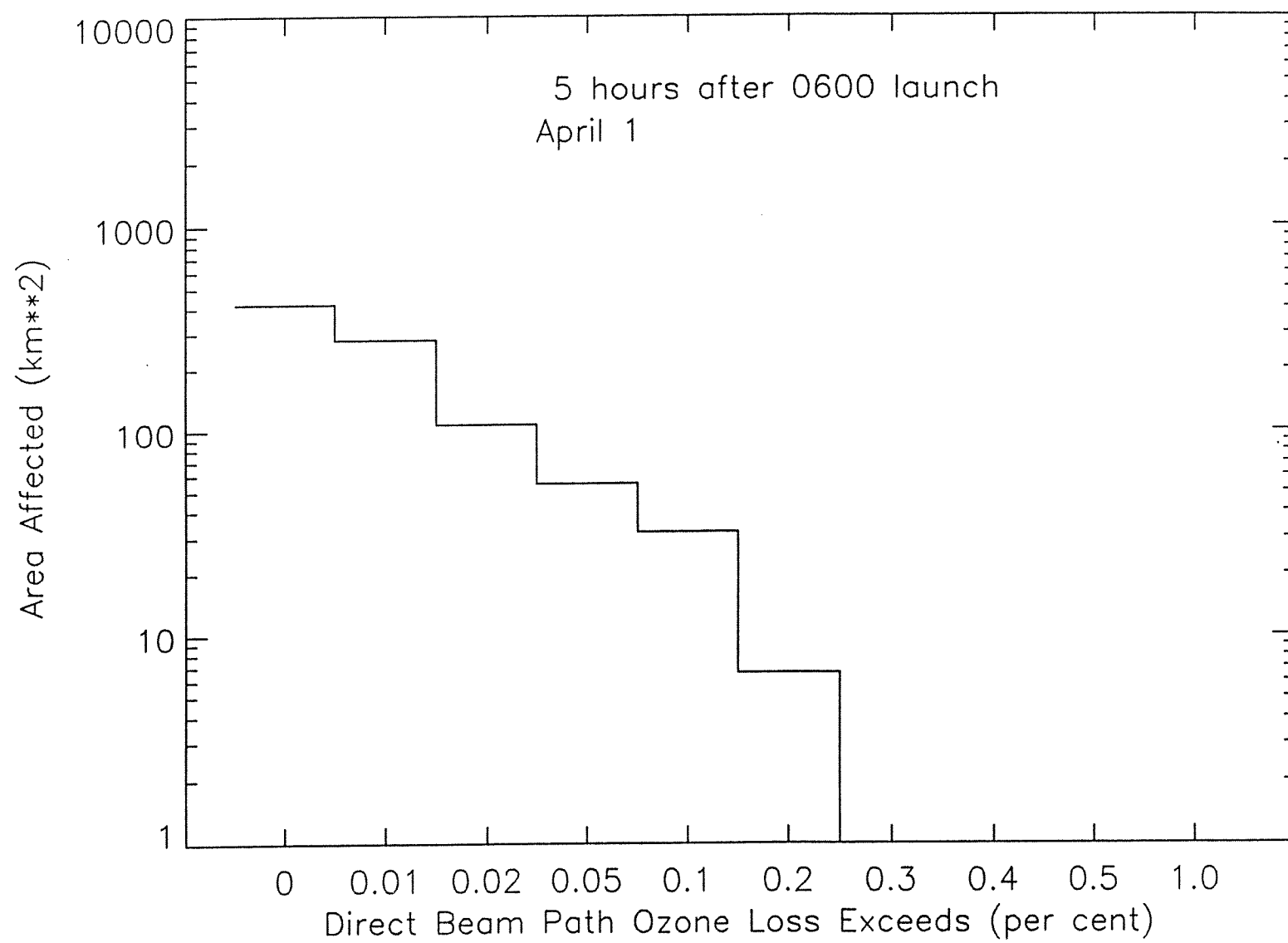


Figure 11c

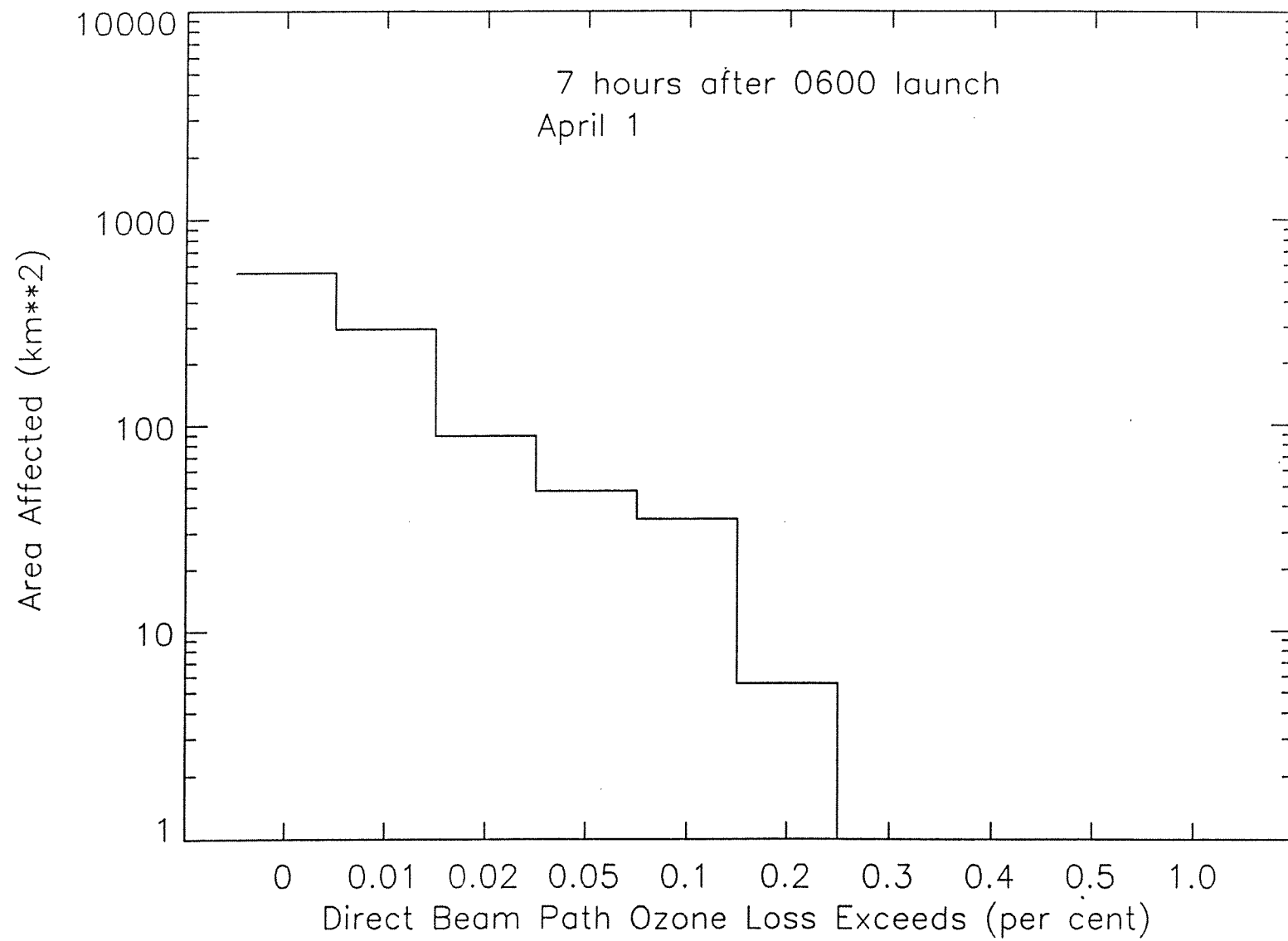


Figure 11d

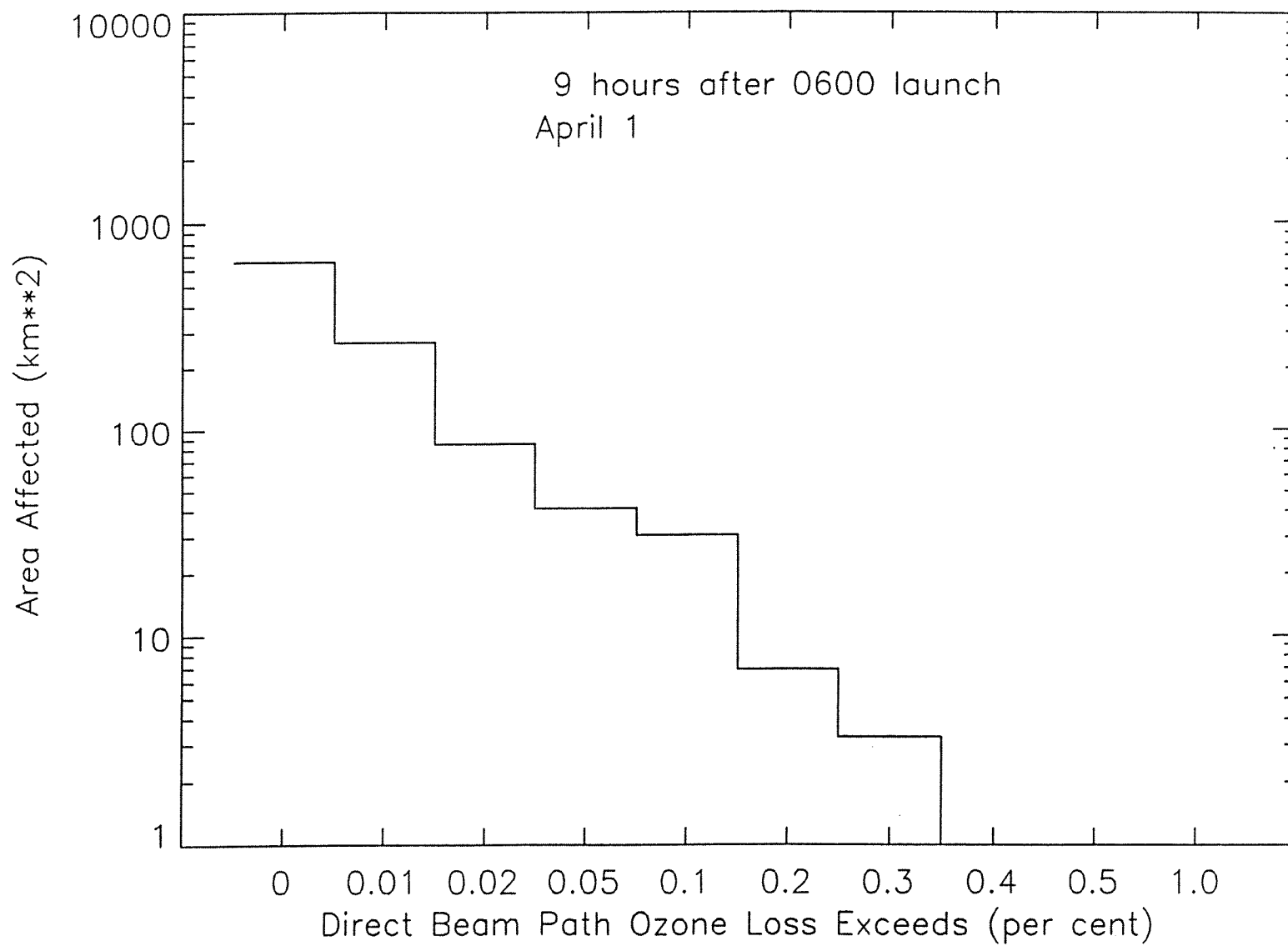


Figure 11e

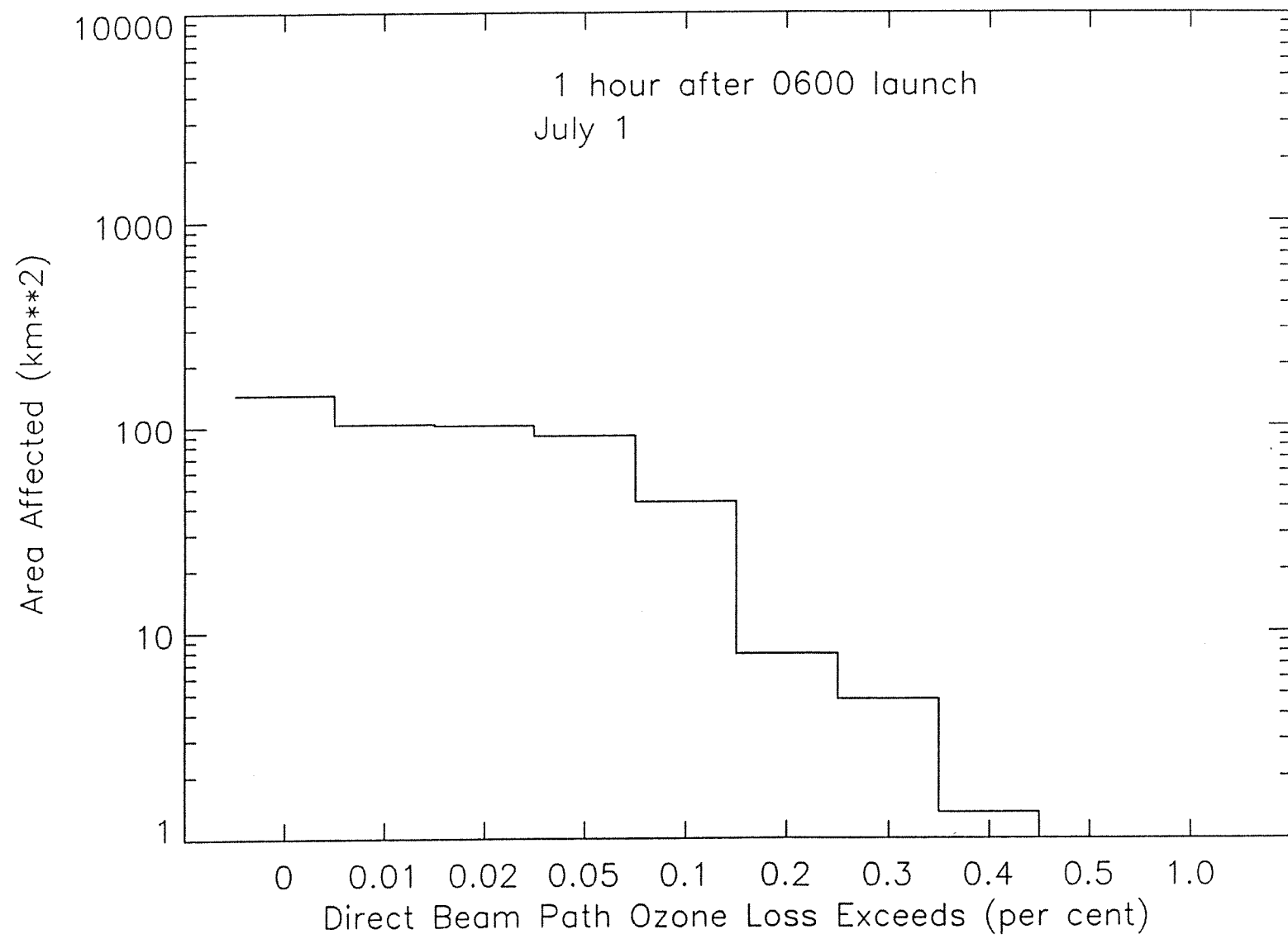


Figure 12a

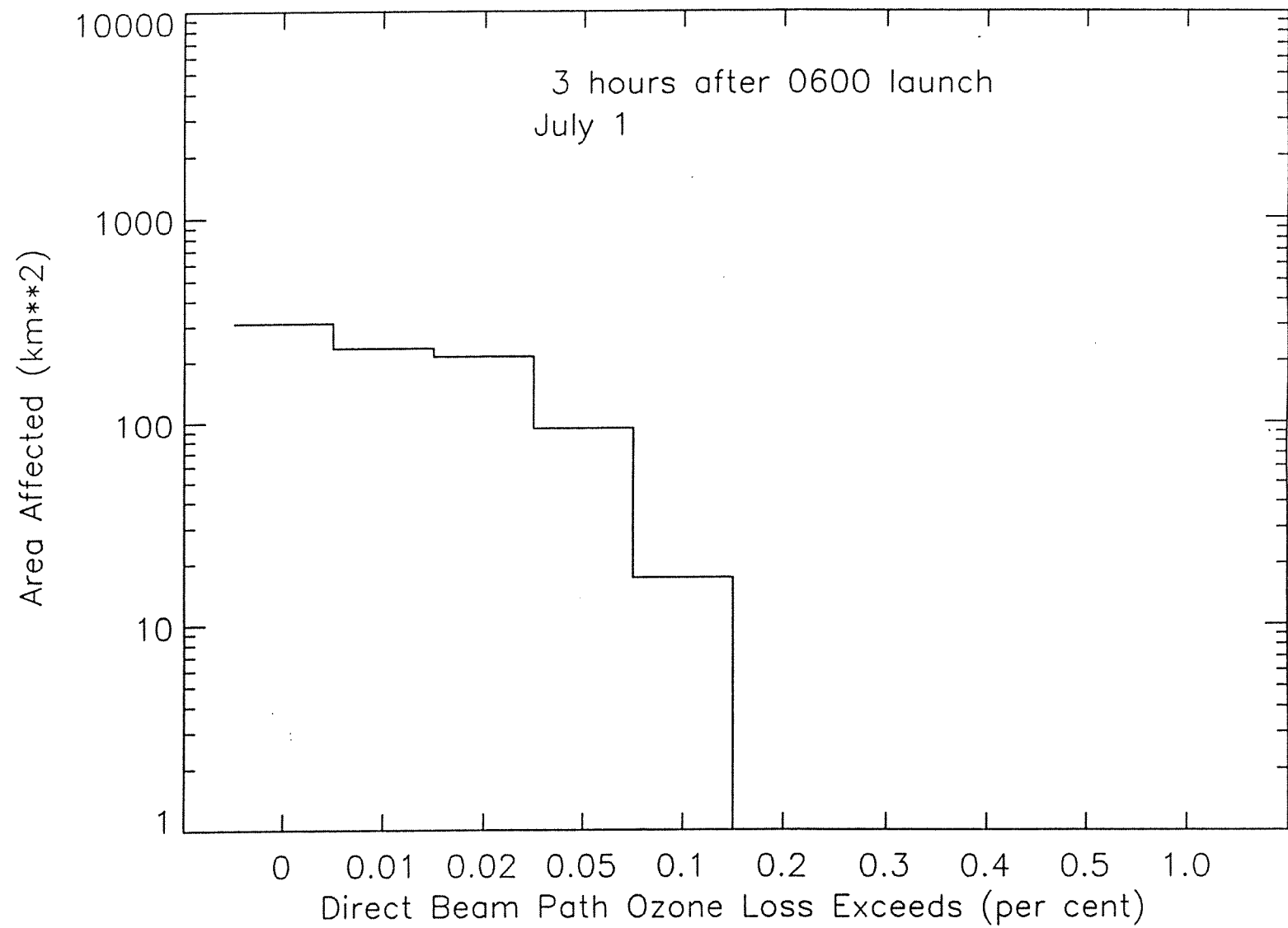


Figure 12b

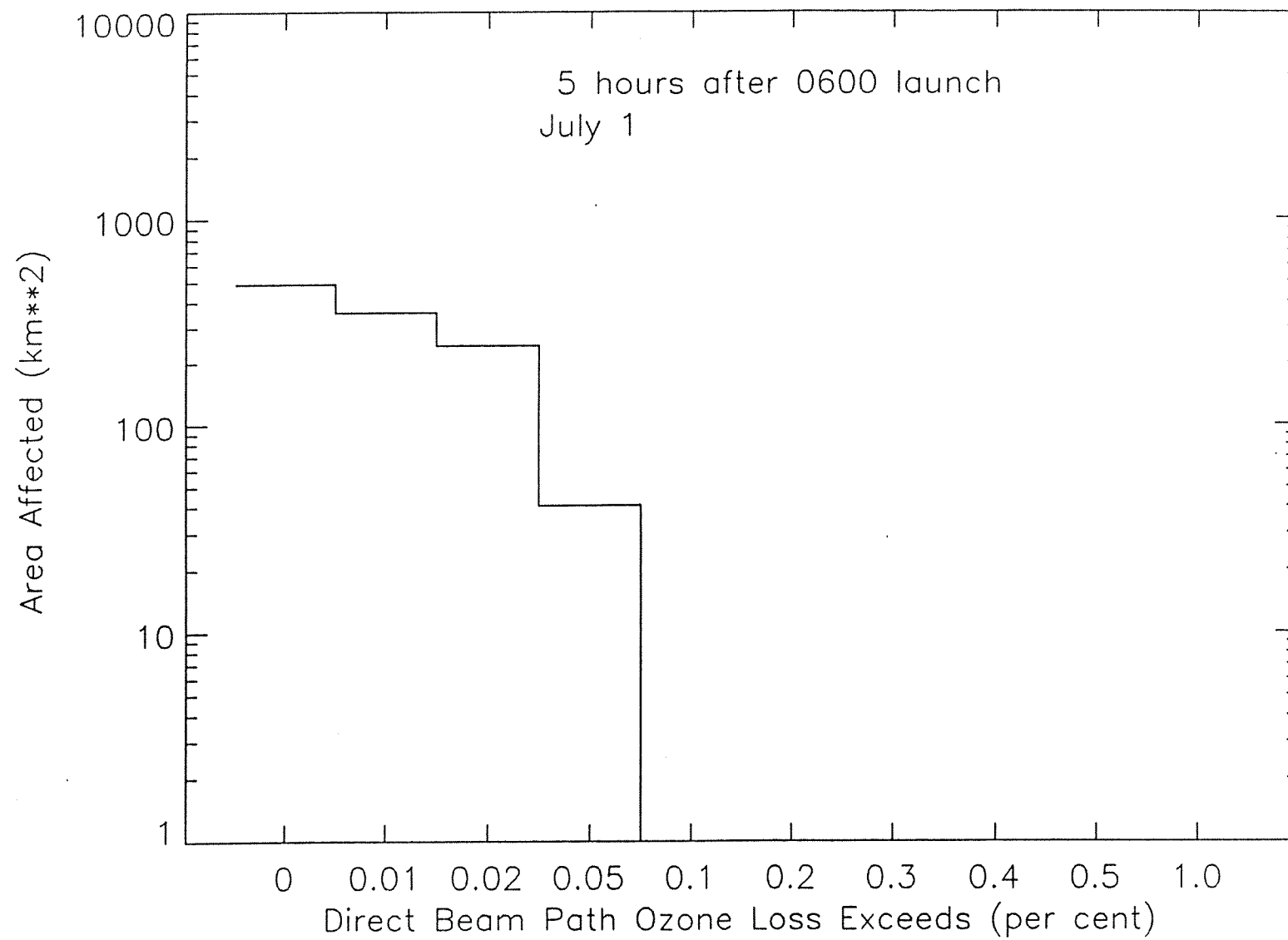


Figure 12c

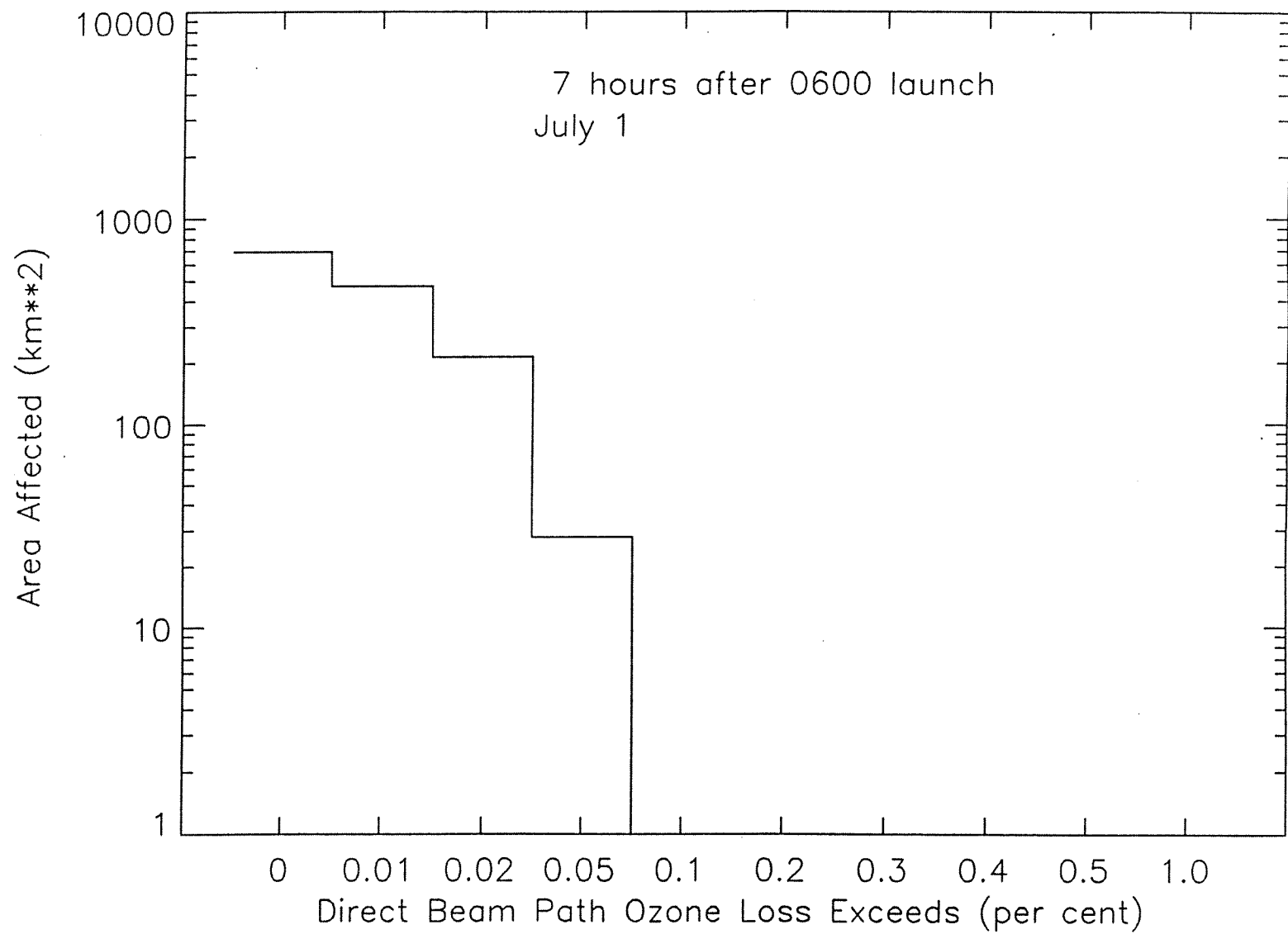


Figure 12d

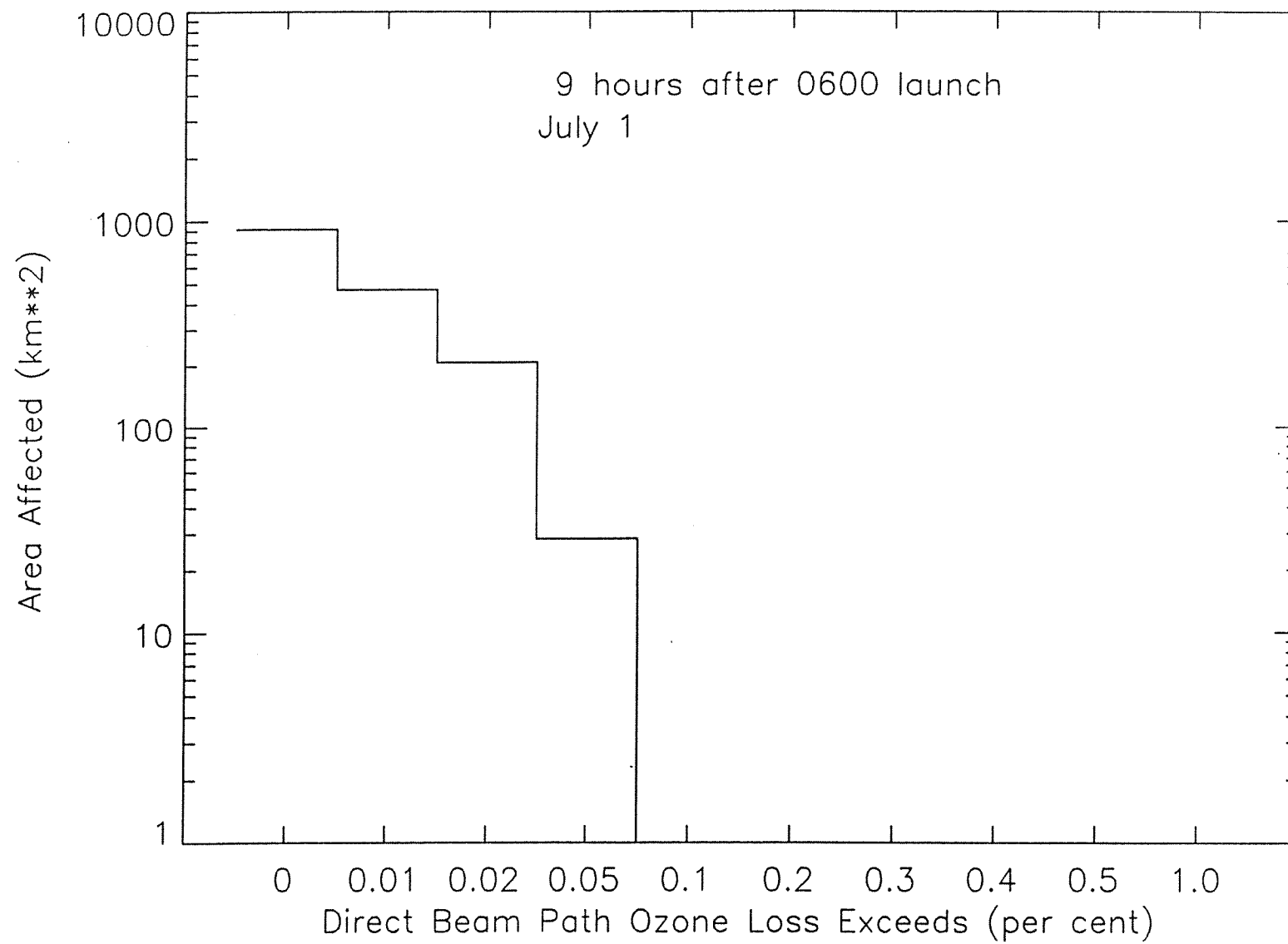


Figure 12e

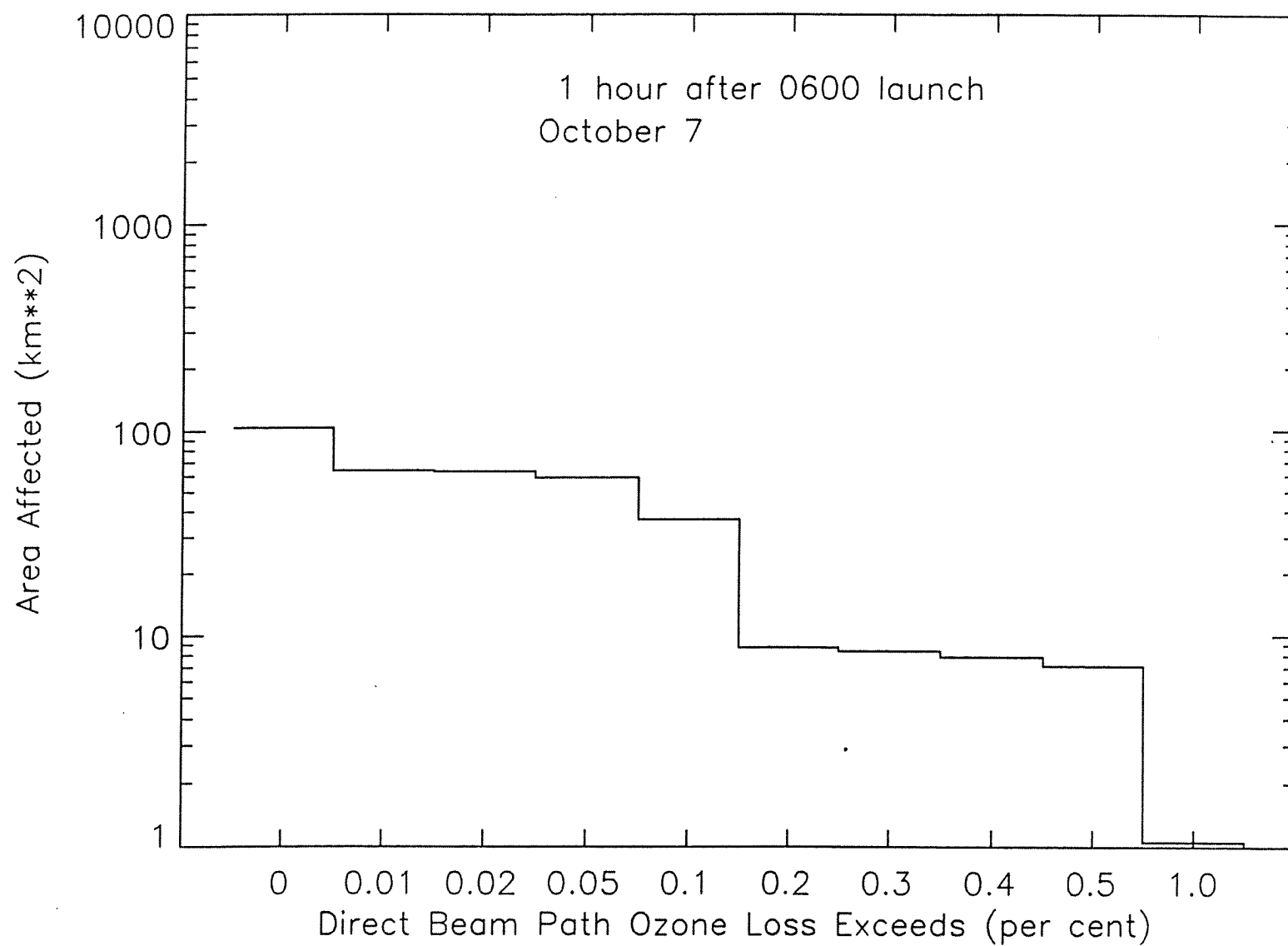


Figure 13a

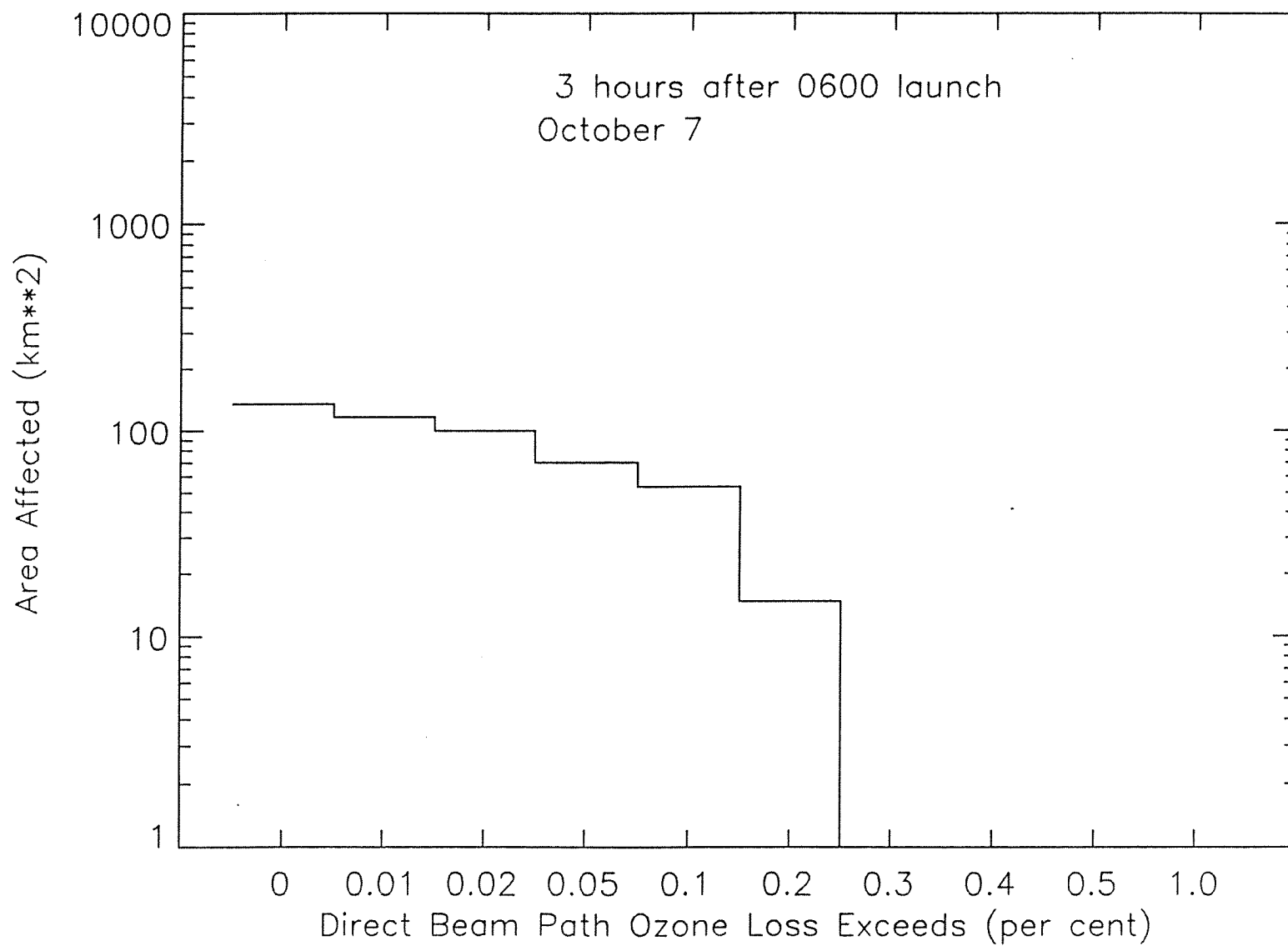


Figure 13b

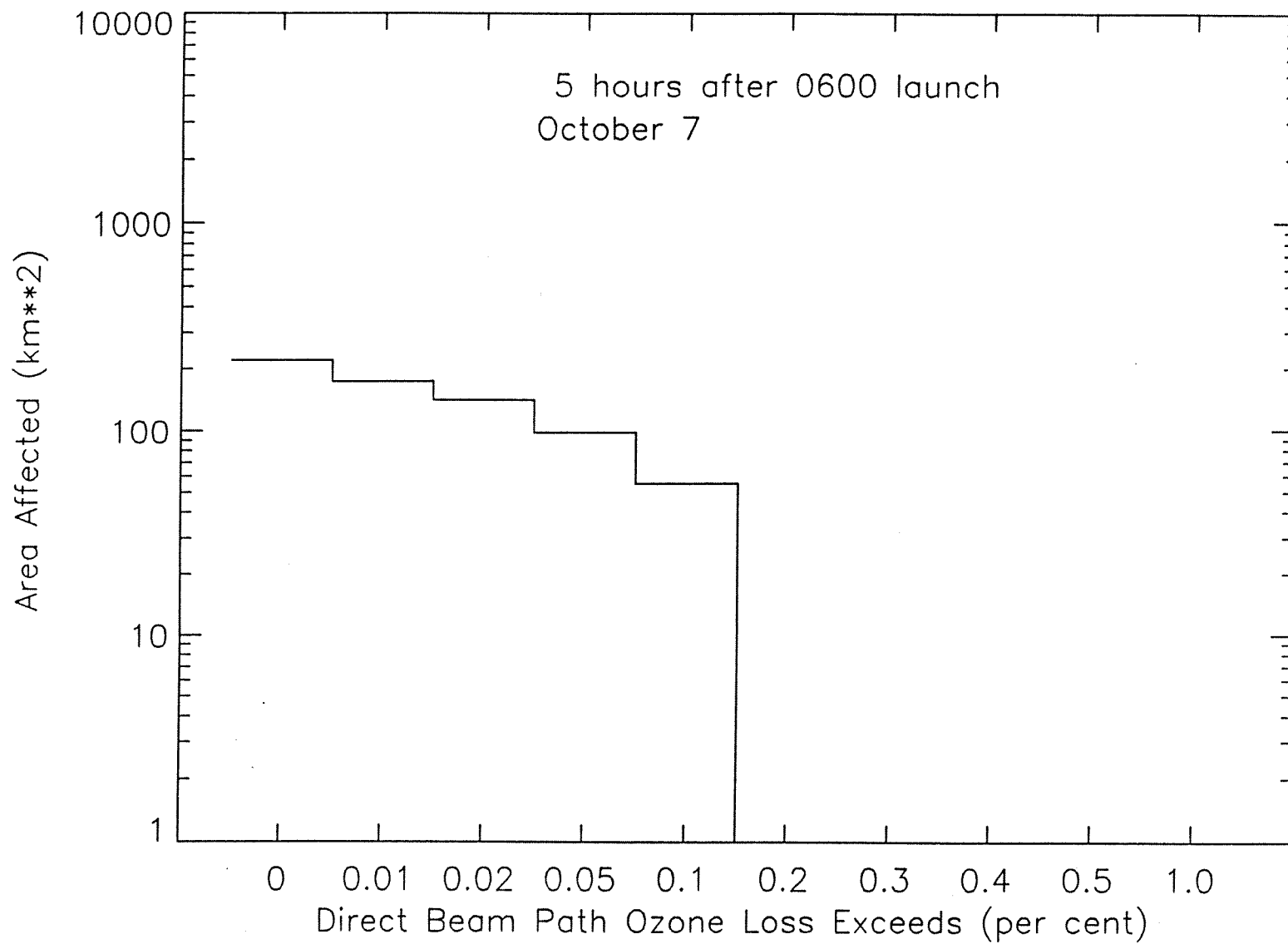


Figure 13c

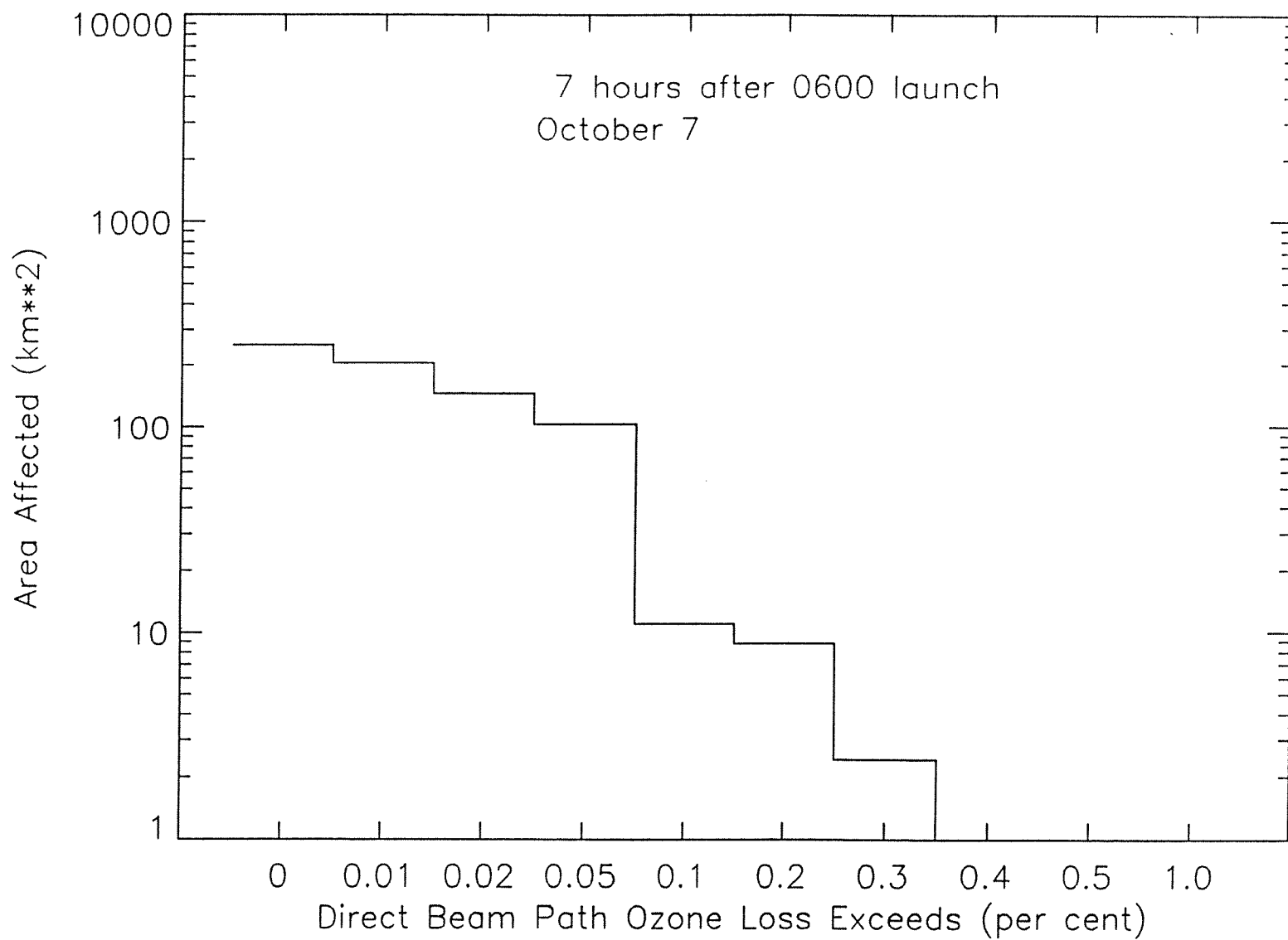


Figure 13d

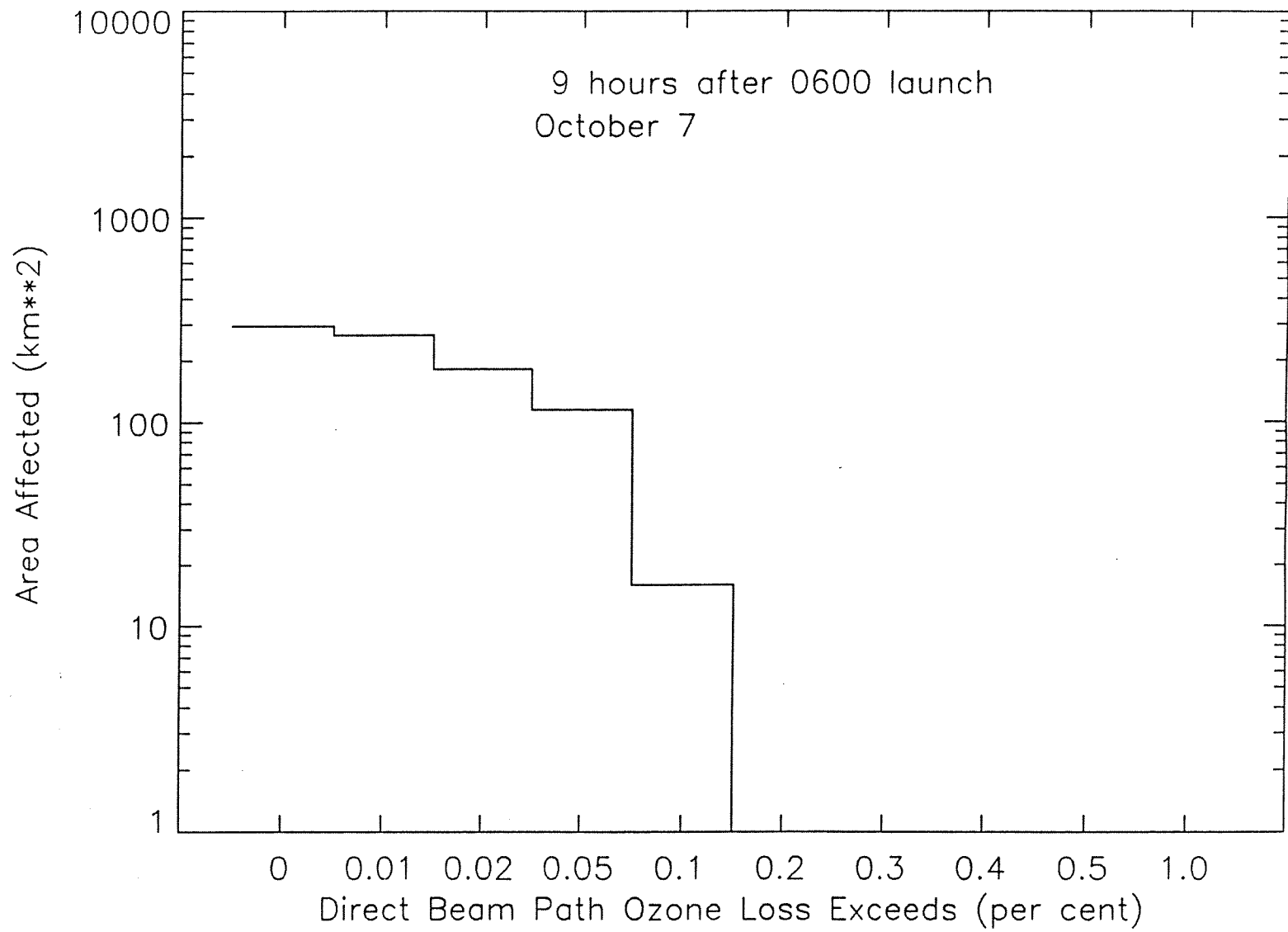


Figure 13e

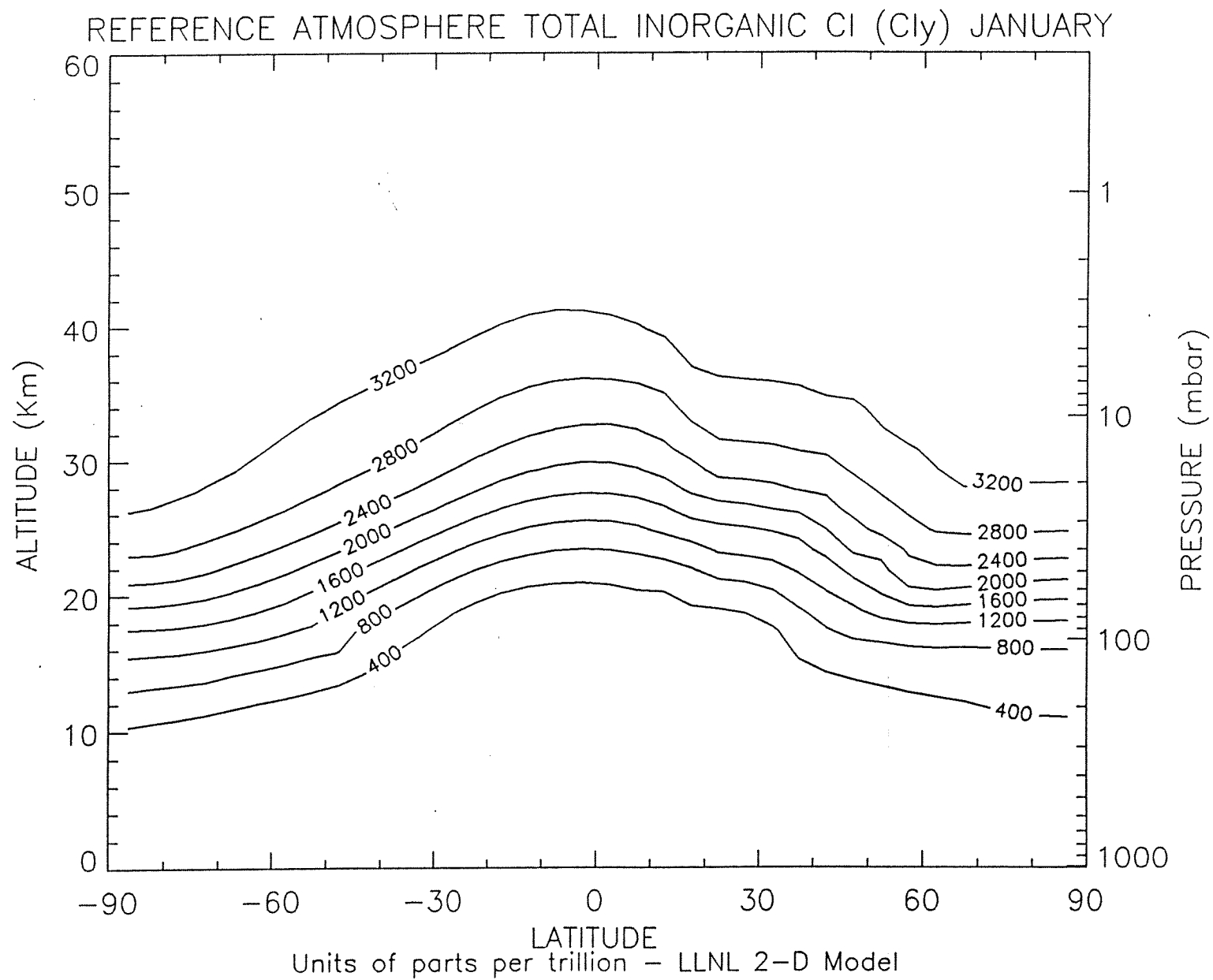


Figure 14a

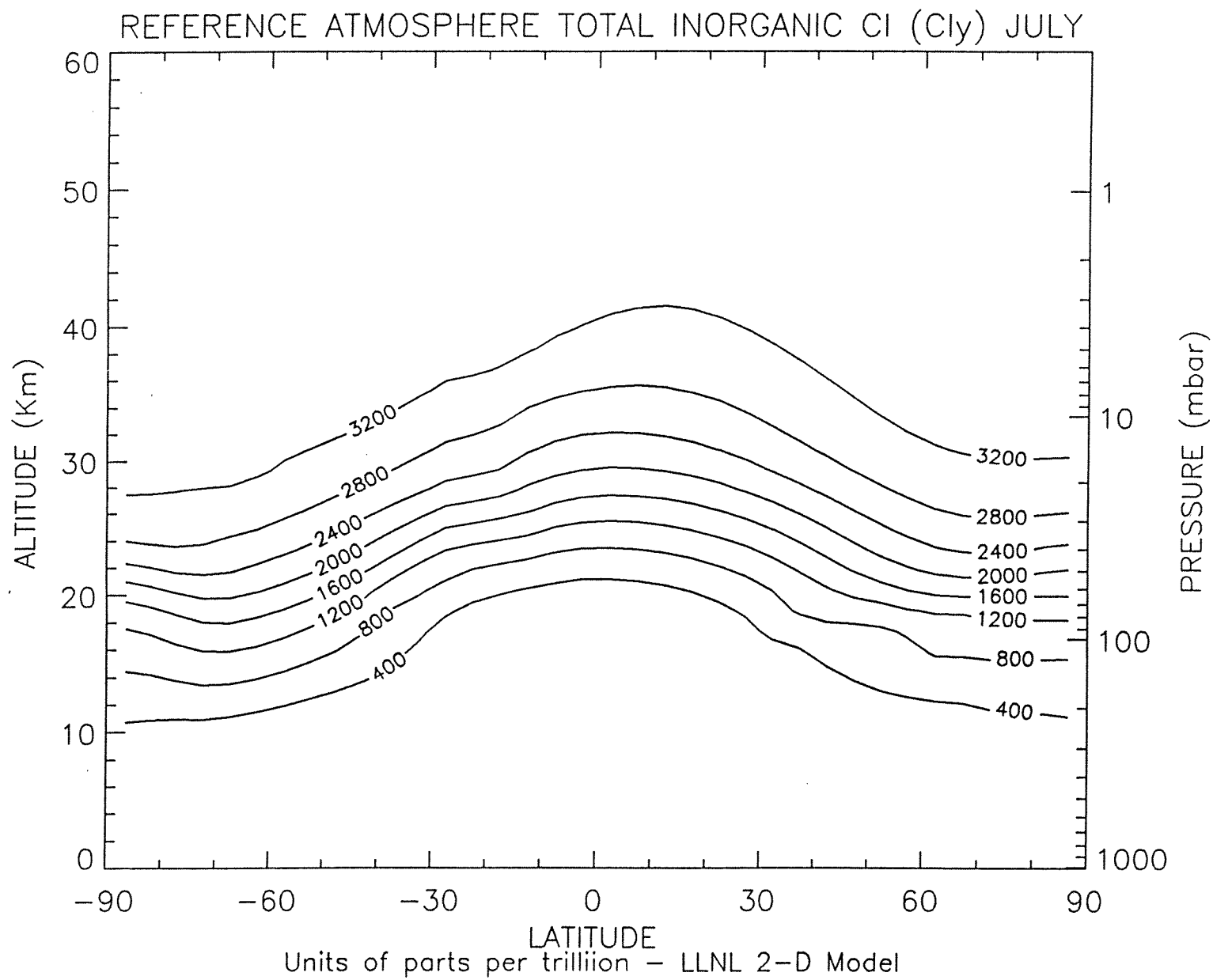


Figure 14b

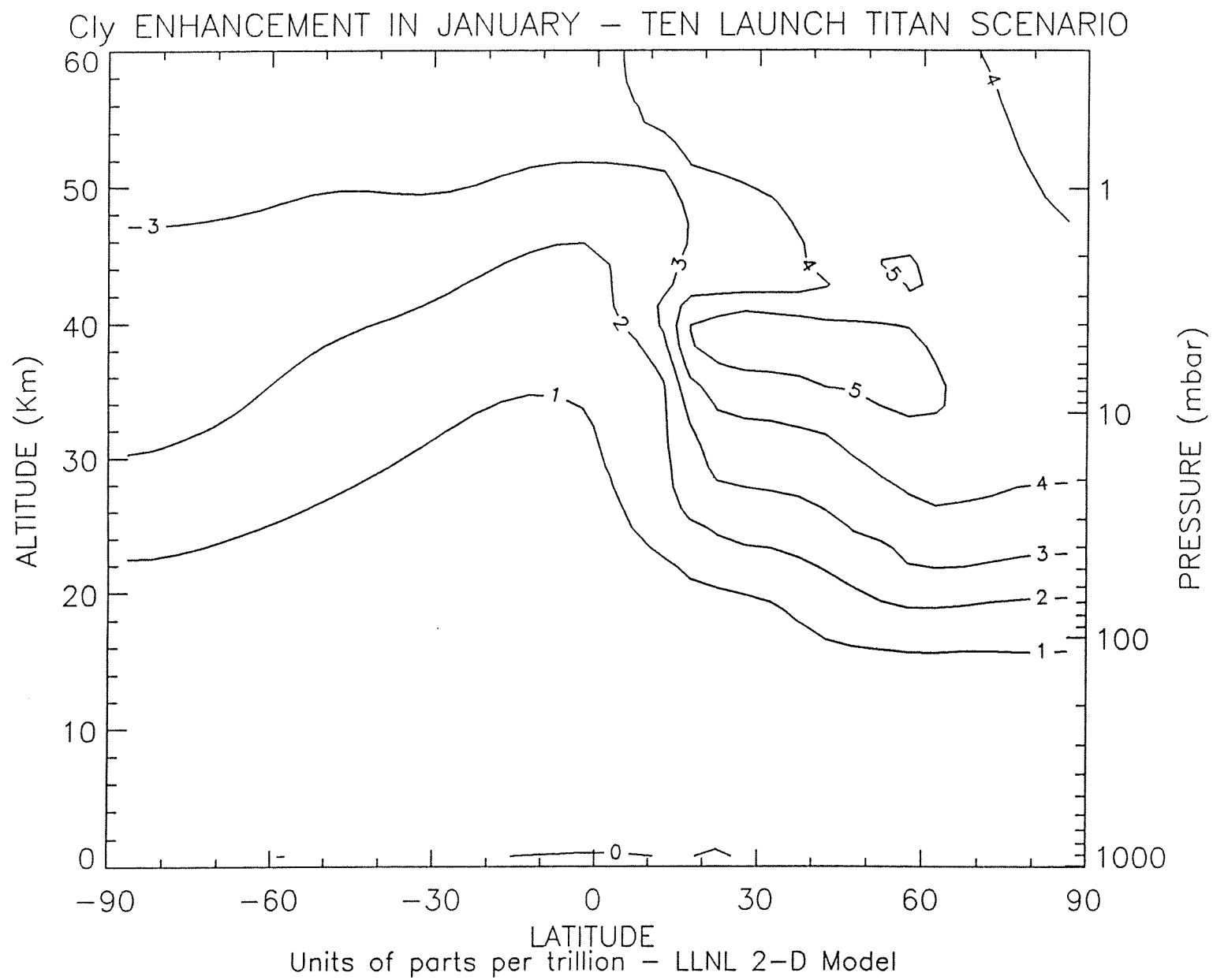


Figure 15a

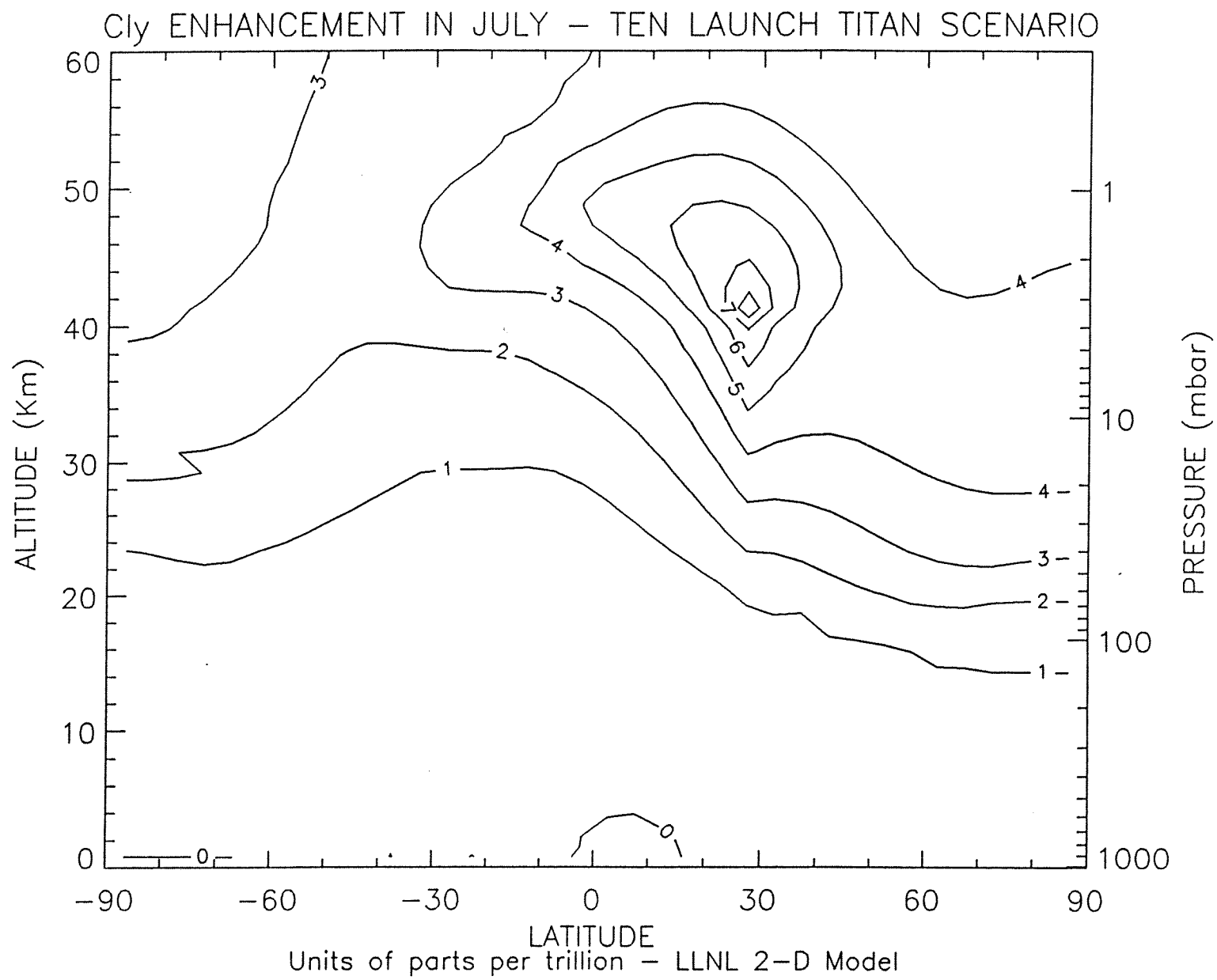


Figure 15b

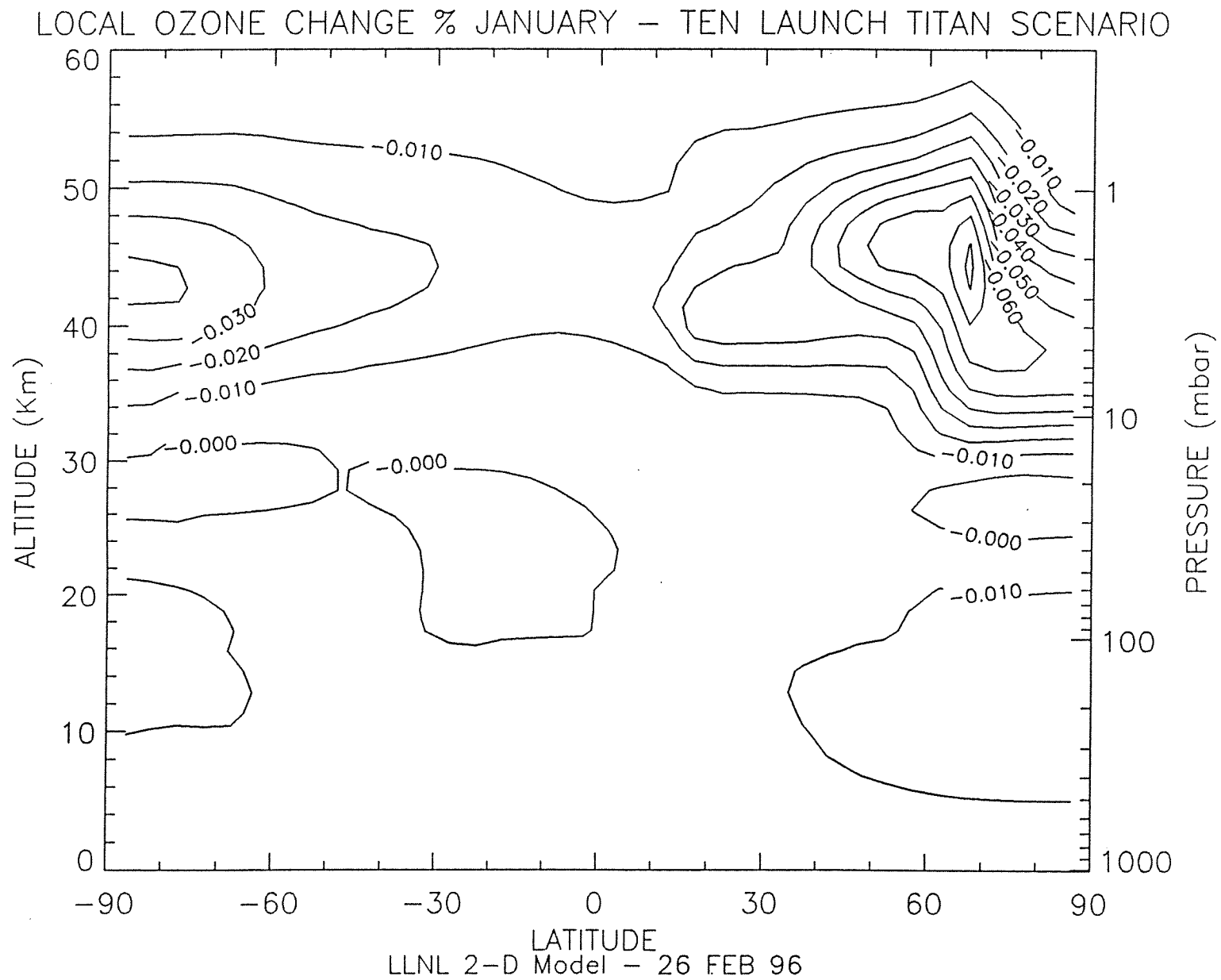


Figure 16a

Figure 16b

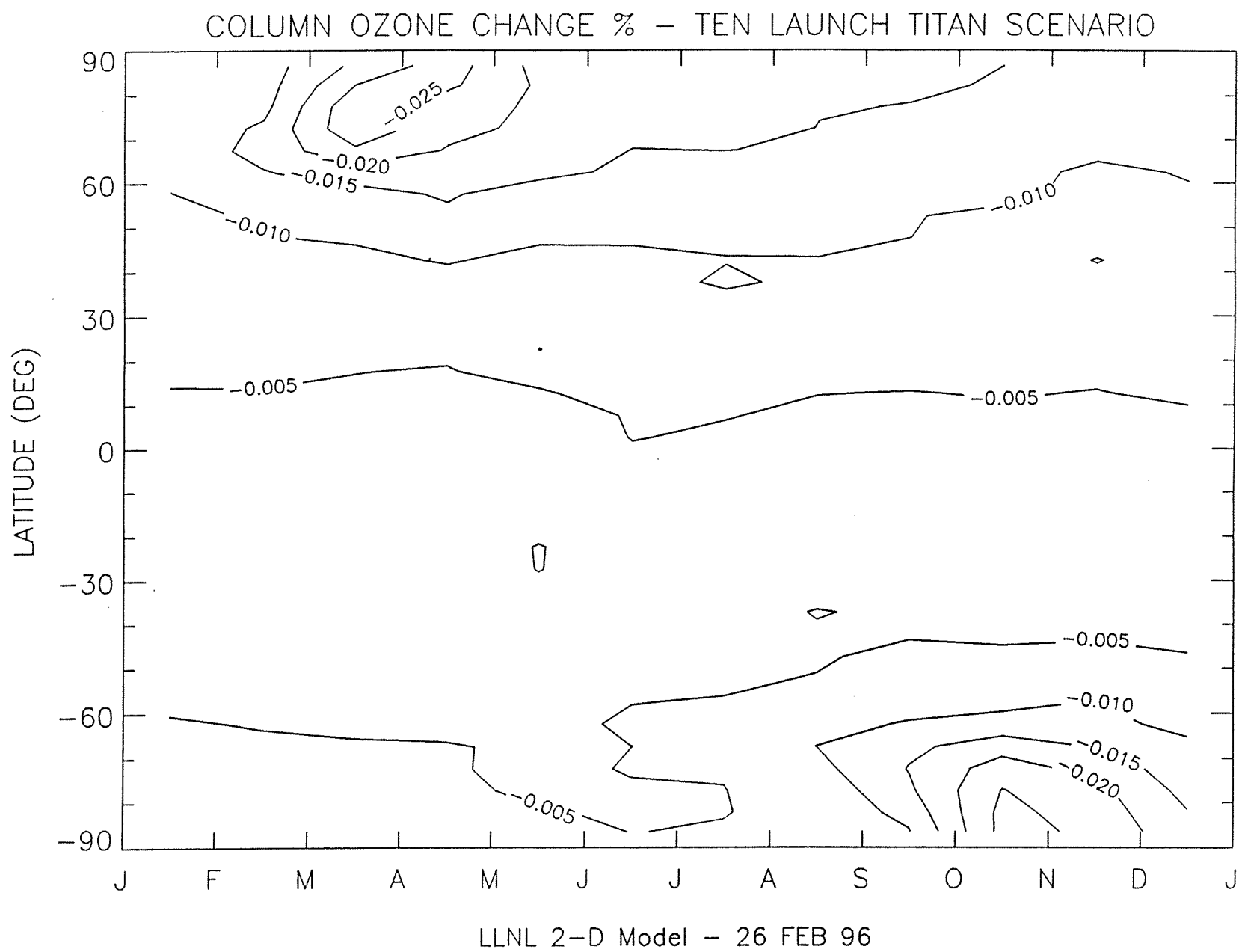


Figure 17

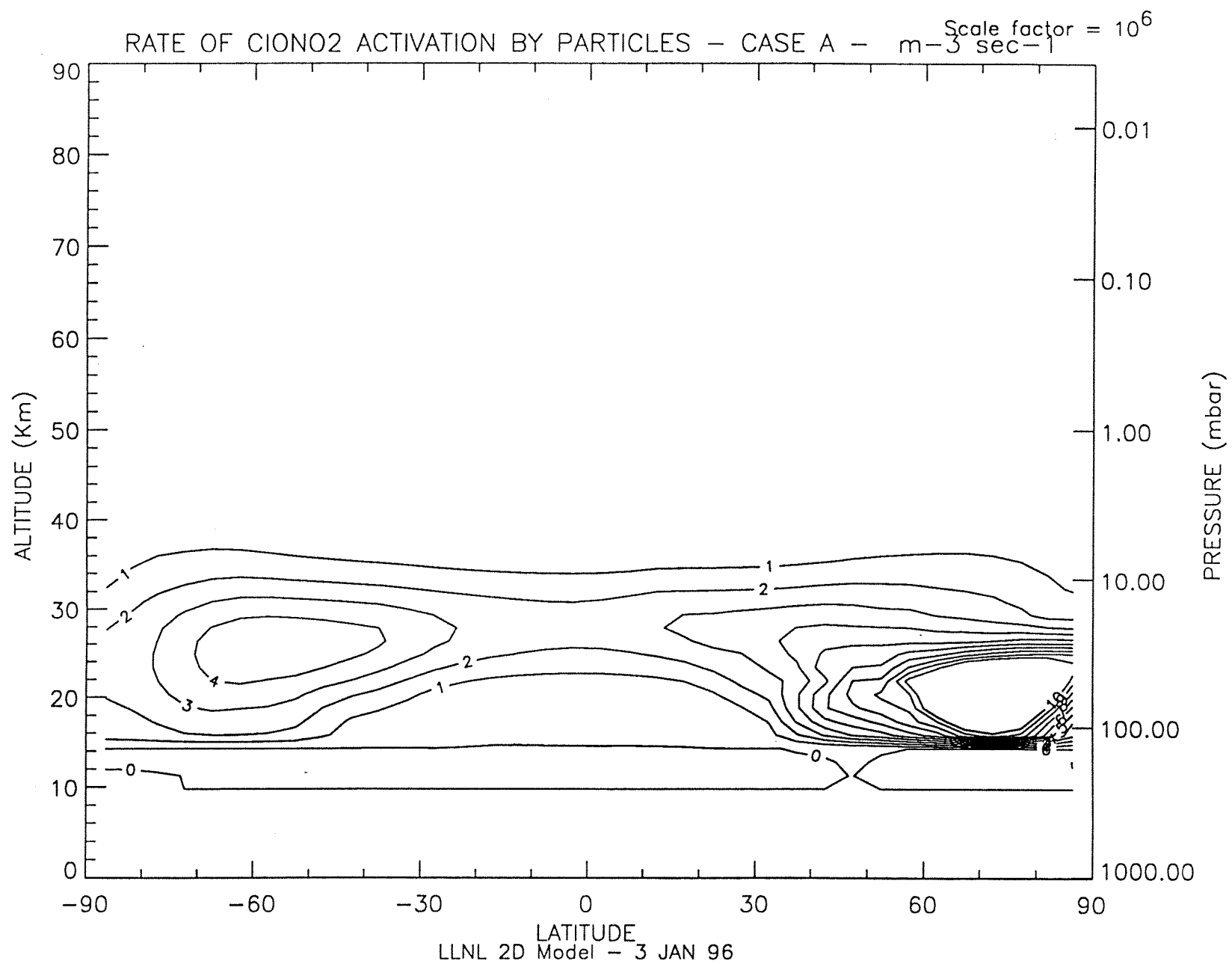


Figure 18

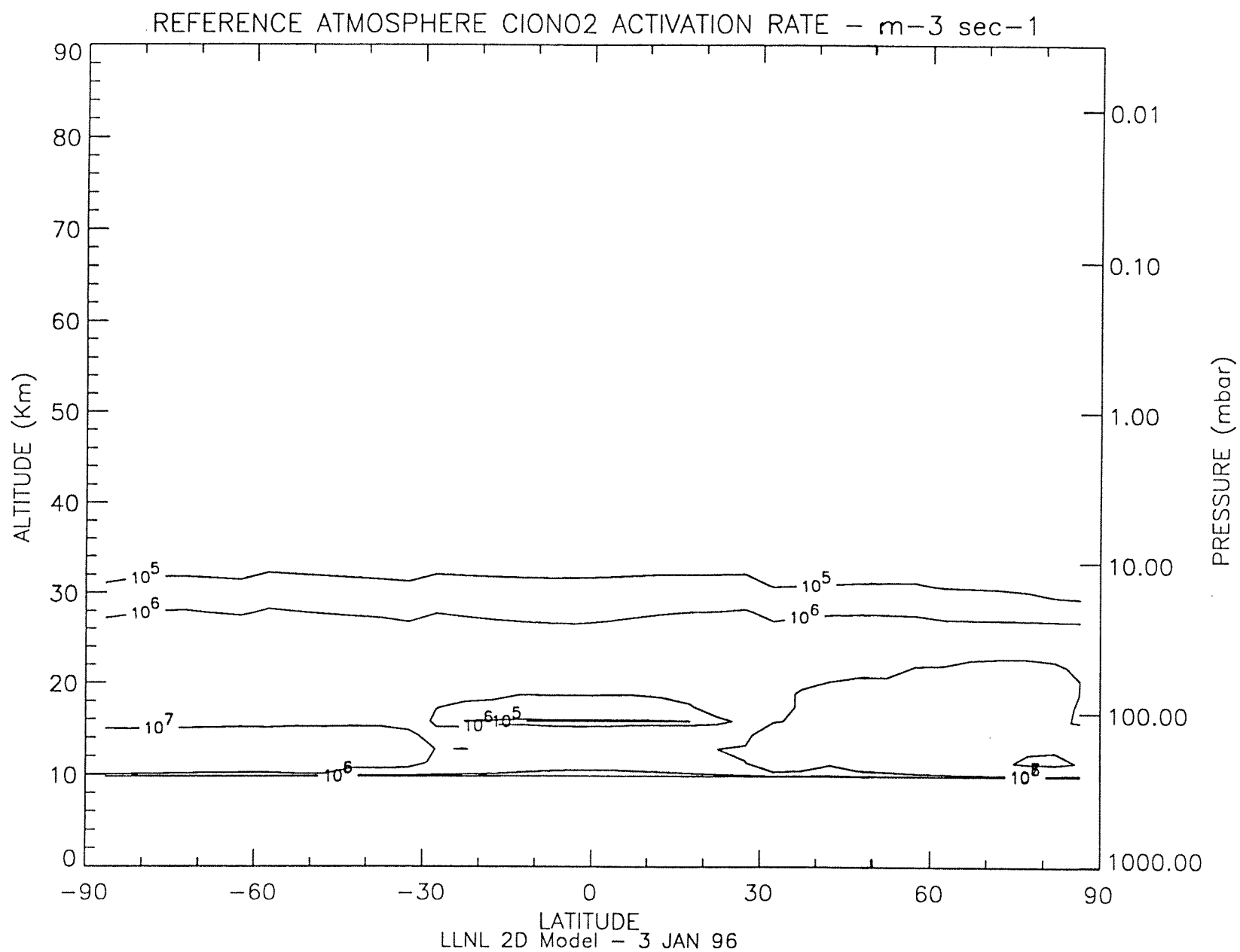


Figure 19

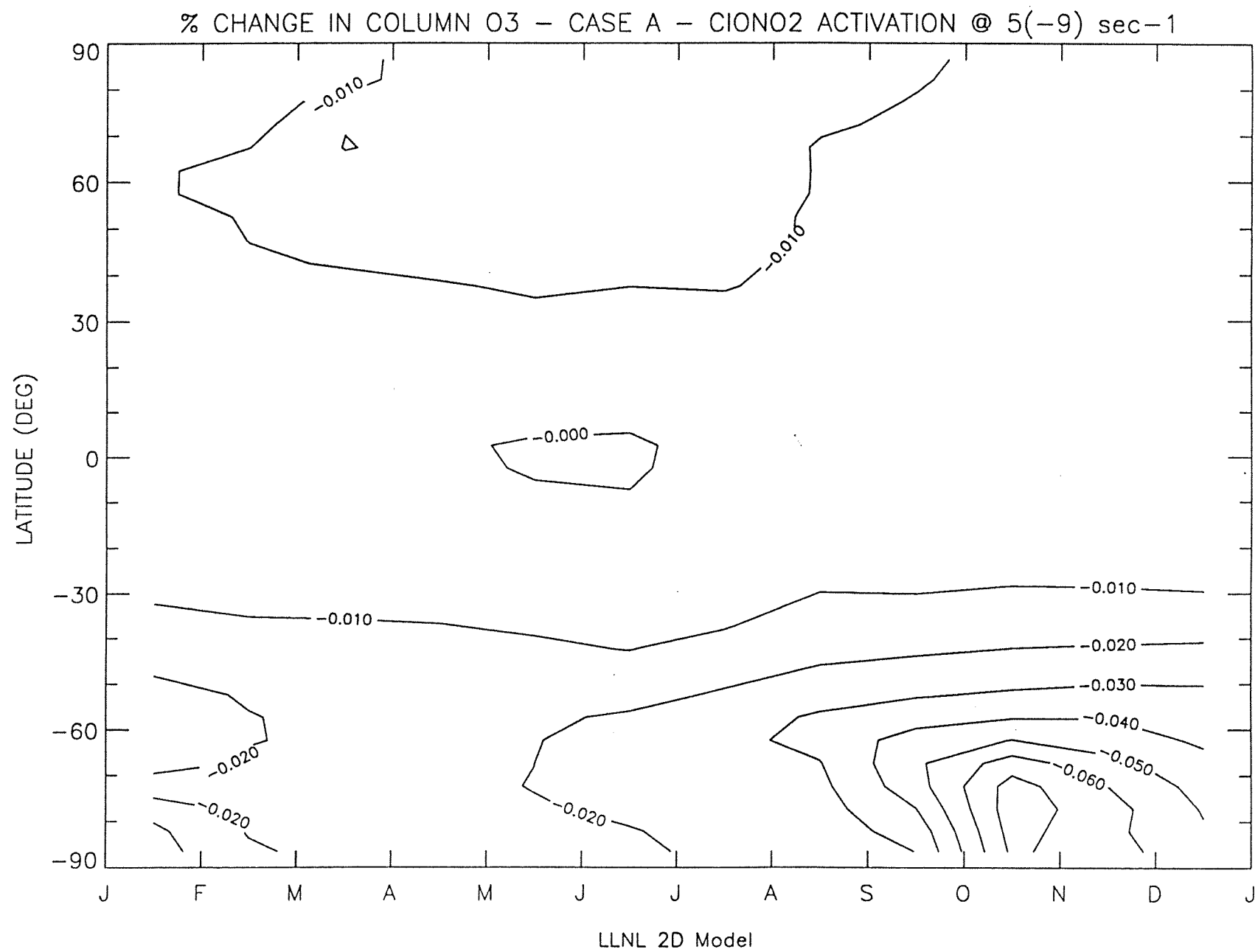


Figure 20